THE CLUSTERING OF EARTHQUAKE MAGNITUDES: FROM LABORATORY FRACTURE TO EARTH SCALE.

Katerina Stavrianaki

A thesis submitted for the degree of Doctor of Philosophy

University College London

January 2018

I, Katerina Stavrianaki confirm that the work presented in this thesis is my own. Where information has been derived from other sources, I confirm that this has been indicated in the thesis.

- -

Abstract

Over the last century statistical seismology has been one of the key methods to describe the nature of the seismic process. The clustering of earthquakes in space and time has been established and is included in statistical models such as the Epidemic Type Aftershock Sequences (ETAS) model to describe earthquake occurrence. On the other hand the clustering in magnitude is considered to be zero. If magnitude correlation exist and included in the statistical models this could lead to better interpretation of the seismicity in the region that can be used to update and improve probabilistic forecasts of seismicity.

This research seeks to test the existence or not of earthquake magnitude correlations by analysing earthquake catalog data from different regions worldwide. In standard models of seismic hazard such as ETAS, the magnitude of each earthquake is independently drawn from a Gutenberg-Richter distribution. As such, there should not be any correlations between magnitude and seismicity if the usual ETAS assumptions are correct, since the increase in the seismicity only affects the number of aftershocks, while having no effect on their magnitude. We have shown that the mean magnitude of earthquakes is larger during periods of high seismicity confirming the existence of correlations.

I additionally studied acoustic emission (AE) data from laboratory triaxial rock deformation experiments. The AE technique provides a means to analyse microcracking activity inside the rock volume and since experiments can be performed to simulate crustal conditions, AE can be used as a proxy for natural processes such as earthquakes. The results have also been analysed in terms of crack length and stress intensity.

Finally, two statistical models, the ETAS model which is most widely used in the field of statistical seismology and a compound poisson model have been tested on their forecasting capabilities.

Acknowledgements

First and foremost I would like to express my immense gratitude to my supervisors Professor Peter Sammonds and Dr Gordon J. Ross.

Peter, thank you for your guidance and support, the enlightening discussions, constant encouragement, your willingness to generously give me your time in meetings and many other unscheduled discussions and for providing the funding opportunity to me which made this PhD possible. Gordon, thank you for your advice, exciting scientific discussions and for your willingness to provide a more advanced supervisory role when was needed.

I am very grateful to all the people who have helped me in various ways during my PhD, in particular I would like to thank: Dr Ilan Kelman, as a graduate advisor your support and extreme patience during the most difficult period of my PhD has been invaluable. Dr Rosanna Smith and Ms Mumtaz Abdul Ghafoor thank you for the administrative support, I really appreciate it. Thanks to Professor P. Meredith, Dr N. Brantut and Dr E. David for your assistance and help with my laboratory experiments and to the technical stuff of the Ice and Rock Physics lab; John Bowles, Neil Hughes, Steve Boon and Jim Davy your help has been of great value to me. Dr S. Kirby, I am very grateful for inviting me to work with you at the USGS in Menlo Park, for the scientific discussions and the laboratory experience and knowledge I gained during my time there.

I would like to acknowledge and appreciate the financial support from the UCL IRDR throughout my PhD and for generously providing me additional funds to attend international conferences, workshops and for funding my travel to the USGS. For this I am enormously grateful. I would also like to thank the European Union (European Social Fund) and Greek national resources under the framework of the Thalis Program: Seismo Fear Hellarc project of the Education & Lifelong Learning Operational Programme for partially funding the first year of my PhD.

I would like to thank all the my friends and colleagues, past and present, in the UCL IRDR , for making the last three and a half years during this PhD a memorable and fun experience. Special thanks to Andria, Sally, Omar, Gianluca, Serena, Mark, Tasnuva and Bayes for being such amazing friends.

Last but not least I would like to thank my parents Nikos and Susan-Carol, my brother Ioannis and my grandfather Peter for being there for me, their support and understanding - I could not have done it without you.

Contents

Author's Declaration **3**

Abstract **5**

Acknowledgements **7**

Table of Contents **9**

List of Figures **11**

List of Tables **18**

Nomenclature **21**

1 Introduction **23**
1.1 Statistical Seismology 23
1.2 Motivation and research questions 28
1.3 Aim of the thesis 30
1.4 Objectives 31
1.5 Thesis layout 32
1.6 Research output 34

2 Literature Review **37**
2.1 Chapter outline 37
2.2 Physical Models 38
2.3 Statistical Models 40
2.4 Statistical models in short term earthquake prediction and long-term seismic hazard analysis and the role of magnitude clustering 44
2.5 The Epidemic Type Aftershock Sequence (ETAS) model 45
2.6 Earthquake catalogs 48
2.7 Magnitude of completeness M_c 55
2.8 Declustering 63
2.9 Magnitude correlations - An overview of existing work 66
2.10 Fracture mechanics 70

3 Magnitude correlations **73**
3.1 Chapter outline 73
3.2 Proposed approach for magnitude correlations assessment 74

3.3 Applications in California . . . 83
3.4 Synthetic catalogs - Validation of the proposed methodology . . . 94
3.5 Stochastic Declustering Methodology . . . 95
3.6 Applications in a variety of tectonic settings . . . 98
3.7 Key findings - discussion . . . 111

4 Triaxial deformation of sandstone 113
4.1 Chapter outline . . . 113
4.2 Rock sample preparation . . . 116
4.3 Triaxial Rock Physics Ensemble . . . 120
4.4 Rock sample assembly . . . 123
4.5 The experimental procedure . . . 125

5 Magnitude correlations in experimental data 129
5.1 Chapter outline . . . 129
5.2 Sensor calibration . . . 135
5.3 Magnitude correlations in experimental data . . . 135
5.4 Interpretation of results . . . 137
5.5 Key findings - discussion . . . 140

6 Forecasting with the ETAS and compound Poisson models 143
6.1 Chapter outline . . . 143
6.2 Forecasting with the bayesian ETAS model . . . 146
6.3 Forecasting with the bayesian ETAS model . . . 149
6.4 Forecasting with the compound poisson model . . . 153
6.5 Conclusions . . . 159

7 Conclusions - Outcomes 161

References 168

Appendices 189

A Synthetic catalogs results 191
A.1 Parkfield - Cut off magnitude 1.1 . . . 191
A.2 Parkfield - Cut off magnitude 2 . . . 215
A.3 Southern California - Cut off magnitude 3.5 . . . 239

B Constant strain rate experiments 241
B.1 Stress-Time plots . . . 241

C Constant load experiments 247
C.1 Axial strain (%)-Time plots . . . 247

D RMS Amplitude Method 249

E The Geiger algorithm 253

List of Figures

1.1 A positive c > 0 in Omori's law means that the singularity in aftershock rate occurs at negative time (t < 0), that is, before the mainshock. We show Omori laws with c = 1 and c =0 here in linear scale and in log-log scale. In statistical analyses of earthquake catalogues, events before the green or black lines may be removed to ensure completeness of aftershock accounting (*Kagan*, 2004). Positive c would fit a relative lack of early aftershocks (either real or apparent), but trends toward a singularity before the mainshock initiation. They propose that the positive empirical value for c is mostly due to the under-reporting of small aftershocks immediately following a mainshock. Figures and caption obtained by *Kagan and Houston* (2005). 27

2.1 Screenshot of the *Hauksson et al.* (2012) earthquake catalog of Southern California. 50

2.2 Format of the *Hauksson et al.* (2012) earthquake catalog of Southern California. 51

2.3 The FMD of a subset of the Southern California earthquake catalog. The M_c estimation is shown with a vertical line and corresponds to magnitude 1.4 56

2.4 b value estimate as a function of magnitude cutoff M_{co} for the subset of the NCSN (Northern California Seismic Network) catalog. For $M_{co} < M_c$, the b value is erroneous because the FMD is not a strict power-law. For $M_{co} > M_c$, the b value estimate starts to stabilise (around 1.0 in the example) before fluctuating again due to undersampling at the higher end of the FMD. Error bars represent $\pm$ 1σ, standard deviation obtained from bootstrapping. Figure and caption taken from *Mignan* (2012). 57

2.5 The temporal variation of M_c calculated with the maximum curvature (MAXC) and median-based analysis of the segment slope (MBASS) methods for the magnitude 7.3 Landers 1992 afterschock sequence. Moving window approach with a window of 1000 events, moved by 250 events.Figures obtained from *Mignan* (2012). 60

2.6 Plot (a) shows the estimated b-values for M_c(t) calculated for different threshold rates r max, showing stable results for values smaller than approximately 200 events per day, in which horizontal lines refer to (a) b = 1:28. Plots (d) shows the corresponding M_c(t) estimations for r max 100, 200 events per day in (d), in which the black curve refers to the empirical result of *Helmstetter et al.* (2006) applied to the mainshock in (d). Figures obtained from *Hainzl* (2016). 62

2.7 Difficulties in estimating ETAS parameters when maximizing the log-likelihood numerically. Except for K0 and a, the starting values (black dots) for the components of θ are set to the true values. The white circles show the estimation results of the numerical maximization routine ($\hat{\theta}$) and the + symbol depicts the location of the true K0 and a. Figure obtained from *Veen and Schoenberg* (2008). 65

2.8 Schematic representation of the nine tensor components. 71

2.9 Stress state during triaxial deformation. 72

3.1 A visual example of a branching structure implied by the ETAS model. The top layer represents the mainshocks, each of which can produce several aftershocks. These aftershocks are also themselves capable of producing further aftershocks. 76

3.2 Applications of the algorithm (Algorithm to Estimate Mc Based on Catalog Data section with N = 10) to estimate the rate-dependent completeness magnitude M_c(t) . Aftershock sequences of (a, d) the Mw 7.3 Landers and (b, e) the Mw 7.1 Hector Mine earthquake, as well as (c, f) the year 2011 swarm in western Bohemia. Plots (a - c) show the estimated b-values for M_c(t) calculated for different threshold rates r max, showing stable results for values smaller than approximately 200 events=day, in which horizontal lines refer to (a) b = 1.28, (b) b = 1.32, and (c) b = 1.22. Plots (d - f) show the corresponding M_c(t) estimations for r max =100; 200 events/day in (d, e) and r max = 300 events/day in (f), in which the black curve refers to the empirical result of *Helmstetter et al.* (2006) applied to the mainshock in (d, e), and to all events in (f). Error bars refer to b-values estimated for successive, nonoverlapping 500 events (plot d) and 200 events (plots e, f). The b-values calculated with constant completeness magnitude (M_c = 2.0 for California and 0.5 for the swarm) are marked by light blue error bars and those determined for the estimatedM_c(t) (with r max 100 in the aftershock sequences)are shown by green bars. Gray points indicate recorded earthquakes with their magnitudes. In all plots, error bars refer to 1 standard deviation. Figure and caption obtained by *Hainzl* (2016). 79

3.3 Flowchart of the main steps of the proposed methodology. 82

3.4 The spatial distribution of seismic activity for 365 days after the magnitude 6 Parkfield earthquake in 2004.Figure obtained from *Shcherbakov et al.* (2006) 84

3.5 Mean earthquake magnitude for the raw data along with the high-/low intensity subcatalogs, for each magnitude of completeness in the Parkfield catalog. The vertical lines indicate 95% confidence intervals. 86

3.6 Power of the Mann-Whitney test for detecting magnitude differences between the low and high intensity catalogs, for each value of the magnitude difference c or size. 88

3.7 Map showing the study area in Southern California. The waveform-relocated epicenters are shown as black dots, the non relocated seismicity (events of type 3d, 1d, and xx) is shown as light grey dots, and earthquakes of M $\geq$ 5.5 are shown as stars. Quaternary faults are depicted as light grey curves. The large earthquake sequences are indicated by year: 1992 Mw 7.3 Landers; 1994 Mw 6.7 North- ridge; 1999 Mw 7.1 Hector Mine; 2010 Mw 7.2 El Mayor Cucapah. The polygon is the SCSN reporting area for local events. Events located outside this polygon are called regional events. US, United States of America. Figure and caption obtained from *Hauksson et al.* (2012). . 89

3.8 Temporal variation of the magnitude of completeness, found using the maximum curvature method from *Mignan* (2012) 90

3.9 Short term aftershock incompleteness period after the Mw 7.1 Hector Mine earthquake. The dashed line defines the boundaries of the excluded events after the mainshock for cut off 3.5 91

3.10 Mean earthquake magnitude for the raw data along with the high-/low intensity subcatalogs, for each cut-off magnitude in the Southern Califonia catalog. The vertical lines indicate 95% confidence intervals 93

3.11 The three main types of tectonic boundaries shown in a cross section. Figure obtained from https://pubs.usgs.gov/gip/dynamic/Vigil.html 99

3.12 Schematic illustration of the relative motion of the rock mass in a normal fault. Figure obtained from https://geomaps.wr.usgs.gov/parks/deform/ 99

3.13 Schematic illustration of the relative motion of the rock mass in a reverse fault. Figure obtained from https://geomaps.wr.usgs.gov/parks/deform/ 100

3.14 Schematic illustration of the relative motion of the rock mass in a strike slip fault. Figure obtained from https://geomaps.wr.usgs.gov/parks/deform/ 100

3.15 The study area of the western Corinth gulf is denoted by a black box. 104

3.16 Rate varying estimation of the b value. 106

3.17 Mean earthquake magnitude for the original (raw data) along with the high/low intensity subcatalogs, for each cut-off magnitude M0 in the western Corinth gulf catalog. The vertical lines indicate 95% confidence intervals 107

3.18 Main geologic structures of the Hellenides and the Aegean Sea (location indicated by inset to Fig. 2c). Barbed lines indicate thrust fronts for the most external unit(s) of the Hellenides. Red and green triangles indicate the modern and Miocene volcanic arcs, respectively. Large arrows with symmetric heads are GPS velocities in the Eurasian reference frame. Central Hellenic Shear Zone (CHSZ); Gulf of Corinth (CG); North Aegean Basin (NAB); North Anatolian Fault (NAF); Kephalonia Transform Fault (KFT); Paxos Zone (PA). Figure taken from *Papanikolaou and Vassilakis* (2010) 108

3.19 Focal mechanism solution of the 01/07/2009 earthquake south of Crete. The image is obtained from the National Observatory of Athens http://bbnet.gein.noa.gr 109

3.20 Rate varying estimation of the b value. 110

4.1 The characteristic stress and strain curves of triaxially deformed Darley Dale sandsone. It is shown that different samples are deformed in the same manner, making Darley Dale an excellent rock to use in the laboratory. 115

4.2 Coring a Darley Dale sandstone sample. 116

4.3 Grinding the sample 117

4.4 Schematic representation of a conventional triaxial compression testing machine, including optional arrangements for pore fluid pressure. The Figure is taken from *Paterson and Wong* (2005) 121

4.5 The triaxial testing cell for rock deformation designed by *Sammonds* (1999). The rock sample is jacketed in a multiple-instrumented plastic sleeve to keep out the confining fluid. Twelve electrical and/or acoustic measurements can be made simultaneously on the sample. The sample is deformed by upper and loading rams. These in turn are loaded by an axial loading piston that is pressure balance so only the differential stress (the total axial stress minus the confining pressure) need be applied, greatly improving the accuracy of load measurement and experimental control. The confining fluid is oil. An internal heater allows temperatures up to 400°C to be used. The caption and the figure are obtained from *Sammonds* (1999). 122

4.6 List of physical variables measured and set at beginning of experiments together with absolute uncertainties. From *Clint* (1999). 122

4.7 The jacket and the AE setup on top of the lower piston. Rubber bands are keeping the threads close to the jacket and prevent them getting caught inside the pressure vessel. 123
4.8 Cross section of the triaxial ensemble. 125

5.1 Figure showing the three stages of deformation of a DDS sample. . . 132
5.2 Figure showing the three stages of deformation of a DDS sample. . . 133
5.3 Figure showing the axial strain %-time plot of the stress stepping experiment. 134
5.4 Figure showing a time series created from the AE data. 136
5.5 Figure showing the ETAS fit to the AE data. 136

6.1 Map showing a part of California. The region inside the black box represents the study area. 149
6.2 Histogram showing the number of mainshocks generated by each simulation and the frequency of their appearance. The mean number of mainshocks was found to be 20. 153
6.3 Histogram showing the number of mainshocks generated by each simulation and the frequency of their appearance. The mean number of mainshocks over magnitude 5 was found to be 11 for the period 2007-2011. 158

B.1 Stress-Time plot. Dry experiment at 30 MPa confining pressure . . . 241
B.2 Stress-Time plot. 50 MPa confining pressure and 20 MPa pore pressure, constant pressure experiment 242
B.3 Stress-Time plot. 50 MPa confining pressure and 20 MPa pore pressure, constant volume experiment 242
B.4 Stress-Time plot. Dry experiment at 80 MPa confining pressure . . . 243
B.5 Stress-Time plot. 100 MPa confining pressure and 20 MPa pore pressure, constant pressure experiment 243
B.6 Stress-Time plot. 100 MPa confining pressure and 20 MPa pore pressure, constant volume experiment 244
B.7 Stress-Time plot. 40 MPa confining pressure and 10 MPa pore pressure, constant pressure experiment 244
B.8 Stress-Time plot. 50 MPa confining pressure and 20 MPa pore pressure, constant volume experiment 245
B.9 Stress-Time plot. 50 MPa confining pressure and 20 MPa pore pressure, constant volume experiment 245

B.10 Stress-Time plot. 50 MPa confining pressure and 20 MPa pore pressure, constant volume experiment. Saw cut sample. 246

C.1 Axial strain (%)-Time plot. 50 MPa confining pressure and 20 MPa pore pressure. 247
C.2 Axial strain (%)-Time plot. 40 MPa confining pressure and 10 MPa pore pressure. 248
C.3 Axial strain (%)-Time plot. 40 MPa confining pressure and 10 MPa pore pressure. 248

List of Tables

3.1 Earthquake magnitude and ETAS intensity correlations in Parkfield. . 85

3.2 Average magnitude of the original earthquake catalogs along with the low and high intensity subcatalogs. 85

3.3 Correlation between the magnitude of each earthquake in the Southern California catalog and the ETAS intensity immediately preceding it, along with 95% confidence interval. Also shown is the p-value of the Mann-Whitney test when comparing the mean earthquake magnitude in the high and low intensity regions. 92

3.4 Mean magnitude of the original earthquake catalogs (raw data) at each cut-off magnitude in the Southern California catalog, along with the low and high intensity subcatalogs that are created by considering only the earthquakes that occur during periods when the ETAS intensity function is below/above a certain threshold. 92

3.5 Quantification of the b value variations between low and high intensity datasets for all the cut off magnitudes. 93

3.6 Correlation between the magnitude of each mainshock and the average magnitude of its aftershocks in the declustered Parkfield catalog, along with 95% confidence interval. 96

3.7 Correlation between the magnitude of each mainshock and the mean magnitude of its aftershocks in the declustered Southern California catalog, along with 95% confidence interval. 97

3.8 Correlation between the magnitude of each earthquake in the western Corinth catalog and the ETAS intensity immediately preceding it, along with 95% confidence interval. Also shown is the p-value of the Mann-Whitney test when comparing the mean earthquake magnitude in the high and low intensity regions. 105

3.9 Correlation between the magnitude of each earthquake in the aftershock sequence and the ETAS intensity immediately preceding it, along with 95% confidence interval. Also shown is the p-value of the Mann-Whitney test when comparing the mean earthquake magnitude in the high and low intensity regions. 111

5.1 Table showing the constant strain rate experiments performed and their experimental conditions. All experiments performed in Darley Dale sandstone and the strain rate used is 10^{-5} s^{-1} 131
5.2 Table showing the constant stress (creep) experiments performed and their experimental conditions. All experiments performed in Darley Dale sandstone and the strain rate used to bring the sample to the desired stress level is 10^{-5} s^{-1} 133
5.3 Table showing the constant strain rate experiments performed and their experimental conditions. All experiments performed in Darley Dale sandstone and the strain rate used is 10^{-5} s^{-1} 137
5.4 Table showing the constant load (creep) experiments performed and their experimental conditions. All experiments performed in Darley Dale sandstone and the initial strain rate used is 10^{-5} s^{-1} 137

6.1 Table showing the number of aftershocks for each mainshock over magnitude 5 in the earthquake catalog. 157

List of Abbreviations

AE	Acoustic Emissions
BMC	Bayesian Magnitude of Completeness
EMR	Entire Magnitude Range
$ETAS$	Epidemic Type Aftershock Sequence
FMD	Frequency Magnitude Distribution
$G-R$	Gutenberg Richter
$M0$	Cut off magnitude
M_c	Magnitude of Completeness
M_L	Location magnitude
M_w	Moment magnitude
$MAXC$	Maximum Curvature
$MBASS$	Median-Based Analysis of the Segment Slope
$MCMC$	Markov chain Monte Carlo
MLE	Maximum Likelihood Estimation
$NCSN$	Northern California Seismic Network
NED	North East Down
OFC	Olami Feder Christensen
$SCEC$	Southern California Earthquake Catalog
$SNDI$	Seismic Network Density Incompleteness
SOC	Self Organised Criticality
$STAI$	Short Term Aftershock Incompleteness

Chapter 1

Introduction

1.1 Statistical Seismology

Seismology is the study of the generation, propagation, and recording of elastic waves in the Earth (and other celestial bodies) and of the sources that produce them (*Lay and Wallace*, 1995). The term Statistical Seismology was introduced by Keiiti Aki in his work *Aki and Furumoto* (1956). The connection between seismology and statistics is discussed in *Vere-Jones and Smith* (1981); *Vere-Jones* (2006) where aspects such as epicentre location, velocity modelling, the interpretation of seismograms, the analysis of building response and its uses in earthquake-resistant design and the assessment of risk from seismic and other geophysical events have been identified as challenges that seismology posed to statistics.

The study of earthquakes with statistics is performed with the use of stochastic (random) models that describe the seismogenic process. The advantage of statistical models over the physical models, e.g. Coulomb stress modelling, is that statistical models don't seek to understand the process fully, and by replacing unknown aspects of the process with random processes allow for quantification of the uncertainties (*Vere-Jones*, 2010). As pointed in *Jeffreys* (1998) and discussed in *Vere-Jones*

(2010) stochastic does not mean without physical meaning. Every physical model should be able to predict the associated uncertainties, in other words *Jeffreys* (1998) argues that every physical model should be based on a stochastic model.

The Milne-Shaw seismograph was the first that was able to provide reliable measurements and therefore marked the beginnings of seismology as a quantitative science (*Vere-Jones*, 2000). During that early period of statistical seismology, in 1894, Fusakichi Omori in his work *Omori* (1894), developed the first empirical law of seismology to describe the decay of aftershocks with time after a mainshock. Omori's law was modified in 1961 by Utsu (*Utsu*, 1961). Utsu added the parameter p which describes the rate of which the aftershocks decay over time. This modification is most commonly used today as it yields a good fit to the data. Another major contribution in statistical seismology is the formulation of the Gutenberg-Richter (G-R) law (*Gutenberg and Richter*, 1944), which describes the relation between the number of earthquakes with their magnitudes in a given region.

In statistical seismology there are three fundamental empirical laws that describe seismicity. These are:

(i) The Gutenberg-Richter law.

The Gutenberg-Richter (G-R) law (*Ishimoto and Iida*, 1939; *Gutenberg and Richter*, 1944) describes the exponential distribution of earthquake magnitudes. The G-R law is given by equation 1.1.0.1 where N(m) is the number of earthquakes with magnitude greater than or equal to m_t, α and b also known as b value are the ordinate intercept and slope, respectively, of the line that relates m_t and log_{10}N(m).

$$\log_{10} N(m) = \alpha - b(m - m_t) \tag{1.1.0.1}$$

The parameter α is the logarithm of the total number of earthquakes above the threshold magnitude M and is a constant that depends on the seismicity rate and the length of the observation time (*Nava et al.*, 2016). The b value describes the relation between small and large earthquakes and is usually close to 1 (*Kagan*, 2013). Studies such as *Scholz* (1968a) has shown the connection of the b value with the level of stress when studying rock deformation in the laboratory and studies of the b value on different faulting regimes such as *Schorlemmer et al.* (2005); *Gulia and Wiemer* (2010) showed that the b value depends inversely on differential stress. The relation of the b value with the differential stress thus provides a physical explanation of the G-R law.

The G-R law corresponds to a power law in terms of the energies which is a typical sign of scale-invariance (*Main*, 1996; *Turcotte*, 1997) and it has been shown to hold for magnitudes as small as -4.4 (*Kwiatek et al.*, 2010). The validity of the G-R law has also been established experimentally e.g. *Mogi* (1963); *Scholz* (1968b); *Lockner* (1993) in acoustic emissions (AE's) that are used as a proxy for studying earthquakes in the lab [see chapter 3 for more details].

(ii) Omori's law and the modified Omori law.

Omori's law (*Omori*, 1894) describes the decay rate of aftershocks after a large earthquake as equation 1.1.0.2, K and c are coefficients, t is the time since the mainshock and n(t) is the aftershock frequency. Despite its empirical nature; Omori's law captures the temporal clustering of earthquakes observed in nature.

$$n(t) = \frac{K}{t + c} \tag{1.1.0.2}$$

The Omori law was modified by Utsu (*Utsu*, 1961) by adding an additional parameter (p) which describes the rate of aftershock decay. The modified Omori law is given by equation 1.1.0.3:

$$n(t) = \frac{K}{(t+c)^p} \tag{1.1.0.3}$$

The c value is usually less than 1 day, and it is thought to be related to changes in the detection level of the operating seismic network and short term aftershock incompleteness (STAI) (*Kagan*, 2004; *Shcherbakov et al.*, 2004; *Hainzl and Marsan*, 2008). In *Enescu et al.* (2009) small c values are calculated and is shown that c values larger than a few minutes are a result of STAI. *Kagan and Houston* (2005) reach the same conclusion and show that the c value that originates from Omori's law in equation 1.1.0.2 shouldn't have positive values since that would mean the singularity in equation 1.1.0.2 occurs before the mainshock. In addition the dependence of the c value on the threshold magnitude (*Shcherbakov et al.*, 2004; *Ogata*, 1998; *Ogata and Zhuang*, 2006) demonstrates the non physical significance of the c value. In Figure 1.1 below, the results of *Kagan and Houston* (2005) are presented. In *Narteau et al.* (2009) a dependence of the c value with the underlying stress suggests physical interpretation. The work of *Davidsen et al.* (2015) also provided evidence of a physical meaning of the c value based on its dependence on the threshold magnitude.

The existence or lack of physical meaning to the c value is currently an open question to statistical seismology.

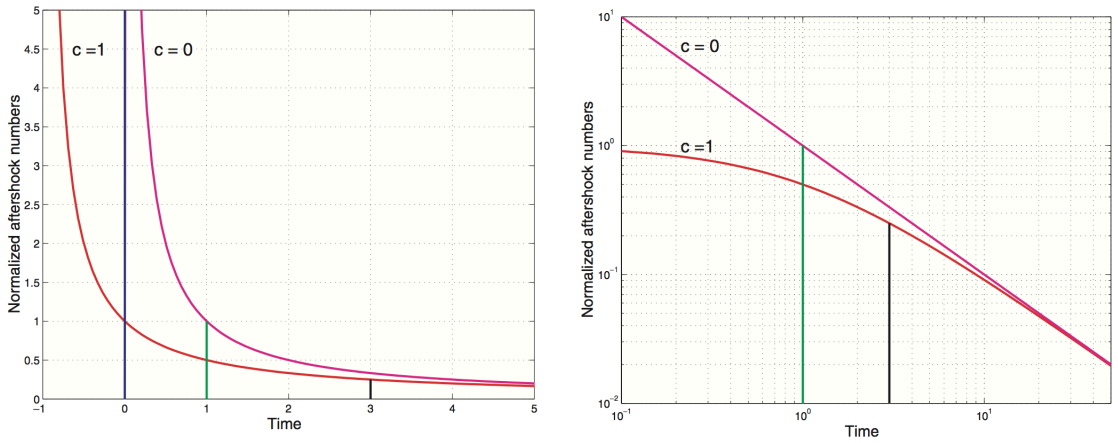

Figure 1.1: A positive c > 0 in Omori's law means that the singularity in aftershock rate occurs at negative time (t < 0), that is, before the mainshock. We show Omori laws with c = 1 and c =0 here in linear scale and in log-log scale. In statistical analyses of earthquake catalogues, events before the green or black lines may be removed to ensure completeness of aftershock accounting (*Kagan*, 2004). Positive c would fit a relative lack of early aftershocks (either real or apparent), but trends toward a singularity before the mainshock initiation. They propose that the positive empirical value for c is mostly due to the under-reporting of small aftershocks immediately following a mainshock. Figures and caption obtained by *Kagan and Houston* (2005).

(iii) The productivity law.

The aftershock productivity law relates the rate of aftershocks triggered by a mainshock to its magnitude. *Ogata* (1989) showed that the total number of aftershocks is proportional to the exponential function of the magnitude of the main shock as follows:

$$N \propto \exp\{\beta M\} \tag{1.1.0.4}$$

Larger magnitude mainshocks produce larger number of aftershocks, however the magnitudes of these aftershocks are independent.

Despite their empirical nature, the Omori law and the G-R law capture features of seismicity such as temporal and spatial clustering, and have been implemented in statistical models developed to describe the occurrence of earthquakes e.g. *Gerstenberger et al.* (2005); *Reasenberg and Jones* (1989); *Ogata* (1988, 1998); *Rhoades and Evison* (2004); *Turcotte et al.* (2007). One such model is the Epidemic Type After-

shock Sequence (ETAS) model developed by Ogata (*Ogata*, 1988, 1998) in which every earthquake can simultaneously be a foreshock, a mainshock and an aftershock and is generated either by a background or a triggered process. A fundamental assumption of the ETAS model is that the magnitudes of each earthquake are independent and identically distributed, i.e. that there are no magnitude correlations. Specifically for ETAS, the magnitude of each earthquake is assumed to be an independent draw from the G-R distribution with a fixed b value. This assumption suggests that the magnitude of earthquakes is unpredictable.

1.2 Motivation and research questions

The assumption of the independence of earthquake magnitudes has been questioned over the last 10 years in research in statistical seismology. Different approaches have been developed by *Lippiello et al.* (2013); *Sarlis* (2011); *Lennartz et al.* (2011); *Nichols and Schoenberg* (2014) to study magnitude correlations between successive earthquakes and between mainshock-aftershock sequences in regional and global catalogs. Studies by *Lippiello et al.* (2008, 2012) suggest that magnitude correlations exist between successive earthquakes in Southern California. *Davidsen and Green* (2011) and *Sarlis* (2011) deny their existence. The key controversy is the quality of the earthquake catalog data used to search for such magnitude correlations. *Davidsen and Green* (2011) claim that earthquake correlations are purely an artefact of an earthquake catalog being incomplete. This makes the study of this aspect of statistical seismology extremely challenging, because the different approaches proposed to treat catalog incompleteness give different results, as well as being controversial, not least because of the implications for earthquake forecasting, which is in itself highly contested. In addition to these studies which directly look for magnitude correlations, there has been increased interest recently in the subject of Short Term Aftershock Incompleteness (STAI). STAI is the main cause of bias in the statistical

analysis of earthquake catalogs. The study of STAI has indirectly contributed to the field of research and is therefore addressed in this thesis. As introduced above, laboratory experiments where AE have been monitored as proxies for earthquakes, have been employed to elucidate the mechanics of earthquakes and the Earth?s crust. But the same issues arise as to the quality of the AE catalogs produced from these experiments when scaling from the laboratory to the crustal scale. In statistics, it is often questioned whether the complexity of the models is always necessary (*Rogers*, 1995). In some cases it has been shown that simple models can perform as well as their more complex counterparts. An example of this in earthquake statistics is the use of the ETAS model. The ETAS model has been the most widely used statistical model in seismology over the last 30 years. A simpler model is the compound Poisson model. The compound Poisson model has been employed a small number of times in the literature (e.g., *Özel and Inal* (2008); *Aktas et al.* (2009); *Özel* (2011)). Despite its simplicity this model performed well in forecasting earthquakes in Turkey. For this reason it is chosen to be compared with the ETAS model in this thesis. This thesis addresses the fundamental research question of the existence or not of correlations in earthquake magnitudes or magnitude clustering. The existence of magnitude correlations would not only leave the possibility of earthquake prediction open but importantly magnitude correlation could be implemented in seismic forecasting models and seismic hazard assessments in order to provide more better forecasts and assessments. But the answer is not straightforward and the subject is considered controversial. A second, related question is whether or not any magnitude clustering scales from the laboratory to the crustal scale. The third question this thesis addresses is the STAI of catalogs. From these research questions, comes the central hypotheses that this thesis seeks to test: earthquake magnitudes are correlated and they are correlated at different scales.

1.3 Aim of the thesis

The principal aim of this is thesis is to address the existence of earthquake magnitude correlations. To achieve this aim the following is necessary: Firstly to understand the different approaches to study earthquake magnitude correlations and why these produce such diametrically opposed results and determine the key factors that limit their performance. Secondly, to develop a new methodology that addresses the limitations identified. Thirdly, apply the methodology to earthquake catalogs to test the hypothesis that earthquake magnitudes are correlated. Finally, apply the methodology to laboratory experimental data to test the hypothesis that magnitudes are correlated at different scales.

The second aim of this thesis is to test the performance of the Bayesian ETAS model and a compound Poisson model in their forecasting capabilities as a comparison between a complex and a simple model.

1.4 Objectives

The fundamental research question of this thesis is to address the question of the existence or not of earthquake magnitude correlations. The main objectives of this thesis are formulated based on this research question and are outlined below:

1. Study the existing methodologies on earthquake magnitude correlations and identify their strengths and limitations.
2. Develop a new methodology for earthquake magnitude correlations that is robust to the limitations identified and that is more robust to STAI to account for both temporal and rate variations of the magnitude of completeness.
3. Apply the proposed new methodology on magnitude correlations to earthquake catalog data. Answer the question if the results support the hypothesis of the existence of magnitude correlations.
4. Plan and perform triaxial rock deformation experiments while recording acoustic emission (AE) in the UCL Rock and Ice Physics Laboratory.
5. Apply the proposed new methodology on magnitude correlations to the AE data. Interpret the results in terms of fracture mechanics and establishing the dependence on experimental conditions. Answer the question if the results from the experiments support the hypothesis of the existence of magnitude correlations and hence scaling from the laboratory to the crust.

Additional objectives based on the comparison of the Bayesian ETAS and the compound Poisson model in forecasting are:

1. Study the existing literature on earthquake forecasting with these two models.
2. Perform earthquake forecasting (point estimates) in California and compare the models. Answer the question if the simple compound Poisson model performs on an equal basis with the more advanced ETAS model.

1.5 Thesis layout

Chapter 2 consists of the literature review. The chapter includes the description and review of the ETAS model which is the model used throughout the thesis as well as other statistical models used in seismology. Other approaches to study earthquakes such as the physical models are discussed briefly. The topic of earthquake catalogs which are the source of data for any statistical earthquake analysis is presented. For the analysis to be valid the quality of the data has to be assessed. Topics such as the magnitude of completeness, declustering (i.e., the separation of earthquakes into mainshocks and aftershocks) and the problems that earthquake catalogs introduce to a statistical analysis are discussed here. These are key concepts that will be used throughout the thesis. Following the background material the concept of magnitude correlations is examined by providing an overview of the existing work. In this chapter short term earthquake prediction and long term seismic hazard analysis techniques are also presented and it is discussed how the methodology proposed in this thesis fits into these frameworks. An introduction to the theory of rock mechanics and deformation in the lab is also included in the chapter. In Chapter 3 the new methodology proposed to study magnitude correlations is described along with applications to Southern California and the Parkfield region in Northern California. The existence of correlations is confirmed and the next step is to apply this method to a variety of faulting types. The rational behind this is the dependance of the b value on the the different types of faulting *Schorlemmer et al.* (2005); *Gulia and Wiemer* (2010). The stability of the b value in the region under study to avoid bias in the results is an important aspect of the methodology. In this chapter the proposed methodology is compared with the stochastic declustering methodology of *Nichols and Schoenberg* (2014). In Chapter 4, the laboratory experimental procedure from the preparation of the rock samples to deformation is presented. In Chapter 5 the proposed methodology for studying magnitude correlations is applied to the AE data from fracturing and the results are interpreted in terms of fracture mechanics.

The recording of the AE, the analysis and calibrations that are needed are also included in this chapter. In Chapter 6, a comparison of the Bayesian ETAS model and the compound Poisson model in their forecasting capabilities is performed. The description of the Bayesian ETAS and compound Poisson models is included in this chapter and the results of the forecasting in California is discussed. Chapter 7 is the final chapter of this thesis. Here, the conclusions of this thesis are given along with a discussion of implications of the results and future work.

1.6 Research output

1.6.1 Papers

K. Stavrianaki, G. J. Ross and P. Sammonds (2017), Are earthquake magnitudes correlated? Study cases in California. Bulletin of the Seismological Society of America. (Under review)

1.6.2 Conference Talks

K. Stavrianaki, G. J. Ross and P. Sammonds (2015), Are Earthquakes Predictable? A Study on Magnitude Correlations in Earthquake Catalog and Experimental Data. AGU Fall Meeting, San Francisco

1.6.3 Conference Posters

K. Stavrianaki, P. Sammonds and G. J. Ross (2016), An experimental view on earthquake magnitude correlations. IUGG Conference on mathematical geophysics, Paris

K. Stavrianaki, F. Vallianatos, P. Sammonds and G. J. Ross (2014), An experimental approach to non - extensive statistical physics and Epidemic type aftershock sequence (ETAS) modeling. The case of triaxially deformed sandstones using acoustic emissions. AGU Fall Meeting, San Francisco

1.6.4 Collaborative work

D. Pohoryles, J. Melo, T. Rossetto, M. Fabian, C. McCague, K. Stavrianaki, B. Lishman and B. Sargeant (2016). Use of DIC and AE for monitoring effective strain

and debonding in FRP and FRCM retrofitted RC beams. Journal of Composites for Construction: 04016057.

This publication is a result of an independent project I undertook during my PhD where my role was to assist in the processing and the interpretation of AE data produced from laboratory experiments in FRP and FRCM retrofitted RC beams.

During my PhD I was also involved with a project studying the rheology of serpentinites under the supervision of Dr S. Kirby. The rheology of serpentine is key for understanding the nucleation and propagation of earthquakes, and the relative weakness of serpentinite can significantly affect geodynamic processes at tectonic plate boundaries (*Hirth and Guillot*, 2013). For this project I was invited by Dr S. Kirby to the United States Geological Survey (USGS) to perform complex experiments in the lab of Dr D. Lockner and Dr D. Moore. The results indicated the need of further experiments in different conditions. The planning, execution and interpretation of this future work far exceeded the time I could allocate to a separate of my PhD project and unfortunately this marked the end of my involvement with this project.

Chapter 2

Literature Review

2.1 Chapter outline

In Chapter 1 the importance of statistical seismology in the study of earthquakes is introduced. This chapter reviews the state-of-the-art approaches to modelling the clustering of earthquakes. Although the focus of this thesis is on statistical modelling, the physical models of stress transfer, earthquake triggering and and fault slip are briefly introduced. The advantages of the Epidemic-type Aftershock (ETAS) model are reviewed and a detailed description of the ETAS model to give an explanation as to why this model is chosen for the analysis of earthquake magnitude correlations in this thesis. The quality of earthquake catalogs as a source of data is then reviewed. Topics such as the magnitude of completeness, declustering (i.e., the separation of earthquakes into mainshocks and aftershocks) and the problems that the use of earthquake catalogs introduce into statistical analyses are discussed. There follows a short review of existing methodologies for determining magnitude correlations. Finally, the theory of rock mechanics and deformation is introduced as this will be drawn on in discussing the physics of correlation phenomena later in the thesis.

2.2 Physical Models

From a statistical perspective, earthquakes can be described as points in space and time; however from a physical perspective, earthquake generation is the result of stress build-up within the brittle crust that leads to rupturing usually pre-existing faults in the crust. Absolute stresses magnitudes are difficult to measure in the crust, however the stress changes induced by earthquakes can be calculated (*Hainzl et al.*, 2010). The Coulomb stress model is the state-of-the-art approach to modelling physically the transfer of stress within the crust following an earthquake and the potential for triggering further earthquakes (*King et al.*, 1994). Many papers have been published on the Coulomb stress transfer principle. Stress changes are quantified by the Coulomb failure function ΔCFF given in equation 2.2.0.1:

$$\Delta CFF = \Delta\tau + \mu(\Delta\sigma_n + \Delta p) \tag{2.2.0.1}$$

where $\Delta\tau$ is the shear stress in the direction of slip, $\Delta\sigma_n$ is the normal stress changes (positive for unclamping or extension), μ is the friction coefficient and Δp is the pore pressure change. Displacements in the elastic upper crust produces a tensorial stress perturbation that can then be resolved into shear and normal components on target (or receiver) faults; an increase in shear stress in the slip direction and a decrease in normal stress, increase the likelihood of future fault rupture (*Hainzl et al.*, 2010). Based in the theory of elasticity, it has been shown qualitatively that an increase in the Coulomb stress for a given region is usually associated with an increase of seismic activity (*Console et al.*, 2006). While the rate-and-state theory of fault fictional slip developed by *Dieterich* (1994) has been able to give a physical justification to the phenomenon known as Omori aftershock decay law (*Console et al.*, 2006).

Hainzl et al. (2010) summarise the input information and related uncertainties. All applications of the stress-triggering model rely on the correct determination

of the relevant stress changes. However, the stress calculation can lead to large uncertainties such as:

1. The unknown distribution of receiver faults.
2. The non-unique inversion results for the slip-models and mainshock fault geometry and extent.
3. Uncalculable small scale slip variability which can lead to strong stress heterogeneities close to the source fault.
4. Spatial inhomogeneity of material and pre-stress conditions.

So although physical models have great value in elucidating earthquake mechanics, the uncertainties are large, which necessitates statistical approaches. The study of magnitude correlations has been done in this thesis and in the literature, using statistical models only. In this thesis the existence of magnitude correlations is demonstrated in a statistically significant way. But like every model, statistical models have their limitations: one of which is the difficulty to attribute the corresponding outcome to underlying physical processes.

Physical and statistical models can be linked through the Gutenberg-Richter (G-R) b value. deformation was the first to report the dependency of the b value on the level of stress when studying rock deformation in the laboratory. Since then a number of studies demonstrated this dependency and the temporal variations of the b value in laboratory studies (e.g., (*Sammonds et al.*, 1992; *Main et al.*, 1992; *Sammonds and Ohnaka*, 1998) and studies on earthquake data (e.g., (*Schorlemmer et al.*, 2005; *Gulia and Wiemer*, 2010). The b value is also linked with fractal statistics (e.g., *Huang and Turcotte* (1988)) where it shown that the b value is inversely proportional to stress and proportional to the fractal dimension of the stress - strength distribution. Fractal statistics are incorporated into the Self Organised Criticality (SOC) models introduced by *Bak et al.* (1987, 1988). Self Organised Criticality refers to a property of dynamical systems to organise spatially and/or temporally in a scale free man-

ner (*Caruso and Kantz*, 2011). Such systems organise themselves into the critical behaviour. The variations of the b value will be analytically discussed on Chapter 3.

An attempt to give physical meaning to earthquake magnitude correlations is by using an experimental approach. The monitoring of AE and their use as proxies for earthquakes provide an insight on the fracturing process which is in turn related to stress changes and the variations of the b value. In this thesis it is demonstrated that magnitude correlations depend on the fracture process that corresponds to different types of experiments and therefore the faulting type it likely to be one of the control factors of magnitude correlations. So fracture mechanics is briefly introduced at the end of this chapter.

2.3 Statistical Models

Some of the most commonly used statistical models are presented in this section. The Epidemic Type Aftershock Sequence model which is used for the analysis of seismicity in this thesis is described in a separate section.

2.3.1 Every Earthquake is a Precursor According to Scale (EEPAS) model

The Every Earthquake is a Precursor According to Scale (EEPAS) was formulated by *Evison and Rhoades* (1997, 1999) based on observations of precursory swarms in New Zealand and Greece. The model was later extended by *Rhoades and Evison* (2004) and uses smaller earthquakes as precursors to forecast larger ones. It is based on the precursory scale increase (Ψ) phenomenon, which corresponds to a long-term precursory increase of seismicity at similar magnitudes to the eventual aftershocks (*Rhoades*, 2007, 2010). The EEPAS models classifies earthquakes into

three categories; mainshocks, swarms and multiplets. The initial hypothesis of the EEPAS model was a one to one relation of swarm activity and mainshock, multiplets were a third type of earthquakes that was considered neither predictable nor precursory (*Rhoades*, 2010). In the EEPAS model each earthquake contributes to the total occurrence rate density, with the scale of its contribution in time, magnitude and location being controlled by its magnitude (*Rhoades*, 2010). The contribution of each earthquake to the future rate density is given from equation 2.2.1.1, where each earthquake i has time t_i, magnitude m_i, location (x_i,y_i inside a surveillance area R, w_i is a weighting factor that may depend on other earthquakes in the vicinity and f_i, g_i, h_i are densities of the probability distributions for time, magnitude, and location respectively (*Rhoades*, 2007).

$$\lambda(t, m, x, y) = w_i f_{1i}(t) g_{1i}(m) h_{1i}(x, y) \tag{2.3.1.1}$$

The total rate density is calculated by summing over all past occurrences which could affect the rate density within R and is given by equation 2.3.1.2 where μ is a parameter, λ_0 is a baseline rate density, t_0 is the start time of the catalog and η is a normalised function (*Rhoades*, 2007).

$$\lambda_i(t, m, x, y) = \mu\lambda_0(t, m, x, y) + \sum_{\{t_i \geq t_0; m_i \geq m_0\}} \eta(m_i)\lambda_i(t, m, x, y) \tag{2.3.1.2}$$

2.3.2 Short-Term Earthquake Probability (STEP) model

STEP is a model developed by *Gerstenberger et al.* (2005) which combines historical earthquakes and fault data to produce a forecast of strong shaking probabilities. The G-R and Omori laws are implemented in this model which consists of a spatially varying Poisson background model to which more complex clustering models are added. The clustering model includes a generic clustering model, a sequence specific clustering model and a spatially heterogeneous model *Gerstenberger et al.*

(2005). The rate at time t is given by equation 2.3.2.1 according to *Reasenberg and Jones* (1989, 1994) where à, b, c and p are constants and M_m is the mainshock magnitude.

$$\lambda(t) = \frac{10^{\grave{a}+b(M_m-M)}}{(t+c)^p} \tag{2.3.2.1}$$

If a sufficient number of aftershocks is produced, the sequence specific model is then calculated using a posteriori values for the parameters of each event in the sequence (*Tiampo and Shcherbakov*, 2012). The spatially heterogeneous model is calculated at nodes where the minimum number of events to obtain a robust estimate of the parameters is met (*Gerstenberger et al.*, 2005). The expected rate of earthquake sources nearby, their magnitudes and distances from the site, propagation effects and local soil conditions at the site control the hazard earthquake shaking (*Gerstenberger et al.*, 2005).

2.3.3 Pattern Informatics (PI) index

The PI approach was introduced in the early 2000's by *Rundle et al.* (2000a,b, 2002, 2003) and *Tiampo et al.* (2000, 2002a,b) and optimised by *Holliday et al.* (2006) and *Tiampo et al.* (2006a,b). In this method anomalous activation patterns or quiescence are used as proxies for changes in the underlying stress that may precede large earthquakes (*Tiampo and Shcherbakov*, 2012). The PI index is calculated over a large area which is divided into a grid and over a long time period with a constant background rate which is equal to the α constant of the G-R law. The seismic activity rate $\psi_{obs}(x_i, t)$ is defined as the number of earthquakes above the threshold magnitude per unit time within a box that has center x_i at time t. The

time-averaged seismicity function is given by equation 2.3.3.1 over the interval (t - t_0)

$$S(x_i, t_0, t) = \frac{1}{(t - t_0)} \int_{t_0}^{t} \psi_{obs}(x_i, t) dt \tag{2.3.3.1}$$

S(x_i,t_0,t) is the i_{th} component of a time-dependent vector evolving in an N - dimensional space where N denotes the total number of locations. Denoting spatial averages over the N boxes by $< >$, the phase function $\hat{S}(x_i,t_0,t)$ is then defined to be the mean-zero, unit-norm function obtained from S and shown in equation 2.3.3.2 (*Tiampo et al.*, 2006b).

$$\hat{S}(x_i, t_0, t) = \frac{S(x_i, t_0, t) - < S(x_i, t_0, t) >}{||S(x_i, t_0, t)||} \tag{2.3.3.2}$$

In 2.3.3.2 the denominator is the square root of the variance (the standard deviation) over all spatial boxes (*Tiampo et al.*, 2006b). The change in the local rate of seismicity serves as measure of the stress change and is given by equation 2.3.3.3 (*Tiampo et al.*, 2002a).

$$\Delta\hat{S}(x_i, t_1, t_2) = \Delta\hat{S}(x_i, t_0, t_2) - \Delta\hat{S}(x_i, t_0, t_1) \tag{2.3.3.3}$$

The PI index at x_i between t_1 and t_2 is given by equation 2.3.3.4 where μ_p is the spatial mean of $\{\Delta\hat{S}(x_i, t_i, t_2)\}^2$.

$$\Delta P(x_i, t_i, t_2) = \{\Delta\hat{S}(x_i, t_i, t_2)\}^2 - \mu_p \tag{2.3.3.4}$$

2.4 Statistical models in short term earthquake prediction and long-term seismic hazard analysis and the role of magnitude clustering

In this thesis the existence of earthquake magnitude correlations is demonstrated with applications to California, Greece and experimental data. It shown that in periods of high seismicity the mean magnitude of earthquakes is increased and this increase can be translated into a variation in the b value. The variations of the b value due to magnitude correlations are not included in the models used to forecast seismicity. In contrast, variations of the b value in space and time have been studied extensively (e.g. *Wiemer and Wyss* (2002); *Schorlemmer et al.* (2005); *Wiemer and Schorlemmer* (2007)) and these variations have important implications for earthquake hazard because local and regional probabilistic seismic hazard assessment (PSHA) is commonly performed using the GR frequency magnitude distribution (*Field*, 2007; *Wiemer and Schorlemmer*, 2007; *Wiemer et al.*, 2009; *Tiampo and Shcherbakov*, 2012). In *Westerhaus et al.* (2002) lower b values are associated with increased seismic hazard. A decrease in the b value is also observed between the low and high intensity data in the proposed methodology. Implementing magnitude correlations into the statistical models that are used for forecasting would improve mostly short term forecasting since the proposed methodology does not incorporate a ground motion model for the estimation of ground shaking at the area under study that is one of the requirements for a seismic hazard analysis. The degree to which implementing magnitude correlations would improve forecasting and seismic hazard is an expansion of this thesis that will be addressed in future work.

2.5 The Epidemic Type Aftershock Sequence (ETAS) model

Earthquake occurrence can be described as a collection of points, where each point represents it's time and/or location. As such earthquakes can be modelled by a stochastic (random) point processes. In the case where each point has additional information information (these are called marks) then the process is called marked point process. A number of stochastic point process models for earthquake occurrence have been proposed e.g. (*Vere-Jones*, 1970; *Kagan*, 1973; *Ogata*, 1988, 1998). However, the multidimensional nature of earthquake occurrence and the properties of their statistical distributions constitute an inhibitory factor for the creation and statistical analysis of such models (*Kagan*, 2013).

The model used in this thesis is the Epidemic Type Aftershock Sequence (ETAS) model developed by Ogata in 1988. It is called epidemic due to the analogy of earthquake generation with the spread of a disease. One of the fundamental properties of ETAS is that each earthquake can be simultaneously a foreshock, a mainshock and an aftershock. The terms mainshock or aftershock are frequently used without a definition. Here I provide the definition of *Utsu* (1970): *It is often observed that a number of earthquakes occur in a group within a limited interval of time and space. The largest earthquake in such a series is called the mainshock, and smaller ones occurring before and after the mainshock are called foreshocks and aftershocks respectively.*

Mathematically the ETAS model is a special case of the marked Hawkes-type self-exciting process. The Hawkes process introduced by *Hawkes* (1971); *Hawkes and Oakes* (1974), is used in seismology applications because of it's ability to be represented twofold; as a cluster process where the clusters are generated by a certain branching structure and via a conditional intensity which gives the normalised prob-

ability that one event will occur in the next instant conditional on the history of the process so far.

The conditional intensity function $\lambda(t|H_t)$ of the ETAS model is shown in Equation 2.5.0.1 and gives the probability of an earthquake occurring in some small time interval $[t, t + \Delta_t]$ where H_t denotes the history of the earthquake catalog prior to t.

$$\lambda(t|H_t) = \mu + \sum_{\{i:S<t_i<t\}} \frac{K_0 e^{a(M_i - M_c)}}{(t - t_i + c)^p} \tag{2.5.0.1}$$

In the above equation, S is the starting time of the catalog, M_c is the catalog magnitude of completeness i.e. the magnitude above which all earthquakes are recorded by the seismic network, μ denotes the background rate, $t_1, \ldots, t_n$ are the occurrence times of the n earthquake which occurred between times S and t, and M_i is the magnitude of the earthquake that occurred at time t_i.

Like in any Hawkes process (*Daley and Vere-Jones*, 2003), the occurrence of an event (earthquake in the case of ETAS) makes the occurrence of additional events more probable due to the increase in the summation part of equation 2.5.0.1. The corresponding process of 2.5.0.1 is equivalent to a branching process where each point can be generated either as a background event or triggered by a specific previous earthquake.

The ETAS model parameters θ are (μ, K_0, α, c, p), where μ represents the rate of the poisson process that forms the arrival of the background earthquakes, the parameters K_0 and α determine the aftershock productivity, the exponent p is the rate of power-law decay over time. The factor c (days) is a scaling time to establish the power-law decay rate and allows a finite number of aftershocks at the origin time of a triggering earthquake (a mainshock).

The estimation of the ETAS parameters is obtained by maximum likelihood estimation (MLE) and in *Ogata* (1988) the non linear Fletcher and Powel technique is used. Likelihood is the probability of a model parameter value given an observation, and maximum likelihood is a method for estimating model parameter values based on maximising the likelihood (*Hawkes*). The log likelihood of the ETAS model is given in equation 2.5.0.2, where $\lambda(t_i;\theta)$ is the parameterised conditional intensity rate and t_i is the occurrence times of the earthquakes in the observed interval [0, T].

$$\log L(\theta) = \sum_{i=1}^{N} \log \lambda(t_i;\theta) - \int_0^T \lambda(t_i;\theta)\ dt \tag{2.5.0.2}$$

The evaluation of the calculated parameters likelihood score such as the Akaike Information Criterion (AIC). The AIC is defined as follows: $2p - 2L(\theta)$, where p is the number of fitted parameters. Lower AIC values correspond to better fit of the model.

2.5.1 ETAS model review

Point process modeling for earthquake occurrence have been developed since the 1960's and '70s by D. Vere - Jones (*Vere-Jones and Davies*, 1966; *Vere-Jones*, 1970). At the time the maximum likelihood estimation of the model parameters was acknowledged theoretically as a suitable method however was not fully feasible (*Ogata*, 1999). In *Ogata* (1988) the restricted trigger model is described in equation 2.5.1.1, where μ is the the background seismicity rate, τ_m the origin times of secondary aftershocks and $\sum_{\{\tau_m<t\}}$ is taken over the triggered events $\{m\}$ that occurred before t.

The triggering eventsτ_m are determined with the residual analysis method (*Ogata*, 1999).

$$\lambda(t|H_t) = \mu + \sum_{\{\tau_m<t\}} \frac{K_m}{(t-\tau_m+c_m)^{p_m}} \tag{2.5.1.1}$$

The original trigger model was proposed by *Vere-Jones and Davies* (1966) and Ogata extended this model (*Ogata*, 1986, 1988, 1989) to describe seismic occurrence in terms of the conditional intensity and proposed the ETAS model. The conditional intensity of the ETAS model is shown in equation 2.5.0.1. Epidemic models where used as early as 1949 to describe population growth in epidemiology (*Kendall*, 1949) but it was *Hawkes* (1971), who modelled these processes with a conditional intensity. Compared to the restricted trigger model, ETAS allows for mainshock and aftershock identification even in cases of swarms where this is inherently difficult (*Ogata*, 1999). *Ogata* (1986, 1988) compares the ETAS model with other alternatives by comparing the goodness of fit. In 1998 the ETAS model was extended from temporal to spatiotemporal model (*Ogata*, 1998). Since then, ETAS is the most widely used statistical model to describe seismic activity with applications to short and long term forecasting in regions worldwide (e.g. (*Console et al.*, 2006, 2007, 2010; *Falcone et al.*, 2010; *Helmstetter et al.*, 2005, 2006, 2007) and the only model used to study earthquake magnitude correlations.

2.6 Earthquake catalogs

Earthquake catalog data are provided from seismic networks and are the source of information to study earthquakes. An earthquake catalog typically contains information about the location, time, magnitude, depth and focal mechanism of the recorded earthquakes. The exact format of the catalog differs between networks of different countries and therefore this information is provided. In Fig-

ures 2.1 and 2.2, we see a typical example of an earthquake catalog and it's format which is provided in a separate file. In this thesis the data are provided from the Southern California Earthquake Data Center (SCEDC) and the National Observatory of Athens (NOA). SCEDC operates at the Seismological Laboratory at Caltech and is the primary archive of seismological data for southern California. The 1932-to-present Caltech/USGS catalog maintained by the SCEDC is the most complete archive of seismic data for any region in the United States (`http:/scedc.caltech.edu/about/index.html`). The National Observatory of Athens is the first research Institution created in Greece in 1842. The first seismograph was installed in the National observatory in 1898 however the seismographic network begin to operate in 1964 (*Chouliaras*, 2009). Since the earthquake catalog data are the only representation of the reality, ensuring the quality of the data is extremely important especially when performing statistical analysis. In this section, I will discuss common problems, properties and artifacts of earthquake catalogs that, if not addressed, introduce bias to the statistical analysis. These are:

1. Data from quarries or explosions.
2. Location errors and artifacts.
3. Magnitude errors.
4. Magnitude of completeness (M_c) estimation.

```
1981 01 01 01 49 29.040  3301561 33.73183 -118.82150 10.230 2.27 21 31  0.16  0  3     0     0  0.500  1.000 99.000 99.000 le 3d
1981 01 01 04 13 55.710  3301565 33.25524 -115.96763  5.664 2.26 45 17  0.21  1  4   260   460  0.300  0.800  0.003  0.003 le ct Poly5
1981 01 01 05 20 14.440  3301566 34.18598 -117.29747  6.519 2.37 52 13  0.17  1  4    92   153  0.100  0.200  0.007  0.006 le ct Poly3
1981 01 01 05 39 56.460  3301567 34.18433 -117.29610  6.621 1.60 29 12  0.17  1  4   372   146  0.200  0.300  0.008  0.004 le ct Poly3
1981 01 01 08 23 18.080  3301570 34.00635 -117.16198 15.480 1.88 42  7  0.17  1  4   372   146  0.200  0.300  0.007  0.004 le ct Poly3
1981 01 01 10 57 34.540  3301572 34.09381 -117.30494 16.351 1.40 22 10  0.12  1  4   378   120  0.200  0.300  0.012  0.017 le ct Poly3
1981 01 01 15 05 24.380  3301576 35.31200 -118.54933  8.980 2.16 18 20  0.18  0  3     0     0  0.100  0.400 99.000 99.000 le 3d
1981 01 01 17 45 59.030  3301578 33.50701 -116.76440  4.752 1.50 15 20  0.15  0  4   195   731  0.200  0.700  0.004  0.002 le ct Poly5
1981 01 01 22 49 35.240  3301586 35.31500 -118.50867  2.480 1.91 12 21  0.17  0  3     0     0  0.300  1.000 99.000 99.000 le 3d
1981 01 02 01 00 38.100  3301590 32.06967 -116.72617 11.410 1.77  6 67  0.10  0  3     0     0  1.100  1.400 99.000 99.000 le 3d
1981 01 02 02 45 54.020  3301591 37.46600 -118.73130  6.000 2.08  0  0  0.00  0  0    99     0 99.000 99.000 99.000 99.000 re xx
1981 01 02 04 11  7.790  3301593 37.48570 -118.73520  6.000 2.45  0  0  0.00  1  0    99     0 99.000 99.000 99.000 99.000 re xx
1981 01 02 04 17 22.610  3301594 34.78643 -118.94714 13.649 1.31 17 26  0.15  1  4  1277    50  0.300  0.900  0.040  0.138 le ct Poly2
1981 01 02 04 46 47.350  3301596 34.04934 -116.43421  9.122 1.71 40 10  0.17  1  4   459    42  0.100  0.300  0.021  0.016 le ct Poly4
1981 01 02 11 04 25.220  3301604 34.39383 -116.47066  6.270 1.40 14 14  0.09  1  3     0     0  0.200  0.400 99.000 99.000 le 3d
1981 01 02 15 03  9.120  3301609 36.04567 -118.27450 11.620 3.13 12 45  0.14  0  3     0     0  0.400  0.900 99.000 99.000 le 3d
1981 01 02 15 28 18.070  3301611 34.26888 -117.01283  5.642 0.92 32  2  0.18  0  4   232    81  0.100  0.100  0.048  0.028 le ct Poly3
1981 01 02 16 45 32.750  3301616 36.04217 -118.27567  0.030 2.59 10 45  0.11  0  3     0     0  0.300  1.200 99.000 99.000 le 3d
1981 01 02 17 17 17.040  3301618 32.38667 -115.18650  4.410 1.90 11 32  0.25  0  3     0     0  2.000  3.500 99.000 99.000 le 3d
1981 01 02 18 54 12.730  3301624 33.03616 -116.40073  6.989 1.69 17 19  0.21  0  4   356    36  0.300  1.100  0.038  0.022 le ct Poly5
1981 01 03 23 53 33.050  3301631 34.10168 -117.20319  6.894 1.45 22  5  0.14  0  4   107    52  0.300  0.400  0.091  0.464 le ct Poly3
1981 01 04 03 56 50.180  3301634 34.26730 -117.01370  5.880 1.10 10  2  0.05  1  4   232    81  0.300  0.400 99.000 99.000 le ct Poly3
1981 01 04 07 11 34.920 12160459 33.53387 -116.79005  3.598 1.00  9 17  0.11  1  4   223   658  0.300  2.500  0.010  0.010 le ct Poly5
1981 01 04 07 11 39.410  3301635 33.53407 -116.79020  3.629 1.44 39 18  0.24  1  4   223   658  0.200  0.600  0.008  0.003 le ct Poly5
1981 01 04 08 07  1.930  3301637 34.36767 -120.80400 11.480 2.30  8 44  0.10  1  3     0     0  1.500  1.100 99.000 99.000 le 3d
1981 01 04 09 14 52.860  3301638 37.46620 -118.79330  0.010 1.92  0  0 99.00  1  0     0     0 99.000 99.000 99.000 99.000 re xx
1981 01 04 09 21 32.270  3301639 32.14817 -115.78200 21.190 2.77 17 51  0.27  1  3     0     0  0.000  2.400 99.000 99.000 le 3d
1981 01 04 13 08 11.190  3301641 33.87099 -116.31469  4.819 1.77 38 14  0.17  1  4   214    12  0.300  0.300  0.210  0.033 le ct Poly4
1981 01 04 13 19 46.560  3301642 34.39650 -116.47150  7.730 1.46 34 14  0.11  1  3     0     0  0.100  0.300 99.000 99.000 le 3d
1981 01 04 13 32 28.560  3301643 37.43900 -118.26220  6.000 1.90  0  0 99.00  1  0     0     0 99.000 99.000 99.000 99.000 re xx
1981 01 04 15 42 10.590  3301645 34.01285 -116.71931 14.462 2.21 50  6  0.14  0  4   270   240  0.100  0.200  0.023  0.016 le ct Poly3
1981 01 04 21 31  2.250  3301648 33.25436 -115.96783  5.390 1.70 25 16  0.20  0  4   260   460  0.400  1.100  0.004  0.004 le ct Poly5
1981 01 04 22 14  0.280  3301650 34.00647 -116.61151 15.594 1.50 25  4  0.10  0  4   200   271  0.100  0.100  0.057  0.034 le ct Poly3
1981 01 04 22 31 37.850  3301651 32.93601 -116.29317  9.993 1.80 14 31  0.21  0  4   236    51  0.300  1.200  0.003  0.005 le ct Poly5
1981 01 06 08 58 42.970  3301665 34.31875 -117.10818  5.212 1.50 27 10  0.20  1  4   113   129  0.100  0.200  0.014  0.021 le ct Poly3
1981 01 06 10 07 59.090  3301667 34.79016 -120.31300  4.910 1.40  6 21  0.07  1  3     0     0  0.200  2.400 99.000 99.000 le 3d
1981 01 06 10 34 51.930  3301668 34.31861 -117.10838  5.296 0.80  7 10  0.05  1  4   113   129  1.200  0.800  0.006  0.010 le ct Poly3
1981 01 07 19 03 39.040  3301692 33.99308 -117.19811 12.207 1.85 40 10  0.13  0  4   629    32  0.100  0.200  0.006  0.007 le ct Poly3
1981 01 07 20 03 17.930  3301698 33.00714 -116.20737  5.085 1.65 17 26  0.26  0  4   287    88  0.700  1.800  0.003  0.004 le ct Poly5
1981 01 07 22 00  3.930  3301718 33.49781 -116.77121  4.064 1.75 37 17  0.23  0  4   195   731  0.100  0.500  0.002  0.002 le ct Poly5
1981 01 07 23 25 30.380  3301728 34.50134 -118.05850 10.650 1.00  9  3  0.07  0  3     0     0  1.000  0.500 99.000 99.000 le 3d
1981 01 07 23 34 54.730  3301730 37.43950 -118.89133  9.760 2.24  5 72  0.14  0  0     0     0  8.300  9.600 99.000 99.000 re 1d
1981 01 08 02 51 24.350  3301740 33.76608 -115.68285  4.032 1.54 21 20  0.15  0  4   327    31  0.200  0.800  0.052  0.080 le ct Poly4
1981 01 08 03 51 56.210  3301746 34.20967 -116.44183  3.410 1.20  9 12  0.13  1  3     0     0  0.500  0.700 99.000 99.000 le 3d
```

Figure 2.1: Screenshot of the *Hauksson et al.* (2012) earthquake catalog of Southern California.

```
LOCATION FILE  FORMAT DESCRIPTION
The locations are in the following custom format with 146 character lines:

1981 01 01 04 13 55.710   3301565 33.25524 -115.96763   5.664  2.26  45  17   0.21   1   4   260   460      76   0.300   0.800   0.003   0.003  le ct Poly5
where
      1981 = year
         1 = month
         1 = day
         4 = hour
        13 = minute
    55.710 = second

   3301565 = SCSN cuspid (up to 9 digits)

  33.25524 = latitude
-115.96763 = longitude
     5.664 = depth (km)
      2.26 = SCSN calculated preferred magnitude (0.0 if unassigned)

        45 = number of P and S picks used for 1D SSST or 3D location (different from old format)
        17 =  to nearest statino in km (different from old format)
      0.21 = rms residual (s) for 1D location; value of 99.0 indicates information not available

         1 = local day/night flag (=0 for day, =1 for night in Calif.)

         4 = location method flag (=1 for SCSN catalog or 1d hypoinverse relocation,
                =2 for 1D SSST,  =3 for 3D, =4 for waveform cross-correlation)
             Superseeded by flag below
       260 = similar event cluster identification number (0 if the event is not relocated with waveform cross-correlation data)

       460 = number of events in similar event cluster (0 if the event is not in similar event clusters)

      76 = number of differential times used to locate this event

     0.300 = est. std. error (km) in absolute horz. position
     0.800 = est. std. error (km) in absolute depth
     0.003 = est. std. error (km) in horz. position relative to other events in cluster
     0.003 = est. std. error (km) in depth relative to other events in cluster

        le = SCSN flag for event type (le=local, qb=quarry, re=regional)
        ct = for location method (ct=cross-correlation; 3d=3d velocity model; xx= not relocated, SCSN location used)
     Poly5= the polygon where the earthquake is located.  We used 5 polygons to
            generate this catlog.
```

Figure 2.2: Format of the *Hauksson et al.* (2012) earthquake catalog of Southern California.

2.6.1 Data from quarries or explosions (Artificial events)

Quarry blasts and other non - tectonic events are sometimes included in earthquake catalogs contaminating the data. Network operators typically remove such events, however, artificial events have been reported near Istanbul, in Alaska, Switzerland and western USA (*Gulia et al.*, 2012, and references therein). Artificial events are of small magnitude, but a plethora of small events can be misinterpreted as an increase in the seismicity rate. Artificial earthquakes can also lead to increased b values due to the increase of the smaller magnitudes and bias studies on earthquake quiescence (*Wiemer and Baer*, 2000). One way to avoid these errors when processing earthquake catalog data is with the use of an appropriate cut off magnitude, however this solution is not optimal since it can also lead to loss of natural earthquake data. Quarry and mine blasts are usually performed during daytime, therefore plotting the number of earthquakes vs the hour of day would produce a peak during the daytime hours if the data are contaminated. *Wiemer and Baer* (2000) proposed an algorithm to identify these events based on a purely statistical criterion. The day to night normalised ratio proposed by *Wiemer and Baer* (2000) is defined by equation 2.6.1.1, where Nd is the total number of events in the daytime, Nn in the night-time period, Ld is the number of hours in the daytime period and Ln in the night-time period (Ln + Ld = 24). The ratio is calculated using a regularly spaced grid covering the area studied and sampling only the N (N = Nd + Nn) closest epicenters to each node.

$$Rq = \frac{NdLn}{NnLd} \tag{2.6.1.1}$$

One of the limitations of this method is that natural events near the nodes with high Rq value (i.e. those that will be removed); will also be removed. The work of *Gulia* (2010) suggests removing events above a fixed threshold magnitude and removing

aftershocks via a process called declustering as a solution to the *Wiemer and Baer* (2000) algorithm.

2.6.2 Earthquake location errors

Earthquake location is determined using a given velocity model for P (longitudinal) and S (shear) seismic waves and therefore an accurate velocity model is crucial to the quality of the earthquake location. A systematic error may be introduced from the lateral variations of the velocity since the seismic networks usually use 1D velocity models (3D models are used less frequently used). To improve the existent velocity models calibration is performed by locating events with known parameters such as mine blasts and quarry blasts or by dividing the network area to smaller regions with different 1D models (*Woessner et al.*, 2010). Given a velocity model, the earthquake location algorithm makes predictions of the arrival times of the P and S waves which are then compared to the observed arrival times. The location with the smallest differences between predicted and observed times correspond to the hypocenter location. Errors can also be introduced to the arrival times that depend on the timing of the recorded waveforms. This error typically affects older recordings where GPS receivers where not available.

Earthquake location can be determined with the use of linear as well as non linear methods. Linear methods use partial derivatives and matrix inversion and non linear by sampling either the entire or only parts of the solution space. Linear methods are computationally faster than the non linear however their performance depends on the quality of the initial guess. Non linear models do not rely on the initial guess and provide a solution that includes uncertainties (*Husen and Hardebeck*, 2010).

Earthquake location errors can be classified based on the following criteria (*Pavlis*, 1986):

1. Measurement errors of seismic arrival times.

2. Modeling errors of calculated travel times.

3. Non linearity of the earthquake location problem.

2.6.3 Magnitude errors

With the term magnitude errors we refer to changes in the type of magnitude (e.g. Local magnitude, Moment magnitude) that is provided or to changes in the algorithms used to estimate the magnitudes. These inconsistencies can make an earthquake catalog inhomogeneous. In *Werner and Sornette* (2008) it is shown how uncertainties in the magnitudes can propagate to seismic rate estimates and forecasts. Additionally, magnitude uncertainties can lead to deviations from the G-R law, which has an impact on M_c estimates *Mignan et al.* (2011). The catalogs used in the thesis are the Waveform Relocated Earthquake Catalog for Southern California (1981 to 2011) (*Hauksson et al.*, 2012), for Parkfield earthquakes within (35.5N - 36.5N, 121W - 120W) during the years 2004 and 2005 which were provided by the Northern California Earthquake Data Center and finally the Corinth dataset contained earthquakes within (37.80N - 38.44N, 21.2E - 22.1E) from 1/1/2011 - 13/6/2016 obtained from the National Observatory of Athens (Institute of Geodynamics). For Corinth and Parkfield the reported magnitudes are M_L and the study period is small (5 and 2 years respectively) in order to minimise biases from magnitude errors. The Southern California catalog spans over a 30 year period during which the seismic network has seen changes in the algorithms used and the density of the network. The catalog by *Hauksson et al.* (2012) provides high quality relocated data. Additionally in 2008 in order to ensure consistency in the Southern California Earthquake Catalog, recalibration of the local magnitudes for events between January 1, 1992 to January 1, 2008 begun. Larger earthquakes are reported in the M_w scale. It has been shown that converting magnitudes from one magnitude scale to another can also introduce biases in the statistical analysis therefore the final cata-

log contained both Local and moment magnitudes. The choice of Parkfield, Corinth and the aftershock sequence where the magnitudes are consistent indicates that the observed correlations are not an effect of magnitude errors.

2.7 Magnitude of completeness M_c

The magnitude of completeness M_c is defined as the lowest magnitude at which all of the earthquakes in an earthquake catalog are detected (*Rydelek and Sacks*, 1989). The reasons of magnitude incompleteness can be (*Mignan*, 2012):

1. The signal is so small that it can not be separated from the background noise.
2. The earthquake is so small, that is not detected by a sufficient number of seismic stations to be recorded.
3. Network operators decided that events below a certain threshold are not of interest.
4. Some events are too small to be detected within the coda of larger events (i.e. increased noise).

M_c is often estimated as the magnitude where the frequency-magnitude distribution (FMD) departs from the G-R law and mathematically is described as follows:

$$\log_{10} N = a - b(m - M_c) \tag{2.7.0.1}$$

where N is the number of events with magnitude at least m, a is the earthquake productivity and b describes the relative distribution of small and large earthquakes (*Gutenberg and Richter*, 1944). Deviations only on the lower end of the FMD should be considered when estimating M_c since the deviations that are often observed at the larger magnitudes can be due to statistical fluctuations due to under-sampling or to a real break in the G-R scaling (*Mignan*, 2012; *Naylor et al.*, 2010; *Wesnousky*,

1994). Figure 2.3 shows the how the M_c is calculated from the FMD of a subset of the Southern California earthquake catalog *Hauksson et al.* (2012).

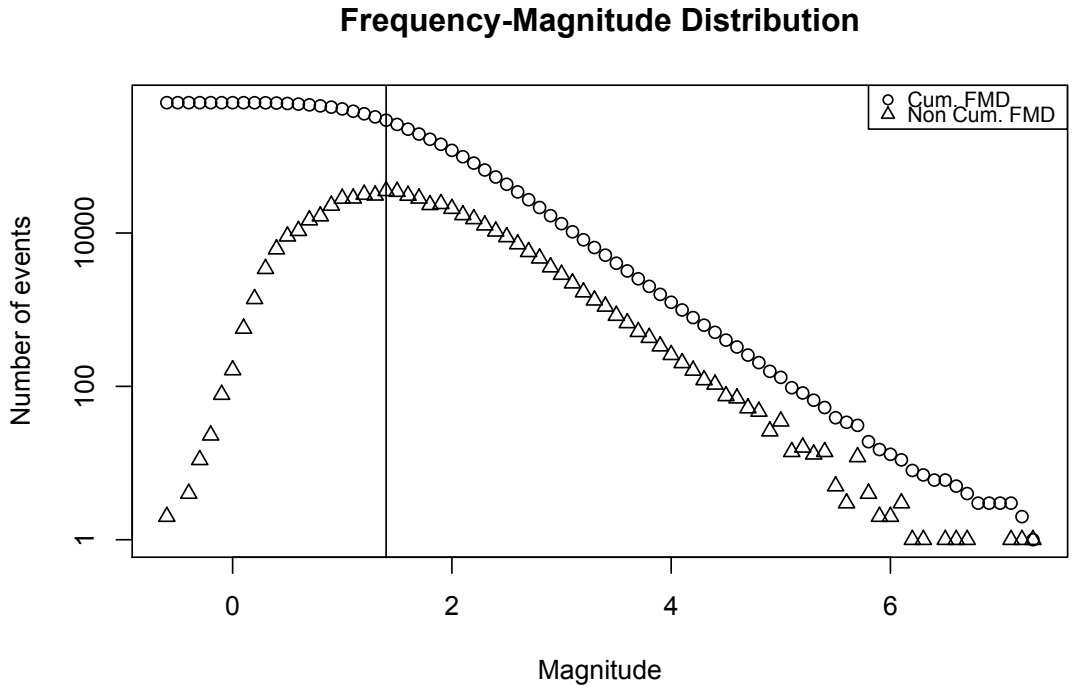

Figure 2.3: The FMD of a subset of the Southern California earthquake catalog. The M_c estimation is shown with a vertical line and corresponds to magnitude 1.4

The magnitude of completeness estimation is an important aspect of every statistical analysis since it has a direct impact on the b value of the G-R law and consequently the a value and all the statistical models in which the G-R law is implemented and are used in seismic hazard assessments and forecasts (*Werner and Sornette*, 2008; *Seif et al.*, 2016). However, this task is not trivial. In Figure 2.4 obtained from *Mignan* (2012) the variation of the b value estimation with respect to the cut-off magnitude M_{co} is shown. When M_c is larger than the cut-off magnitude the b value estimate is erroneous because a power law has not been established whereas in the case where M_c is smaller than the cut-off magnitude the b value is stable around the value 1 before fluctuating again due to under-sampling (*Mignan*, 2012).

A number of methods to determine the M_c have been developed, for example the Maximum Curvature method and the Goodness of Fit Test by *Wiemer and Wyss*

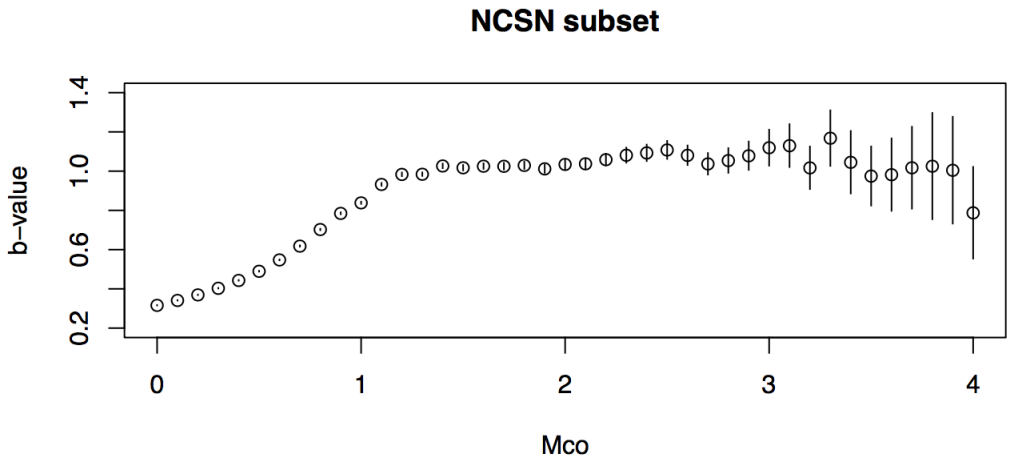

Figure 2.4: b value estimate as a function of magnitude cutoff M_{co} for the subset of the NCSN (Northern California Seismic Network) catalog. For $M_{co} < M_c$, the b value is erroneous because the FMD is not a strict power-law. For $M_{co} > M_c$, the b value estimate starts to stabilise (around 1.0 in the example) before fluctuating again due to under-sampling at the higher end of the FMD. Error bars represent $\pm$ 1σ, standard deviation obtained from bootstrapping. Figure and caption taken from *Mignan* (2012).

(2000), the M_c from the Entire Magnitude Range (EMR) by *Woessner and Wiemer* (2005) and the Median-Based Analysis of the Segment Slope (MBASS) method by *Amorèse* (2007). These are catalog based methods and can be classified into two categories, the parametric e.g. the EMR where the evaluation of M_c is based on fitting the FMD, and the non parametric (e.g. MBASS) which are based on the evaluation of changes in the FMD. In network based methods the probability level of an earthquake detected by a network given the sensor sensitivity and station distribution is calculated. These methods use waveform or phase picked data, e.g., *Schorlemmer and Woessner* (2008) instead of catalog data. In this thesis only catalog based methods for the estimation of the M_c will be used, since they are considered the norm in the literature. Specifically, the EMR and MBASS methods are used in order to include both a parametric and a non parametric approach. All methods have advantages and disadvantages and the choice can be made on a case to case basis, however for consistency the above methods are chosen for all the applications. The EMR and MBASS are described below:

1. Entire Magnitude Range (EMR)

EMR is a method to estimate the magnitude and the associated uncertainties by *Woessner and Wiemer* (2005) that uses the entire dataset in the analysis including the magnitude ranges that are reported incompletely. It is similar to the work of *Ogata and Katsura* (1993) and consists of two parts: the G-R law to model the complete part, and the cumulative normal distribution q(M|μ,σ) which describes the detection capability of the seismic network as a function of the magnitude for the incomplete part of the FMD. The choice of the normal distribution was made after modelling a variety of catalogs and does not have a physical meaning. The selection of the normal distribution was criticized by *Kagan* (2002) in terms of the stability of smaller earthquakes and their negative influence on the results. The best fitting model is the one that maximises the log likelihood function of four parameters, the a and b of the G-R law and the μ and σ of the detection function that correspond to the magnitude at which 50% of the earthquakes are detected and the standard deviation describing the width of the range where earthquakes are partially detected, respectively. The fitness of the model is tested with a Kolmogorov - Smirnov test at the 0.05 significance level where the null hypothesis of the test is that the two samples are drawn from the same distribution and the uncertainties are estimated using bootstraping. The idea of a bootstrap to obtain standard errors, confidence intervals and other measures of uncertainty is to resample the original data, directly or via a fitted model, to create datasets from which the variability of the quantities of interest can be assessed without analytical calculation. The name bootstrap comes from the use of existing data to generate more data which seems analogous to a trick used by a fictional Baron Munchausen, who when he found himself at the bottom of a lake got out by pulling himself up by his bootstraps (*Davison and Hinkley*, 1997). The bootstrap method was developed by *Efron* (1981).

2. Median-based analysis of the segment slope (MBASS)

MBASS is a method developed by *Amorèse* (2007). It is a non parametric method, which is applied for the detection of change points in the non cumulative FMD. The magnitude that corresponds to the lowest magnitude where the G-R law still applies is denoted m_0 and it is required for a reliable b value estimation. The author discusses that the break point at the lowest magnitude is referred as magnitude of completeness by some authors e.g. *Woessner and Wiemer* (2005), however other authors, e.g. *Aki* (1987), *Main* (1987), interpret the discrepancies at the low magnitude implying a departure from self-similarity for the small earthquakes. *Amorèse* (2007), adopts the notation m_0 instead of M_c of other earlier authors such as *Aki* (1965) when computing b values. The detection of the m_0 point is performed with the multiple change-point procedure of *Lanzante* (1996), which is commonly used in time series. This method is applied on segment slopes of the incremental FMD as follows: If M1 and M2 are the magnitudes of two consecutive points of the FMD the segment slope for M = M2 is defined in equation 2.7.0.2.

$$s(M_2) = \frac{\log[N(M_1)] - \log[N(M_2)]}{M_1 - M_2} \tag{2.7.0.2}$$

The author uses the non parametric Mann Whitney test to accept or reject the null hypothesis that there is no change in the sequence. The uncertainties in the MBASS method are calculated using a bootstrap approach.

As discussed in the beginning of this section, magnitude incompleteness M_c can be caused by a variety of reasons. Changes in the seismic networks and large earthquakes that cause smaller aftershocks to become undetected in their coda, a phenomenon that is referred as short term aftershock incompleteness (STAI) (*Kagan*, 2004) are responsible for temporal variations of the magnitude of completeness in a given area. A common practise is to calculate the magnitude of completeness with a methodology such as the EMR by using a moving window technique. This allows

as to monitor the changes of the M_c throughout a specified time period and subsequently choose a a data set where the M_c remains stable. However this technique has a smoothing effect on the data and hence does not capture the temporal variations to their full extent. In the Figure 2.5 below the time varying M_c calculation for the 1992 Landers earthquake using the maximum curvature (MAXC) and MBASS techniques are shown.

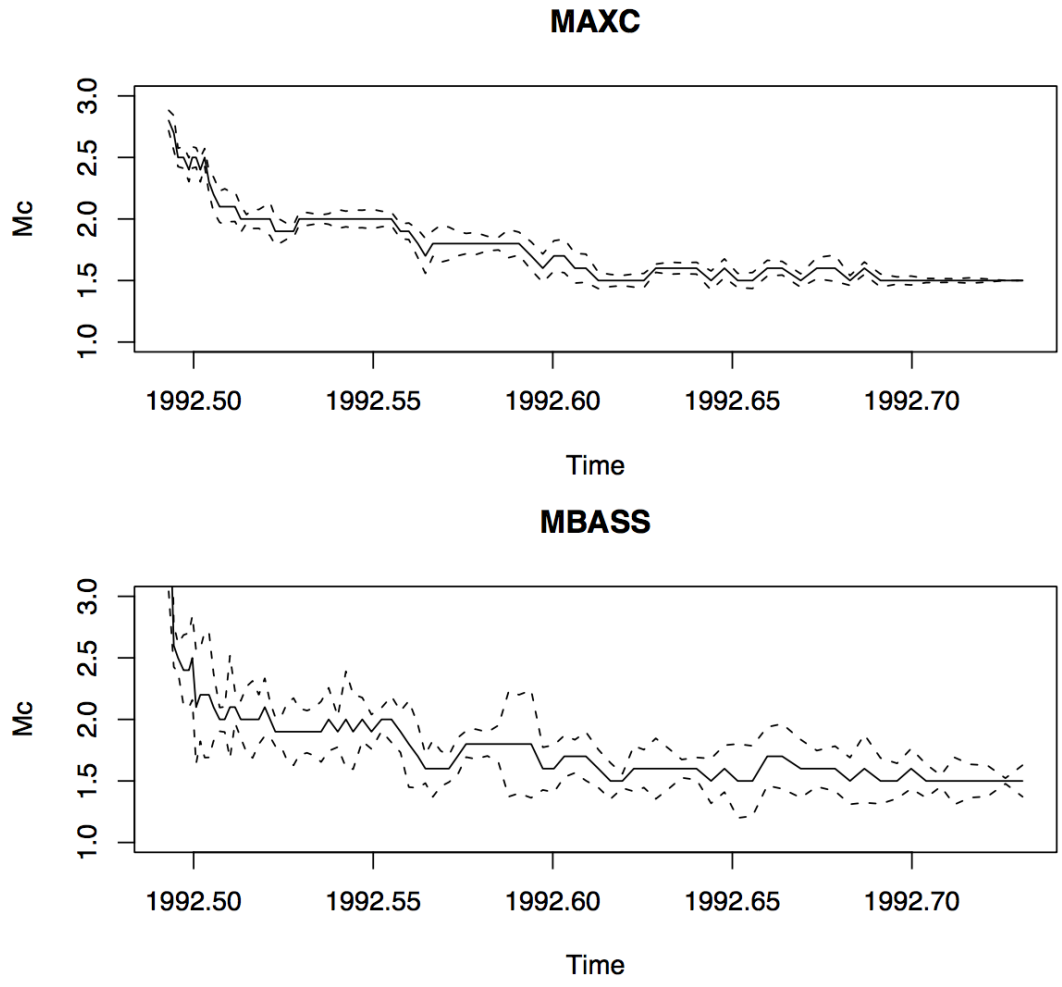

Figure 2.5: The temporal variation of M_c calculated with the maximum curvature (MAXC) and median-based analysis of the segment slope (MBASS) methods for the magnitude 7.3 Landers 1992 afterschock sequence. Moving window approach with a window of 1000 events, moved by 250 events.Figures obtained from *Mignan* (2012).

It can be seen an increase in the M_c magnitude immediately after the 7.3 magnitude earthquake to the magnitude 3 with the MBASS method and a little below 3 with the MAXC method. However more recent research has shown that these methods do not

fully capture the effect of incompleteness. In his paper *Hainzl* (2016) demonstrates how the magnitude of completeness varies with the seismicity rate. *Hainzl* (2016) firstly calculates the b values with a maximum likelihood method for the data under study as a function of the estimated local earthquake rate. Assuming a constant FMD, incomplete recordings should result in an apparent decrease of the estimated b-value. The rate at which the b value decrease is observed and is then used to estimate the time varying magnitude of completeness. The *Hainzl* (2016) method will be discussed in more detail in the next chapter where the methodology proposed by this thesis is analysed. In Figure 2.6 the application of the rate dependent magnitude of completeness is shown for the M 7.3 Landers aftershock sequence. If we compare it with Figure 2.5 we can clearly see that the increase of the M_c after the mainshock is significantly larger.

The variations of the M_c are not limited is the temporal and seismicity rate domain, they are also spatial. To estimate the spatially varying magnitude a mapping approach is typically used in which the FMD is generated from from events located in a cylindrical volume of fixed radius R or of fixed number of events N, centered on each node of a spatial grid e.g. *Wyss et al.* (1999); *Wiemer and Wyss* (2000). In the constant radius method a minimum number of events is assigned to avoid instable M_c results. R must be large enough to have a sufficient number of nodes but small enough to avoid over smoothing. For the fixed number of events approach, the maximum radius R max is fixed to avoid over-smoothing. The number of events must be large enough to obtain reliable M_c estimates but small enough to avoid gaps *Mignan* (2012). To avoid the limitations of the above mapping technique *Mignan et al.* (2011) proposed the Bayesian Magnitude of Completeness (BMC) spatial mapping method. In the BMC method a spatial resolution optimization to minimize spatial heterogeneities and uncertainties in Mc estimates is firstly performed and secondly a Bayesian approach to merge prior information on the relationship between M_c and

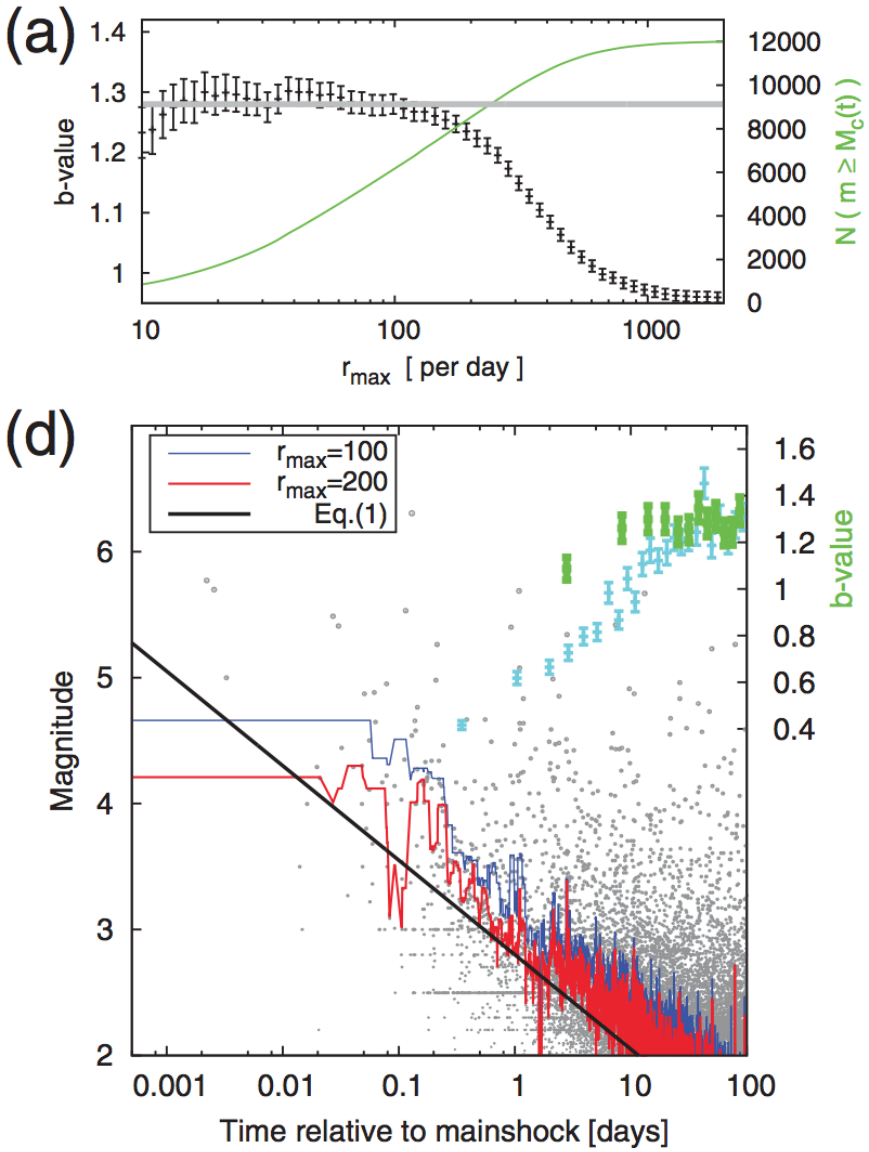

Figure 2.6: Plot (a) shows the estimated b-values for M_c(t) calculated for different threshold rates r max, showing stable results for values smaller than approximately 200 events per day, in which horizontal lines refer to (a) b = 1:28. Plots (d) shows the corresponding M_c(t) estimations for r max 100, 200 events per day in (d), in which the black curve refers to the empirical result of *Helmstetter et al.* (2006) applied to the mainshock in (d). Figures obtained from *Hainzl* (2016).

the density of seismic stations with locally observed M_c, weighted by their respective uncertainties.

The EMR and MBASS calculations estimated in this thesis are performed during the Matlab based software tool for seismological analysis ZMAP (*Wiemer*, 2001). ZMAP is software that uses the corrected version of the maximum likelihood esti-

mation of the b value that minimises uncertainties and therefore using ZMAP the estimation of the magnitude of completeness is more robust.

2.8 Declustering

Seismicity declustering is the process of separating an earthquake catalog into foreshocks, mainshocks and aftershocks. In the ETAS section earlier in this chapter I showed that seismicity in this model is represented by background and triggered events. With declustering the aim is to identify the independant background events, or mainshocks, from the triggered events (aftrshocks, foreshocks) that occur in clusters. Declustering is commonly used procedure in many seismological applications however the quality of the earthquake catalog data must be assessed first, since missing magnitudes and other catalog artifacts can bias the results. There are three main categories of declustering algorithms, the window methods, the cluster methods and the stochastic methods. The window based techniques are the simplest. For each earthquake in the catalog with magnitude M, the subsequent shocks are identified as aftershocks if they occur within a specified time interval T(M), and within a distance interval L(M) (*Van Stiphout et al.*, 2012). The algorithms of *Knopoff and Gardner* (1972); *Gardner and Knopoff* (1974) are examples of windowing techniques. The algorithm of *Reasenberg* (1985) is the most well known cluster approach to declustering. The triggered events are identified by linking earthquakes to clusters according to spatial and temporal interaction zones *Van Stiphout et al.* (2012). Stochastic declustering is a probabilistic approach for separating background from triggered events using clustering models such as the ETAS, e.g. *Zhuang et al.* (2002).

There are many limitations associated with the declustering algorithms. Window based and cluster methods contain arbitrary parameters for defining the aftershock window sizes or the link distances in both space and time. Different parameters give different declustered catalogs and thus a different estimate of the background

seismicity. These conventional declustering algorithms have difficulty making an optimal choice of parameters (*Zhuang et al.*, 2002). A better option is to assign probabilities to each event for being either background or triggerred. However ETAS and other branching process models are commonly estimated using Maximum Likelihood (ML). The vector of parameters that maximises the log likelihood $\hat{\theta}$ are obtained by using a numerical optimization routine, since no closed form solution is generally available. In the cases where the log likelihood function is extremely flat in the vicinity of its maximum, such optimization routines can have convergence problems and can be substantially influenced by arbitrary choices of starting values (*Veen and Schoenberg*, 2008). Figure 2.7 shows a graphical representation of the difficulties in the parameters estimation using the maximum likelihood approach. The numerical maximization routine converges to an estimate close to θ in only two cases. It fails to converge in two cases and seems incapable of improving the K0 estimate for the four starting configurations in which K0 is modified by 33%. This could be due to the relative flatness of the log-likelihood function (shown in grey-levels) with respect to variations of K0.

The unreliable nature of stochastic declustering using the ETAS model is also discussed in the work of *Sornette and Utkin* (2009b). They conclude that the estimated rates of triggered events suffer from large errors along with the branching ratio n which quantifies the fraction of events that have been triggered by previous events. Errors tend to be smaller and perhaps acceptable in some cases for small triggering efficiency and branching ratios (*Sornette and Utkin*, 2009b).

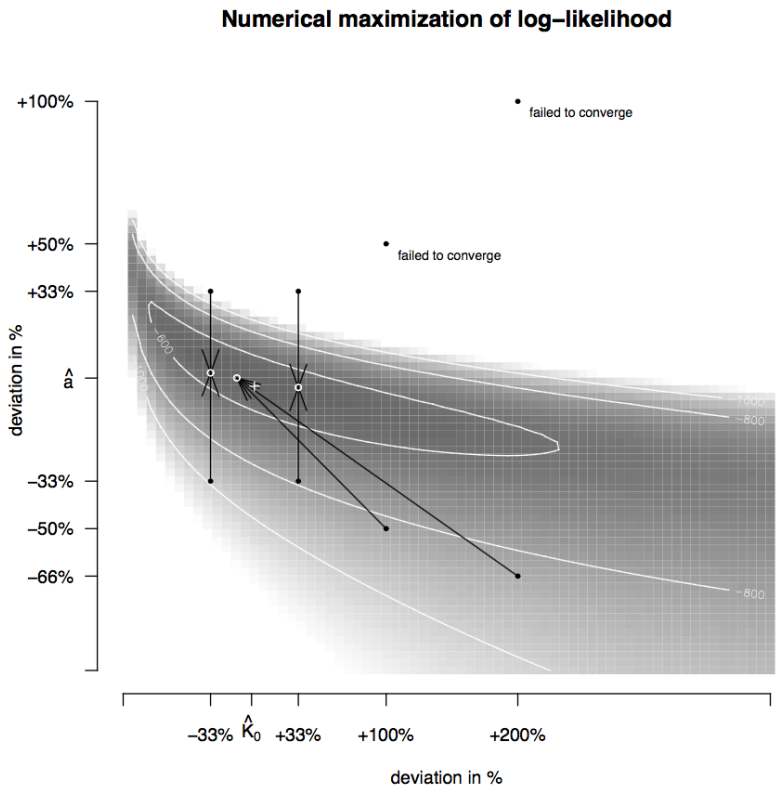

Figure 2.7: Difficulties in estimating ETAS parameters when maximizing the log-likelihood numerically. Except for K0 and a, the starting values (black dots) for the components of θ are set to the true values. The white circles show the estimation results of the numerical maximization routine ($\hat{\theta}$) and the + symbol depicts the location of the true K0 and a. Figure obtained from *Veen and Schoenberg* (2008).

2.9 Magnitude correlations - An overview of existing work

Earthquake activity varies in space and time and while the temporal and spatial clustering of earthquakes has been established to be greater from what would be expected from a purely random process e.g. *Main et al.* (1999), the correlation between the earthquake magnitudes is assumed to be zero. Recently this assumption has been questioned with some some studies supporting the existence of magnitude correlations and other studies claiming the correlation is purely caused by the properties of the earthquake catalog and more specifically the short term aftershock incompleteness (STAI). As described below, previous work can be broadly separated into two main categories:

1. Magnitude correlations between successive earthquakes.

   In this category we find the work by *Lippiello et al.* (2008, 2012) who demonstrate the existence of magnitude correlations in Southern California and their relationship with Δt and Δr. Δt corresponds to the elapsed time between successive earthquakes and Δr to the distance between subsequent epicentres. They conclude that earthquakes occur with higher probability close in time, space and magnitude to previous events and that the next earthquake tends to have a magnitude similar but smaller than the previous one (*Lippiello et al.*, 2008). In the work of *Davidsen and Green* (2011), it is shown that the above mentioned correlations are an effect of short term aftershock incompleteness (STAI) and seismic network density incompleteness (SNDI) in the earthquake catalogs. *Davidsen and Green* (2011) stated that considering the magnitudes of only the earthquakes that are close in space and/or in time to the directly subsequent one can bias the estimation of the magnitude correlation. This is due to dependency of the magnitude on the parameters of the modified Omori law and should also be observable in models such as

the ETAS where the modified Omori law is implemented. In *Lippiello et al.* (2012), the earthquake magnitude correlations were re-analyzed in terms of STAI and SNDI. Following their methodology from *Lippiello et al.* (2008), they showed that magnitude correlations are more important for earthquakes close in time and cannot be attributed to STAI or SNDI. The paper provides detailed description of their methodology and the steps they followed to explore the role of STAI and SNDI. Adopting a different methodology *Lippiello et al.* (2013), continued the search for magnitude correlations, this time using the Olami-Feder-Christensen (OFC) model for earthquake activity. The OFC model considers a discrete system of blocks interconnected with elastic springs and the total force F_i acting on a given block i increases at constant rate when F_i is smaller than a threshold force value F_c. When F_i exceeds the threshold value, the force on block i reduces to zero and the force on the four neighbour blocks is increased by a value α and therefore on the neighbour block the total force is: $F_j = F_j + \alpha$ (*Lippiello et al.*, 2013). The OFC model is a statistical model that can reproduce the Gutenberg Richter and Omori laws to describe earthquake activity. It is considered one of the simplest models of the Self Organised Criticality (SOC) regime, as introduced by *Bak et al.* (1987, 1988). Self Organised Criticality refers to a property of dynamical systems to organise spatially and/or temporally in a scale free manner (*Caruso and Kantz*, 2011; *Golyk*). Such systems organise themselves into the critical behaviour. The goal of *Lippiello et al.* (2013) was to examine whether correlations found in real data can be found in these simple models. This study examines the role of the dissipation parameter α described above on magnitude correlations. They documented their results and concluded that the parameter α controls the magnitude correlations and that for intermediate α values the magnitudes of subsequent earthquakes in the OFC model are correlated. In terms of STAI, *Lippiello et al.* (2013) argues that the similarities between the results from numerical catalogs which are not affected form catalog incompleteness with

experimental catalogs demonstrates that the existence of magnitude correlations are not resulting from STAI. When analyzing the earthquake catalog of Southern California using the natural time domain, *Sarlis* (2011) suggests that magnitude correlations observed in the region become lower as the catalog the cut-off (M0) magnitude increases, and essentially become insignificant above $M0 = 3.1$. This suggests that catalog incompleteness is the cause. The cut-off magnitude$M0$ is the minimum magnitude used in a statistical analysis and does not correspond to the magnitude of completeness, M_c. In contrast using the natural time domain and fluctuation analysis *Lennartz et al.* (2011) search for magnitude correlations in time, their conclusion suggests the existence of such correlations.

2. Magnitude correlations between a mainshock and it's aftershocks.

   In *Nichols and Schoenberg* (2014), the approach used to search for magnitude correlations does not involve subsequent events but instead directly investigates the relationship between the magnitude of each mainshock in the catalog, and the average magnitude of its subsequent aftershocks. Positive correlations would imply that larger mainshocks tend to have larger aftershocks, which would suggest the existence of magnitude correlations. This approach was applied on a global earthquake catalog, where evidence of small magnitude correlations was found.

In the previous work described in this section, it is clear that research has been mainly focused in the correlation between the magnitude of successive earthquakes. Although finding correlations in the magnitudes between successive earthquakes in time, is an exciting outcome, the question of interest especially on seismic hazard assessments is the correlation in the magnitudes of a mainshock with its aftershocks. Short term aftershock incompleteness and seismic network density incompleteness are the obvious parameters that bias the results of both types of research, however the identification of successive earthquakes i.e. to define the branching structure

of the earthquake catalog and obrtain mainshock - aftershock sequences is not a trivial task. To find the branching structure we need to decluster the earthquake catalog. Declustering refers to a range of statistical methodologies e.g. (*Knopoff and Gardner*, 1972; *Zhuang et al.*, 2002; *Reasenberg*, 1985) that are used to identify and separate mainshocks from aftershocks. The process of declustering introduces new biases to the research. In the following sections I am aiming to introduce a new method that is more robust to the above mentioned biases and looks for correlations in the magnitudes of earthquakes in specific region rather than successive events without relying in declustering.

2.10 Fracture mechanics

Fracture mechanics is the study of mechanical behaviour of cracked materials subjected to an applied load. It has been linked to stress, strain, displacement and deformation (*Perez*, 2017).

(i) Stress: The stress at a point on a body represents the internal resistance of a body due to an external force. The load (P) and the cross-sectional area (A) are related to stress as indicated by the equation 2.10.0.1 of equilibrium of forces. It is measure of force per unit area, typically thought to control earthquake occurrence; stress is accumulated via loading by plate tectonics and released by deformation.

$$\sum F_y = P - \sigma A = 0 \tag{2.10.0.1}$$

$$\sigma = \frac{P}{A} \tag{2.10.0.2}$$

If stress is not equal from all directions then we say that the stress is a differential stress. Three kinds of differential stress occur: tensional, compressional and shear.

(ii) Strain: A geometric quantity, which depends on the relative movement of two or three points in a body. A strain is a change in size, shape, or volume of a material.

(iii) Deformation: The movement of points in a solid body relative to each other. When a rock is subjected to increasing stress it passes through three successive stages of deformation. Elastic deformation wherein the strain is reversible, ductile deformation wherein the wherein the strain is irreversible and finally fracture where the strain is irreversible ad the material breaks. Post failure frictional sliding may be observed.

(iv) Dispalcement: The movement of a point in a vector quantity in a body subjected to loading.

Stress at a point in an isotropic body can be described with a second order tensor consisting of nine components as shown in equation 2.10.0.3.

$$\sigma_{i,j} = \begin{Bmatrix} \sigma_{11} & \sigma_{12} & \sigma_{13} \\ \sigma_{21} & \sigma_{22} & \sigma_{23} \\ \sigma_{31} & \sigma_{32} & \sigma_{33} \end{Bmatrix} \tag{2.10.0.3}$$

The subscript notation used for the nine stress components have the following meaning: $\sigma_{x,y}$: Stress on the x plane along y direction.

Figure 2.8 shows a schematic representation of the tensor components.

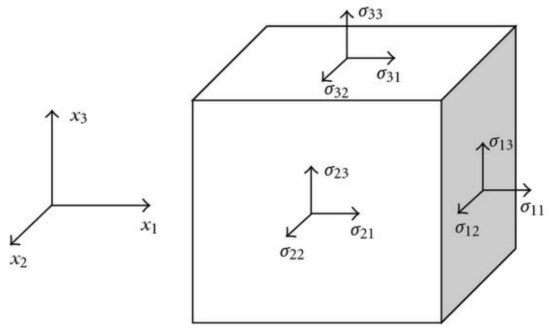

Figure 2.8: Schematic representation of the nine tensor components.

The diagonal components of equation 2.10.0.1 σ_1, σ_2, σ_3 are called principal stresses and define planes of no shear stress normal to them.

All the experiments performed and described in this thesis correspond to triaxial deformation. The stress state during these conditions ($\sigma_1 > \sigma_2 = \sigma_3$) is shown in Figure 2.9. The convention is that compression is taken to be positive.

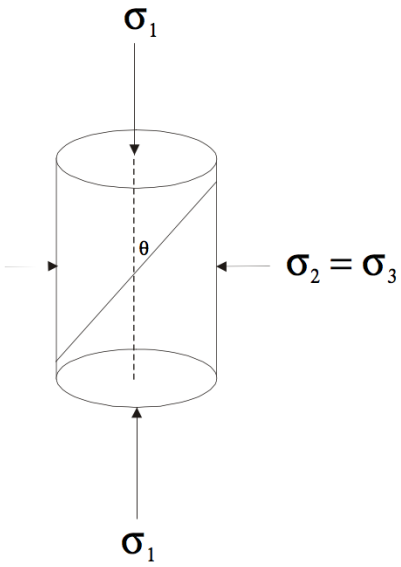

Figure 2.9: Stress state during triaxial deformation.

Chapter 3

Magnitude correlations

3.1 Chapter outline

The concept of correlation in the magnitude of the earthquakes is controversial. Although the number of aftershocks that are generated from an earthquake depends on the mainshock magnitude, the magnitude of the aftershocks it is generally believed to be independent from the magnitude of the mainshock. Many widely used seismicity models adopt this approach, which implies that earthquake magnitudes are essentially unpredictable (*Ogata*, 1988, 1998; *Turcotte et al.*, 2007; *Reasenberg and Jones*, 1989). Over the past 10 years, some studies suggested the existence of magnitude correlations, while other studies argue that such correlations are a statistical artifact due to the incompleteness of earthquake catalogs [1]. These studies gave impetus to the work presented in this thesis and the developing of a new methodology which is more robust to potential incompleteness. In this chapter, a detailed description of a novel methodology developed for the purposes of this thesis is described with applications to different regions and tectonic settings.

[1]The magnitude of completeness M_c of an earthquake catalog denotes the magnitude above which all earthquakes are recorded

3.2 Proposed approach for magnitude correlations assessment

Previous work such as *Lippiello et al.* (2008, 2012) and *Nichols and Schoenberg* (2014), gave the impetus to develop a new methodology for studying earthquake magnitude correlations. The hypothesis proposed by this thesis is that the average magnitude of earthquakes is likely to be higher in the time periods following previous large earthquakes. These previous studies test the hypothesis directly by looking at the correlation between observed mainshocks and aftershocks, where these are identified using either direct temporal succession, or declustering. It has been observed by (*Davidsen and Green*, 2011; *Hainzl*, 2016) that these methods are potentially unreliable due to STAI, we instead seek a more robust measure of recent seismic activity.

The approach proposed here uses the ETAS model (*Ogata*, 1988, 1989), which is one of the most widespread models used for statistical earthquake forecasting. A fundamental assumption of the ETAS model is that the magnitudes of each earthquake are independent and identically distributed, i.e. that there are no magnitude correlations. Specifically, the magnitude of each earthquake is assumed to be an independent draw from the Gutenberg-Richter distribution with a fixed b-value. ETAS is a special case of the marked Hawkes self-exciting point process (*Hawkes*, 1971; *Hawkes and Oakes*, 1974). In such a model, it is assumed that the probability of an earthquake occurring in some small time interval $[t, t + \Delta_t]$ as $\Delta_t \to 0$, can be modelled by a conditional intensity function $\lambda(t|H_t)$ where H_t denotes the history of the earthquake catalog prior to t. In the ETAS model, the form of the conditional intensity function is given by:

$$\lambda(t|H_t) = \mu + \sum_{\{i:S<t_i<t\}} \frac{Ke^{a(M_i-M_c)}}{(t-t_i+c)^p} \tag{3.2.0.1}$$

where S is the starting time of the catalog, M_c is the catalog magnitude of completeness, μ denotes the background seismicity rate, K, and α control the productivity of an earthquake with magnitude M_i, c is a constant and p represents the rate of the aftershock decay according to the modified Omori law, $t_1, \ldots, t_n$ are the occurrence times of the n earthquakes that occur between times S and t, and M_i is the magnitude of the earthquake that occurs at time t_i. The intuition behind the ETAS model is that whenever an earthquake occurs, it becomes more likely that additional aftershock earthquakes will occur shortly after, due to the increased intensity in the summation term. Larger earthquakes will produce more additional earthquakes, to an extent which is controlled by the α parameter. Such a model naturally reproduces the earthquake clustering patterns which are empirically observed in real catalogs.

Like all Hawkes processes, the ETAS model can be rephrased in terms of a branching point process model (*Hawkes and Oakes*, 1974). This comes from noticing in Equation 3.2.0.1 that the conditional intensity λ of the ETAS model at time t is a linear superposition of the background rate μ and the intensity spikes from the m previous earthquakes prior to t. By the basic theory of point processes (*Veen and Schoenberg*, 2008) each earthquake in the catalog can hence be viewed as having been generated either by the background process, or by a specific previous earthquake. This leads to a declustering of the catalog into mainshocks and aftershocks, where the mainshocks are the earthquakes produced by the background process, and the aftershocks are those triggered by a previous earthquake. This representation is used in the stochastic declustering of earthquake catalogs into mainshocks and aftershocks (*Zhuang et al.*, 2002). To illustrate this, Figure 3.1 shows a simplified version of a branching structure. The top row represents the background events and the rows below represent the triggered events. Triggered events can trigger their own earthquakes as well acting as foreshocks, mainshocks and aftershocks at the same time, which is a fundamental feature of the ETAS model.

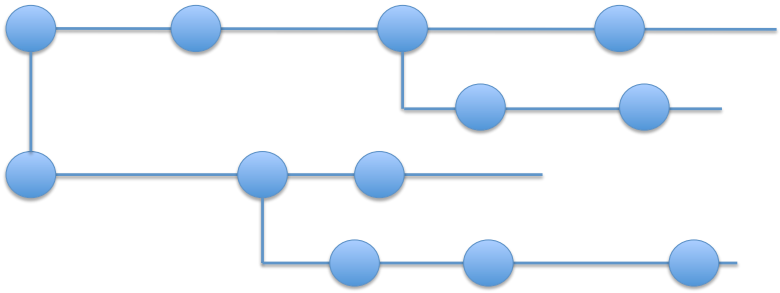

Figure 3.1: A visual example of a branching structure implied by the ETAS model. The top layer represents the mainshocks, each of which can produce several aftershocks. These aftershocks are also themselves capable of producing further aftershocks.

The proposed methodology for studying magnitude correlations in a catalog has the following steps. First, the magnitude of completeness (M_c) of the catalog is calculated using the standard Median-Based Analysis of the Segment Slope (MBASS) and the Entire Magnitude Range (EMR) methods (*Amorèse*, 2007; *Woessner and Wiemer*, 2005). These produce values of 1.9 and 1.5 in the Southern California catalog, and 1.1 in Parkfield.

Next, the ETAS model is fitted to the catalog using maximum likelihood to estimate its parameters, as in *Veen and Schoenberg* (2008). Given the estimated parameters, we can then use Equation 3.2.0.1 to evaluate the conditional intensity $\lambda(t_i|H_{t_i})$ at each observed earthquake time $t_1, \ldots, t_n$ in the catalog. This gives a sequence of n pairs (CI_i, M_i) where CI_i denotes the conditional intensity $\lambda(t_i|H_{t_i})$ at time t_i, and M_i denotes the magnitude of the earthquake that occurred at t_i. These pairs can then be plotted in order to get a visual representation of whether the magnitude depends on the conditional intensity, which acts as a measure of the level of recent seismicity prior to each earthquake in the catalog.

Recently it has been shown in *Hainzl* (2016) that methods such as the maximum curvature for estimating the magnitude of completeness M_c do not accurately capture STAI after a large earthquake, and the time varying magnitude of completeness estimation is smoothed over the period of the whole catalog. *Hainzl* (2016) demonstrates the dependance of M_c with the seismicity rate and shows the rapid increase of

M_c minutes, hours or sometimes days after a large mainshock. The rate dependent estimation of the magnitude of completeness $M_c(t)$ as described in *Hainzl* (2016) is then applied to all the mainshocks above magnitude 6 in the catalog since changes in the rate are caused by larger earthquakes. To make sure that magnitude 6 was the right choise, a small number number of earthquakes with magnitudes between 5.7 and 5.9 where analysed and the results showed no increase in the rate. Firstly, the mainshocks in the data are identified using the declustering algorithm described in *Helmstetter* (2003). According to this desclustering method, an earthquake is a mainshock if a year before this earthquake and within 50 km there is not a larger earthquake. The aftershocks are selected using equation 3.2.0.2 proposed by *Wells and Coppersmith* (1994) and used in *Hainzl* (2016). All the earthquakes within 100 days following a mainshock and with distance (d) less than 5 times the rupture length (L) are aftershocks:

$$L = 10^{-2.44+0.59M} km \tag{3.2.0.2}$$

For every aftershock sequence the G-R b value is calculated for different seismicity rates using the maximum likelihood method (*Aki*, 1965; *Marzocchi and Sandri*, 2003) for magnitude bins with at least 100 magnitudes (*Hainzl*, 2016). Equation E.0.0.10 shows the b value calculation.

$$\hat{b} = \frac{1}{ln(10)\langle m - (M_c - 0.5\Delta m)\rangle} \tag{3.2.0.3}$$

where $\langle \ldots \rangle$ refers to the average value, M_c is the magnitude of completeness and Δm is the binning interval of the reported magnitudes. In California $\Delta m = 0.01$. The binning of the magnitudes is used to correct for biases in the b value calculation the original maximum likelihood estimation by *Aki* (1965) introduces. For example, the average magnitude μ of a continuous random variable with a power law distribution is different from the average of the same binned random variable

and second that the threshold magnitude is not equal to the minimum magnitude *Marzocchi and Sandri* (2003). The corrected formula E.0.0.10 drastically improves the accuracy of the b value estimation and its used throughout the thesis.

Hainzl (2016) demonstrates a decrease in the b value at higher rates as a result of STAI. The value of seismicity rate where the b value decreases is then used to calculate the rate dependent magnitude of completeness. In Figure 3.2 we show the results of his analysis for the Hector Mine and Landers earthquakes in California and for a swarm in western Bohemia.

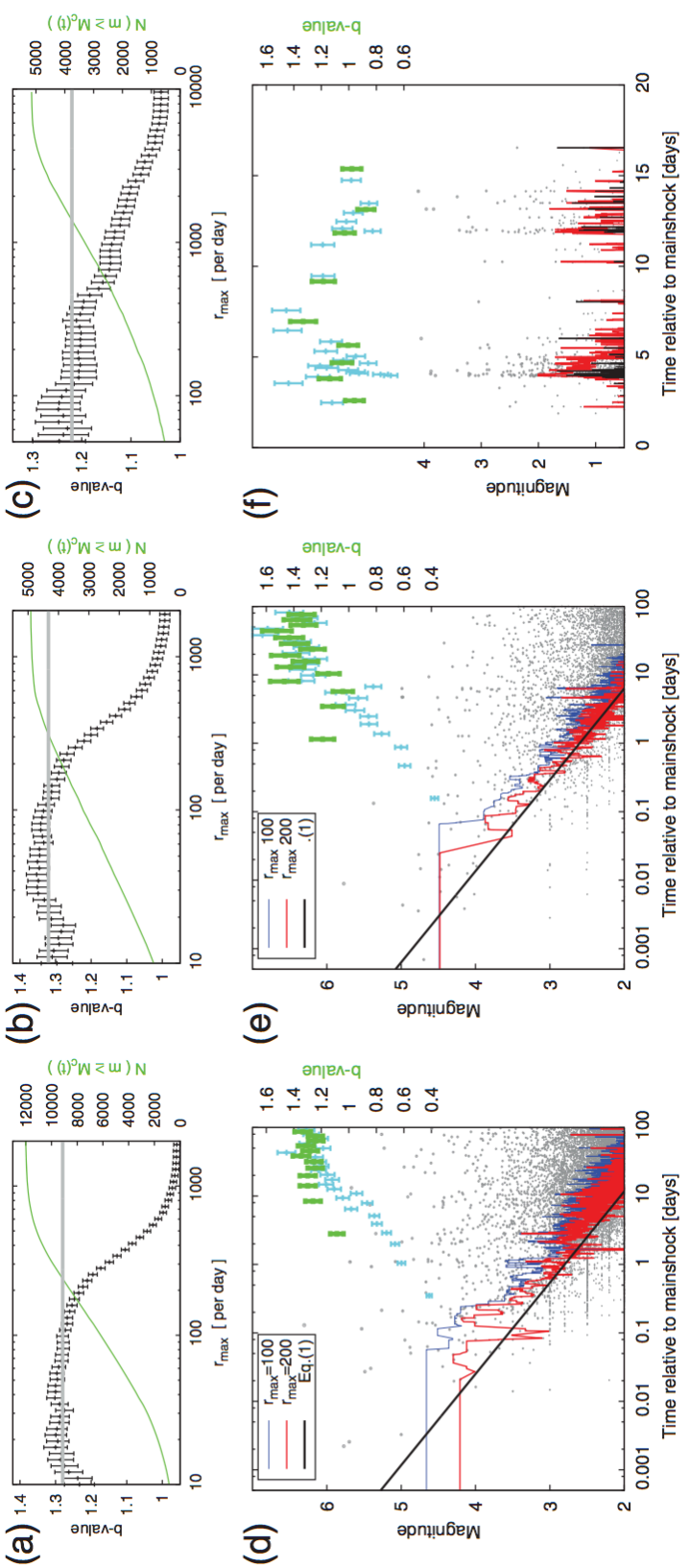

Figure 3.2: Applications of the algorithm (Algorithm to Estimate Mc Based on Catalog Data section with N = 10) to estimate the rate-dependent completeness magnitude M_c(t) . Aftershock sequences of (a, d) the Mw 7.3 Landers and (b, e) the Mw 7.1 Hector Mine earthquake, as well as (c, f) the year 2011 swarm in western Bohemia. Plots (a - c) show the estimated b-values for M_c(t) calculated for different threshold rates r max, showing stable results for values smaller than approximately 200 events=day, in which horizontal lines refer to (a) b = 1.28, (b) b = 1.32, and (c) b = 1.22. Plots (d - f) show the corresponding M_c(t) estimations for r max =100; 200 events/day in (d, e) and r max = 300 events/day in (f), in which the black curve refers to the empirical result of *Helmstetter et al.* (2006) applied to the mainshock in (d, e), and to all events in (f). Error bars refer to b-values estimated for successive, nonoverlapping 500 events (plot d) and 200 events (plots e, f). The b-values calculated with constant completeness magnitude (M_c = 2.0 for California and 0.5 for the swarm) are marked by light blue error bars and those determined for the estimatedM_c(t) (with r max 100 in the aftershock sequences)are shown by green bars. Gray points indicate recorded earthquakes with their magnitudes. In all plots, error bars refer to 1 standard deviation. Figure and caption obtained by *Hainzl* (2016).

The same analysis is performed to all mainshocks above magnitude 6 in my dataset. In order to remove the effect of STAI during these periods of higher rate I remove from the data all the aftershocks between the mainshock and the time where the $M_c(t)$ drops to a level that doesn't exceed our cut off magnitude.

Finally, we perform a formal statistical analysis of the (CI_i, M_i) pairs of the updated catalog to find whether there is any difference between the magnitude distribution during the low and high intensity periods. If so, this suggests that the observed magnitudes of earthquakes during periods of high recent seismicity are different to the magnitudes observed during periods of low seismicity, demonstrating the existence of magnitude correlations. For consistency I always use 10 % of the highest intensities as the high intensity dataset and the bottom 10 % of the intensities as the low intensity dataset. We test this hypothesis in two ways:

1. A 95% confidence interval for the Pearson correlation coefficient between earthquake magnitudes and the conditional intensity is calculated using a nonparametric bootstrap method (*Efron*, 1981). If the correlation is positive and the confidence interval does not include zero, this serves as a nonparametric hypothesis test which rejects the hypothesis of zero correlation at the 0.05 significance level, and hence suggests the existence of magnitude correlations.

2. Since the correlation coefficient is only a measure of linear dependence and cannot capture non-linear dependence, we also split each catalog into two, corresponding to the low and high intensity periods. The mean magnitude for both these periods is then calculated, and a nonparametric Mann-Whitney (*Mann and Whitney*, 1947) test is used to test whether the two means are equal. If the null hypothesis of equality is rejected, this also demonstrates the existence of magnitude correlations. The Mann-Whitney test is selected as the appropriate tool since its nonparametric nature means that the computed test statistic does not depend on the (unknown) magnitude distribution.

The flowchart below summarises the main steps of the proposed methodology.

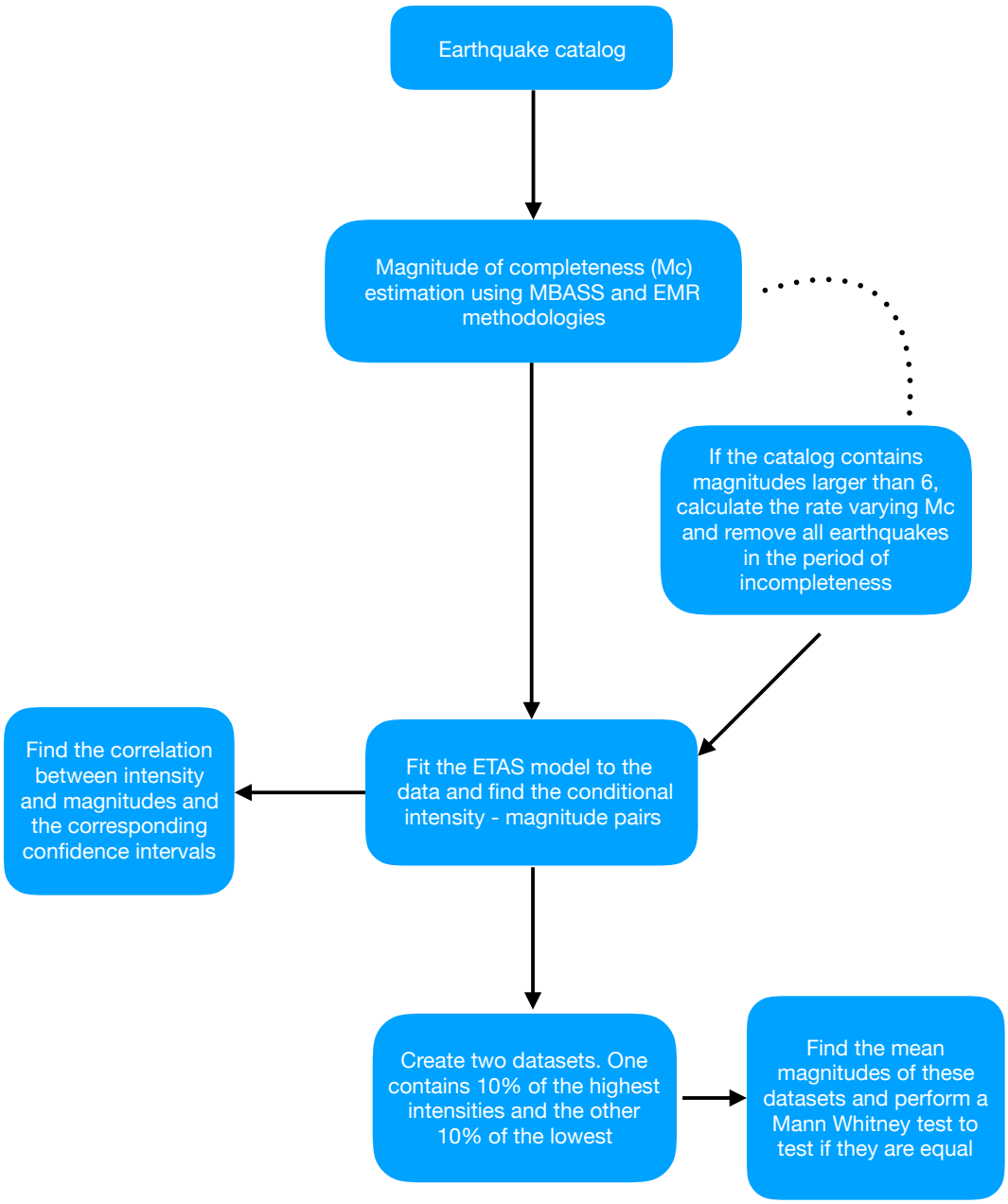

Figure 3.3: Flowchart of the main steps of the proposed methodology.

3.3 Applications in California

We study two earthquake catalogs, taken from different regions and time periods in California. The first region is in Parkfield and includes earthquakes within (35.5N - 36.5N, 121W - 120W) during the years 2004 and 2005. It also includes the magnitude 6 earthquake that occurred in September 28, 2004. The earthquake catalog we used was provided by the Northern California Earthquake Data Center. The Parkfield segment of the San Andreas fault is a well-studied seismological zone with a dense network of seismic stations (*Shcherbakov et al.*, 2006).The second region region includes the earthquakes from the Waveform Relocated Earthquake Catalog for Southern California (1981 to 2011) provided by the Southern California Earthquake Data Center (*Hauksson et al.*, 2012). These datasets are chosen for their high quality which is essential when performing statistical analysis and to prove that this methodology is not unique to one study area.

3.3.1 Parkfield: Conditional Intensity - Magnitude Correlation

The Parkfield section of the San Andreas fault is a region with very dense seismic network. Figure 3.4 shows the study area.

The magnitude of completeness was found to be as low as 1.1, using both the parametric (EMR) and nonparametric (MBASS) methods. Applying a threshold at this level gives a catalog containing 7312 earthquakes. Since previous studies (*Sarlis*, 2011; *Davidsen and Green*, 2011) have shown that spurious magnitude correlations arising due to STAI tend to disappear as the cut-off magnitude is increases, we consider the cut-off values $M0$ of 1.5, 2, and 3. Threshold at this level gives catalogs containing 3752, 1520 and 106 earthquakes respectively.

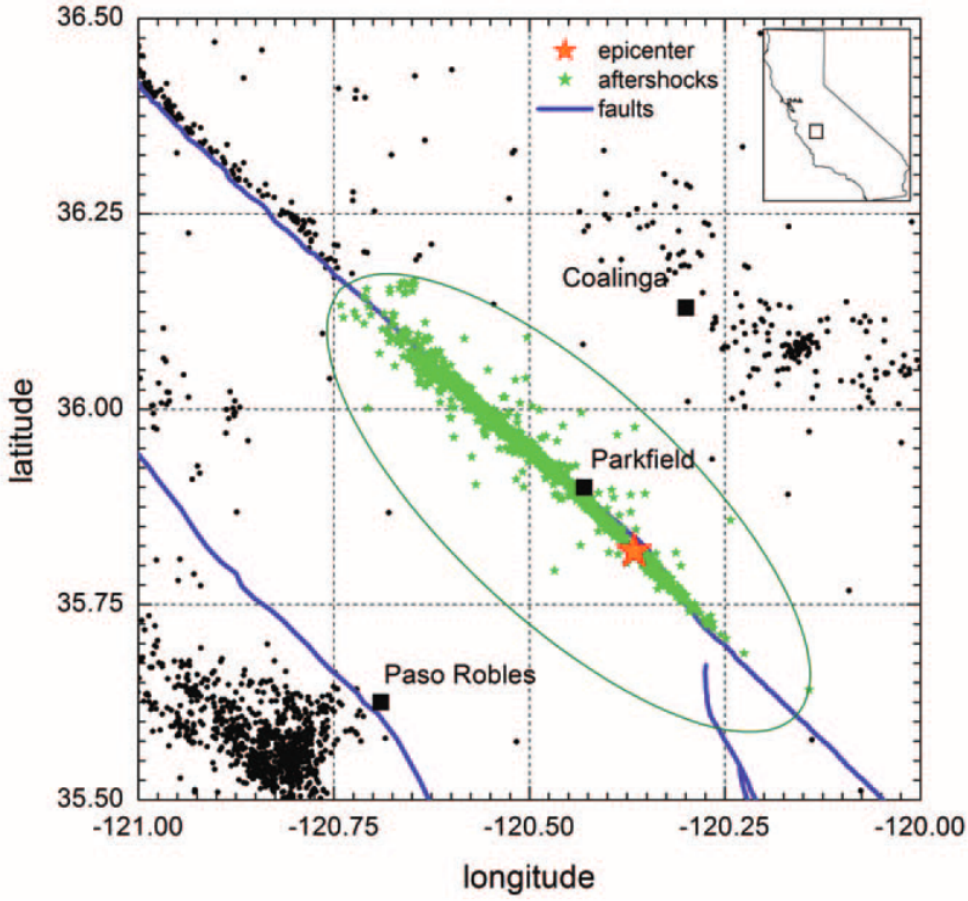

Figure 3.4: The spatial distribution of seismic activity for 365 days after the magnitude 6 Parkfield earthquake in 2004.Figure obtained from *Shcherbakov et al.* (2006)

This region contains only one earthquake with magnitude over 6, to which the *Hainzl* (2016) method of rate dependant magnitude of completeness is applied. Firstly the b value variations are calculated and are shown to be stable with rate. Therefore in Parkfield no data where removed.

For each cut-off magnitude, the ETAS model is fitted to the catalog as described in the previous section. Table 3.1 shows the resulting correlations between the magnitude of each earthquake, and the value of the estimated intensity function immediately before the earthquake occurred. It can be seen that magnitude correlations are both positive and significant since the confidence interval does not include zero and persist even as the cut-off magnitude is raised well above its MBASS/EMR value. This suggests that the correlations are genuine rather than being a statistical

Table 3.1: Earthquake magnitude and ETAS intensity correlations in Parkfield.

M0	Correlation	Confidence Interval	Mann - Whitney test
1.1	0.08	[0.04, 0.11]	< 0.001
1.5	0.10	[0.05, 0.14]	< 0.001
2	0.11	[0.04, 0.18]	< 0.001
3	0.26	[-0.01, 0.50]	0.06

[1]Correlation between the magnitude of each earthquake in the Parkfield catalog and the ETAS intensity immediately preceding it, along with 95% confidence interval. Also shown is the p-value of the Mann-Whitney test when comparing the mean earthquake magnitude in the high and low intensity regions.

Table 3.2: Average magnitude of the original earthquake catalogs along with the low and high intensity subcatalogs.

	Original		Low Intensity		High Intensity	
M0	Mean magnitude	Confidence Interval	Mean magnitude	Confidence Interval	Mean magnitude	Confidence Interval
1.1	1.65	[1.64, 1.66]	1.64	[1.63, 1.65]	1.86	[1.77, 1.96]
1.5	1.98	[1.97, 2.00]	1.98	[1.96, 1.99]	2.19	[2.09, 2.29]
2	2.36	[2.35, 2.39]	2.37	[2.35, 2.39]	2.59	[2.46, 2.74]
3	3.42	[3.35, 3.52]	3.40	[3.33, 3.50]	3.90	[3.43, 4.37]

[2]Mean magnitude of the original earthquake catalogs (raw data) at each cut-off magnitude in the Parkfield catalog, along with the low and high intensity subcatalogs that are created by considering only the earthquakes that occur during periods when the ETAS intensity function is below/above a certain threshold.

artefact, implying that larger earthquakes are more common during periods where there has been a large amount of recent seismic activity, in contrast to the independence assumption used in most mainstream models of seismic hazard (*Ogata*, 1988, 1998; *Turcotte et al.*, 2007; *Reasenberg and Jones*, 1989).

To better understand how substantial these correlations are, we also directly compare the average earthquake magnitudes during periods of high and low seismic activity. For each cut-off magnitude, we plot the calculated values of intensity against the magnitudes. As expected from Equation 3.2.0.1, low intensities dominate the dataset. This allows us to make a distinction between low and high intensity data. The average magnitude during both the high and low intensity period is shown in Table 3.2, along with a 95% confidence interval computed using a parametric bootstrap. The difference between the two periods can clearly be seen at all cut-off magnitudes, again implying that the magnitude correlations are genuine. Note that the wide confidence interval when using a cut-off magnitude 3 is due to the small number of large earthquakes in the catalog at that threshold level.

To aid interpretation, a visual representation of the above results is shown in Figure 3.5. This plot clearly shows that as the intensity increases, larger magnitudes are observed, therefore an increase in the seismic activity in the region can lead to earthquakes with higher magnitudes than average. These results persist through the different cut off magnitudes, although bigger error bars are observed when the cut off magnitude $M0$ is 3 due to significantly smaller data set.

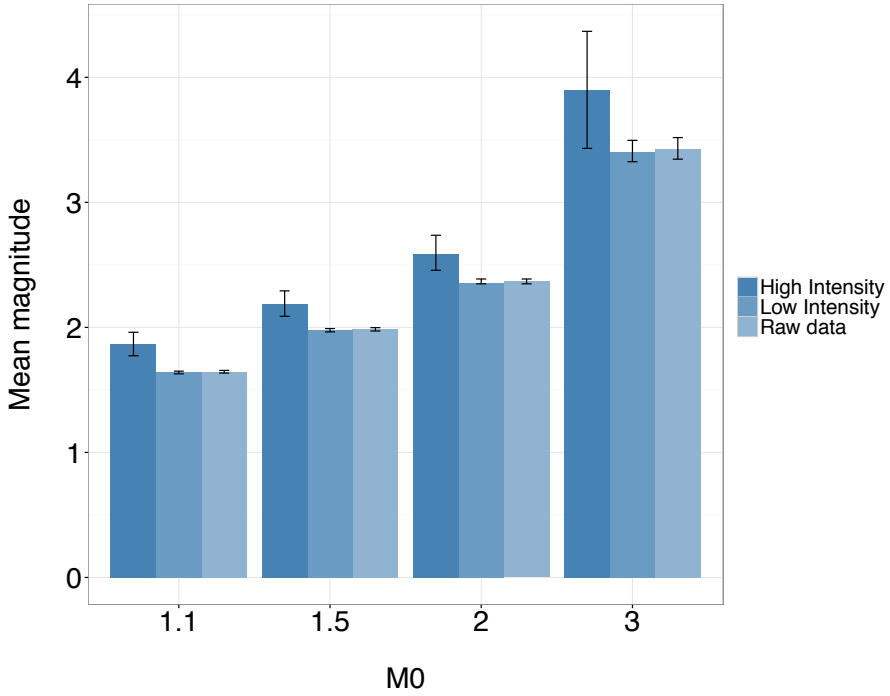

Figure 3.5: Mean earthquake magnitude for the raw data along with the high/low intensity subcatalogs, for each magnitude of completeness in the Parkfield catalog. The vertical lines indicate 95% confidence intervals.

As discussed in the previous section, the correlation coefficient only measures linear rather than nonlinear dependence. As such, we also directly compare the mean earthquake magnitudes during periods of high and low seismic activity. For each cut-off magnitude, subcatalogs containing the high and low intensity earthquakes were created using the top and bottom 10 % of the original data respectively and a Mann-Whitney test was used to compare the means. The resulting p-values are shown in the right hand column of Table 3.1, and the null hypothesis of equal magnitudes between the low and high intensity dataset is rejected when the cut-off magnitude is less than 3, again strongly confirming the existence of magnitude

correlations. For the cut-off magnitude of 3, the p-value of the test is 0.06 which is not quite significant at the standard 0.05 level. However since there are only 106 earthquakes with magnitude greater than 3, this is likely to be due to the small sample size. To investigate further, we performed a power analysis in order to establish whether the data set is big enough to detect the correlation when $M0 = 3$. This was done by repeatedly simulating synthetic high and low intensity catalogs from the original data using a bootstrap procedure, each with the same sample size as the observed high/low intensity catalogs. For each simulated dataset, a fixed value c between 0.01 and 0.5 was added to each earthquake in the high intensity catalog, so that the mean magnitude of that catalog would be on average c greater than the low intensity catalog. Then the Mann-Whitney test was performed on the simulated catalogs. Figure 3.6 shows the resulting power curves, which is the percentage of times the Mann-Whitney test correctly rejects the null hypothesis for each value of c. It can be seen that the power of the test is lower than 0.5 when c is less than around 0.3. Looking at Table 3.2, we can see based on the catalogs with a lower cut-off magnitude that we should expect the difference between the low and high intensity catalogs to only be around 0.2. As such, the most likely reason for obtaining a p-value slightly greater than 0.05 in the $M0 = 3$ case is due to the low power due to the small sample size.

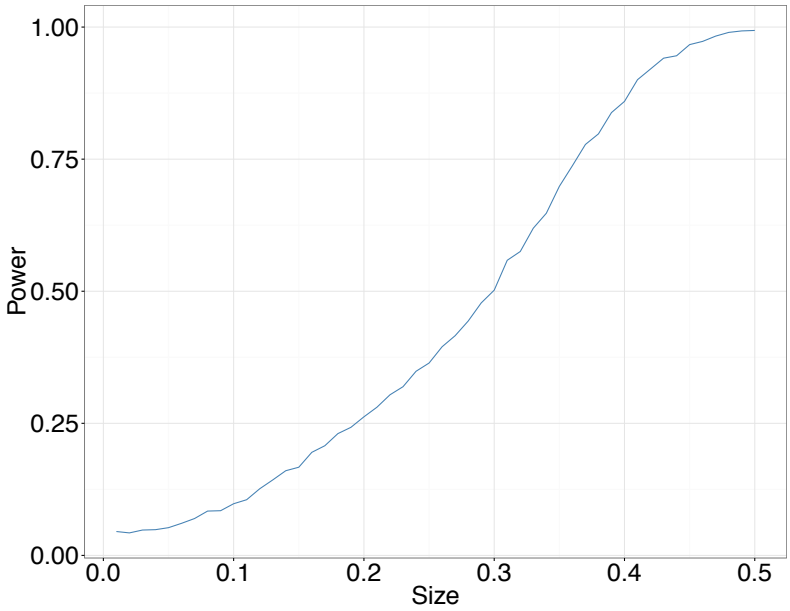

Figure 3.6: Power of the Mann-Whitney test for detecting magnitude differences between the low and high intensity catalogs, for each value of the magnitude difference c or size.

3.3.2 Southern California Conditional Intensity - Magnitude Correlation

To show that our findings about the existence of magnitude correlations are not unique to Parkfield, we also analyse a well-known Southern Californian catalog. Figure 3.7 shows the study area.

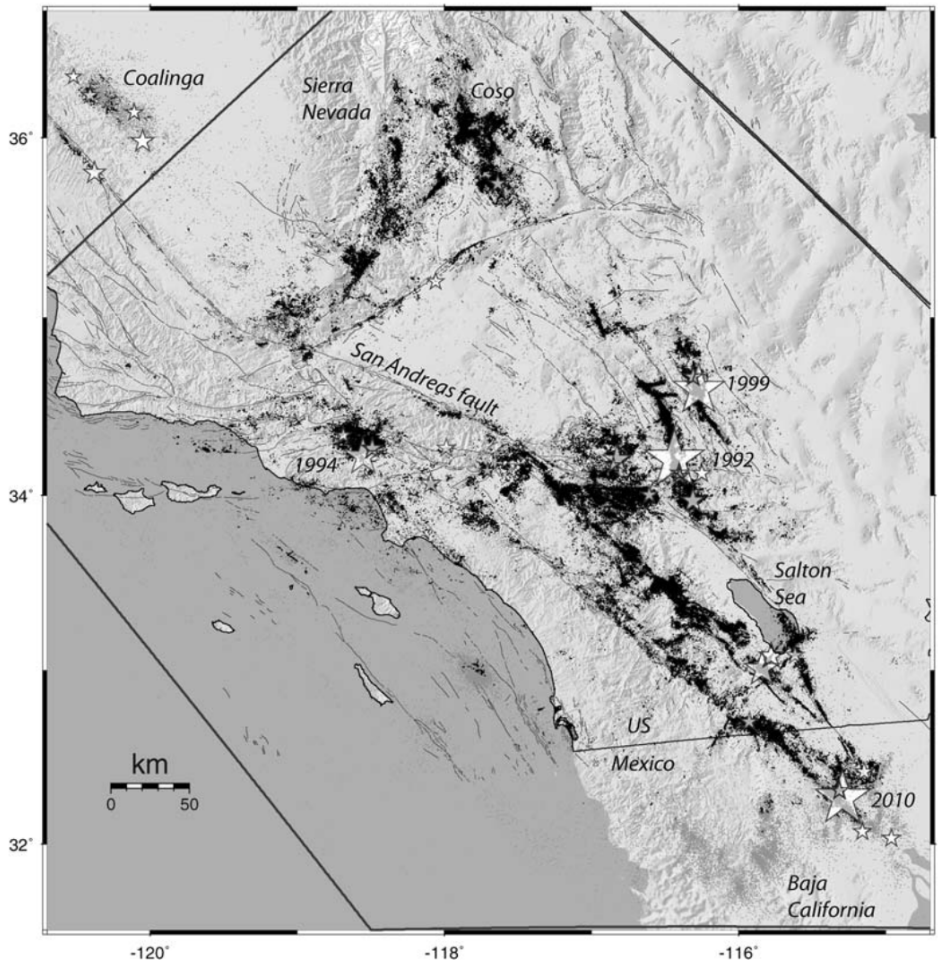

Figure 3.7: Map showing the study area in Southern California. The waveform-relocated epicenters are shown as black dots, the non relocated seismicity (events of type 3d, 1d, and xx) is shown as light grey dots, and earthquakes of M $\geq$ 5.5 are shown as stars. Quaternary faults are depicted as light grey curves. The large earthquake sequences are indicated by year: 1992 Mw 7.3 Landers; 1994 Mw 6.7 North- ridge; 1999 Mw 7.1 Hector Mine; 2010 Mw 7.2 El Mayor Cucapah. The polygon is the SCSN reporting area for local events. Events located outside this polygon are called regional events. US, United States of America. Figure and caption obtained from *Hauksson et al.* (2012).

The magnitude of completeness was estimated to be 1.9 using MBASS, and 1.5 using EMR. Additionally, due to the larger extent of this region, we also investigated how the magnitude of completeness varies over time due to catalog incompleteness, using the maximum curvature method from *Mignan* (2012) with window size of 500 events and 200 bootstraps. The resulting temporal variation of the magnitude of completeness can be seen in Figure 3.8, and is less than 2.7 across the whole catalog.

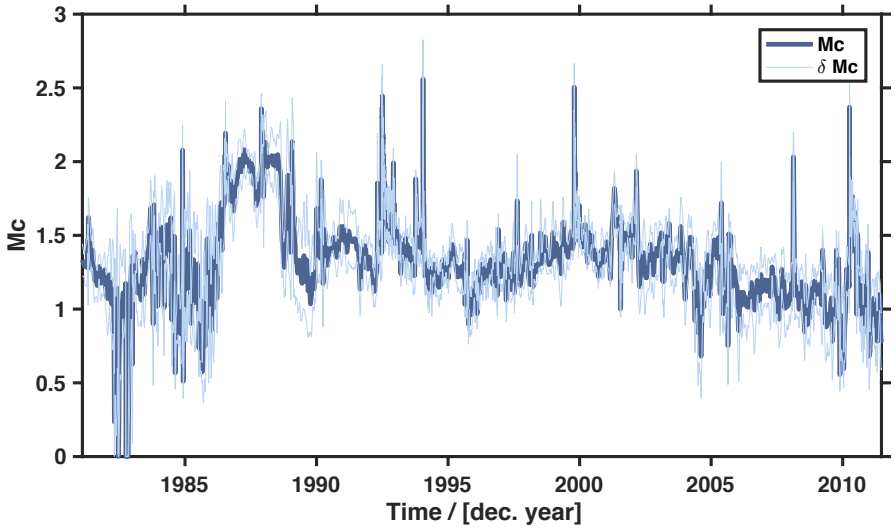

Figure 3.8: Temporal variation of the magnitude of completeness, found using the maximum curvature method from *Mignan* (2012)

The rate dependent estimation of the magnitude of completeness $M_c(t)$ was performed for all the mainshocks above magnitude 6 in the catalog. Figure 3.9 shows the results of this method on the 7.1 Hector Mine earthquake in 1999. In order to remove the effect of STAI during these periods of higher rate we remove from the data all the aftershocks between the mainshock and the time where the $M_c(t)$ drops to a level that doesn't exceed our cut off magnitude. In Figure 3.9 we show how this method is applied when the cut off magnitude is 3.5. All the aftershocks for a time period of 0.13 days were removed.

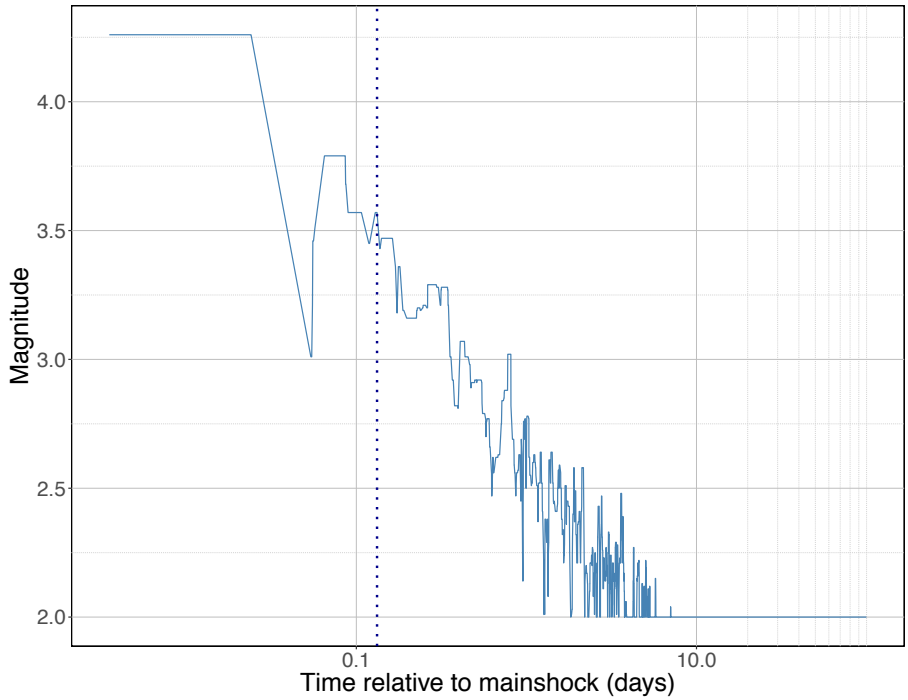

Figure 3.9: Short term aftershock incompleteness period after the Mw 7.1 Hector Mine earthquake. The dashed line defines the boundaries of the excluded events after the mainshock for cut off 3.5

By comparing Figures 3.8 and 3.9 we can see that only by applying the rate dependent magnitude of completeness we can capture the true effects of STAI immediately after a large earthquake.

Table 3.3 shows the correlation between the estimated ETAS intensity function, along with the associated 95% confidence interval and the p-values from the Mann-Whitney test comparing the mean magnitude of the earthquakes during the low and high intensity periods. Both results point strongly to the existence of magnitude correlations, even when using high cut-off magnitudes, suggesting that these are genuine rather than statistical artifacts.

In Table 3.4, we show the observed mean magnitude for the original catalog (raw data), along with the mean magnitudes during the high and low intensity periods. Again, the mean magnitude is substantially higher during high intensity periods, indicating that earthquake magnitude is indeed responsive to recent seismicity, rather

Table 3.3: Correlation between the magnitude of each earthquake in the Southern California catalog and the ETAS intensity immediately preceding it, along with 95% confidence interval. Also shown is the p-value of the Mann-Whitney test when comparing the mean earthquake magnitude in the high and low intensity regions.

M0	Correlation	Confidence Interval	Mann - Whitney test
2.5	0.19	[0.18, 0.21]	< 0.001
3	0.19	[0.16, 0.22]	< 0.001
3.5	0.18	[0.12, 0.22]	< 0.001
4	0.13	[0.05, 0.21]	0.02

than being independent as in the standard ETAS model. Figure 3.10 shows a graphical summary of these results.

Table 3.4: Mean magnitude of the original earthquake catalogs (raw data) at each cut-off magnitude in the Southern California catalog, along with the low and high intensity subcatalogs that are created by considering only the earthquakes that occur during periods when the ETAS intensity function is below/above a certain threshold.

	Original		Low Intensity		High Intensity	
M0	Mean magnitude	Confidence Interval	Mean magnitude	Confidence Interval	Mean magnitude	Confidence Interval
2.5	2.93	[2.90, 2.96]	2.90	[2.83, 2.98]	2.96	[2.88, 3.04]
3	3.43	[3.43, 3.44]	3.43	[3.43, 3.44]	3.54	[3.52, 3.56]
3.5	3.94	[3.93, 3.95]	3.94	[3.93, 3.95]	4.01	[3.98, 4.05]
4	4.45	[4.42, 4.47]	4.45	[4.42, 4.47]	4.49	[4.43, 4.56]

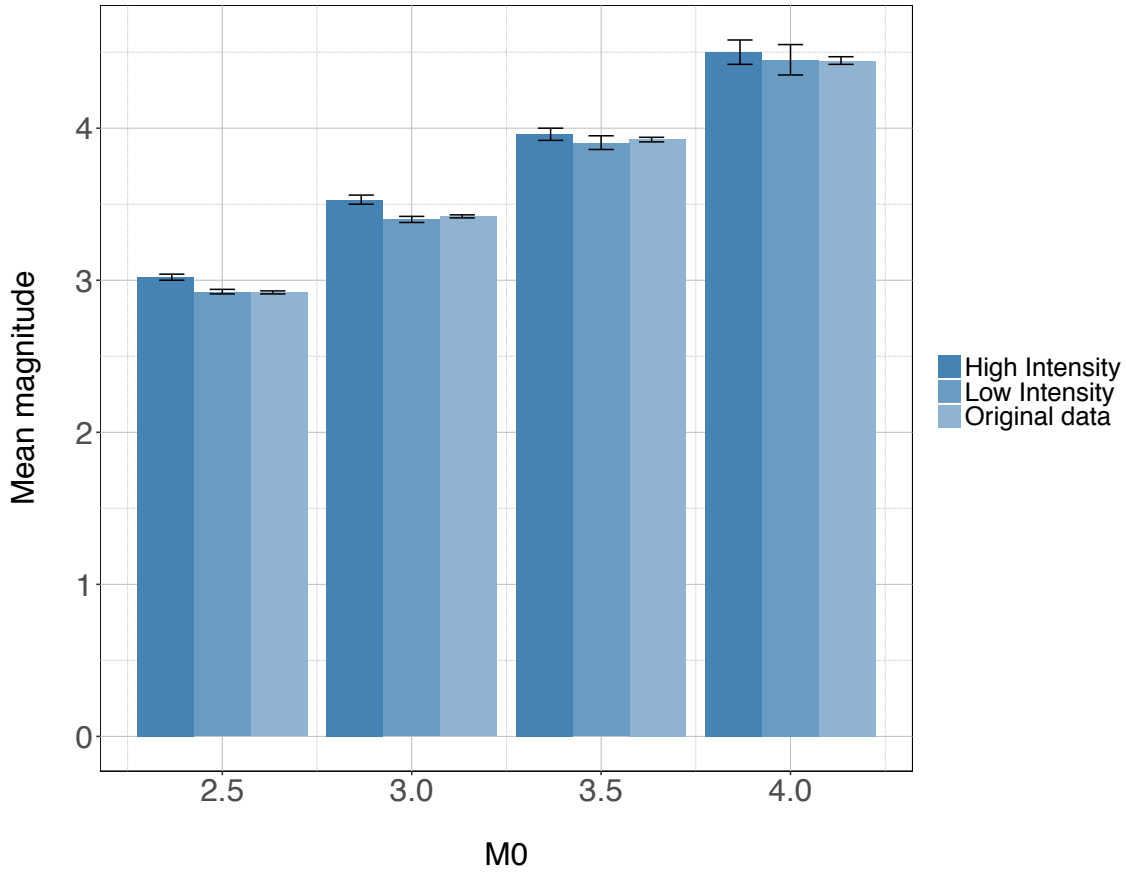

Figure 3.10: Mean earthquake magnitude for the raw data along with the high/low intensity subcatalogs, for each cut-off magnitude in the Southern Califonia catalog. The vertical lines indicate 95% confidence intervals

Using equation E.0.0.10 we can calculate the b value of the low and high intensity datasets from the mean magnitudes and find their difference. The resulting b values are shown in Table 3.5.

Table 3.5: Quantification of the b value variations between low and high intensity datasets for all the cut off magnitudes.

	Original		Low Intensity		High Intensity	
M0	Mean magnitude	b value	Mean magnitude	b value	Mean magnitude	b value
2.5	2.93	0.99	2.90	1.07	2.96	0.93
3	3.43	0.99	3.43	0.99	3.54	0.8
3.5	3.94	0.98	3.94	0.98	4.01	0.85
4	4.45	0.95	4.45	0.95	4.49	0.88

We can observe a decrease in the b value of about 0.1 between the low and high intensity data. As discussed previously in the thesis the ETAS model uses a constant b value for all the data and therefore introduces a bias to the resulting forecast. The significance of a 0.1 change in the b value during the periods of low and high intensity

in the probability of larger earthquakes is beyond the scope of this thesis however this is an interesting result and should be fully addressed in future work.

3.4 Synthetic catalogs - Validation of the proposed methodology

In this section the proposed methodology is applied to synthetic catalogs generated by the ETAS model with a constant b value and without correlations in the earthquake magnitudes. This aims to benchmark the significance of the results of the methodology developed in this thesis and to prove that earthquake magnitude correlations are not a spurious effect of the earthquake catalog and the ETAS model. If the proposed methodology is correct and the earthquake magnitude correlations are genuine then the synthetic catalogs should produce zero correlations. To generate the synthetic catalogs the Bayesian ETAS model of *Ross* (2017) was used. Using the b value and the ETAS parameters that were calculated when fitting the ETAS model to the original catalog as initial parameters we sampled 1000 posterior samples. Each posterior sample is a vector that contains a set of ETAS parameters. Each set was then used to generate a synthetic catalog in a specified period of time which was chosen to be equal with the maximum time of the original catalog and with a specified cut off magnitude. The first region that was chosen to validate the methodology was Parkfield. The small spatial extent, the lack of large earthquakes, and the stability of the b value make this area ideal for testing. Following the procedure described above, we generated 1000 synthetic catalogs for cut off magnitude 1.1 and 1000 catalogs for cut off magnitude 2 and applied the magnitude correlation methodology to each of these catalogs. In the case of cut off magnitude 1.1, 3 out of 1000 synthetic catalogs produced earthquake correlations and when the cut off magnitude was 2, 2 out of 1000 synthetic catalogs had magnitude correlations. This result is not statistically significant and demonstrates that the earthquake mag-

nitude correlations can not be due to spurious effects of the earthquake catalog. Synthetic catalogs were also generated for the Southern California. Due to the large number of events over the period of 30 years were this catalog was studied and for a cut off magnitude 3.5 it was computationally challenging to generate 1000 synthetic catalogs keeping in mind that conditions of subcriticality have to be met in order ETAS to generate a finite amount of events (*Helmstetter and Sornette*, 2002). For this region 2 catalogs were generated and the methodology was applied. These catalogs did not produce significant correlations. The results are presented in Appendix A.

3.5 Stochastic Declustering Methodology

Our proposed methodology for detecting magnitude correlations is based on the intensity function of the ETAS model. An alternative approach is to investigate directly the relationship between the magnitude of each mainshock in the catalog, and the average magnitude of its subsequent aftershocks. Positive correlations would imply that larger mainshocks tend to have larger aftershocks, which would suggest the existence of magnitude correlations. This approach was previously pursued by *Nichols and Schoenberg* (2014) on a global earthquake catalog, where evidence of small magnitude correlations was found. However it is unclear to what extent their results are biased by the extreme heterogeneity of earthquake behaviour across widely seperated seismic regions. As such, we repeat their analysis on the more local Parkfield catalog, and compare it to our results above.

The *Nichols and Schoenberg* (2014) method first declusters the catalog so that each earthquake is labelled as either a mainshock or aftershock. This is based on the stochastic declustering approach of *Zhuang et al.* (2002), which has been known to be quite inaccurate (*Sornette and Utkin*, 2009a). Next, for each such identified

Table 3.6: Correlation between the magnitude of each mainshock and the average magnitude of its aftershocks in the declustered Parkfield catalog, along with 95% confidence interval.

M0	Correlation	Confidence Interval
1.1	0.13	[0.09, 0.17]
1.5	0.05	[-0.01, 0.11]
2	0.06	[-0.01, 0.12]

mainshock, the average magnitude of its aftershocks is computed, and the correlation between the two quantities is obtained over the whole catalog.

Table 3.6 shows the results of applying this method to the Parkfield catalog. It can be seen that when using a cut-off magnitude of 1.1, substantial magnitude correlations are detected. However as the cut-off magnitude increases, this drops substantially suggesting that the observed correlations are at least partially due to STAI. Additionally during the periods of higher rate, the missing smaller earthquakes could lead us to wrongly infer that the mean magnitude of the higher rates has increased. Since declustering does not remove the STAI periods and adds additional bias *Veen and Schoenberg* (2008). For cut-off magnitude, $M0 = 3$, the number of data points were too small to find correlations.

In contrast, the proposed methodology is able to discover larger correlations, which are stable even when the cut-off magnitude is increased well above the value estimated by MBASS. From Table 3.6 its clear to see that only when the cut-off magnitude is 1.1 we obtain significant correlation.

As in the case of Parkfield, we also applied the declustering methodology of *Nichols and Schoenberg* (2014) to the Southern Californian catalog. We use the same cut-off magnitudes of 2.5, 3, 3.5, and 4 that were used above, and perform the declustering and correlation analysis. The results are shown in Table 6, where it can be seen that the estimated correlation sharply decreases as the cut-off magnitude is raised, disappearing entirely when it reaches a value of 5. Again this suggests that the correlations may be spurious. In contrast, the correlations found using our approach persist across the whole range of cut-offs as shown in Table 3.7.

Table 3.7: Correlation between the magnitude of each mainshock and the mean magnitude of its aftershocks in the declustered Southern California catalog, along with 95% confidence interval.

M0	Correlation	Confidence Interval
2.5	0.11	[0.10,0.13]
3	0.08	[0.04,0.11]
3.5	0.07	[0.004, 0.14]
4	-0.01	[-0.11, 0.09]

Similarly to Southern California the intensity - magnitude correlation methodology had better performance than the stochastic declustering methodology.

3.6 Applications in a variety of tectonic settings

In the previous section, the existence of small but significant earthquake magnitude correlations in California was confirmed. In this section I seek to test the methodology in different regions worldwide. The regions were chosen based on their tectonic setting because of the variations of the earthquake size distribution in different stress regimes (*Scholz*, 1968a; *Narteau et al.*, 2009; *Schorlemmer et al.*, 2005; *Smith*, 1981; *Gulia and Wiemer*, 2010; *Sammonds et al.*, 1992; *Main et al.*, 1992; *Sammonds and Ohnaka*, 1998; *Urbancic et al.*, 1992; *Huang and Turcotte*, 1988). As discussed in the previous section, stable b values across the study area ensures that rate changes will not cause increase in the magnitude of completeness and secondly reduces the bias introduced by the ETAS assumption of a singular b value for the entire region under study. Firstly I will provide the basic theory of tectonic plate theory, the different types of faults associated with each boundary and then explain how this is related to the statistical analysis of earthquake catalog and experimental data.

3.6.1 Tectonic boundaries and faulting type

There are three types of tectonic settings *Lay and Wallace* (1995):

1. Divergent boundaries, where two plates are moving apart and new lithosphere is produced or old lithosphere is thinned. Midoceanic ridges and continental rifts are examples of divergent boundaries.

2. Convergent boundaries, where lithosphere is thickened or consumed by sinking into the mantle. Subduction zones and alpine belts are examples of convergent plate boundaries.

3. Transcurrent boundaries, where plates move past one another without either convergence or divergence. Transform faults and other strike-slip faults are examples of transcurrent boundaries.

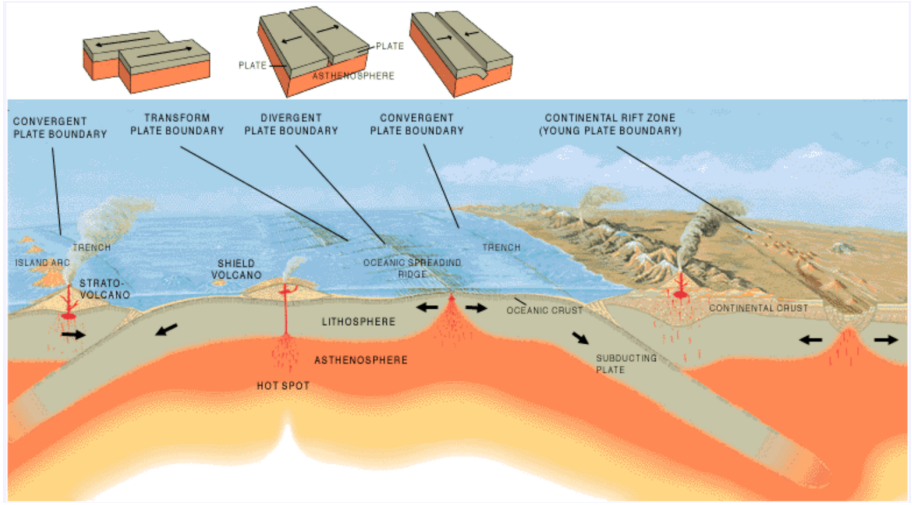

Figure 3.11: The three main types of tectonic boundaries shown in a cross section. Figure obtained from https://pubs.usgs.gov/gip/dynamic/Vigil.html

A fault is a planar fracture or discontinuity in a volume of rock, across which there has been displacement as a result of rock mass movement. In a normal fault the hanging wall moves downwards compared to the footwall as shown in Figure 3.12. Normal faults are common in divergent boundaries.

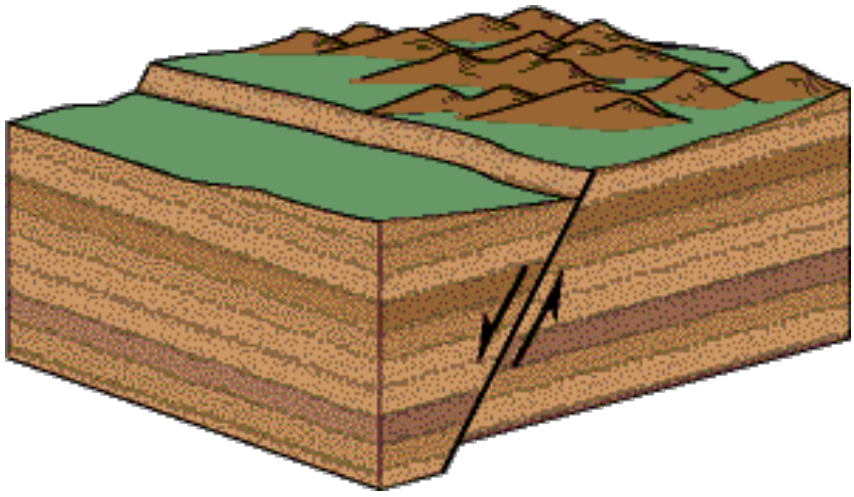

Figure 3.12: Schematic illustration of the relative motion of the rock mass in a normal fault. Figure obtained from https://geomaps.wr.usgs.gov/parks/deform/

In a reverse/thrust fault the hanging wall moves upwards compared to the footwall as shown in Figure 3.13. These faults are common in convergent boundaries.

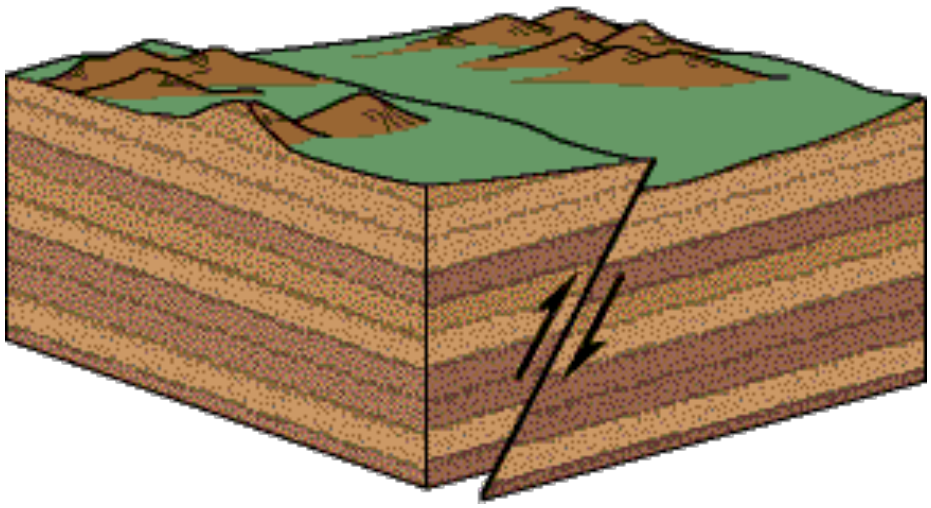

Figure 3.13: Schematic illustration of the relative motion of the rock mass in a reverse fault. Figure obtained from https://geomaps.wr.usgs.gov/parks/deform/

In a strike slip fault the hanging wall moves upwards compared to the footwall as shown in Figure 3.14. Strike slip faults are found on transcurrent boundaries.

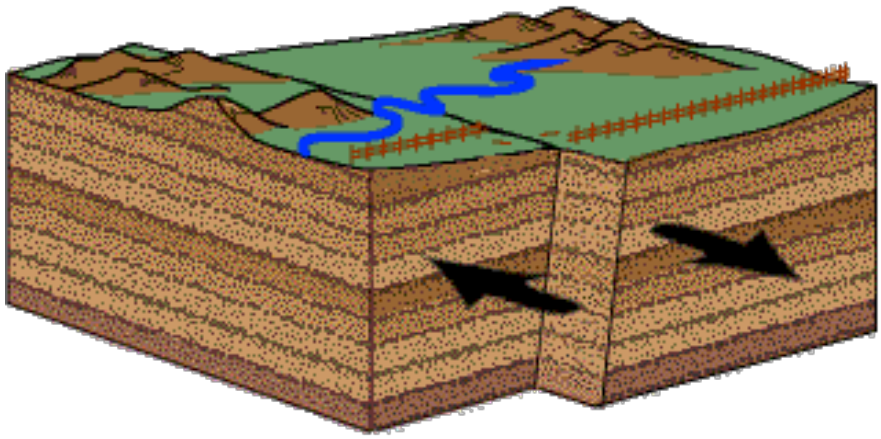

Figure 3.14: Schematic illustration of the relative motion of the rock mass in a strike slip fault. Figure obtained from https://geomaps.wr.usgs.gov/parks/deform/

3.6.2 Variations of the b value

Scholz (1968a), was the first to report the dependancy of the b value to the level of stress when studying rock deformation in the laboratory. The b value was determined from acoustic emission (AE) measurements. Since then the dependency of the b value with stress expanded to studies of earthquake catalog data. In *Schorlemmer et al.* (2005) the b value variations and their dependence on different styles of faulting are shown. The earthquakes associated with each type of faulting was on the basis of the rake angle λ[1], within a range $\pm\ \gamma$. The faulting type is characterised strike slip when $\lambda = 0$ or $\lambda = \pm 180\,^{\circ}$, thrust when $\lambda = 90\,^{\circ}$ and normal when $\lambda = -90\,^{\circ}$. According to this study normal faulting events have the highest b values, thrust faulting the lowest and strike slip intermediate values. Since thrust faults tend to be under higher stress than normal faults he concludes that the b value depends inversely on differential stress.

The paper of *Gulia and Wiemer* (2010), also reaches the same conclusion regarding the relationship of the b value with the stress levels and suggest that the faulting type to be included into the recurrence rates estimation in probabilistic seismic hazard assessments.

Fractals and fractal statistics, are commonly used to describe a variety of natural processes. In *Huang and Turcotte* (1988), the authors used a fractal distribution of stress and strength to simulate a two dimensional fault zone and concluded that the b value is inversely proportional to stress and proportional to the fractal dimension of the stress - strength distribution[2]. The fractal dimension of the stress - strength distribution is also associated with the temporal changes of the b value during an earthquake cycle.

[1]Rake is the angle between a line [or a feature] and the strike line of the plane in which it is found, measured on the plane.

[2]The fractal dimension for regional seismic activity is twice the b value.

Double shear frictional sliding experiments in granite and monitoring of AE 's are studied in *Sammonds and Ohnaka* (1998). It is shown that steady stable sliding on smooth surfaces produces lower b values than rough surfaces, and that the b value decreases before a stick slip instability.

The temporal variation of the b value (the b value is increasing prior a large earthquake) during an earthquake cycle in New Zealand has been shown by *Smith* (1981).

In *Main et al.* (1992) a theoretical model that relates the mean energy release $\langle G \rangle$, the event rate N and the b value with the state of damage of a fractal population of cracks is developed. Based on the relation of the b value with the mean energy release $\langle G \rangle$ they define three types of quiescence. The model can be used to detect changes in $\langle G \rangle$ from AE. Higher b values correspond to lower stress intensity [3] or greater material heterogeneity. The authors report that the inverse relation of stress and b value as shown in *Scholz* (1968a) does not apply for a whole failure cycle in laboratory experiments.

The work of *Sammonds et al.* (1992) expands this idea and describes the role of pore fluids in the temporal variation of the b value. The authors showed that experiments in Darley Dale sandstone performed under constant pore fluid pressure are significantly weaker compared to experiments in air dried samples due to the additional chemical influence of the pore fluid on the sample. Prior to failure, a short term b value minimum is observed (as with the air dried samples) as well as a second intermediate b value minimum. During experiments with constant pore fluid pressure a single b value minimum is observed.

[3] The stress intensity factor predicts the stress intensity near the tip of a crack caused by a remote load or residual stresses.

3.6.3 The role of b value in the study of magnitude correlations

Statistical models like ETAS generate the earthquake magnitudes independently from a Gutenberg - Richter law with a constant b value. As discussed previously the b value is negatively correlated with the differential stress and consequently the faulting type; therefore when studying a region characterised by a variety of faulting types it is likely the time and space varying b value will bias the ETAS estimates. To ensure our methodology is robust, in this section we select regions dominated by a single type of faulting. The regions at first instance are chosen based on published scientific studies that describe faulting type in the area and then the variations of the b value are calculated to ensure stability. The quality of the data and the timeframes during which I performed my analysis where carefully selected in order to avoid biases from changes in the seismic network, the velocity models and the location algorithms.

3.6.4 Application in the western Corinth Gulf, Greece

The western Corinth Gulf is located in the north - west part of Peloponnesos, Greece. It is characterised by extension and is considered one of the most seismically active regions in the world. The opening rate is between 11 and 16 mm yr^{-1} and is dominated by North dipping normal faults and South dipping antithetic faults (*Avallone et al.*, 2004; *Bell et al.*, 2008). The western Corinth gulf is among the highest hazard regions in Greece and Europe (*Segou*, 2016) and has experienced destructive historical earthquakes (*Papazachos et al.*, 1997), moderate modern seismicity that ranges between Mw 5 and Mw 6.5 and frequent swarm [5]activity.

[5]Swarms are sequences of earthquakes that are clustered in space and time and are not associated with an identifiable mainshock.

The area of study includes earthquakes within (37.80N - 38.44N, 21.2E - 22.1E) from 1/1/2011 - 13/6/2016 and is shown in 3.15. The dataset is obtained from the National Observatory of Athens (Institute of Geodynamics). Information about the history, development and quality of the seismic network can be found at *Chouliaras* (2009); *Mignan and Chouliaras* (2014)

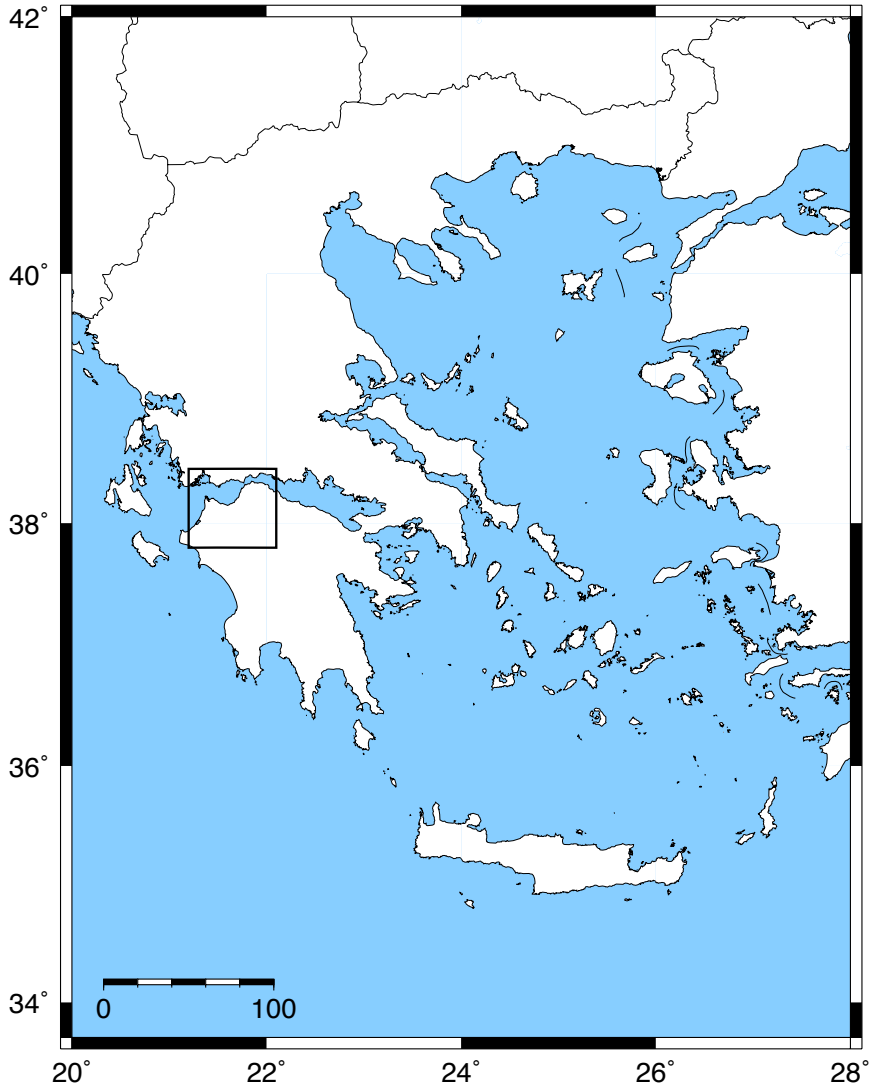

Figure 3.15: The study area of the western Corinth gulf is denoted by a black box.

Table 3.8: Correlation between the magnitude of each earthquake in the western Corinth catalog and the ETAS intensity immediately preceding it, along with 95% confidence interval. Also shown is the p-value of the Mann-Whitney test when comparing the mean earthquake magnitude in the high and low intensity regions.

M0	Correlation	Confidence Interval	Mann - Whitney test
1.5	0.07	[0.04, 0.10]	< 0.001
2	0.05	[0.01, 0.10]	< 0.03

I have chosen this region for the following reasons:

1. The local strain rate is larger and the microseismic activity are higher in the western part of the gulf (*Bernard et al.*, 2006). That insures abundance of data to perform the analysis.

2. Recent seismicity does not include earthquakes over Mw 6 which are the main causes for STAI in earthquake catalogs.

3. The b value is stable with increasing rate.

As in the previous case studies in California, I start by calculating the magnitude of completeness (Mc) using the EMR and MBASS methods. The Mc was found to be 1.5 and the cut off magnitudes (M0) chosen to perform my analysis are 1.5 and 2. At these cut off magnitudes the catalog contains 5753 and 1840 earthquakes, respectively.

The variations of the b value with increasing seismicity rate is shown in Figure 3.16. Since the b value is stable, the impact of STAI in the determination of magnitude correlations is minimum.

The analysis described in section 3.2 is applied in western Corinth gulf showing positive magnitude correlations and increase in the mean magnitude in the high intensity data. Table 3.8 below shows the results. The mean magnitudes of the raw, low and high intensity data are shown in figure 3.17.

Applying the methodology in a region dominated by one faulting type and with stable b values during the time period studied provided the opportunity to validate the

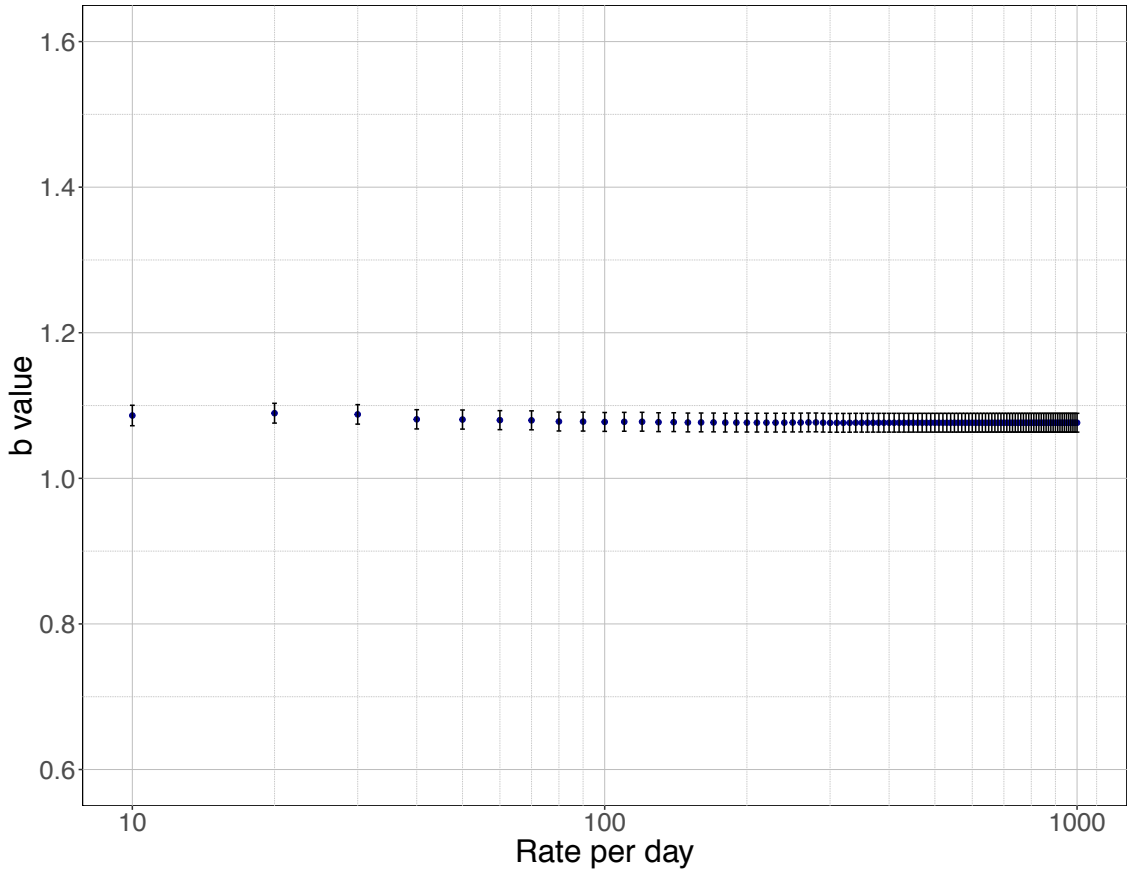

Figure 3.16: Rate varying estimation of the b value.

robustness of the technique. The results showed positive and significant magnitude correlations using both the direct intensity-magnitude correlation and confidence intervals but also by comparing the mean magnitudes of the low and high and low intensity data with the non parametric Mann Whitney test. Compared to California, in this region smaller correlations were observed.

3.6.5 Application in an aftershock sequence south of Crete, Greece

The Hellenic Subduction Zone (HSZ), where the African and Aegean tectonic plates converge is one of the most seismically active regions worldwide. The complex active tectonics of the region became the centre of interest for many studies such as *McKenzie* (1970, 1972); *Angelier et al.* (1982); *Jackson* (1994); *Papanikolaou and*

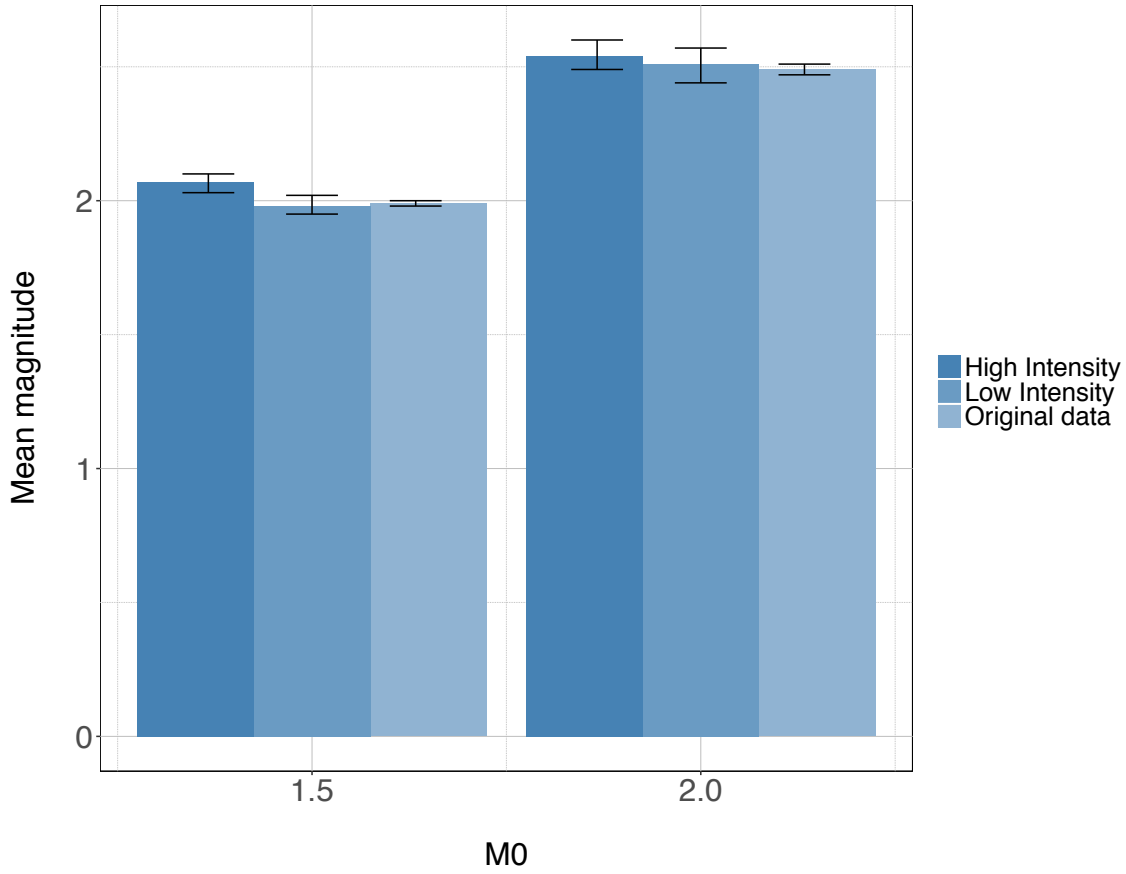

Figure 3.17: Mean earthquake magnitude for the original (raw data) along with the high/low intensity subcatalogs, for each cut-off magnitude M0 in the western Corinth gulf catalog. The vertical lines indicate 95% confidence intervals

Vassilakis (2010); *Royden and Papanikolaou* (2011) among others. In Figure 3.18 the HSZ is shown along with the main geologic structures of the Hellenides.

Here we analyse the aftershock sequence of a Mw 6.3 earthquake that occurred on 01/07/2009 at 33.84N 25.43E. It is a shallow (depth=7Km) thrust faulting earthquake that according to *Shaw and Jackson* (2010) occurred along a splay [6] in the overriding Aegean plate. In the same study this earthquake is compared to an earthquake that occurred 20 km to the west with depth 43 km. This deeper earthquake it shown to be in the subduction zone interface. From this comparison they infer that splay faults branch from the main subduction zone.

[6]Splay faults are one of a series of branching synthetic faults near the termination of a major fault which spread the displacement over a large area.

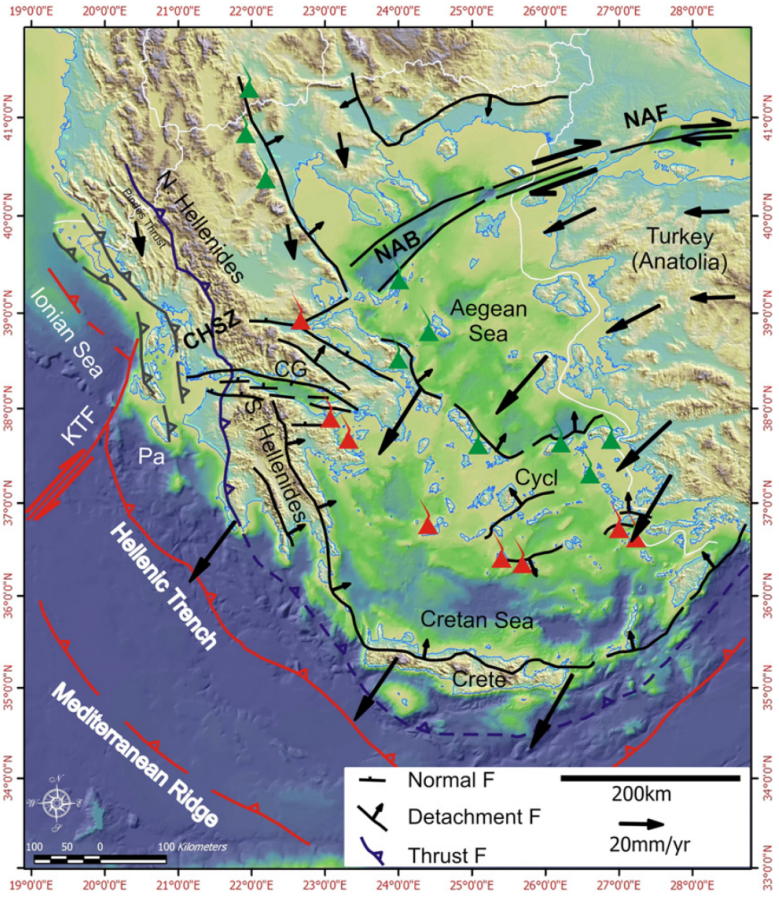

Figure 3.18: Main geologic structures of the Hellenides and the Aegean Sea (location indicated by inset to Fig. 2c). Barbed lines indicate thrust fronts for the most external unit(s) of the Hellenides. Red and green triangles indicate the modern and Miocene volcanic arcs, respectively. Large arrows with symmetric heads are GPS velocities in the Eurasian reference frame. Central Hellenic Shear Zone (CHSZ); Gulf of Corinth (CG); North Aegean Basin (NAB); North Anatolian Fault (NAF); Kephalonia Transform Fault (KFT); Paxos Zone (PA). Figure taken from *Papanikolaou and Vassilakis* (2010)

In figure 3.19 the focal mechanism [7] of this earthquake is shown. From this is confirmed that thrust is the faulting mechanism.

[7]The focal mechanism is constructed for representing the geometry of an earthquake as an infinitesimal planar fault upon which slip has occurred; defined by its strike (angle between map-view representation of the fault plane and North), dip (angle between in-plane representation of the fault plane and the surface of the earth), and rake (the direction the hanging wall moves during rupture, measured relative to strike

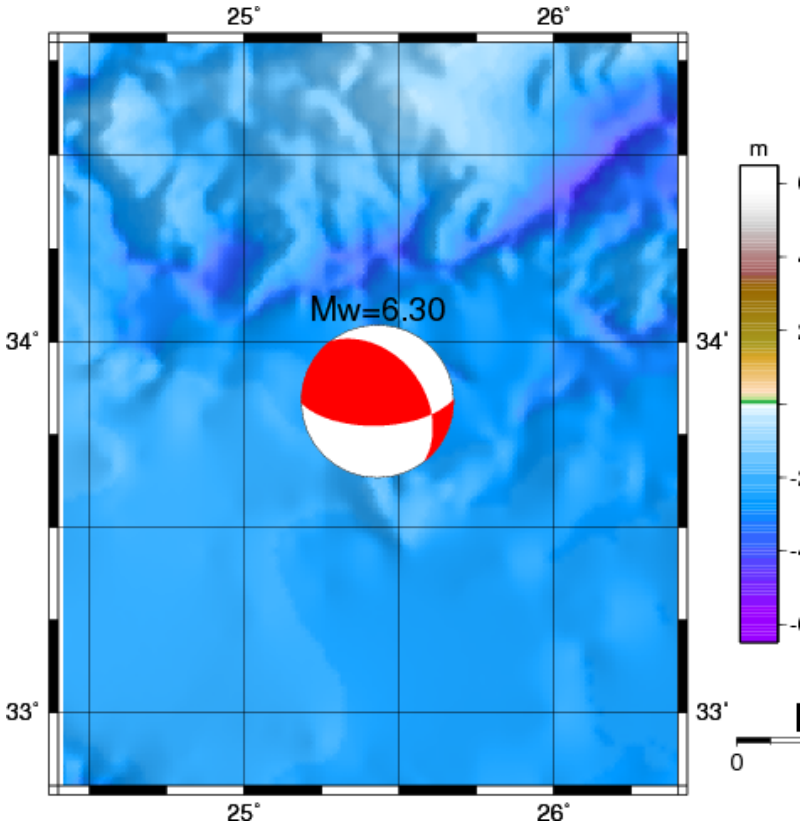

Figure 3.19: Focal mechanism solution of the 01/07/2009 earthquake south of Crete. The image is obtained from the National Observatory of Athens http://bbnet.gein.noa.gr

I have chosen this region for the following reasons:

1. After examining earthquake magnitude correlations in strike slip and normal faulting environments we seek to test our methodology in convergence tectonic setting such as a subduction zone. The HSZ is one of the most seismically active regions and therefore it was considered a study area. However, the complex active tectonics that govern this area comprises of thrust, normal and strike slip faults and it is difficult to distinguish a region that thrust faulting dominates. As such, we focused on an Mw 6.3 earthquake aftershock sequence generated by a thrust fault.

2. This earthquake occurred on the HSZ interface (*Shaw and Jackson*, 2010)

3. The b value is stable with increasing rate of seismicity.

The data we used contain all the earthquakes in 2009 and 2010 within a distance five times the rupture length as defined in equation 3.2.0.2. This corresponds to 17.13 km radius.

As before, we calculate the rate dependent magnitude of completeness. The b value is stable throughout the different rates as shown in 3.20 and therefore we can proceed to the magnitude correlation analysis without removing any data. For this dataset the magnitude of this data was estimated at 3.1 with the EMR method.

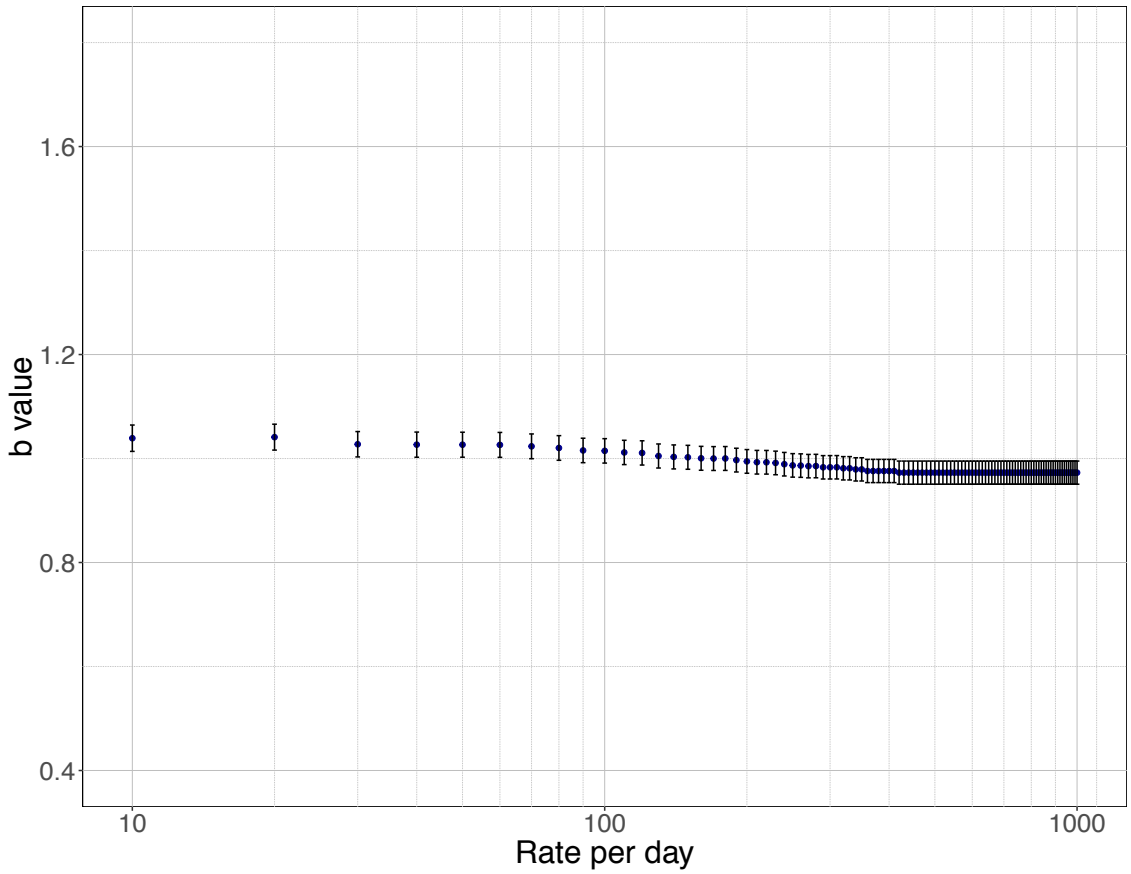

Figure 3.20: Rate varying estimation of the b value.

We apply the magnitude correlation method thresholding at M0= 3.1 and obtain the results shown in table 3.9. We can conclude that the magnitudes are correlated.

Table 3.9: Correlation between the magnitude of each earthquake in the aftershock sequence and the ETAS intensity immediately preceding it, along with 95% confidence interval. Also shown is the p-value of the Mann-Whitney test when comparing the mean earthquake magnitude in the high and low intensity regions.

M0	Correlation	Confidence Interval	Mann - Whitney test
3.1	0.08	[0.004, 0.17]	< 0.03

3.7 Key findings - discussion

The scope of this chapter was to develop a new methodology to search for earthquake magnitude correlations, and to hence demonstrate their existence. To validate our methodology we used two different study areas n California and regions in Greece based on the dominate faulting type:

(i) Parkfield, which lies in the creeping section of the San Andreas Fault

(ii) The entire Southern California region.

(iii) The Western Corinth Gulf, which is dominated by normal faults.

(iv) An aftershock sequence South of Crete with a thrust fault focal mechanism.

Strong evidence of magnitude correlations is found, with the earthquake magnitudes being substantially larger during periods where the ETAS intensity function is high, which corresponds to high degree of recent seismicity.

Unlike the methodology of *Lippiello et al.* (2008, 2012) which only considered correlations between pairs of successive earthquakes, our method uses the whole catalog simultaneously and is hence robust to the criticism of *Davidsen and Green* (2011) who claimed that correlations are due to incompleteness. Indeed, incompleteness after large earthquakes can bias the results of any statistical analysis therefore we performed a rate dependent calculation of the magnitude of completeness in order to remove events during this period and to ensure the high quality of the data.

The correlations found persist even when the cut-off magnitude is raised well above the estimated value for the catalogs. In relation to the faulting type, larger correla-

tions were observed on the strike slip environment. The thrust and normal faulting earthquakes have similar correlation values. As such, we cannot draw conclusions on the influence of the stress level to the magnitude correlations.

The fact that earthquake magnitudes seem to be dependent on recent seismic activity has strong implications for earthquake forecasting, since it implies there may be a degree of predictability of aftershock magnitude, based on the associated magnitude of the mainshock. This may allow for more accurate forecasts than those given by standard seismicity models such as ETAS, which make strong assumptions of independence.

The approach developed here uses the conditional intensity of the Epidemic Type Aftershock Sequence (ETAS) model as a proxy for the local level of seismic activity. Several regions in California and Greece have been studied using this methodology, and is found that the mean magnitude of earthquakes is higher during periods of high seismic activity, demonstrating the existence of small but significant correlations.

Chapter 4

Triaxial deformation of sandstone

4.1 Chapter outline

In the previous Chapters the concept of magnitude correlations is discussed and a new methodology to analyse earthquake catalog data is developed. To take the analysis one step further AE data from triaxial deformation experiments in sandstone samples are analysed and used as proxies for earthquakes. In this chapter the experimental procedure; from preparing samples to deformation will be described. In the following chapter the analysis of the data collected from these experiments is described.

The rock type used for all the experiments is Darley Dale sandstone, a Millstone Grit of Carboniferous age. It is poorly graded quartz-feldspathic sandstone bound with siliceous cement. Approximately 75% of the mineral content is quartz, 10% feldspar (plagioclase and microcline) and 15% clay and other minerals forming the remainder; grains show angular to sub-angular geometry ranging between 0.1 and 0.3mm (*Eccles et al.*, 2005). It is widely used in rock physics due to excellent

experiment reproducibility (*Clint*, 1999) and for its relative homogeneity (*Baud and Meredith*, 1997). All the samples were cored from the same batch of sandstone blocks and prepared to be used in the triaxial apparatus.

In Figure 4.1 below the stress stress strain curves of two laboratory experiment is shown. Darley Dale samples deform in the same manner, and this reproducibility makes them ideal for study in the laboratory.

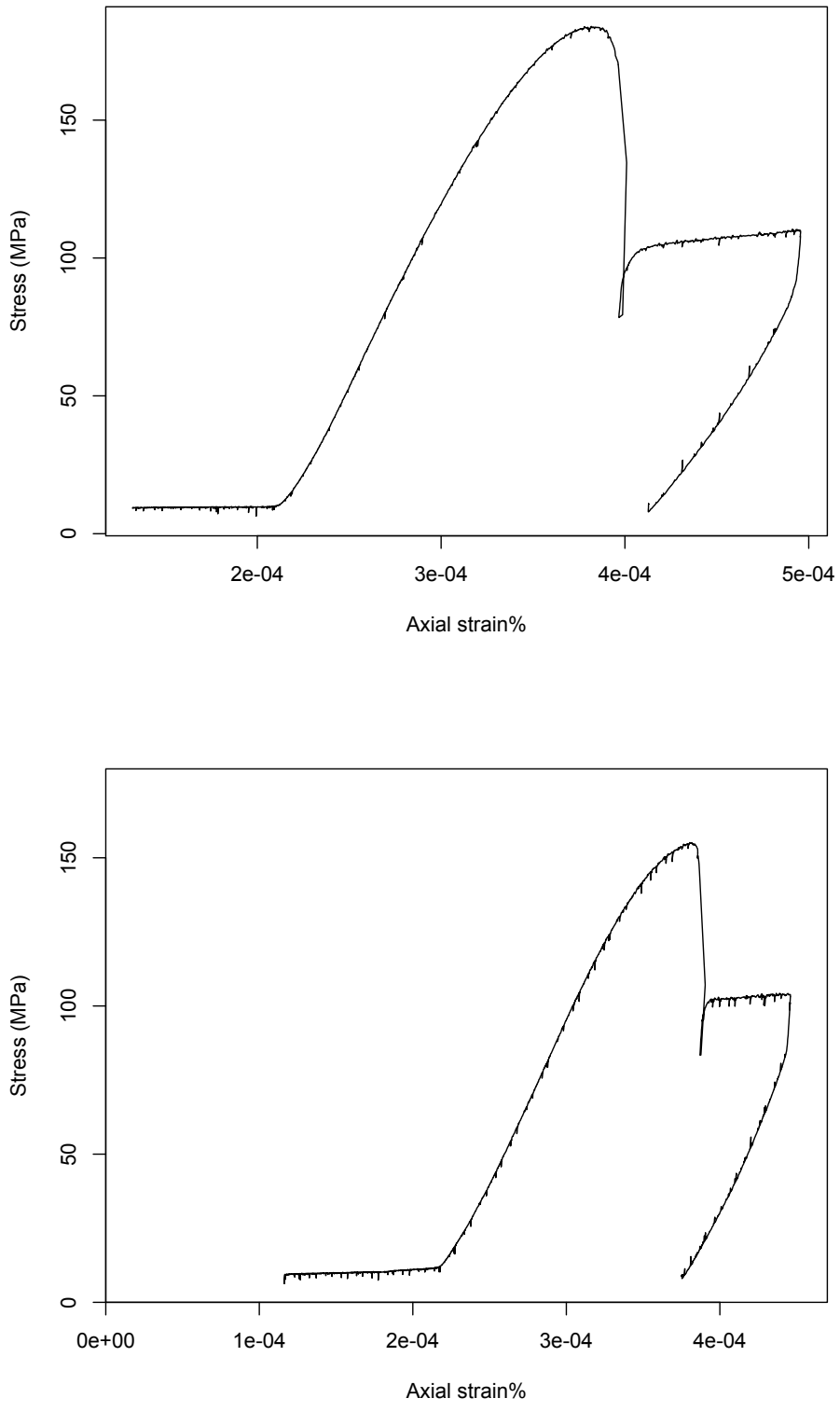

Figure 4.1: The characteristic stress and strain curves of triaxially deformed Darley Dale sandsone. It is shown that different samples are deformed in the same manner, making Darley Dale an excellent rock to use in the laboratory.

4.2 Rock sample preparation

4.2.1 Coring and grinding

Rock preparation is an essential element of the experiment procedure. A systematic approach helps to eliminate errors and therefore comparisons between results of different samples can be made. Cylindrical samples of 40mm diameter and 130mm length are initially cored using a using a diamond impregnated coring drill. The sandstone block is clamped into place and the coring drill is lowered at a steady rate to avoid damaging the sample. Throughout coring; water is used to cool the coring drill. Figure 4.2 shows the drilling of the sample.

Figure 4.2: Coring a Darley Dale sandstone sample.

The ends of the sample are cut further using a diamond sintered circular saw before to be ground to exactly100mm (±0.02 mm) with a diamond sintered grinding wheel. This is to ensure all samples have a 2:5:1 length:diameter ratio (*Mogi*, 1966). As shown in figure 4.3 below, during grinding the sample is held in place with two

stainless steel blocks that are magnetically attached to the machine. A water-oil (Ultragrind lubrication oil) mixture was used to lubricate the grinding wheel whilst it was slowly lowered onto the sample in very small increments to prevent damaging the sample and grinding apparatus. The grinding ensures that both ends of the sample are flat and parallel, so that an even distribution of stress is applied to the sample during the experiment (*Hawkes and Mellor*, 1970).

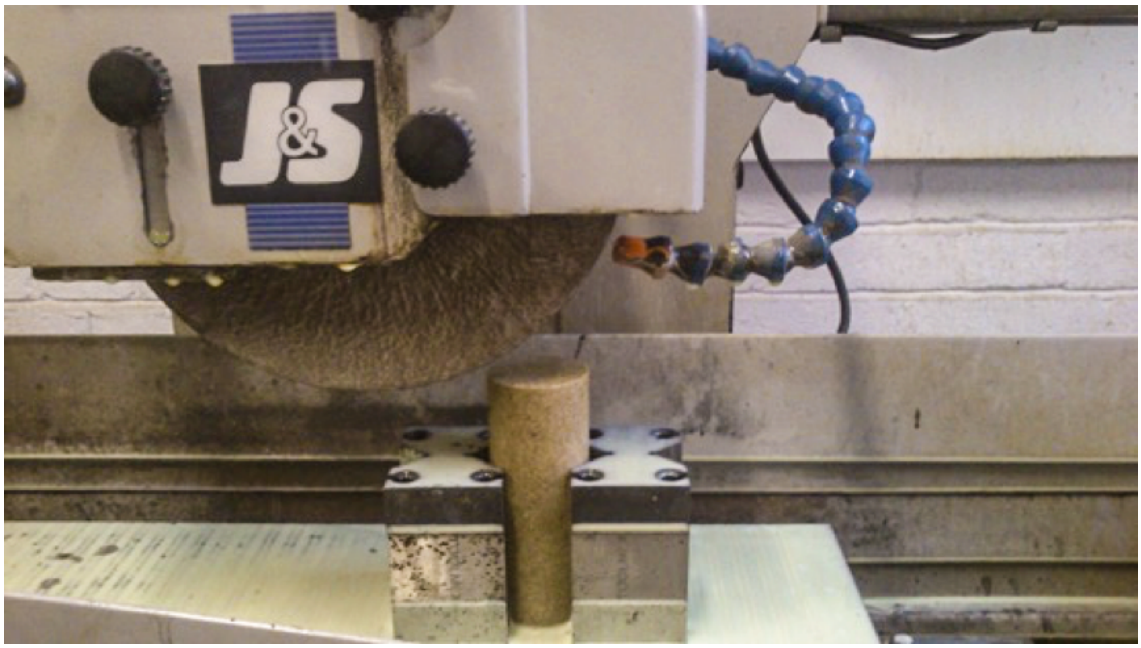

Figure 4.3: Grinding the sample

The samples are washed with water to remove oil that remained from grinding. They were placed in an oven to air dry at 60°C. At this temperature thermal cracking is not observed (*Glover et al.*, 1995).

The procedure above refers to the preparation of intact samples. For my experiments I additionally made a saw cut sample. The difference from the intact sample is that I made a cut in a 30° angle to the sample. Each side of the cut surfaces as well as the top and bottom sides where ground to be flat and parallel and to ensure the sure the total length is 100 mm. The saw cut sample was made to study fracture in conditions were fractures pre-exist. This is a realistic scenario since earthquakes typically occur on pre-existing faults in the crust.

4.2.2 Saturation

The majority of the experiments performed in water saturated samples. The air dried samples are submerged in a bell jar with distilled water. The jar then closes and connects to a vacuum pump. Sandstones have high porosity therefore the time spent under vaccum was approximately 10 minutes. Then the vaccum pump was closed and the samples remained in the jar for 24 hours.

4.2.3 Porosity calculation

To be able to compare results from different experiments we had to ensure that the porosity between the samples had no more than 2% difference (*Heap*, 2009). As such, porosity calculations were made to select the samples to be used in the experiments.

We use Archimedes's Principle which states that an object submerged in a fluid is buoyed by a force that is equal to the weight of the displaced fluid, to calculate the porosity.

Porosity ϕ is fraction of the volume of voids over the total volume as shown in equation 4.2.3.1.

$$\frac{V_p}{V_b} \tag{4.2.3.1}$$

The volume of fluids (V_p) is defined defined as:

$$V_p = \frac{W_{sat} - W_{dry}}{p_f} \tag{4.2.3.2}$$

were W_{sat} is the weight of the sample saturated with water, W_{dry} is the weight of the air dried sample and p_f is the density of the water.

The total volume (V_b) is defined as:

$$V_b = \frac{W_{sat} - W_{sub}}{p_f} \tag{4.2.3.3}$$

were W_{sub} is the weight of the saturated sample submerged in water. Porosity is calculate according to equation 4.2.3.4 were M_{sat}, M_{dry} and M_{sub} is the mass of the water saturated , air dried and submerged sample respectively.

$$\phi = \frac{M_{sat} - M_{dry}}{M_{sat} - M_{sub}} \tag{4.2.3.4}$$

4.3 Triaxial Rock Physics Ensemble

To simulate the stress conditions in the earth's crust and study rock fracture we used the triaxial rock physics apparatus designed by *Sammonds* (1999) at the Rock and Ice Physics Lab, University College London.

The most common way to achieve triaxial state of stress is to superimpose a hydrostatic pressure and a uniaxial stress. This means that normal stress σ_2 and σ_3 are equal during the experiment. The advantage of the triaxial test is that captures the dependence of rock failure on both normal and shear stress especially during brittle fracture is observed (*Paterson and Wong*, 2005). Figure 4.4 shows the elements of any triaxial cell. Confining pressure is achieved from a liquid at high pressure that surrounds the specimen. A piston is advanced to apply axial force.

The triaxial deformation apparatus at the Rock and Ice Physics lab is shown in Figure 4.5

Axial load is applied via a 1500 kN servo-controlled hydraulic actuator that rests on a hemispherical seat to ensure even loading of the test specimen. The triaxial cell incorporates a pressure balanced piston to improve the accuracy of the load measurement (*Sammonds*, 1999). Experiments can be performed at constant strain rates or constant stress (e.g. creep) and the specimen deformation is measured by external linear variable displacement transducers (LVDTs) (*Eccles et al.*, 2005). The apparatus can operate at confining pressures as high as 400 MPa and temperatures up to 400°C. Silicone oil is the confining medium.

Pore fluid pressure and volume measured at control of the rock specimen was achieved using two servo- controlled pressure intensifier systems. These intensifiers with 10 and 22 cm^3 volumes and were placed at either end of the specimen to allow for constant or changing pore pressure gradients depending on test conditions (*Eccles et al.*, 2005).

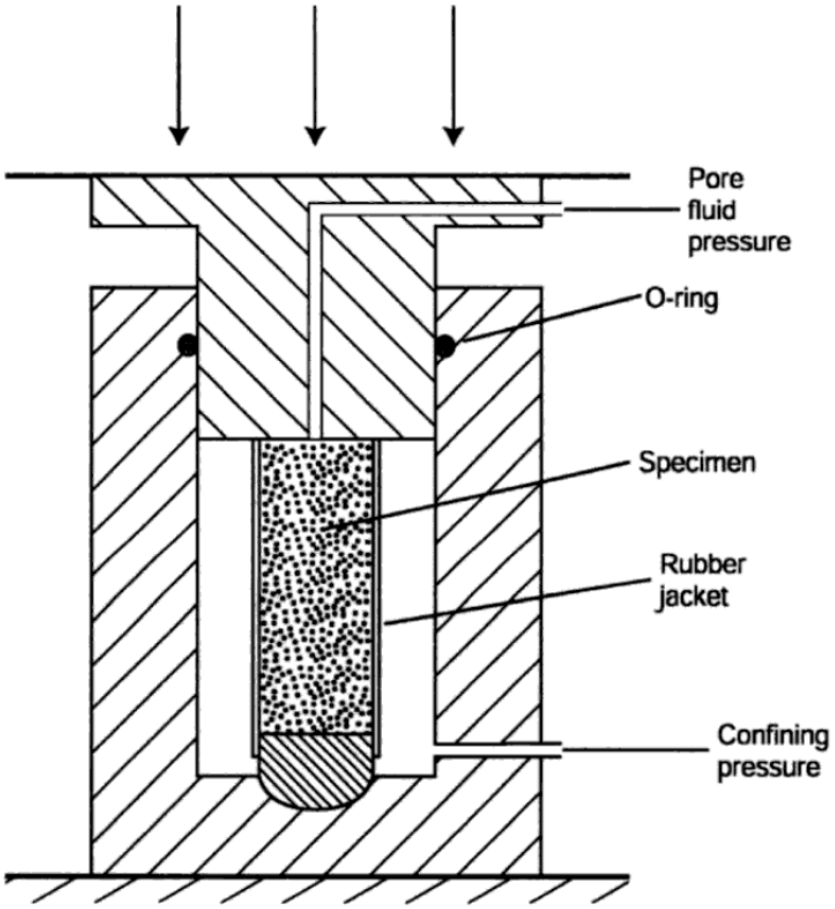

Figure 4.4: Schematic representation of a conventional triaxial compression testing machine, including optional arrangements for pore fluid pressure. The Figure is taken from *Paterson and Wong* (2005)

The uncertainties of the various measurements during a triaxial deformation test are shown in Figure 4.6 below:

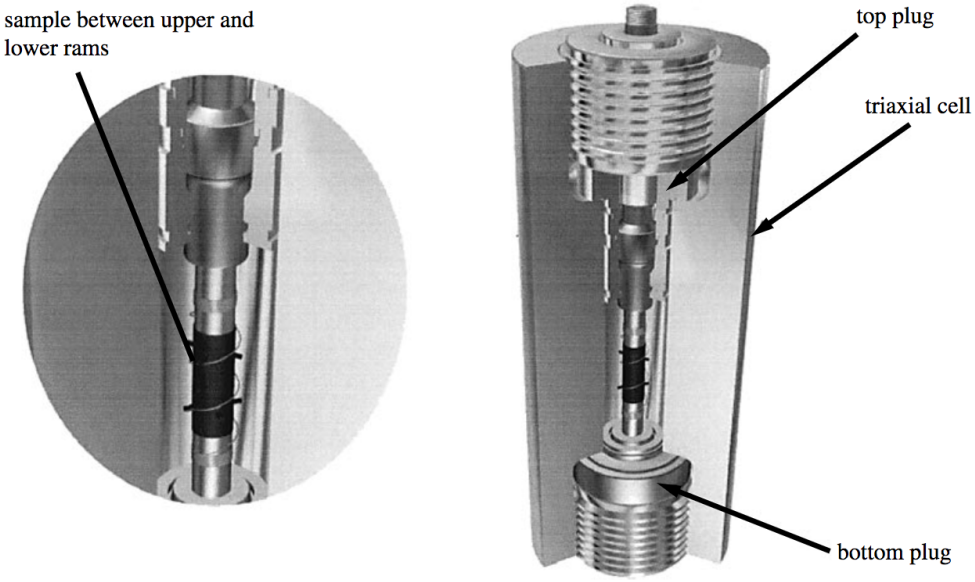

Figure 4.5: The triaxial testing cell for rock deformation designed by *Sammonds* (1999). The rock sample is jacketed in a multiple-instrumented plastic sleeve to keep out the confining fluid. Twelve electrical and/or acoustic measurements can be made simultaneously on the sample. The sample is deformed by upper and loading rams. These in turn are loaded by an axial loading piston that is pressure balance so only the differential stress (the total axial stress minus the confining pressure) need be applied, greatly improving the accuracy of load measurement and experimental control. The confining fluid is oil. An internal heater allows temperatures up to 400°C to be used. The caption and the figure are obtained from *Sammonds* (1999).

Variable	Absolute Uncertainty
Confining Pressure	± 0.1MPa
Pore Pressure	± 0.4MPa
LVDT	± 0.005mm
Mass of Sample	± 0.005g
Length of Sample	± 0.01mm
Parallelism of Sample	± 0.01mm
Angle of Failure	± 0.5°
Conductivity of Pore Fluid	± 1μS

Figure 4.6: List of physical variables measured and set at beginning of experiments together with absolute uncertainties. From *Clint* (1999).

4.4 Rock sample assembly

The rock sample assembly is shown in Figure 4.7 below.

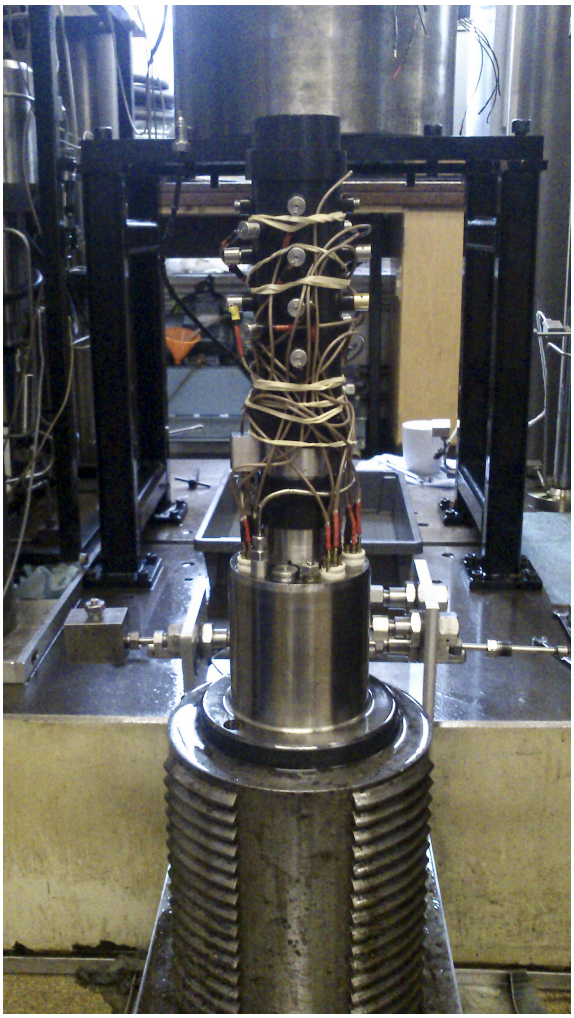

Figure 4.7: The jacket and the AE setup on top of the lower piston. Rubber bands are keeping the threads close to the jacket and prevent them getting caught inside the pressure vessel.

The sample is located inside a jacketing system which isolates the sample from the confining pressure medium but allows for pore fluid to enter. The jacketing system used is designed by Professor Peter Sammonds (*Sammonds*, 1999). It is made out of fluoroelastomer nitrile and can seal the rock efficiently from confining pressures up to 400MPa and temperatures up to 100°C (*Clint*, 1999). Pore fluid distribution plates are placed on the top and bottom end of the sample and nitrile cufs are placed over the jacket to seal the sample. The jackets consist of specially designed

holes were concave stainless steel inserts are placed and are in direct contact with the sample. These are the locations were the piezoelectric transducers are placed in order to record acoustic emissions (AE). The transducers have 5mm diameter and 2mm thickness and are made by PI Ceramics. The transducers have frequency 1.2 MHz and were pre amplified with a 40 db gain.

During the experiments the rock sample assembly is positioned inside the pressure vessel and its relative position in the triaxial deformation ensemble is shown in Figure 4.8 below.

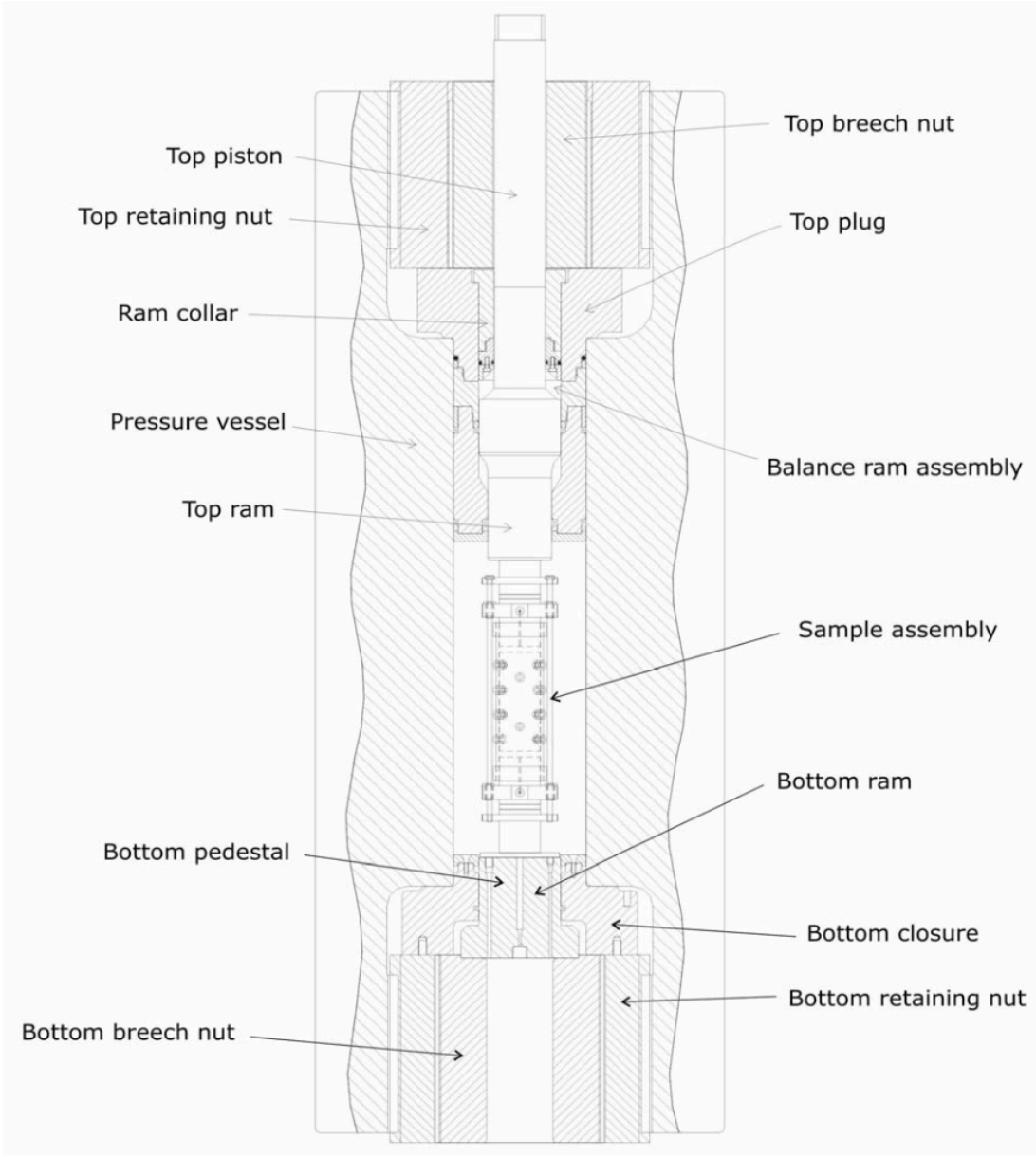

Figure 4.8: Cross section of the triaxial ensemble.

4.5 The experimental procedure

In this section a description of the experimental procedure of the triaxial deformation is provided. The experiments we performed can be classified into two categories:

1. Constant strain rate experiments (strength tests). The strain rate used is 10^{-5} s^{-1} The experiments where done both with constant pore fluid pressure and with constant pore fluid volume.

2. Constant load experiments in which deformation rate varie over time.

I performed both type of experiments to air dried and water saturated samples.

In summary the experimental procedure is described as follows:

1. The sample is placed inside the jacket. The pore fluid distribution plates are placed on the top and bottom and the nitrile cufs are placed over the jacket to seal the sample.

2. The jacket is placed on the bottom piston and the AE are connected to the leads.

3. The bottom piston with the sample is slid below the pressure vessel and then the top piston is placed. At this stage the pore fluid is connected.

4. The machine is switched on and we move from actuator to crosshead control.

5. The pressure vessel is initially lifted to be released from the supporting frame and then carefully lowered down and locked in place.

6. Once the pressure vessel is lowered we can connect the confining pressure tubing and linear variable displacement transducers (LVDTs).

7. At this stage we start the logging of mechanical data (i.e. load, displacement, pressure) and the AE data.

8. The oil pump is turned on. It requires approximately 40 bars of oil pressure to fill the vessel. When the vessel is full , oil will flow from the side valve. We allow for some oil to come out and then we close valve and allow the vessel to settle.

9. Confining pressure and pore pressure is set and the sample is left to settle for about an hour.

10. Switch to displacement control and set the strain rate (if we are to perform a constant strain rate experiment). If we are to perform a creep experiment

start deforming at a constant strain rate until we reach the desired level of axial stress. This is usually between 80 % and 90 % of the short term strength. Then we stop loading and keep load constant while the strain rates varies.

11. Start deformation. When the rock fractures we allow some extra time for frictional sliding and then stop.
12. Remove load from the vessel.
13. Return to displacement control.
14. Remove the displacement transducers and hemispherical seats.
15. Remove pore fluid pressure and the confining pressure.
16. Lift the vessel and remove the sample.
17. Switch off servo hydraulics.

Chapter 5

Magnitude correlations in experimental data

5.1 Chapter outline

In Chapter 3 the subject of magnitude correlations was introduced as well as the development of a new methodology to study them. Applying the methodology to several datasets in regions across the world demonstrated the existence of positive correlations in the earthquake magnitudes with the local level of seismicity which is quantified with the conditional intensity of the ETAS model and that in periods of higher seismicity the mean magnitude of the earthquakes increases. The aim of this chapter is to take the analysis one step further and analyse acoustic emission (AE) data from triaxial deformation experiments in sandstone samples. Applying the ETAS model to experimental data will allow the validation of the results obtained from the earthquake catalog data and provide for the first time a holistic view on the correlation of earthquake magnitudes.

The majority of continental earthquakes occur within the seismogenic layer (T_s) on the upper 20 km of Earth's crust where brittle deformation (the rock fractures

when subjected to stresses greater than the its strength) prevails (*Watts and Burov*, 2003). Parameters such as the applied stress, the rate and duration of loading, pressure, temperature, the presence of fluids and previous deformation history all control the overall mechanical response (*Sammonds*, 1999). In the laboratory we can simulate the Earth's crust conditions and since the main stresses in the crust are compressive (*Main*, 1996) rock deformation under compression can be used to draw analogies with seismicity (*Baró et al.*, 2013). The advantage of studying earthquakes with laboratory experiments, is the ability to control parameters such as the stress, the strain rate, the pressure and temperature upon which fracturing depends and monitor the behaviour of each parameter individually through time. On Earth's scale, portion of the energy that is released during frictional sliding along the faults is converted to seismic waves that propagate outwards. On a laboratory scale, when microfractures occur they generate elastic waves similar to those generated by earthquakes (*Scholz*, 1968b). These waves are called acoustic emissions (AE). There are many similarities between earthquakes and AE events. Statistical laws that describe seismicity such as the Gutenberg-Richter and the Omori law are obeyed in AE events (*Mogi*, 1963; *Scholz*, 1968b; *Sammonds et al.*, 1992; *Lockner*, 1993) and therefore AE provides a great tool to study the seismogenic process.

In this chapter firstly the experiments performed in the laboratory and the recording of the AE's are described. Then, the results of the magnitude correlations in the experimental data following the methodology described in Chapter 3 will be presented and the results will be explained in terms of fracture mechanics i.e. the study of how cracks form and interact under stress within a sample or in Earth's crust until failure (fracture). The formation and fracturing of cracks within the sample is analogous of fracturing in the crust and therefore the magnitudes of the AE events or earthquakes strongly depend in this process. The fracture mechanics model used in this study is discussed as well as the different conditions of the experiments, that

can influence crack formation and subsequently the AE magnitudes. The results of the magnitude correlation method will be explained on this basis.

5.1.1 Constant strain rate experiments and AE analysis

Table 5.1 shows all the constant strain experiments performed and the conditions/ settings used. The stress-time plots of all the experiments are shown in Appendix B.

Table 5.1: Table showing the constant strain rate experiments performed and their experimental conditions. All experiments performed in Darley Dale sandstone and the strain rate used is $10^{-5}\ s^{-1}$

Name of experiment	Confining Pressure (MPa)	Pore Pressure (MPa)	Notes
DDS1	30	0	Dry
DDS2	50	20	Constant Pressure
DDS3	50	20	Constant Volume
DDS4	80	0	Dry
DDS5	100	20	Constant Pressure
DDS6	100	20	Constant Volume
DDS7	40	10	Constant Pressure
DDS8	50	20	Constant Volume
DDS9	50	20	Constant Volume
DDS10	50	20	Constant Volume; Sawcut sample

In Figure 5.1 an example of a 50 MPa confining pressure, 20 MPa pore fluid pressure experiment. The plot is divided to five areas representing different stages of the experiment. During the first stage we observe closing of the most favourable orientated microcracks. This stage may be absent at higher confining pressures. During the second stage quasi-linear elastic deformation is dominant and crack closure is still prevalent. In the third stage, the stress-strain curve begins to deviate from linearity becoming concave downwards and a process of strain hardening occurs. Axial orientated microcracks are formed at this stage. During stage 4 the rock sample undergoes strain softening as its ability to withstand further increases in stress is reduced. Crack formation is accelerated during this stage. In the final stage, stable sliding occurs on the macroscopic fault plane and stress becomes independent of strain (*Clint*, 1999).

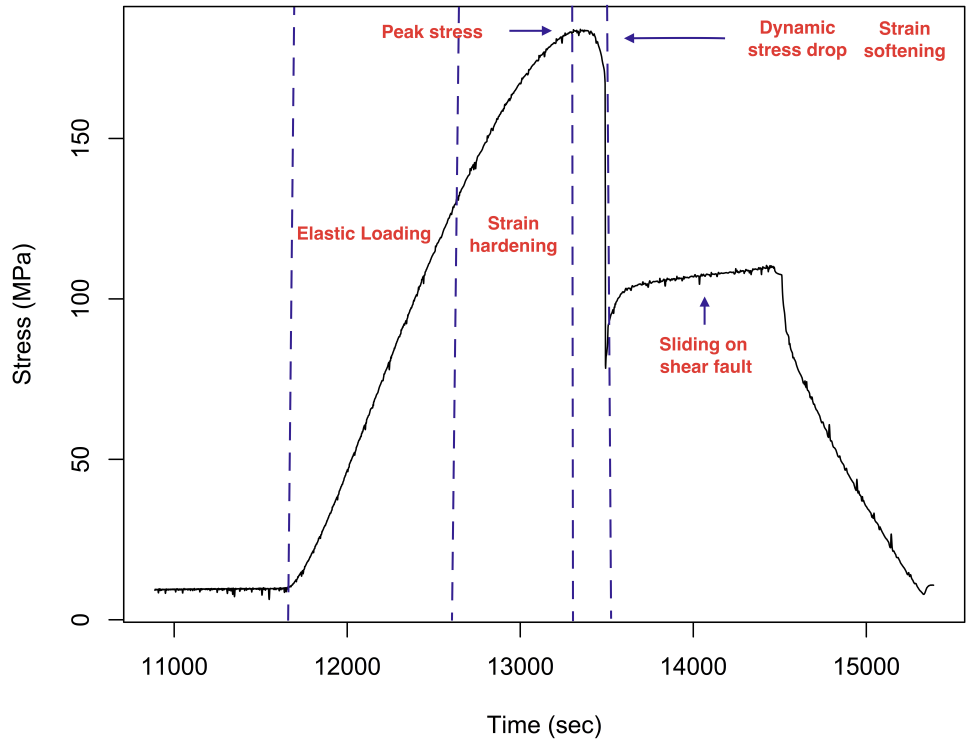

Figure 5.1: Figure showing the three stages of deformation of a DDS sample.

5.1.2 Constant stress (creep) experiments and AE analysis

To conduct a constant load experiment the sample is initially loading with a constant strain rate (10^{-5} s^{-1}) up to the desired differential stress level. Then the load remains constant and the strain rate varies over time. The differential stress which the sample is initially loaded has significant influence on the duration of the experiment. With a decrease in the stress the duration of the experiments increases (*Baud and Meredith*, 1997; *Heap et al.*, 2009)

Three stages can be identified during a creep experiment:

1. Primary creep; The strain rate is initially high and then decreases to a stable value that marks the start of the next stage.

2. Secondary or steady state creep.

3. Tertiary creep; The strain rate is increased until the failure of the sample.

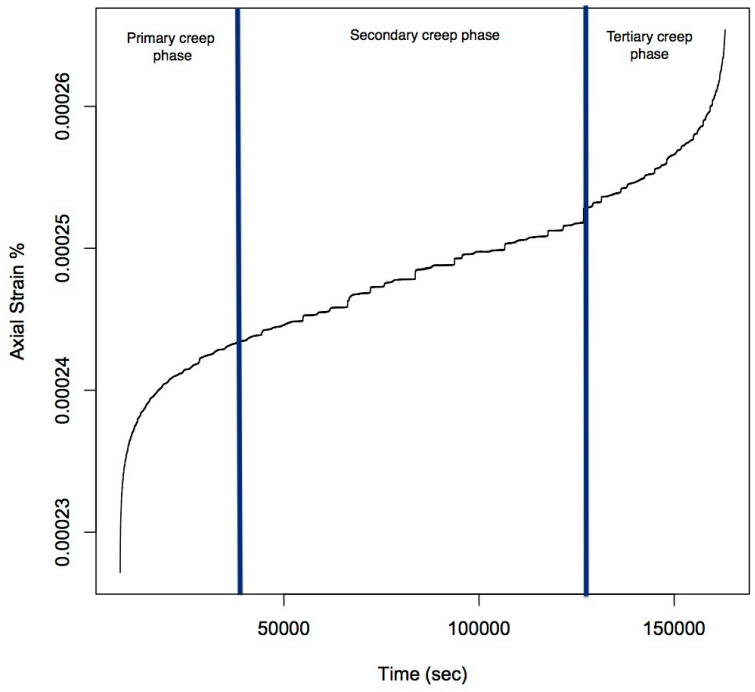

Figure 5.2: Figure showing the three stages of deformation of a DDS sample.

Table 5.2 shows all the constant stress (creep) experiments performed for the purposes of this thesis and the conditions/ settings used. The axial strain (%)-time plots are shown in Appendix C.

Table 5.2: Table showing the constant stress (creep) experiments performed and their experimental conditions. All experiments performed in Darley Dale sandstone and the strain rate used to bring the sample to the desired stress level is 10^{-5} s^{-1}

Name of experiment	Confining Pressure (MPa)	Pore Pressure (MPa)	Load (kN)	Notes
DDSC1	50	20	211	Constant Pressure
DDSC2	40	10	207	Constant Pressure
DDSC3	40	10	217	Constant Pressure

Prior to these tests we conducted a series of constant strain rate experiments and a step test to determine the initial value of differential stress at which the creep test would start. The methodology of *Heap et al.* (2009) where they studied time dependent brittle creep in Darley Dale sandstone is appled. To overcome the influence of stress to the creep behaviour by selecting samples with porosity difference

smaller than 0.5 % for the creep experiments. The sample variability is overcome by conducting a stress stepping experiment in which multiple creep experiments are performed in the same sample. The level of stress for the first step is crucial since the sample will not creep within the elastic regime. Our experiment started at 85% of the short term strength determined from the constant strain rate experiments corresponding at 211kN. The axial strain %-time plot is shown in Figure 5.3. Once the sample had undergone approximately 0.2 mm of axial shortening during secondary creep, the stress was stepped up by 6kN.

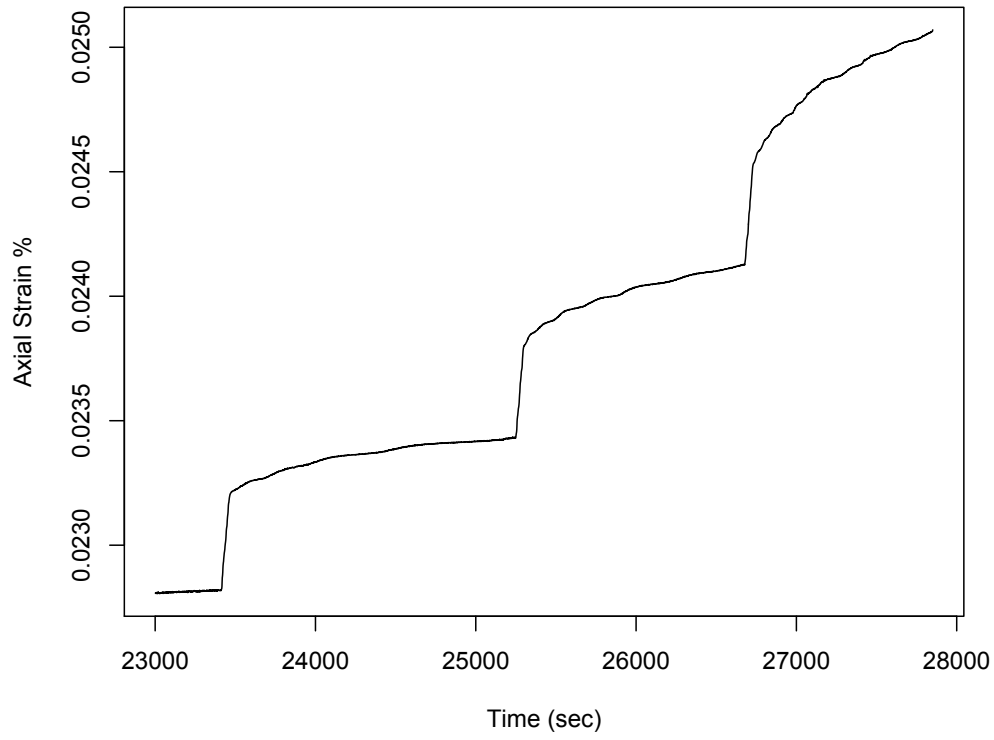

Figure 5.3: Figure showing the axial strain %-time plot of the stress stepping experiment.

AE's where recorded during the creep experiments and analysed as described in 5.1.1 The experimental conditions correspond to depths in the upper 5km of the Earth's crust.

5.2 Sensor calibration

In *McLaskey et al.* (2015) it shown the importance of sensor calibration in AE recording in order to compare the size of AE's with earthquakes and other AE's recorded by different sensor and systems. To that end, we perform a simple calibration technique to determine the voltage that corresponds to a 1 mm crack. At a 30MPa confining pressure a single layer of 1mm diameter glass beads are placed between metal cylindrical parts of 5cm length and 2cm width each to ensure the correct dimensions prior placing them inside the jacket. The initial strain rate was set at 10^{-6} s^{-1} to avoid rapid breaking of the glass beads and damaging of the jacketing system. Later on the experiment it was decided that this strain rate was too low and it was increased to 10^{-5} s^{-1}. We found that -4.92 V correspond to 1mm breaking.

5.3 Magnitude correlations in experimental data

AE data from the experiments were analysed in order to determine their time and magnitudes. The magnitudes are calculated using a built in algorithm of the software used to process the AE's. These data were used to create experimental catalogs analogous to earthquake catalogs and analysed in the way described in Chapter 3 to determine wether the magnitudes are correlated.

An example time series for a constant strain rate experiment with 100 MPa confining pressure and 20 MPa pore pressure is shown in Figure 5.4

Figure 5.5 shows the variations of the ETAS intensity with time and the variations of stress with time during the experiment. This plot shows that the ETAS intensity which corresponds to the rate fits well with the variations in stress.

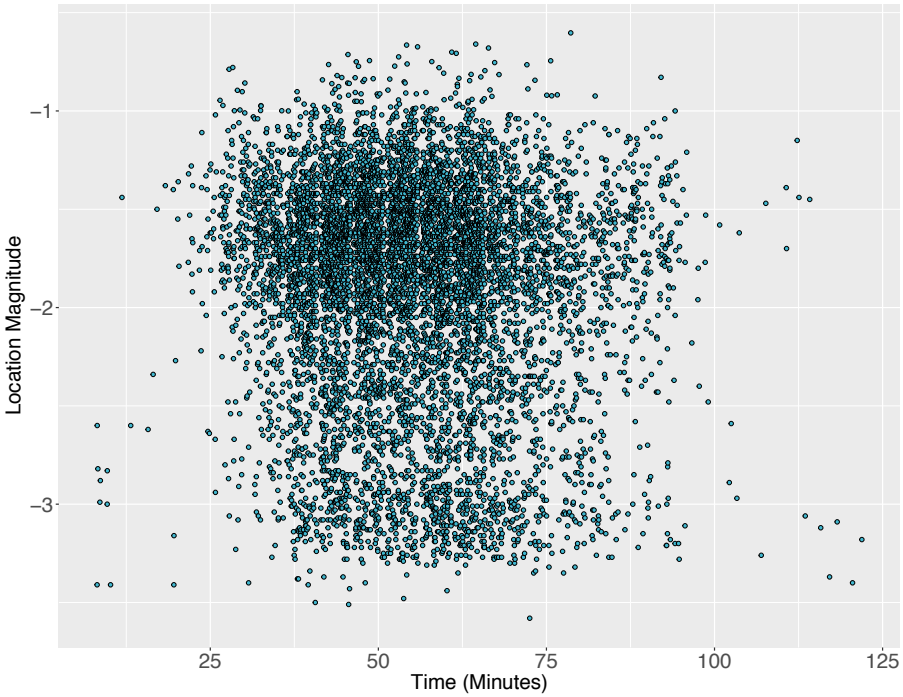

Figure 5.4: Figure showing a time series created from the AE data.

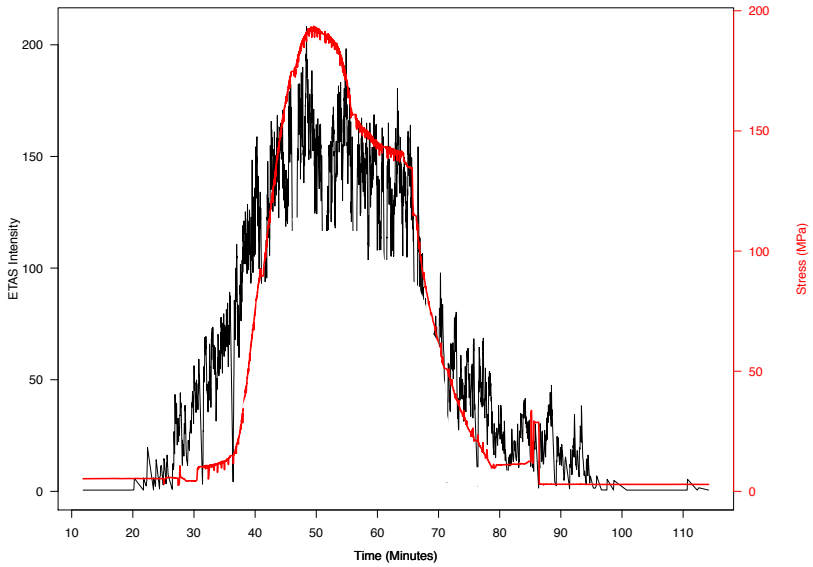

Figure 5.5: Figure showing the ETAS fit to the AE data.

The results from the constant strain rate experiments are shown in Table 5.3

The results from the constant load (creep) experiments are shown in Table 5.4

The correlation between the ETAS intensity and the magnitudes was slightly positive in most cases but the 95% confidence intervals included zero making the results

Table 5.3: Table showing the constant strain rate experiments performed and their experimental conditions. All experiments performed in Darley Dale sandstone and the strain rate used is 10^{-5} s^{-1}

CP (MPa)	PP (MPa)	Pearson Correlation	Confidence Intervals	Mann-Whitney test	Pore fluid	Notes
40	10	0.040	[0, 0.08]	0.08	Constant pressure	No correlation
50	20	-0.007	[-0.07,0.06]	0.38	Constant pressure	No correlation
50	20	0.140	[0.05,0.22]	0.04	Constant volume	Correlation
100	20	0.004	[-0.02,0.02]	0.96	Constant pressure	No correlation
50	20	0.03	[0.01,0.07]	0.05	Constant volume	Correlation

Table 5.4: Table showing the constant load (creep) experiments performed and their experimental conditions. All experiments performed in Darley Dale sandstone and the initial strain rate used is 10^{-5} s^{-1}

CP (MPa)	PP (MPa)	Load (kN)	Pearson Correlation	Confidence Intervals	Mann-Whitney test	Pore fluid	Notes
40	10	211	0.002	[-0.05, 0.06]	0.68	Constant pressure	No correlation
50	20	217	0.05	[-0.13,0.26]	0.28	Constant pressure	No correlation

not significant. Only the 50MPa confining pressure-20MPa pore pressure with constant volume experiments showed significant results. This in an interesting result that shows how the fracture process can affect the existence of correlations in the magnitudes. In the following section the results are interpratated based on fracture mechanics.

5.4 Interpretation of results

For the first time in this thesis, an earthquake magnitude correlation methodology is applied to AE data from experiments. The motivation behind this attempt is to provide some physical explanation on the occurrence of the magnitude correlations that are observed in earthquake catalogs. The results were consistent between two types of experiments; constant pressure experiments showed no correlation and constant volume experiments showed correlations. Since no literature exists for guidance into the interpretation, the logical step was to consider what is difference between these types of experiments. The difference is the fracturing process; i.e. the way cracks form, extend and interact in the sample during the deformation. Several models have been developed to describe this process. The model chosen in this thesis explicitly details with clustering of fractures from a fracture mechanics

viewpoint and relates this to statistical approaches through the fractal dimension and Hurst number, which other approaches do not.

According to *Main et al.* (1993); *Ashby and Sammis* (1990); *Scholz* (1990); *Costin* (1983); *Rundle and Klein* (1989) the stability of the initial crack growth may be attributed to:

1. Tensile relief of differential stress in an overall compressional stress field.

2. A reduction of the rate of subcritical crack growth as the local stress intensity increases due to crack growth itself.

3. The development of an anelastic process zone of smaller scale damage ahead of the crack tip.

4. The mechanism of dilatant hardening in the presence of a pore fluid.

5. To the material heterogeneity itself as the crack runs into a stronger grain.

The stability of this initial stage is due to the negative feedback between the increase in crack length and the stress intensity, represented by the term (d - a)/d in equation 5.4.0.1, where S_r is the remote stress, d is the radius of the "domain" where the stress intensity is relieved and a is the crack half length (*Henderson et al.*, 1992).

$$K \propto S_r \frac{d-a}{d} (\pi\alpha)^{1/2} \tag{5.4.0.1}$$

When the crack density reach a critical density, the cracks begin to interact. During this process the stress intensity at the tip of a crack is increased by the presence of a neighbour, and the stress in the intervening region is also increased. This corresponds to a positive feedback in the crack's growth process, eventually leading to a runaway instability (*Henderson et al.*, 1992; *Main et al.*, 1993). The stress

intensity factor is now described by equation 5.4.0.2 where c is the centre-to-centre distance between adjacent cracks.

$$K \propto S_r(c\tan(\frac{\pi\alpha}{2c}))^{1/2} \tag{5.4.0.2}$$

According to the fracture mechanical model of *Henderson et al.* (1992) the Hurst number (H) shown in Equation 5.4.0.3, where n is the Euclidean dimension of the system and D is the fractal dimension calculated using a box counting method separates the system into two categories.

$$H = n - D \tag{5.4.0.3}$$

The Hurst number was introduced in *Hurst et al.* (1965) initially to study the record of floods and droughts on the river Nile where he consider the river flow as a time series. His analysis is extended to many time series since then and the Hurst number is considered a quantitative measure of persistence and anti - persistence (*Turcotte*, 1997). In a persistent time series an increase in values will most likely be followed by an increase in the short term and a decrease in values will most likely be followed by another decrease in the short term. In an anti-persistent time series an increase will most likely be followed by a decrease or vice-versa (i.e., values will tend to revert to a mean). This means that future values have a tendency to return to a long-term mean. In the model of *Henderson et al.* (1992) n=1, and therefore $0 < D < 1$, while $1 > H > 0$. A Hurst number > 0.5 suggests a predictability or persistence of the system. This is more likely to occur on Earth in macrocracks and faults at high intensities (*Main et al.*, 1990). A Hurst number < 0.5 suggests clustering and anti persistence behavior. In this case at low stress intensities it less likely that fracture will recur at that site due to the strain relief stabilisation of fracture at one locality. This results in distributed damage. In the limiting case of $H = 1$, dynamic rupture occurs at critical stress intensities (*Main et al.*, 1990). When the

experiment is performed under constant volume the pore fluid pressure is changing and consequently the effective pressure. This affects the crack length growth. The stability of this cracking is due to negative feedback between the increase in crack length and the stress intensity (*Sammonds and Ohnaka*, 1998). This corresponds to a persistence fracture process as described by *Henderson et al.* (1992). Constant pressure experiments give positive feedback and anti-persistent type of fracture. The results indicate that only when the fracture process is persistent we observe significant magnitude correlations. This is an interesting result that coincides with the magnitude correlation analysis and demonstrates the complexity of the subject. The existence of magnitude correlations, which indicates a sense of predictability in the earthquake magnitudes; is found when the the fracture process is persistent which also indicates a sense of predictability.

5.5 Key findings - discussion

The scope of this chapter was to test the newly developed methodology applied in Chapter 3 to search for earthquake magnitude correlations in the magnitudes of AE data from triaxial deformation laboratory experiments. Applying the methodology to the magnitudes of the AE data two outcomes can be distinguished. First; during constant pressure experiments where the Hurst number is < 0.5 an anti persistent behaviour is observed and positive feedback between the crack length and the stress intensity. In this environment no correlations are observed. During the constant volume experiments a persistent behaviour and negative feedback between the crack length and the stress intensity describes the system. Here the Hurst number is $>$ 0.5 suggesting predictability in the system. During these conditions we observe magnitude correlations. In the earthquake catalog data the study of magnitude correlations in different tectonic zones and fault types consistently showed significant results and no differentiation was observed. As such, I cannot draw conclusions

on the influence of the stress level to the magnitude correlations. However, it is demonstrated that the fracturing process and as a result, stress levels, affect the magnitude correlations. With the fracture mechanics interpretation shown in this Chapter and the dependence of the magnitude on the Hurst number which is a measure of predictability in a system this work can be extended in the future to study the fracture process of individual faults, find their Hurst number and compare the results with the analysis of the earthquake catalog data for this fault.

Chapter 6

Forecasting with the ETAS and compound Poisson models

6.1 Chapter outline

Although earthquakes are a phenomenon of great complexity, certain simple general laws govern the statistics of their occurrence. The development of stochastic models that implement these laws, the significant increase in the number of seismic networks which are the source of earthquake catalog data as well as the significant improvement on the quality the data provided. These gave the impetus to improve our scientific understanding of earthquakes, the evaluation and testing of earthquake forecasts, earthquake early warning, and seismic hazards assessments; tasks of great societal importance (*Michael and Wiemer*, 2010).

Statistical models such as *Gerstenberger et al.* (2005); *Reasenberg and Jones* (1989); *Ogata* (1988, 1998); *Rhoades and Evison* (2004); *Turcotte et al.* (2007) are frequently used to perform short term, long term and real time forecasts and to assess seismic hazard. It is shown that these models produce reliable forecasts during an aftershock sequence, and also retrospective comparative tests have shown that these models can

be used as a reasonable null hypothesis to test future forecasting and/ or predictions models (*Marzocchi and Lombardi*, 2009). Out of these models ETAS is the most frequently used, however over the last decade a less mainstream and much simpler model has been used to forecast earthquakes in Turkey by *Özel and Inal* (2008); *Özel* (2011). Here, earthquake occurrence is modelled by a compound Poisson model that uses a homogenous Poisson distribution for the occurrence of the earthquake times and a geometric distribution to describe the number of aftershocks.

The choice of a statistical model to describe a complex phenomenon such as seismogenesis is not trivial and among statisticians it is often debated whether model complexity is always necessary with simpler models performing as equal as their more advanced ones (*Rogers*, 1995). In the work of *Helmstetter and Werner* (2014) the same question is asked with case study a time-dependent forecast in California. The authors compared the ETAS model with two new models that make simpler assumptions about seismicity. Their results showed that the ETAS model performs better, nevertheless the simpler models performed well.

The aim of this Chapter is to compare the complex Bayesian ETAS model with the simple compound Poisson model in forecasting earthquakes larger than magnitude 5 during a 5 year period in Southern California and to test the assumption that the number of aftershocks follows a geometric distribution. It is shown that the number of aftershocks in Southern California do not follow a geometric distribution showing that simpler models can not perform as well as the most advanced ones and cannot be applied worldwide to describe seismicity.

For this purpose the catalog of *Hauksson et al.* (2012) from 1981 to 2011 was used with the last 5 years i.e. from 2007 to 2011 serving as the period over which the forecast will be performed. The results of each model will be compared to the observed data from the catalog.

The Bayesian ETAS model is a more advanced version of the ETAS model described in Chapter 2 and used throughout this thesis. As I will describe in this Chapter, Bayesian statistics account for uncertainty in the estimation of the model's parameters in contrast with frequentist statistics where point estimates are treated as true values. Even though frequentist statistics provide methods to estimate uncertainty it is difficult to translate this into information about forecast uncertainty (*Ross*, 2017). The complexity of the ETAS however makes implementation in a purely bayesian framework a challenging procedure. The bayesian ETAS of *Ross* (2017) used in this Chapter is available to download as package in the R programming language under the name bayesianETAS (`https://cran.r-project.org/web/packages/bayesianETAS/index.html`

The compound Poisson model it is a much simpler model that is defined as follows (from `http://www.math.uah.edu/stat/poisson/Compound.html`):

Suppose we have a Poisson process with rate $\lambda \in (0, \infty)$. In the Poisson process the inter-arrival times is a sequence denoted by X = (X_1, X_2, ...) with X being a sequence of independent random variables, each having the exponential distribution on [0, ∞) with rate λ , the sequence of arrival times is T = (T_1, T_2, ...) and the counting process $\{N_t\colon t \in [0, \infty)\}$. For t $\in$ [0, ∞), the number of arrivals N_t has a Poisson distribution with parameter λt.

If we assume Y = (Y_1, Y_2, ...) is a sequence of independent and identically distributed random variables independent from the Poisson process then the compound poisson process associated with the given Poisson process N and the sequence Y is the stochastic process V = $V_t\colon t \in [0, \infty)\}$ where:

$$V_t = \sum_{n=1}^{N_t} Y_n \tag{6.1.0.1}$$

V_t is the total value for all of the arrivals in (0,t]

In this case, a homogenous Poisson process is used to generate the times of earthquake occurrence and a geometric distribution is used for the number of aftershocks generated by one event. The choice of the geometric distribution is based on previous studies e.g. *Christophersen and Smith* (2000); *Özel and Inal* (2008).

The results of my comparison showed significant different between the two models.

6.2 Forecasting with the bayesian ETAS model

6.2.1 Key concepts of Bayesian inference

Statistical inference is the procedure of drawing conclusions about a population or process based on a sample. It can be separated into two categories based on the definition of probability. In frequentist statistics probability is viewed as an event's frequency after a large number of trials. In contrast Bayesian inference express degrees of belief and thus allowing room for prior knowledge or ignorance to be included in the calculations.

The fundamental steps of undertaking a Bayesian analysis are described in *Glickman and van Dyk* (2007) and are presented below:

1. Formulate a probability model for the data.

   If we have n amount of observed values y_1, y_2, ..., y_n and the vector of unknown parameters is θ, assuming that the observations are made independently, we are interested in choosing a probability function $\mathrm{p}(y_i \mid \theta)$ for the data.

2. Decide on a prior distribution.

The prior distribution represents the current state of knowledge, or current description of uncertainty, about the model parameters prior to data being observed. Prior distributions can be divided into:

(i) Informative prior distribution.

The choice of this distribution is been made by the statistician based on his or her beliefs for the unknown parameters. For example, the statistician can make this decision based on other data.

(ii) Non-informative prior distribution.

The non-informative prior represents ignorance about the parameters. In this case no prior knowledge about the parameters exists before observing the data. This is implemented in practise by assigning equal probability to all values of the parameter.

3. Observe the data and construct the likelihood function based on the data and the probability model formulated in Step 1. Then the likelihood is combined with the prior distribution to form the posterior distribution which quantifies the uncertainty in the values of the unknown model parameters after the data are observed.

The likelihood is the joint probability function of the data, but viewed as a function of the parameters, treating the observed data as fixed quantities. Assuming that the data values y = (y_1, $y_2 \ldots Y_n$) are independent the likelihood function is:

$$L(\theta|y) = p(y_1 \ldots y_n|\theta) = \prod_{i=1}^{n} p(y_i|\theta) \qquad (6.2.1.1)$$

Values of the parameters that correspond with the largest values of the likelihood are the parameters that are most supported by the data.

The posterior distribution is obtained by applying Bayes theorem:

$$\begin{aligned} p(\theta|y) &= \frac{p(\theta)p(\theta|y)}{\int p(\theta)p(y|\theta)d\theta} \\ &= \frac{p(\theta)L(\theta|y)}{p(y)} \\ &\propto p(\theta)L(\theta|y) \end{aligned} \tag{6.2.1.2}$$

The expressions in equation 6.2.1.2 are equal when the right-most term is multiplied by a normalising constant that does not depend on θ. In principle to obtain the posterior distribution, multiply the prior distribution by the likelihood and then determine the constant (not depending on θ) that forces the expression to integrate to 1.

4. Summarise important features of the posterior distribution, or calculate quantities of interest based on the posterior distribution.

6.2.2 Markov chain Monte Carlo (MCMC) methods

In the Bayesian ETAS model and many other applications of Bayesian statistics the analytical computation of the posterior distribution is too complicated to be directly simulated. In this case a common approach is to simulate samples from the posterior distribution. The method used in the Bayesian ETAS model to acquire samples from the posterior distribution is the Markov chain Monte Carlo (MCMC) method. As the name indicates, for this method to produce acceptable approximations to integrals and to other functionals depending on a distribution of interest, it is enough to generate a Markov chain $(\theta^{(m)})$m with limiting distribution the distribution of interest (*Robert*, 2007). The model which is used for in this application, introduces an alternative methodology with the use of latent variables, i.e. variables that are inferred from other observed variables (*Ross*, 2017).

6.3 Forecasting with the bayesian ETAS model

The Southern California earthquake catalog of *Hauksson et al.* (2012) which contains earthquakes between 1981 to 2011 in the region between 30° and 37° longitude, -113° and -122° latitude is used for the forecast. The data from 2007 - 2011 were removed from the original catalog in order to become the forecasted period. Figure 6.1 shows a map of the region.

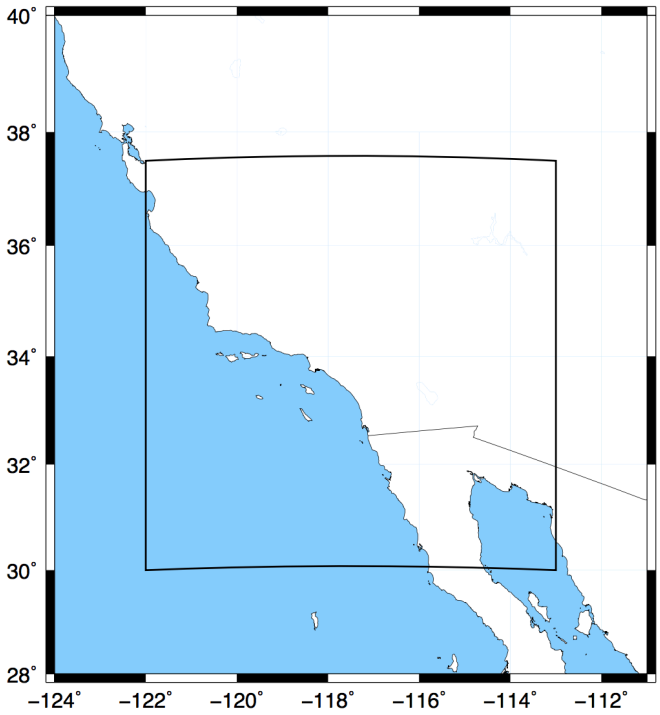

Figure 6.1: Map showing a part of California. The region inside the black box represents the study area.

The first step was to draw samples from the Bayesian posterior distribution of the ETAS model with the latent variable MCMC scheme from *Ross* (2017). Each sample contained a set of the five parameters of the temporal ETAS model (μ, K, α, c, p).

The data above are then used to simulate sample data from the ETAS model over a specified period of time, in this case 5 years. The average number of mainshocks that are generated from the simulations will represent the forecast outcome. However this was not a straightforward procedure and in some cases infinite amount of

earthquakes are produced in a finite period of time. In the following paragraphs, I will discuss the conditions that lead to this result.

The conditional intensity of the temporal ETAS model is given by equation 6.3.0.1:

$$\lambda(t|H_t) = \mu + \sum_{\{i:S<t_i<t\}} \frac{K_o e^{a(M_i - M_c)}}{(t - t_i + c)^p} \tag{6.3.0.1}$$

where S is the starting time of the catalog, M_c is the catalog magnitude of completeness, μ denotes the background rate, $t_1, \ldots, t_n$ are the occurrence times of the n earthquakes which occurred between times S and t, and M_i is the magnitude of the earthquake that occurred at time t_i.

Looking at 6.3.0.1 the ETAS model can be interpreted as a superposition of different poisson processes; the background rate μ and the intensity spikes from the m previous earthquakes prior to t. According to the theory of point processes (*Daley and Vere-Jones*, 2007; *Veen and Schoenberg*, 2008) each earthquake is generated either by the background process, or by a specific previous earthquake and therefore ETAS is considered a branching model.

In *Helmstetter and Sornette* (2002) the topic of explosive increase of the seismic rate is analysed and it is shown that this occurs in the "supercritical" regime, while in the "subcritical" regime we obtain finite results. The terms "supercritical" and "subcritical" correspond to the value of the branching ratio, n i.e. the mean number of aftershocks triggered per event and the term θ which is a positive constant. In relation to θ the work of *Sornette and Sornette* (1999) showed that an earthquake can produce an aftershock sequence according to a "local" Omori law with an exponent $1+\theta$. They also found that the "global" Omori law has two distinct power law regimes. The first has exponent $p_- =$ p - θ for time t $< t^\star \sim \kappa^{-1/\theta}$, where $0 < 1 < \kappa$ represents the fraction of triggered aftershocks per triggering earthquake and the second has an exponent p_+ for times larger than $t^\star$. The work of *Sornette and Sornette* (1999) refers to the case where $\alpha = 0$, whereas in the work of *Helmstetter*

and Sornette (2002) α is > 0. The three regimes that correspond to the values of n, θ are:

1. The subcritical regime, where n < 1. In this case the exponents p_- and p_+ of *Sornette and Sornette* (1999) are obtained.

2. The supercritical regime, where n > 1 and $\theta > 0$. In this case the the seismicity rate has an explosive exponential increase.

3. When θ is < 0,(the local p value is < 1) *Helmstetter and Sornette* (2002) finds a transition from 1- $\mid \theta \mid$ to an explosive exponential increase. The transition time τ is different than the time $t^\star$.

4. For n $= 1$, *Helmstetter and Sornette* (2002) reports there is exactly one earthquake on average triggered per earthquake and the process is exactly at the critical point between death on the long run and exponential proliferation.

Finally it is shown that the following conditions must be satisfied in order to avoid infinite results:

1. $\theta > 0$ ensures finite results at large times.

2. At short times a constant c is introduced in the Omori law.

3. A necessary condition for finite triggered events is: $a <$ b.

4. The role of a cut-off m_0 magnitude. In the absence of such magnitude, small earthquakes dominate the dynamics of the system therefore including m_0 is important.

To avoid infinite number of triggered aftershocks only the parameters that correspond to the subcritical regime were included in the forecast. Another approach would be to include the parameters from the supercritical regime but only to consider the predictive distribution p(N$\mid$ N $< \infty$). Since the compound model does generate magnitudes, only number of aftershocks, the impact of magnitude uncertainties as reported in *Helmstetter and Werner* (2014) was not taken into account.

The following step was to simulate data, the average number of earthquakes over magnitude 5 that where generated was 20. The Bayesian ETAS model forecast was almost exact the real observations, which included 19 earthquakes.

The results of the ETAS forecast are shown in Figure 6.2 below:

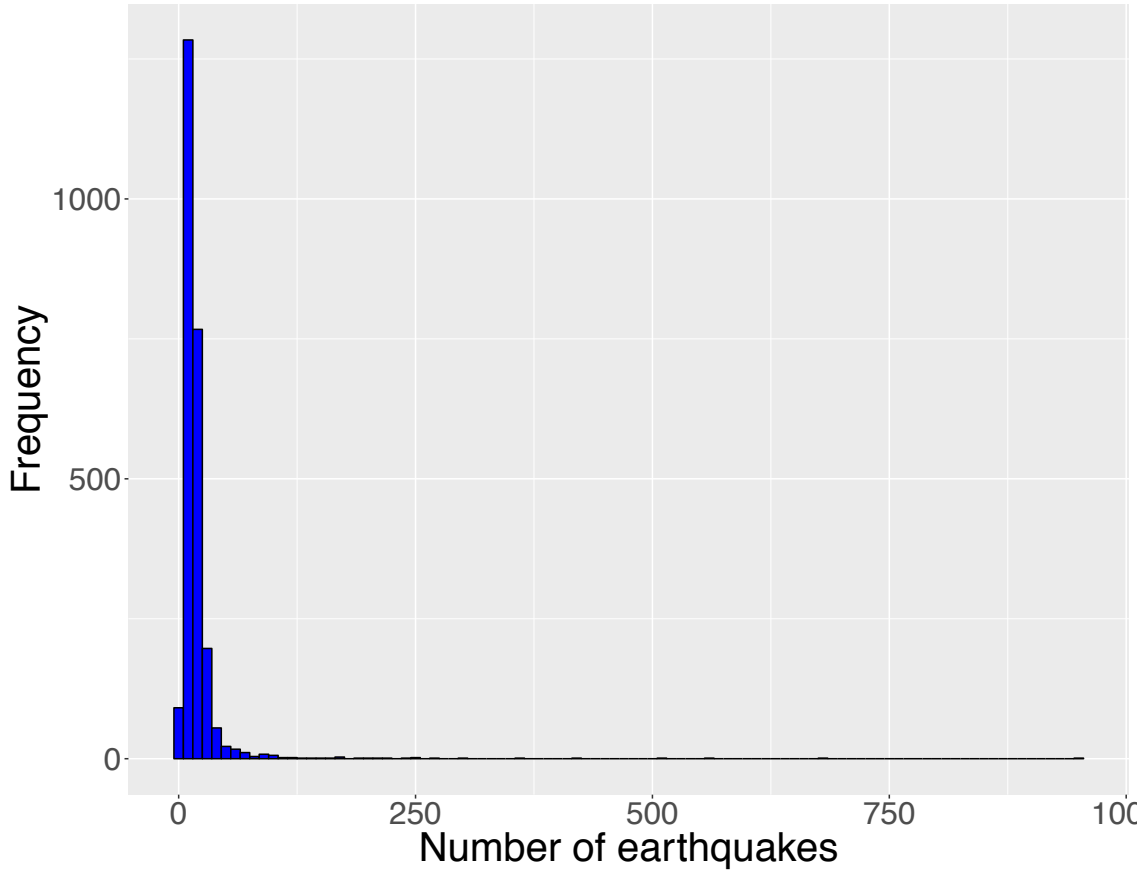

Figure 6.2: Histogram showing the number of mainshocks generated by each simulation and the frequency of their appearance. The mean number of mainshocks was found to be 20.

6.4 Forecasting with the compound poisson model

The model (the same model is used in *Özel and Inal* (2008)) uses a homogeneous poisson model to model the times of earthquake occurrence and a geometric distribution to model the number of aftershocks each of these events will produce. The poisson distribution gives the probability of a number of independent events occurring in a time interval [0,T] with rate or intensity λ. A random variable X is said

to have geometric distribution with parameter p if X takes values in $\{1, 2, 3, \dots\}$ with probabilities:

$$P(Y = k) = (1 - p)^k p \tag{6.4.0.1}$$

X is the random variable that marks the time the first success has come up. If we model the number of failures until the first success then the probabilities are given by:

$$P(X = k) = (1 - p)^{k-1} p \tag{6.4.0.2}$$

To forecast with this model the parameter λ for the homogeneous poisson model and p for the geometric distribution must be calculated. The parameter λ is the rate of mainshocks over magnitude 5 in a year and was found equal to 2.2. The number of the aftershocks for each mainshock over magnitude 5 has to be determined for the calculation of the geometric parameter p; as such the earthquake catalog has to be declustered. The declustering method adopted for this application is by *Helmstetter* (2003). According to this method an earthquake is not a mainshock if there exists a previous larger earthquake within 1 year and 50 km radius. Then all the earthquakes within a rupture length (L) and 1 year after the mainshock are considered as aftershocks. The rupture length I have used for the aftershocks it is different from the one of *Helmstetter* (2003) due it's applicability of the latter only to magnitudes above 6. Instead I have used 5 times the rupture length as defined in *Wells and Coppersmith* (1994) and used in *Hainzl* (2016) and throughout Chapter 3 due to it's applicability to magnitudes smaller than 6.

$$L = 10^{-2.44+0.59M} km \tag{6.4.0.3}$$

The declustering algorithm detected 57 mainshocks. The number of their aftershocks is shown in Table 6.1. Although the geometric distribution has been used in the literature as an appropriate distribution to model the number of aftershocks, the results below indicate that is not the case for Southern California. The parameter p calculated for the geometric distribution based on these lengths is 0.009.

Mainshocks (Index number)	Number of aftershocks
1	493
2	231
3	1277
4	40
5	452
6	5
7	508
8	300
9	131
10	2570
11	1058
12	164
13	172
14	351
15	2
16	78
17	27
18	148
19	870
20	70
21	10

22	46
23	3320
24	0
25	8
26	0
27	41
28	2879
29	6
30	121
31	2502
32	1833
33	1311
34	171
35	209
36	920
37	41
38	3792
39	2064
40	251
41	33
42	633
43	28
44	149
45	155
46	294
47	55
48	1

49	6
50	190
51	2226
52	1134
53	13372
54	26
55	4585
56	9343
57	72

Table 6.1: Table showing the number of aftershocks for each mainshock over magnitude 5 in the earthquake catalog.

The parameters λ and p calculated from the data are now used to produce 10000 synthetic datasets that include times and length of aftershocks. The value we are interested in in the forecast is the number of mainshocks, that is the number of events generated by the compound poisson model at each time. The mean value of generated events for the selected period of 5 years represents the forecast. The value calculated was 11 earthquakes, this is an under-prediction of the 19 observed earthquakes. In this model, the number of aftershocks each mainshock produces is calculated however there is no information on the magnitude.

Figure 6.3 below shows the histogram of the generated earthquakes with their frequency.

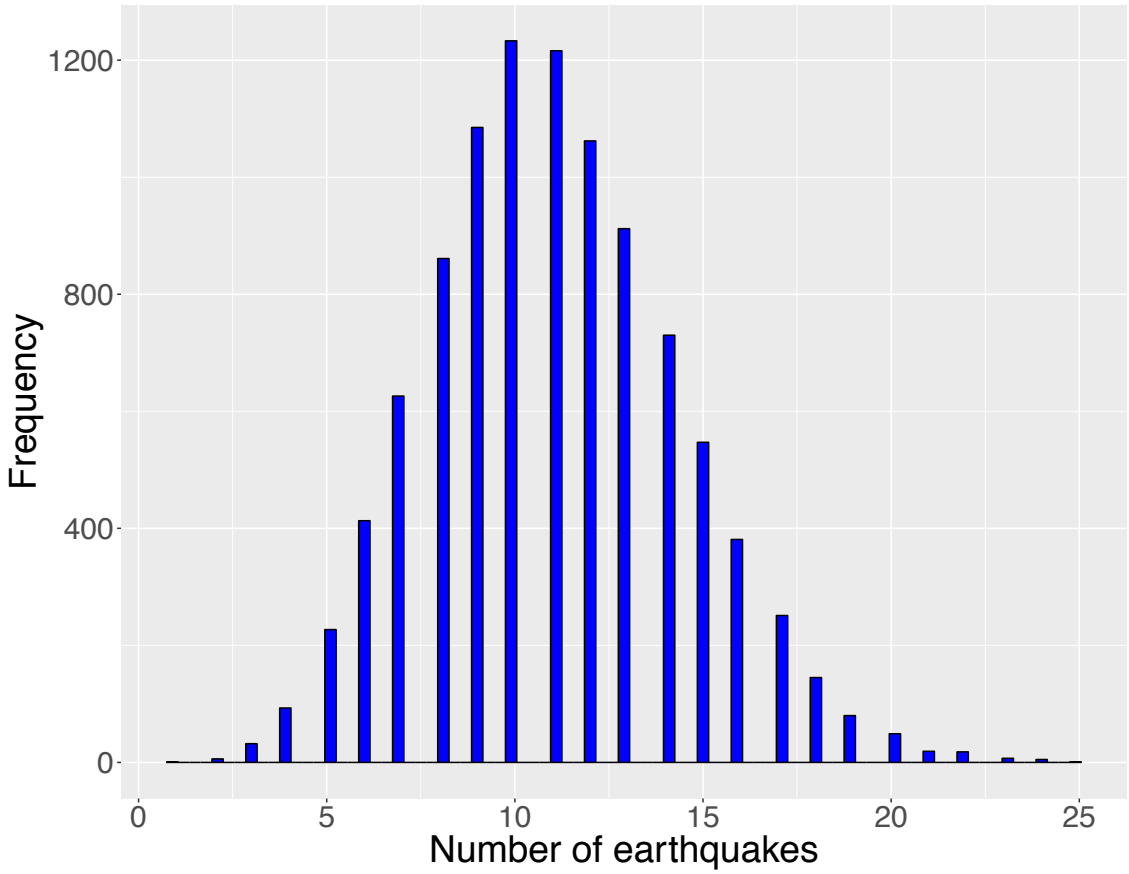

Figure 6.3: Histogram showing the number of mainshocks generated by each simulation and the frequency of their appearance. The mean number of mainshocks over magnitude 5 was found to be 11 for the period 2007-2011.

6.5 Conclusions

The frequentist ETAS model is commonly used for short term and long term forecasts e.g. *Console et al.* (2007); *Ogata* (2011); *Marzocchi and Lombardi* (2009); *Werner et al.* (2011); *Lombardi and Marzocchi* (2010). In contrast the compound model is less frequently used e.g. (*Aktas et al.*, 2009; *Özel and Inal*, 2008; *Özel*, 2011). The aim of this chapter is to address a common question in the statistical community of whether simple models can perform as well as complex models with an application in earthquake forecasting in California.

A 5 year period for forecasting between 2007-2011 was chosen in Southern California during which 19 earthquakes occurred. First a simple compound poisson model that simulates times with a homogenous poisson distribution and the number of aftershocks with a geometric distribution was used. The model under-predicted the real number of earthquakes by forecasting 11 earthquakes. The results also showed that the geometric distribution does not describe the number of aftershocks generated by the mainshocks and therefore the compound Poisson model is not recommended for forecasting in Southern California. A power law distribution described better the number of aftershocks. However, despite the simplicity the compound Poisson model forecasted 60 % of the observed results. The Bayesian ETAS model, almost predicted the exact number of earthquakes with a 20 earthquakes forecast. It is shown that the Bayesian ETAS model is a far superior to the compound model. In this Chapter only point estimates of earthquake occurrence where estimated. A future step would be to fully use the Bayesian ETAS capabilities and the Bayesian framework advantages and estimate the probabilities and the uncertainty of the occurrence of large earthquakes.

Chapter 7

Conclusions - Outcomes

The main objective of this thesis was to develop a new methodology that is robust to the bias that is introduced by incomplete recording of earthquakes from the seismic networks in order to determine if earthquake magnitudes are correlated. The existence of magnitude correlations can be implemented in seismic forecasting models and advance seismic hazard assessments. To achieve this aim the following was necessary: firstly to understand the literature on this subject and to determine the key factors that are likely to limiting their performance. Second, to develop a new methodology that addresses the identified issues. Finally test the methodology not only to earthquake catalog data but also to experimental data and provide a holistic view on the subject.

The second aim of this thesis was to test the performance of the Bayesian ETAS model and a compound Poisson model in their forecasting capabilities. The compound Poisson model, has been increasingly used over the last years in earthquake statistics. In statistics, there is often a questioning wether the complexity of the models is always necessary (*Rogers*, 1995). In some cases it has been shown that simple models can perform equally to their more complex rivals. An application of this question in earthquake statistics with the comparison of the simple compound poisson model and the ETAS model is performed in California.

In this Chapter, the conclusions and outcomes of the research in relation to each of the detailed objectives are described.

1. An extended literature review has identified the strengths and limitations of the pre existing work on earthquake magnitude correlations. It has been found that the majority of previous work has focused on the correlation of earthquake magnitudes between successive events however the correlations found are attributed to the phenomenon of short term aftershock incompleteness (STAI) after a large earthquake. That is the saturation of the seismic networks from the increased seismicity rate and the loss of smaller earthquakes in the coda of large events. Studies that use declustering to separate mainshocks from aftershocks and study their correlations are subjected to additional bias during the declustering procedure. Additionally, studies on the phenomenon of STAI are also studied since this is the greatest obstacle in the study of magnitude correlations.

2. A new methodology to study magnitude correlations has been developed. This method is more robust to STAI than previous methodologies since the earthquake magnitudes are correlated with the local level of seismicity as this is quantified by the conditional intensity of the ETAS model and the precise identification of successive events and the use of unreliable declustering techniques are not necessary.

3. The temporal variations of the magnitude of completeness M_c it is demonstrated to bias the statistical analysis. Window based techniques estimating the M_c through time smooth out the results over time and do not capture accurately the extent of the STAI effect. Another methodology which calculates the magnitude of completeness as a function of rate and time has been shown to capture the full extent of STAI. This rate and time varying M_c has been implemented in my methodology in order to remove period of incompleteness and thus making the methodology more robust.

4. Statistical models like ETAS generate the earthquake magnitudes independently from a Gutenberg - Richter law with a constant b value. The b value is negatively correlated with the differential stress and consequently the faulting type; therefore when studying a region characterised by a variety of faulting types it is likely the time and space varying b value to bias the ETAS estimates. To ensure the methodology is robust, I select regions dominated by a single type of faulting. Additionally the variations of the b value with the seismicity rate are calculated, the stability of these variations is ensured before applying my methodology into the different tectonic regions.

5. The existence of magnitude correlations which is the main objective of this thesis has been demonstrated in two ways: A 95% confidence interval for the Pearson correlation coefficient between earthquake magnitudes and the conditional intensity is calculated using a nonparametric bootstrap method. If the correlation is positive and the confidence interval does not include zero, this serves as a nonparametric hypothesis test which rejects the hypothesis of zero correlation at the 0.05 significance level, and hence suggests the existence of magnitude correlations.

   Since the correlation coefficient is only a measure of linear dependence and cannot capture non-linear dependence, we also split each catalog into two, corresponding to the low and high intensity periods. The mean magnitude for both these periods is then calculated, and a nonparametric Mann-Whitney test is used to test whether the two means are equal. If the null hypothesis of equality is rejected, this also demonstrates the existence of magnitude correlations. The Mann-Whitney test is selected as the appropriate tool since its nonparametric nature means that the computed test statistic does not depend on the (unknown) magnitude distribution.

6. For the first time a holistic approach on the subject of earthquake magnitude correlations is provided with the application of the proposed methodology

to experimental data from triaxial deformation experiments on Darley Dale sandstone. The experiments were performed in the Rock and Ice Physics Laboratory at UCL.

7. Two types of experiments where performed into a variety of confining and pore fluid pressure conditions that simulate the conditions on Earth's upper crust and the microfracturing activity was monitored with the recording of acoustic emissions (AE's). The results where interpreted in terms of the fracture and indicate that only when is persistent significant correlations are observed. The Hurst number is a quantitative measure of persistence and anti - persistence. The existence of magnitude correlations, which indicates a sense of predictability in the earthquake magnitudes; is found when the the fracture process is persistent which also indicates a sense of predictability. The study of magnitude correlations in different tectonic zones and fault types consistently showed significant results and no differentiation was observed.

8. Forecasting in Southern California over a 5 year period showed that Bayesian ETAS model is a far superior to the compound model. The forecast included point estimate predictions, where the Bayesian ETAS predicted 19/20 earthquakes and the compound Poisson model 11/20 earthquakes. The assumption that simple statistical models can perform in an equal basis with the more advanced models has not been validated.

9. Studies in Turkey has shown that the number of aftershocks of large earthquakes over magnitude 5 follow a geometric distribution. This was tested in Southern California and it was shown that the number aftershocks do not follow a geometric distribution, instead a power law distribution is observed.

7.0.1 Limitations

This section discusses the limitations of this thesis as it currently stands.

1. Limitations on the earthquake catalog applications

   Throughout the thesis has been shown that the quality of the earthquake catalog data are the biggest source of bias to the study of earthquake magnitude correlations followed by the variations of the G-R b value in space, time and with the seismicity rate which are not taken into consideration in previous studies. The methodology proposed in this thesis provides a robust solution to the study of earthquake magnitude correlations however it has some limitations. The main limitation is that it can be applied only to regions with high quality data and dense seismic networks. The methodology would be more accurate when applied to areas with the same type of faulting and stable b values, in periods of time where the algorithms for calculating the magnitudes do not change and the magnitude that is reported is of the same type (e.g. ML). Regions like California, Japan and Greece provide information about the evolution of their seismic networks and algorithms used however other regions with high seismicity like Nepal have poor seismic network which makes the application of the method not possible. A solution would be to divide the area under study into a grid where each grid ensures b value stability and one dominant faulting type.

2. Limitations on the experimental applications

   During this thesis a number of experiments have been conducted with the simultaneous recording of AE's in different conditions that represent conditions in the upper 5 km of the earth's crust. This poses a limitation since seismicity is not limited to these depths. The inclusion of experiments that represent larger crustal depths it is one of the proposed improvements for the experimental work and part of future work. The choice of one type of rock (sandstone) for

all the experiments could be a limitation however it was deliberately chosen due to the excellent reproducibility.

7.0.2 Future work

Future work to further develop and validate the research in this thesis are presented. These are:

1. Study different regions and tectonic environments. For example Japan that includes a variety of fault types and experiences earthquakes of very large magnitude could be ideal for studying. Japan has a dense seismic network and provides high quality data. The effect of STAI would have to be carefully removed since it can last for several days after a magnitude 9 earthquake. However the variations of the b value spatially and separated by faulting type along with the corresponding magnitude correlation outcome would be an idea for future work.

2. Quantify the extend to which applying the proposed methodology would improve current forecasting and seismic hazard approaches.

3. The experimental work can be extended in the future to study the fracture process of individual faults, find their Hurst number and compare the results with the analysis of the earthquake catalog data for this fault.

4. The compound Poisson model can be applied to make forecasts to regions that the geometric distribution has a better fit to the length of the aftershocks in that region.

References

Aki, K. (1965), Maximum likelihood estimate of b in the formula logn= a-bm and its confidence limits, *Bulletin of the Earthquake Research Institute*, *43*, 237–239.

Aki, K. (1987), Magnitude-frequency relation for small earthquakes: A clue to the origin of max of large earthquakes, *Journal of Geophysical Research: Solid Earth*, *92*(B2), 1349–1355.

Aki, K., and A. S. Furumoto (1956), *Some problems in statistical seismology*, Hawaii Institute of Geophysics, University of Hawaii.

Aktas, S., H. Konsuk, and A. Yî?îter (2009), Estimation of change point and compound poisson process parameters for the earthquake data in turkey, *Environmetrics*, *20*(4), 416–427.

Amorèse, D. (2007), Applying a change-point detection method on frequency-magnitude distributions, *Bulletin of the Seismological Society of America*, *97*(5), 1742–1749.

Angelier, J., N. Lybéris, X. Le Pichon, E. Barrier, and P. Huchon (1982), The tectonic development of the hellenic arc and the sea of crete: a synthesis, *Tectonophysics*, *86*(1-3), 159165,167–163,196.

Ashby, M., and C. Sammis (1990), The damage mechanics of brittle solids in compression, *Pure and Applied Geophysics*, *133*(3), 489–521.

Avallone, A., et al. (2004), Analysis of eleven years of deformation measured by gps in the corinth rift laboratory area, *Comptes Rendus Geoscience*, *336*(4), 301–311.

Bak, P., C. Tang, and K. Wiesenfeld (1987), Self-organized criticality: An explanation of the 1/f noise, *Phys. Rev. Lett.*, *59*, 381–384, doi: 10.1103/PhysRevLett.59.381.

Bak, P., C. Tang, and K. Wiesenfeld (1988), Self-organized criticality, *Physical review A*, *38*(1), 364.

Baró, J., Á. Corral, X. Illa, A. Planes, E. K. Salje, W. Schranz, D. E. Soto-Parra, and E. Vives (2013), Statistical similarity between the compression of a porous material and earthquakes, *Physical review letters*, *110*(8), 088,702.

Baud, P., and P. Meredith (1997), Damage accumulation during triaxial creep of darley dale sandstone from pore volumometry and acoustic emission, *International Journal of Rock Mechanics and Mining Sciences*, *34*(3-4), 24–e1.

Bell, R. E., L. C. McNeill, J. M. Bull, and T. J. Henstock (2008), Evolution of the offshore western gulf of corinth, *Geological Society of America Bulletin*, *120*(1-2), 156–178.

Bernard, P., et al. (2006), Seismicity, deformation and seismic hazard in the western rift of corinth: New insights from the corinth rift laboratory (crl), *Tectonophysics*, *426*(1), 7–30.

Caruso, F., and H. Kantz (2011), Prediction of extreme events in the ofc model on a small world network, *The European Physical Journal B-Condensed Matter and Complex Systems*, *79*(1), 7–11.

Chouliaras, G. (2009), Investigating the earthquake catalog of the national observatory of athens, *Natural Hazards and Earth System Science*, *9*(3), 905–912.

Christophersen, A., and E. G. Smith (2000), A global model for aftershock behaviour, in *Proceedings of the 12th World Conference on Earthquake Engineering,*

Auckland, New Zealand. Paper, vol. 379.

Clint, O. C. (1999), Electrical potential changes and acoustic emissions generated by fracture and fluid flow during experimental triaxial rock deformation, Ph.D. thesis, University of London.

Console, R., M. Murru, and F. Catalli (2006), Physical and stochastic models of earthquake clustering, *Tectonophysics*, *417*(1), 141–153.

Console, R., M. Murru, F. Catalli, and G. Falcone (2007), Real time forecasts through an earthquake clustering model constrained by the rate-and-state constitutive law: Comparison with a purely stochastic etas model, *Seismological Research Letters*, *78*(1), 49–56.

Console, R., D. Jackson, and Y. Kagan (2010), Using the etas model for catalog declustering and seismic background assessment, *Pure and applied geophysics*, *167*(6-7), 819–830.

Costin, L. (1983), A microcrack model for the deformation and failure of brittle rock, *Journal of Geophysical Research: Solid Earth*, *88*(B11), 9485–9492.

Daley, D., and D. Vere-Jones (2003), Basic properties of the poisson process, *An Introduction to the Theory of Point Processes: Volume I: Elementary Theory and Methods*, pp. 19–40.

Daley, D. J., and D. Vere-Jones (2007), *An introduction to the theory of point processes: volume II: general theory and structure*, Springer Science & Business Media.

Davidsen, J., and A. Green (2011), Are earthquake magnitudes clustered?, *Phys. Rev. Lett.*, *106*, 108,502, doi: 10.1103/PhysRevLett.106.108502.

Davidsen, J., C. Gu, and M. Baiesi (2015), Generalized omori–utsu law for aftershock sequences in southern california, *Geophysical Journal International*, *201*(2), 965–978.

Davison, A. C., and D. V. Hinkley (1997), *Bootstrap methods and their application*, vol. 1, Cambridge university press.

Dieterich, J. (1994), A constitutive law for rate of earthquake production and its application to earthquake clustering, *Journal of Geophysical Research: Solid Earth*, *99*(B2), 2601–2618.

Eccles, D., P. Sammonds, and O. Clint (2005), Laboratory studies of electrical potential during rock failure, *International journal of rock mechanics and mining sciences*, *42*(7), 933–949.

Efron, B. (1981), Nonparametric estimates of standard error: the jackknife, the bootstrap and other methods, *Biometrika*, pp. 589–599.

Enescu, B., J. Mori, M. Miyazawa, and Y. Kano (2009), Omori-utsu law c-values associated with recent moderate earthquakes in japan, *Bulletin of the Seismological Society of America*, *99*(2A), 884–891.

Evison, F., and D. Rhoades (1997), The precursory earthquake swarm in new zealand: hypothesis tests, *New Zealand Journal of Geology and Geophysics*, *40*(4), 537–547.

Evison, F., and D. Rhoades (1999), The precursory earthquake swarm and the inferred precursory quarm, *New Zealand Journal of Geology and Geophysics*, *42*(2), 229–236.

Falcone, G., R. Console, and M. Murru (2010), Short-term and long-term earthquake occurrence models for italy: Etes, ers and ltst, *Annals of Geophysics*, *53*(3), 41–50.

Field, E. H. (2007), Overview of the working group for the development of regional earthquake likelihood models (relm), *Seismological Research Letters*, *78*(1), 7–16.

Gardner, J., and L. Knopoff (1974), Is the sequence of earthquakes in southern california, with aftershocks removed, poissonian?, *Bulletin of the Seismological*

Society of America, *64*(5), 1363–1367.

Gerstenberger, M. C., S. Wiemer, L. M. Jones, and P. A. Reasenberg (2005), Real-time forecasts of tomorrow's earthquakes in california, *Nature*, *435*(7040), 328–331.

Glickman, M. E., and D. A. van Dyk (2007), Basic bayesian methods, *Topics in Biostatistics*, pp. 319–338.

Glover, P., P. Baud, M. Darot, P. Meredith, S. Boon, M. LeRavalec, S. Zoussi, and T. Reuschle (1995), α/β phase transition in quartz monitored using acoustic emissions, *Geophysical Journal International*, *120*(3), 775–782.

Golyk, V. A. (), Self-organized criticality.

Gulia, L. (2010), Detection of quarry and mine blast contamination in european regional catalogues, *Natural hazards*, *53*(2), 229–249.

Gulia, L., and S. Wiemer (2010), The influence of tectonic regimes on the earthquake size distribution: A case study for italy, *Geophysical Research Letters*, *37*(10).

Gulia, L., S. Wiemer, and M. Wyss (2012), Catalog artifacts and quality control, *Community Online Resource for Statistical Seismicity Analysis*, *10*.

Gutenberg, B., and C. F. Richter (1944), Frequency of earthquakes in california, *Bulletin of the Seismological Society of America*, *34*(4), 185–188.

Hainzl, S. (2016), Rate-dependent incompleteness of earthquake catalogs, *Seismological Research Letters*, *87*(2A), 337–344.

Hainzl, S., and D. Marsan (2008), Dependence of the omori-utsu law parameters on main shock magnitude: Observations and modeling, *Journal of Geophysical Research: Solid Earth*, *113*(B10).

Hainzl, S., S. Steacy, and D. Marsan (2010), Seismicity models based on coulomb stress calculations.

Hauksson, E., W. Yang, and P. M. Shearer (2012), Waveform relocated earthquake catalog for southern california (1981 to june 2011), *Bulletin of the Seismological Society of America*, *102*(5), 2239–2244.

Hawkes, A. (), Adamopoulos (1973), *Cluster models for earthquakesregional*.

Hawkes, A. G. (1971), Spectra of some self-exciting and mutually exciting point processes, *Biometrika*, pp. 83–90.

Hawkes, A. G., and D. Oakes (1974), A cluster process representation of a self exciting process, *Journal of Applied Probability*, *11*(03), 493–503.

Hawkes, I., and M. Mellor (1970), Uniaxial testing in rock mechanics laboratories, *Engineering Geology*, *4*(3), 179–285.

Heap, M., P. Baud, P. Meredith, A. Bell, and I. Main (2009), Time-dependent brittle creep in darley dale sandstone, *Journal of Geophysical Research: Solid Earth (1978–2012)*, *114*(B7).

Heap, M. J. (2009), Creep: time-dependent brittle deformation in rocks, Ph.D. thesis, UCL (University College London).

Helmstetter, A. (2003), Is earthquake triggering driven by small earthquakes?, *Physical Review Letters*, *91*(5), 058,501.

Helmstetter, A., and D. Sornette (2002), Subcritical and supercritical regimes in epidemic models of earthquake aftershocks, *Journal of Geophysical Research: Solid Earth (1978–2012)*, *107*(B10), ESE–10.

Helmstetter, A., and M. J. Werner (2014), Adaptive smoothing of seismicity in time, space, and magnitude for time-dependent earthquake forecasts for california, *Bulletin of the Seismological Society of America*, *104*(2), 809–822.

Helmstetter, A., Y. Y. Kagan, and D. D. Jackson (2005), Importance of small earthquakes for stress transfers and earthquake triggering, *Journal of Geophysical Research: Solid Earth*, *110*(B5).

Helmstetter, A., Y. Y. Kagan, and D. D. Jackson (2006), Comparison of short-term and time-independent earthquake forecast models for southern california, *Bulletin of the Seismological Society of America*, *96*(1), 90–106.

Helmstetter, A., Y. Y. Kagan, and D. D. Jackson (2007), High-resolution time-independent grid-based forecast for m 5 earthquakes in california, *Seismological Research Letters*, *78*(1), 78–86.

Henderson, J., I. Main, P. Meredith, and P. Sammonds (1992), The evolution of seismicity at parkfield: observation, experiment and a fracture-mechanical interpretation, *Journal of Structural Geology*, *14*(8-9), 905–913.

Hirth, G., and S. Guillot (2013), Rheology and tectonic significance of serpentinite, *Elements*, *9*(2), 107–113.

Holliday, J. R., J. B. Rundle, K. F. Tiampo, W. Klein, and A. Donnellan (2006), Systematic procedural and sensitivity analysis of the pattern informatics method for forecasting large (m¿ 5) earthquake events in southern california, *pure and applied geophysics*, *163*(11), 2433–2454.

Huang, J., and D. Turcotte (1988), Fractal distributions of stress and strength and variations of b-value, *Earth and Planetary Science Letters*, *91*(1-2), 223–230.

Hurst, H. E., R. P. Black, and Y. Simaika (1965), *Long-term storage: an experimental study*, Constable.

Husen, S., and J. Hardebeck (2010), Earthquake location accuracy, community online resource for statistical seismicity analysis.

Ishimoto, M., and K. Iida (1939), Observations sur les seismes enregistres par le microsismographe construit dernierement (1), *Bull. Earthq. Res. Inst. Univ. Tokyo*, *17*, 443–478.

Jackson, J. (1994), Active tectonics of the aegean region, *Annual Review of Earth and Planetary Sciences*, *22*(1), 239–271.

Jeffreys, H. (1998), Theory of probability, 1967, reprinted in oxford classic texts in the physical sciences.

Kagan, Y. (1973), Statistical methods in the study of seismic processes, *Bull. Int. Statist. Inst*, *45*, 437–453.

Kagan, Y. Y. (2002), Seismic moment distribution revisited: I. statistical results, *Geophysical Journal International*, *148*(3), 520–541.

Kagan, Y. Y. (2004), Short-term properties of earthquake catalogs and models of earthquake source, *Bulletin of the Seismological Society of America*, *94*(4), 1207–1228.

Kagan, Y. Y. (2013), *EARTHQUAKES: models, statistics, testable forecasts*, John Wiley & Sons.

Kagan, Y. Y., and H. Houston (2005), Relation between mainshock rupture process and omoris law for aftershock moment release rate, *Geophysical Journal International*, *163*(3), 1039–1048.

Kendall, D. G. (1949), Stochastic processes and population growth, *Journal of the Royal Statistical Society. Series B (Methodological)*, *11*(2), 230–282.

King, G. C., R. S. Stein, and J. Lin (1994), Static stress changes and the triggering of earthquakes, *Bulletin of the Seismological Society of America*, *84*(3), 935–953.

Knopoff, L., and J. Gardner (1972), Higher seismic activity during local night on the raw worldwide earthquake catalogue, *Geophysical Journal International*, *28*(3), 311–313.

Kwiatek, G., K. Plenkers, M. Nakatani, Y. Yabe, G. Dresen, et al. (2010), Frequency-magnitude characteristics down to magnitude-4.4 for induced seismicity recorded at mponeng gold mine, south africa, *Bulletin of the Seismological Society of America*, *100*(3), 1165–1173.

Lanzante, J. R. (1996), Resistant, robust and non-parametric techniques for the analysis of climate data: theory and examples, including applications to historical radiosonde station data, *International Journal of Climatology*, *16*(11), 1197–1226.

Lay, T., and T. C. Wallace (1995), *Modern global seismology*, vol. 58, Academic press.

Lennartz, S., A. Bunde, and D. Turcotte (2011), Modelling seismic catalogues by cascade models: Do we need long-term magnitude correlations?, *Geophysical Journal International*, *184*(3), 1214–1222.

Lippiello, E., L. de Arcangelis, and C. Godano (2008), Influence of time and space correlations on earthquake magnitude, *Physical review letters*, *100*(3), 038,501.

Lippiello, E., C. Godano, and L. Arcangelis (2012), The earthquake magnitude is influenced by previous seismicity, *Geophysical Research Letters*, *39*(5).

Lippiello, E., C. Godano, and L. de Arcangelis (2013), Magnitude correlations in the olami-feder-christensen model, *EPL (Europhysics Letters)*, *102*(5), 59,002.

Lockner, D. (1993), The role of acoustic emission in the study of rock fracture, in *International Journal of Rock Mechanics and Mining Sciences & Geomechanics Abstracts*, vol. 30, pp. 883–899, Elsevier.

Lombardi, A. M., and W. Marzocchi (2010), The etas model for daily forecasting of italian seismicity in the csep experiment, *Annals of Geophysics*.

Main, I. (1996), Statistical physics, seismogenesis, and seismic hazard, *Reviews of Geophysics*, *34*(4), 433–462.

Main, I., et al. (1999), Is the reliable prediction of individual earthquakes a realistic scientific goal, *Nature*, *397*(1).

Main, I. G. (1987), A characteristic earthquake model of the seismicity preceding the eruption of mount st. helens on 18 may 1980, *Physics of the earth and planetary interiors*, *49*(3-4), 283–293.

Main, I. G., S. Peacock, and P. G. Meredith (1990), Scattering attenuation and the fractal geometry of fracture systems, *pure and applied geophysics*, *133*(2), 283–304.

Main, I. G., P. G. Meredith, and P. R. Sammonds (1992), Temporal variations in seismic event rate and b-values from stress corrosion constitutive laws, *Tectonophysics*, *211*(1-4), 233–246.

Main, I. G., P. R. Sammonds, and P. G. Meredith (1993), Application of a modified griffith criterion to the evolution of fractal damage during compressional rock failure, *Geophysical Journal International*, *115*(2), 367, doi: 10.1111/j.1365-246X.1993.tb01192.x.

Mann, H. B., and D. R. Whitney (1947), On a test of whether one of two random variables is stochastically larger than the other, *The annals of mathematical statistics*, pp. 50–60.

Marzocchi, W., and A. M. Lombardi (2009), Real-time forecasting following a damaging earthquake, *Geophysical Research Letters*, *36*(21).

Marzocchi, W., and L. Sandri (2003), A review and new insights on the estimation of the b-valueand its uncertainty, *Annals of geophysics*.

McKenzie, D. (1970), Plate tectonics of the mediterranean region, *Nature*, *226*, 239–243.

McKenzie, D. (1972), Active tectonics of the mediterranean region, *Geophysical Journal International*, *30*(2), 109–185.

McLaskey, G. C., D. A. Lockner, B. D. Kilgore, and N. M. Beeler (2015), A robust calibration technique for acoustic emission systems based on momentum transfer from a ball drop, *Bulletin of the Seismological Society of America*, *105*(1), 257–271.

Michael, A. J., and S. Wiemer (2010), Theme i–introductory material.

Mignan, A. (2012), Estimating the magnitude of completeness for earthquake catalogs, *Community Online Resource for Statistical Seismicity Analysis*.

Mignan, A., and G. Chouliaras (2014), Fifty years of seismic network performance in greece (1964–2013): spatiotemporal evolution of the completeness magnitude, *Seismological Research Letters*, *85*(3), 657–667.

Mignan, A., M. Werner, S. Wiemer, C.-C. Chen, and Y.-M. Wu (2011), Bayesian estimation of the spatially varying completeness magnitude of earthquake catalogs, *Bulletin of the Seismological Society of America*, *101*(3), 1371–1385.

Mogi, K. (1963), Magnitude-frequency relation for elastic shocks accompanying fractures of various materials and some related problems in earthquakes (2nd paper).

Mogi, K. (1966), Pressure dependence of rock strength and transition from brittle fracture to ductile flow.

Narteau, C., S. Byrdina, P. Shebalin, and D. Schorlemmer (2009), Common dependence on stress for the two fundamental laws of statistical seismology, *Nature*, *462*(7273), 642–645.

Nava, F., V. Márquez-Ramírez, F. Zúñiga, L. Ávila-Barrientos, and C. Quinteros (2016), Gutenberg-richter b-value maximum likelihood estimation and sample size, *Journal of Seismology*, pp. 1–9.

Naylor, M., K. Orfanogiannaki, and D. Harte (2010), Exploratory data analysis: Magnitude, space, and time, *Community Online Resource for Statistical Seismicity Analysis*, *10*.

Nichols, K., and F. P. Schoenberg (2014), Assessing the dependency between the magnitudes of earthquakes and the magnitudes of their aftershocks, *Environmetrics*, *25*(3), 143–151.

Ogata, Y. (1986), Statistical models for earthquake occurrences and residual analysis for point processes, *Mathematical Seismology*, *1*, 228–281.

Ogata, Y. (1988), Statistical models for earthquake occurrences and residual analysis for point processes, *Journal of the American Statistical association*, *83*(401), 9–27.

Ogata, Y. (1989), Statistical model for standard seismicity and detection of anomalies by residual analysis, *Tectonophysics*, *169*(1-3), 159–174.

Ogata, Y. (1998), Space-time point-process models for earthquake occurrences, *Annals of the Institute of Statistical Mathematics*, *50*(2), 379–402.

Ogata, Y. (1999), Seismicity analysis through point-process modeling: A review, *Pure & Applied Geophysics*, *155*(2-4), 471.

Ogata, Y. (2011), Significant improvements of the space-time etas model for forecasting of accurate baseline seismicity, *Earth, planets and space*, *63*(3), 217–229.

Ogata, Y., and K. Katsura (1993), Analysis of temporal and spatial heterogeneity of magnitude frequency distribution inferred from earthquake catalogues, *Geophysical Journal International*, *113*(3), 727–738.

Ogata, Y., and J. Zhuang (2006), Space-time etas models and an improved extension, *Tectonophysics*, *413*(1), 13–23.

Omori, F. (1894), *On the after-shocks of earthquakes*, vol. 7, The University.

Özel, G. (2011), A bivariate compound poisson model for the occurrence of foreshock and aftershock sequences in turkey, *Environmetrics*, *22*(7), 847–856.

Özel, G., and C. Inal (2008), The probability function of the compound poisson process and an application to aftershock sequence in turkey, *Environmetrics*, *19*(1), 79–85.

Papanikolaou, D., and E. Vassilakis (2010), Thrust faults and extensional detachment faults in cretan tectono-stratigraphy: implications for middle miocene extension, *Tectonophysics*, *488*(1), 233–247.

Papazachos, V., B. Papazachos, C. Papazachou, and K. Papazachou (1997), *The earthquakes of Greece*, Editions Ziti.

Paterson, M. S., and T.-f. Wong (2005), *Experimental rock deformation-the brittle field*, Springer Science & Business Media.

Pavlis, G. L. (1986), Appraising earthquake hypocenter location errors: A complete, practical approach for single-event locations, *Bulletin of the Seismological Society of America*, *76*(6), 1699–1717.

Perez, N. (2017), Introduction to fracture mechanics, in *Fracture Mechanics*, pp. 53–77, Springer.

Reasenberg, P. (1985), Second-order moment of central california seismicity, 1969–1982, *Journal of Geophysical Research: Solid Earth*, *90*(B7), 5479–5495.

Reasenberg, P., and L. Jones (1994), Earthquake aftershocks: update, *Science*, *265*(5176), 1251–1253.

Reasenberg, P. A., and L. M. Jones (1989), Earthquake hazard after a mainshock in california, *Science*, *243*(4895), 1173.

Rhoades, D. A. (2007), Application of the eepas model to forecasting earthquakes of moderate magnitude in southern california, *Seismological Research Letters*, *78*(1), 110–115.

Rhoades, D. A. (2010), Lessons and questions from thirty years of testing the precursory swarm hypothesis, *Pure and applied geophysics*, *167*(6-7), 629–644.

Rhoades, D. A., and F. F. Evison (2004), Long-range earthquake forecasting with every earthquake a precursor according to scale, *Pure and applied geophysics*, *161*(1), 47–72.

Robert, C. (2007), *The Bayesian choice: from decision-theoretic foundations to computational implementation*, Springer Science & Business Media.

Rogers, A. (1995), Population forecasting: Do simple models outperform complex models?, *Mathematical Population Studies*, *5*(3), 187–202.

Ross, G. J. (2017), Bayesian estimation of the etas model for earthquake occurrences.

Royden, L. H., and D. J. Papanikolaou (2011), Slab segmentation and late cenozoic disruption of the hellenic arc, *Geochemistry, Geophysics, Geosystems*, *12*(3).

Rundle, J., K. Tiampo, W. Klein, and J. S. Martins (2002), Self-organization in leaky threshold systems: The influence of near-mean field dynamics and its implications for earthquakes, neurobiology, and forecasting, *Proceedings of the National Academy of Sciences*, *99*(suppl 1), 2514–2521.

Rundle, J. B., and W. Klein (1989), Nonclassical nucleation and growth of cohesive tensile cracks, *Physical review letters*, *63*(2), 171.

Rundle, J. B., W. Klein, K. Tiampo, and S. Gross (2000a), Dynamics of seismicity patterns in systems of earthquake faults, *Geocomplexity and the Physics of Earthquakes*, pp. 127–146.

Rundle, J. B., W. Klein, K. Tiampo, and S. Gross (2000b), Linear pattern dynamics in nonlinear threshold systems, *Physical Review E*, *61*(3), 2418.

Rundle, J. B., D. L. Turcotte, R. Shcherbakov, W. Klein, and C. Sammis (2003), Statistical physics approach to understanding the multiscale dynamics of earthquake fault systems, *Reviews of Geophysics*, *41*(4).

Rydelek, P. A., and I. S. Sacks (1989), Testing the completeness of earthquake catalogues and the hypothesis of self-similarity, *Nature*, *337*(6204), 251–253.

Sammonds, P. (1999), Understanding the fundemental physics governing the evolution and dynamics of the earth'crust and ice sheets, *Philosophical Transactions of the Royal Society of London A: Mathematical, Physical and Engineering Sciences*, *357*(1763), 3377–3401.

Sammonds, P., and M. Ohnaka (1998), Evolution of microseismicity during frictional sliding, *Geophysical Research Letters*, *25*(5), 699–702.

Sammonds, P., P. Meredith, and I. Main (1992), Role of pore fluids in the generation of seismic precursors to shear fracture, *Nature*, *359*(6392), 228–230.

Sarlis, N. (2011), Magnitude correlations in global seismicity, *Physical Review E*, *84*(2), 022,101.

Scholz, C. (1968a), The frequency-magnitude relation of microfracturing in rock and its relation to earthquakes, *Bulletin of the Seismological Society of America*, *58*(1), 399–415.

Scholz, C. (1968b), The frequency-magnitude relation of microfracturing in rock and its relation to earthquakes, *Bulletin of the Seismological Society of America*, *58*(1), 399–415.

Scholz, C. H. (1990), *The mechanics of earthquakes and faulting*, Cambridge university press.

Schorlemmer, D., and J. Woessner (2008), Probability of detecting an earthquake, *Bulletin of the Seismological Society of America*, *98*(5), 2103–2117.

Schorlemmer, D., S. Wiemer, and M. Wyss (2005), Variations in earthquake-size distribution across different stress regimes, *Nature*, *437*(7058), 539–542.

Segou, M. (2016), Physics-based and statistical earthquake forecasting in a continental rift zone: the case study of corinth gulf (greece), *Geophysical Journal International*, *204*(1), 591, doi: 10.1093/gji/ggv467.

Seif, S., A. Mignan, J. Zechar, M. Werner, and S. Wiemer (2016), Estimating etas: the effects of truncation, missing data, and model assumptions, *Journal of Geophysical Research: Solid Earth*.

Shaw, B., and J. Jackson (2010), Earthquake mechanisms and active tectonics of the hellenic subduction zone, *Geophysical Journal International*, *181*(2), 966–984.

Shcherbakov, R., D. L. Turcotte, and J. B. Rundle (2004), A generalized omori's law for earthquake aftershock decay, *Geophysical research letters*, *31*(11).

Shcherbakov, R., D. L. Turcotte, and J. B. Rundle (2006), Scaling properties of the parkfield aftershock sequence, *Bulletin of the Seismological Society of America*, *96*(4B), S376–S384.

Smith, W. D. (1981), The b-value as an earthquake precursor, *Nature*, *289*, 136–139.

Sornette, A., and D. Sornette (1999), Renormalization of earthquake aftershocks, *arXiv preprint cond-mat/9905314*.

Sornette, D., and S. Utkin (2009a), Limits of declustering methods for disentangling exogenous from endogenous events in time series with foreshocks, main shocks, and aftershocks, *Physical Review E*, *79*(6), 061,110.

Sornette, D., and S. Utkin (2009b), Limits of declustering methods for disentangling exogenous from endogenous events in time series with foreshocks, main shocks, and aftershocks, *Physical Review E*, *79*(6), 061,110.

Tiampo, K., J. Rundle, S. McGinnis, S. Gross, and W. Klein (2000), Observation of systematic variations in non-local seismicity patterns from southern california, *Geocomplexity and the Physics of Earthquakes*, pp. 211–218.

Tiampo, K., J. Rundle, S. McGinnis, S. Gross, and W. Klein (2002a), Mean-field threshold systems and phase dynamics: An application to earthquake fault systems, *EPL (Europhysics Letters)*, *60*(3), 481.

Tiampo, K., J. Rundle, and W. Klein (2006a), Premonitory seismicity changes prior to the parkfield and coalinga earthquakes in southern california, *Tectonophysics*, *413*(1), 77–86.

Tiampo, K., J. Rundle, W. Klein, and J. Holliday (2006b), Forecasting rupture dimension using the pattern informatics technique, *Tectonophysics*, *424*(3), 367–376.

Tiampo, K. F., and R. Shcherbakov (2012), Seismicity-based earthquake forecasting techniques: Ten years of progress, *Tectonophysics*, *522*, 89–121.

Tiampo, K. F., J. B. Rundle, S. A. McGinnis, and W. Klein (2002b), Pattern dynamics and forecast methods in seismically active regions, *Earthquake Processes: Physical Modelling, Numerical Simulation and Data Analysis Part II*, pp. 2429–2467.

Turcotte, D., J. Holliday, and J. Rundle (2007), Bass, an alternative to etas, *Geophysical Research Letters*, *34*(12).

Turcotte, D. L. (1997), *Fractals and chaos in geology and geophysics*, Cambridge university press.

Urbancic, T., C. Trifu, J. Long, and R. Young (1992), Space-time correlations ofb values with stress release, *Pure and Applied Geophysics*, *139*(3), 449–462.

Utsu, T. (1961), A statistical study on the occurrence of aftershocks., *Geophysical Magazine*, *30*(4).

Utsu, T. (1970), Aftershocks and earthquake statistics (1): Some parameters which characterize an aftershock sequence and their interrelations, *Journal of the Faculty of Science, Hokkaido University. Series 7, Geophysics*, *3*(3), 129–195.

Van Stiphout, T., J. Zhuang, and D. Marsan (2012), Seismicity declustering. community online resource for statistical seismicity analysis. doi: 10.5078/corssa-52382934.

Veen, A., and F. P. Schoenberg (2008), Estimation of space–time branching process models in seismology using an em type algorithm, *Journal of the American Statistical Association*, *103*(482), 614–624.

Vere-Jones, D. (1970), Stochastic models for earthquake occurrence, *Journal of the Royal Statistical Society. Series B (Methodological)*, pp. 1–62.

Vere-Jones, D. (2000), Seismologya statistical vignette, *Journal of the American Statistical Association*, *95*(451), 975–978.

Vere-Jones, D. (2006), The development of statistical seismology: A personal experience, *Tectonophysics*, *413*(1), 5–12.

Vere-Jones, D. (2010), How to educate yourself as a statistical seismologist, *Community Online Resource for Statistical Seismicity Analysis*, *10*.

Vere-Jones, D., and R. Davies (1966), A statistical survey of earthquakes in the main seismic region of new zealand: Part 2time series analyses, *New Zealand journal of geology and geophysics*, *9*(3), 251–284.

Vere-Jones, D., and W. Smith (1981), Statistics in seismology, *Communications in Statistics-Theory and methods*, *10*(15), 1559–1585.

Watts, A., and E. Burov (2003), Lithospheric strength and its relationship to the elastic and seismogenic layer thickness, *Earth and Planetary Science Letters*, *213*(1), 113–131.

Wells, D. L., and K. J. Coppersmith (1994), New empirical relationships among magnitude, rupture length, rupture width, rupture area, and surface displacement, *Bulletin of the seismological Society of America*, *84*(4), 974–1002.

Werner, M. J., and D. Sornette (2008), Magnitude uncertainties impact seismic rate estimates, forecasts, and predictability experiments, *Journal of Geophysical Research: Solid Earth*, *113*(B8).

Werner, M. J., A. Helmstetter, D. D. Jackson, and Y. Y. Kagan (2011), High-resolution long-term and short-term earthquake forecasts for california, *Bulletin of the Seismological Society of America*, *101*(4), 1630–1648.

Wesnousky, S. G. (1994), The gutenberg-richter or characteristic earthquake distribution, which is it?, *Bulletin of the Seismological Society of America*, *84*(6), 1940–1959.

Westerhaus, M., M. Wyss, R. Yilmaz, and J. Zschau (2002), Correlating variations of b values and crustal deformations during the 1990s may have pinpointed the rupture initiation of the m w= 7.4 izmit earthquake of 1999 august 17, *Geophysical Journal International*, *148*(1), 139–152.

Wiemer, S. (2001), A software package to analyze seismicity: Zmap, *Seismological Research Letters*, *72*(3), 373–382.

Wiemer, S., and M. Baer (2000), Mapping and removing quarry blast events from seismicity catalogs, *Bulletin of the Seismological Society of America*, *90*(2), 525–530.

Wiemer, S., and D. Schorlemmer (2007), Alm: An asperity-based likelihood model for california, *Seismological Research Letters*, *78*(1), 134–140.

Wiemer, S., and M. Wyss (2000), Minimum magnitude of completeness in earthquake catalogs: Examples from alaska, the western united states, and japan, *Bulletin of the Seismological Society of America*, *90*(4), 859–869.

Wiemer, S., and M. Wyss (2002), Mapping spatial variability of the frequency-magnitude distribution of earthquakes, *Advances in geophysics*, *45*, 259–V.

Wiemer, S., D. Giardini, D. Fäh, N. Deichmann, and S. Sellami (2009), Probabilistic seismic hazard assessment of switzerland: best estimates and uncertainties, *Journal of Seismology*, *13*(4), 449.

Woessner, J., and S. Wiemer (2005), Assessing the quality of earthquake catalogues: Estimating the magnitude of completeness and its uncertainty, *Bulletin of the Seismological Society of America*, *95*(2), 684–698.

Woessner, J., J. Hardebeck, and E. Hauksson (2010), Theme iv–understanding seismicity catalogs and their problems.

Wyss, M., A. Hasegawa, S. Wiemer, and N. Umino (1999), Quantitative mapping of precursory seismic quiescence before the 1989, m 7.1 off-sanriku earthquake,

japan.

Zhuang, J., Y. Ogata, and D. Vere-Jones (2002), Stochastic declustering of space-time earthquake occurrences, *Journal of the American Statistical Association*, *97*(458), 369–380.

Appendices

Appendix A

Synthetic catalogs results

A.1 Parkfield - Cut off magnitude 1.1

The correlation, the Confidence intervals and the corresponding p value between the low and high intensity data for 1000 synthetic catalogs are shown in the table below.

Correlation	Confidence Interval	Confidence interval2	p value
0.0004	-0.0267	0.0299	0.888
0.0024	-0.0236	0.0291	0.995
0.0021	-0.027	0.0314	0.594
-0.002	-0.0323	0.0308	0.952
-0.0001	-0.0326	0.0336	0.412
-0.0138	-0.0352	0.0115	0.294
-0.0087	-0.0268	0.0098	0.294
0.0209	-0.0039	0.0465	0.706
-0.0012	-0.02	0.0184	0.099
-0.0092	-0.0272	0.01	0.326
-0.0405	-0.0706	-0.0098	0.005
-0.0087	-0.0403	0.0246	0.519
0.0061	-0.022	0.0362	0.877
0.0129	-0.0189	0.0464	0.135
0.0069	-0.0175	0.0331	0.621
-0.0048	-0.0293	0.0216	0.476
-0.0236	-0.0469	0.0001	0.009
0.0024	-0.0266	0.033	0.524
0.004	-0.027	0.0371	0.509
-0.0073	-0.0376	0.0255	0.373
-0.004	-0.0253	0.0176	0.886
-0.0281	-0.0531	0.0002	0.764
-0.0096	-0.0274	0.0091	0.618
0.0028	-0.0197	0.0258	0.505
0.0188	-0.0156	0.0548	0.876
-0.0042	-0.0329	0.0257	0.402
0.0305	-0.0143	0.0792	0.61
0.0322	-0.0022	0.0691	0.043
-0.005	-0.0221	0.0127	0.624
0.0025	-0.0398	0.0517	0.503
0.01	-0.0192	0.0418	0.421
-0.0121	-0.0401	0.019	0.186
-0.0136	-0.0447	0.0187	0.081
0.0026	-0.0245	0.0312	0.624
0.027	-0.0076	0.0631	0.993
0.0005	-0.0343	0.0419	0.282
0.0081	-0.0234	0.042	0.92
-0.0186	-0.0408	0.0049	0.266
0.0087	-0.015	0.035	0.964
-0.0156	-0.0429	0.014	0.389
0.0002	-0.0217	0.0227	0.968
-0.0096	-0.0371	0.023	0.116
-0.0003	-0.0231	0.0226	0.603
-0.0107	-0.0376	0.0163	0.643

-0.0321	-0.0607	-0.0007	0.296
-0.0005	-0.0239	0.0247	0.42
-0.0056	-0.0314	0.0203	0.476
0.0085	-0.0184	0.0369	0.513
-0.0121	-0.0331	0.0103	0.192
0.0006	-0.0289	0.0325	0.63
-0.005	-0.0221	0.0127	0.624
0.002	-0.0157	0.0204	0.952
0.0037	-0.0186	0.0274	0.026
-0.025	-0.0463	-0.0019	0.544
-0.0224	-0.0437	-0.0014	0.683
-0.01	-0.0414	0.0228	0.381
-0.0278	-0.0549	0.0016	0.718
0.0012	-0.0212	0.0247	0.664
0.0034	-0.0363	0.0472	0.266
-0.0127	-0.0384	0.0151	0.054
-0.0115	-0.0341	0.0112	0.926
-0.0075	-0.031	0.0179	0.51
0.0164	-0.016	0.0505	0.779
0.0005	-0.0137	0.0149	0.256
0.0141	-0.0205	0.0509	0.381
0.0125	-0.0301	0.0621	0.492
-0.0005	-0.024	0.025	0.949
0.0127	-0.0309	0.058	0.421
-0.0135	-0.0294	0.0027	0.854
-0.0157	-0.0416	0.0131	0.96
-0.0021	-0.0297	0.0279	0.156
-0.0048	-0.0386	0.031	0.765
-0.0106	-0.0336	0.0134	0.434
-0.0036	-0.0296	0.0243	0.139
-0.0142	-0.0522	0.0277	0.608
0.0019	-0.0173	0.0219	0.08
-0.0075	-0.033	0.0193	0.748
-0.0043	-0.0382	0.0302	0.997
0.0111	-0.0133	0.0374	0.605
-0.0018	-0.0289	0.0257	0.212
-0.0207	-0.0526	0.0128	0.342
-0.0096	-0.0284	0.0101	0.637
-0.0295	-0.0532	-0.0043	0.252
-0.0196	-0.041	0.0037	0.334
-0.0266	-0.0471	-0.0052	0.768
0.0334	-0.0121	0.0839	0.806
-0.0286	-0.0503	-0.0062	0.141
-0.0195	-0.0386	0.0022	0.844
0.011	-0.021	0.0444	0.168

-0.0289	-0.0569	0.0004	0.614
-0.0058	-0.0252	0.0132	0.969
-0.019	-0.0447	0.0089	0.115
-0.0099	-0.0335	0.0148	0.507
-0.0168	-0.0427	0.0108	0.995
-0.0005	-0.0227	0.0225	0.343
-0.007	-0.0367	0.0229	0.713
0.0075	-0.0208	0.0388	0.88
0.0019	-0.0219	0.0269	0.88
0.0188	-0.0135	0.0535	0.128
-0.0104	-0.0382	0.0183	0.392
-0.0446	-0.074	-0.012	0.192
0.003	-0.0177	0.0247	0.445
0.0024	-0.0397	0.0558	0.928
-0.0047	-0.041	0.0358	0.884
-0.0242	-0.0487	0.0032	0.281
-0.0363	-0.0604	-0.0105	0.552
-0.0226	-0.0495	0.0074	0.311
-0.0267	-0.0587	0.0111	0.742
-0.0014	-0.0349	0.0347	0.358
0.0221	-0.009	0.0555	0.553
0.0015	-0.0337	0.0404	0.941
0.0124	-0.0174	0.0455	0.586
-0.0107	-0.0443	0.0282	0.727
0.0031	-0.0283	0.035	0.592
-0.0019	-0.0323	0.0305	0.363
-0.0181	-0.0415	0.0059	0.402
-0.0309	-0.061	0.0011	0.086
-0.029	-0.0628	0.0062	0.031
0.0012	-0.0301	0.0338	0.581
-0.0173	-0.0441	0.0109	0.334
-0.0062	-0.0339	0.0233	0.386
0.0068	-0.0198	0.036	0.08
-0.0079	-0.0354	0.0208	0.497
0.0079	-0.0222	0.0402	0.211
-0.0069	-0.0409	0.0325	0.529
0.0021	-0.027	0.034	0.885
0.0183	-0.0154	0.0552	0.191
0.011	-0.0272	0.0551	0.123
0.007	-0.0252	0.0416	0.577
-0.0314	-0.0684	0.0123	0.022
-0.0326	-0.0611	-0.0025	0.918
-0.013	-0.0419	0.0178	0.774
0.0069	-0.0249	0.0409	0.941
0.0132	-0.0198	0.0488	0.318

-0.0124	-0.0447	0.0206	0.805
-0.0295	-0.0515	-0.0043	0.358
-0.0113	-0.0435	0.0237	0.975
0.0117	-0.03	0.0592	0.36
0.0024	-0.0397	0.0558	0.928
-0.0104	-0.0463	0.0301	0.185
0.0139	-0.0113	0.0414	0.525
0.01	-0.0139	0.0357	0.297
0.0001	-0.0308	0.0334	0.378
-0.0166	-0.0396	0.0071	0.263
0.0115	-0.0258	0.0534	0.787
-0.0026	-0.0309	0.028	0.678
0.0052	-0.0246	0.0385	0.004
0.0106	-0.0174	0.0388	0.343
0.0075	-0.0236	0.0405	0.466
-0.0194	-0.0553	0.0184	0.004
0.0161	-0.0192	0.0531	0.704
0.0206	-0.0221	0.0687	0.611
0.0146	-0.0231	0.0574	0.061
0.0137	-0.0185	0.0482	0.709
-0.0208	-0.0447	0.0045	0.658
-0.0212	-0.042	0.0003	0.177
0.0115	-0.0163	0.0424	0.6
-0.0014	-0.025	0.023	0.722
-0.0023	-0.0328	0.0316	0.264
-0.0108	-0.0401	0.0199	0.393
-0.0036	-0.0424	0.0362	0.767
0.02	-0.0128	0.0551	0.993
0.0018	-0.0251	0.0296	0.912
0.0206	-0.0121	0.0561	0.345
0.0183	-0.0147	0.0538	0.103
-0.0104	-0.0317	0.013	0.364
0.0315	-0.0021	0.0664	0.498
0.0197	-0.0185	0.0586	0.273
-0.0065	-0.0455	0.0416	0.909
-0.01	-0.0385	0.0212	0.184
0.0095	-0.012	0.0325	0.173
0.0027	-0.0257	0.033	0.334
-0.0254	-0.0479	-0.0016	0.216
-0.049	-0.0772	-0.0179	0.006
0.0006	-0.0281	0.0306	0.667
-0.0059	-0.0332	0.023	0.647
-0.026	-0.0496	0.0018	0.434
-0.0105	-0.0486	0.0292	0.575
-0.0051	-0.0356	0.0271	0.951

-0.0093	-0.0419	0.0282	0.948
-0.0044	-0.0337	0.0254	0.45
0.0082	-0.0201	0.0368	0.846
-0.0017	-0.0253	0.0237	0.65
0.0251	-0.0108	0.0641	0.277
-0.0243	-0.0471	0.0003	0.97
-0.0202	-0.0521	0.0168	0.711
-0.0142	-0.045	0.018	0.321
-0.0064	-0.0373	0.0273	0.423
0.0001	-0.0278	0.0312	0.279
0.0065	-0.0237	0.0405	0.268
0.0147	-0.0145	0.0463	0.081
-0.0001	-0.0307	0.0334	0.759
0.0184	-0.0227	0.0655	0.436
0.0153	-0.0201	0.0597	0.588
-0.0056	-0.0354	0.0295	0.212
0.0079	-0.0298	0.0495	0.666
-0.0163	-0.0438	0.0141	0.732
-0.0166	-0.0379	0.0052	0.465
-0.0093	-0.038	0.0227	0.386
-0.0065	-0.0321	0.0218	0.768
0.0129	-0.0238	0.0543	0.991
-0.0179	-0.0414	0.0072	0.618
-0.0185	-0.0425	0.0101	0.349
-0.0244	-0.0442	-0.0032	0.736
-0.0165	-0.0493	0.0211	0.348
-0.0136	-0.0471	0.0228	0.597
-0.0064	-0.0401	0.0307	0.642
-0.0022	-0.0252	0.0229	0.429
0.0057	-0.0302	0.0436	0.742
-0.0087	-0.0409	0.0251	0.882
-0.0003	-0.0263	0.0272	0.907
0.031	-0.0051	0.0692	0.83
-0.0197	-0.0458	0.0096	0.052
0.032	-0.0002	0.0648	0.006
0.0123	-0.016	0.0434	0.764
0.0036	-0.0194	0.0267	0.65
-0.0153	-0.0373	0.0083	0.472
-0.0117	-0.0359	0.0143	0.007
-0.0126	-0.0362	0.012	0.216
0.0301	-0.0015	0.0623	0.844
-0.0158	-0.0413	0.0129	0.969
-0.0066	-0.0309	0.0184	0.828
-0.0177	-0.0477	0.0136	0.314
0.0248	-0.0148	0.0667	0.936

-0.0194	-0.0431	0.0065	0.527
0.0022	-0.0164	0.0211	0.523
0.0008	-0.0229	0.0258	0.217
0.0057	-0.0209	0.0341	0.567
0.0122	-0.0191	0.0451	0.897
-0.0077	-0.0331	0.0201	0.673
0.0021	-0.0257	0.0313	0.187
0.035	-0.001	0.0735	0.059
-0.007	-0.0341	0.0208	0.726
-0.0017	-0.0253	0.0237	0.65
0.0085	-0.0226	0.0414	0.906
0.0115	-0.019	0.0438	0.482
-0.0093	-0.0367	0.0201	0.66
-0.0296	-0.0538	-0.0035	0.034
0.0016	-0.0318	0.0419	0.835
-0.0019	-0.0268	0.0248	0.522
-0.0006	-0.0282	0.0288	0.648
-0.0086	-0.0331	0.0182	0.184
-0.0073	-0.0308	0.0172	0.577
0.0019	-0.0225	0.0275	0.365
-0.0234	-0.0493	0.0101	0.032
-0.0017	-0.0253	0.0237	0.65
0.0292	0.0003	0.059	0.867
-0.0131	-0.0331	0.0083	0.857
0.0149	-0.0144	0.0467	0.252
0.0071	-0.0273	0.0431	0.712
-0.0011	-0.0265	0.0254	0.986
0.0188	-0.0091	0.0508	0.85
0.0108	-0.0224	0.0443	0.135
0.0057	-0.0292	0.0426	0.548
0.0022	-0.0247	0.0316	0.974
0.0024	-0.0264	0.0344	0.96
0.0055	-0.0262	0.0398	0.496
0.0181	-0.0128	0.0518	0.546
0.0105	-0.0218	0.0446	0.984
-0.0015	-0.0255	0.024	0.245
0.0158	-0.0265	0.0676	0.166
-0.0108	-0.0429	0.0202	0.172
-0.0236	-0.0532	0.0085	0.339
0.0097	-0.0187	0.0399	0.686
-0.0183	-0.0496	0.0165	0.845
-0.0018	-0.0293	0.0298	0.837
-0.0201	-0.0459	0.0067	0.042
-0.0196	-0.0492	0.0136	0.115
0.0013	-0.0303	0.0353	0.686

-0.0101	-0.0457	0.0281	0.972
0.0044	-0.0268	0.0402	0.941
0.0165	-0.0164	0.0521	0.538
-0.0196	-0.0438	0.0079	0.441
-0.0173	-0.0474	0.0157	0.788
-0.0034	-0.0291	0.0249	0.817
-0.0295	-0.053	-0.0023	0.637
-0.0035	-0.0362	0.0315	0.262
0.0488	0.0058	0.0921	0.281
0.0105	-0.0087	0.0298	0.69
-0.0046	-0.0295	0.0229	0.165
-0.0197	-0.0473	0.0082	0.584
-0.009	-0.0304	0.0134	0.553
-0.0094	-0.0383	0.0227	0.115
0.01	-0.0159	0.0379	0.08
0.0118	-0.0156	0.0409	0.401
-0.0129	-0.0431	0.0203	0.407
0.0078	-0.0233	0.0395	0.508
-0.0202	-0.0445	0.0063	0.831
-0.0071	-0.0349	0.0246	0.606
-0.0198	-0.0537	0.0185	0.59
-0.0082	-0.0363	0.0207	0.94
0.0069	-0.0371	0.0527	0.506
0.0047	-0.0209	0.0326	0.848
0.0016	-0.0245	0.0298	0.595
0.0216	-0.0134	0.0596	0.835
0.0229	-0.0047	0.0515	0.9
-0.0319	-0.0582	-0.0037	0.025
-0.0103	-0.041	0.0211	0.683
0.0161	-0.0107	0.0443	0.554
-0.0315	-0.0546	-0.0066	0.004
0.0039	-0.0215	0.0311	0.536
0.0047	-0.0308	0.0399	0.074
-0.003	-0.0369	0.0328	0.698
-0.0269	-0.0528	0.001	0.884
-0.0043	-0.0255	0.0188	0.06
0.0025	-0.024	0.0304	0.85
0.0215	-0.0136	0.0595	0.799
-0.0122	-0.0396	0.0152	0.967
0.0012	-0.0262	0.0307	0.111
0.0285	-0.0076	0.0663	0.025
0.0196	-0.0193	0.0634	0.3
0.0092	-0.0245	0.0456	0.162
-0.0034	-0.0359	0.0305	0.037
-0.0149	-0.0448	0.0173	0.706

-0.0074	-0.0323	0.0185	0.612
-0.012	-0.0387	0.0198	0.495
-0.0013	-0.0264	0.0253	0.845
0.001	-0.023	0.0269	0.166
-0.0025	-0.0251	0.0219	0.516
0.0147	-0.0113	0.0408	0.163
-0.0554	-0.0831	-0.0273	0.005
0.026	-0.009	0.0616	0.627
-0.0069	-0.0355	0.0244	0.855
0.0204	-0.0141	0.0581	0.047
-0.0058	-0.0401	0.0312	0.444
-0.0105	-0.0384	0.0192	0.775
0.0036	-0.0262	0.0372	0.646
0.0082	-0.0166	0.034	0.643
-0.0112	-0.0368	0.0169	0.574
0.0016	-0.024	0.0283	0.314
-0.009	-0.0363	0.0199	0.318
0.0055	-0.016	0.0271	0.999
0.0017	-0.0304	0.0369	0.778
0.0008	-0.0264	0.0304	0.951
0.004	-0.027	0.0371	0.509
-0.0173	-0.0411	0.0085	0.073
-0.0035	-0.0311	0.0261	0.506
0.0026	-0.0205	0.0268	0.02
0.0159	-0.0109	0.048	0.357
-0.0183	-0.0351	-0.0004	0.185
-0.008	-0.0335	0.0202	0.185
-0.0196	-0.0405	0.0024	0.013
-0.0133	-0.0383	0.0154	0.054
-0.0069	-0.0278	0.0152	0.722
0.0038	-0.0153	0.0242	0.085
0.0256	-0.0062	0.063	0.296
0.0081	-0.0267	0.0441	0.746
0.0001	-0.026	0.0277	0.4
0.0148	-0.0118	0.0438	0.324
-0.0073	-0.0257	0.012	0.121
-0.0436	-0.0605	-0.0258	0.146
0.0048	-0.0195	0.031	0.787
0.0037	-0.023	0.032	0.228
0.0118	-0.0162	0.0417	0.113
0.0197	-0.0126	0.0563	0.657
-0.0213	-0.0438	0.0034	0.457
0.0024	-0.039	0.0453	0.553
0.0106	-0.0182	0.0409	0.572
-0.0141	-0.0411	0.0148	0.575

-0.0164	-0.0351	0.0043	0.271
0.0172	-0.0085	0.043	0.428
-0.0126	-0.0385	0.0168	0.979
-0.0209	-0.0398	-0.0017	0.833
-0.0187	-0.0387	0.0025	0.179
0.0019	-0.0227	0.0297	0.269
0.005	-0.0237	0.0356	0.795
0.0078	-0.022	0.0402	0.324
-0.0037	-0.0238	0.0186	0.557
-0.0169	-0.0431	0.0098	0.183
-0.03	-0.0521	-0.0055	0.007
-0.0205	-0.0402	0.001	0.605
-0.0002	-0.0205	0.022	0.666
0.0119	-0.0166	0.0417	0.392
-0.0166	-0.0395	0.0078	0.863
-0.0176	-0.036	0.0024	0.953
0.0006	-0.0259	0.0281	0.145
0.0056	-0.0213	0.035	0.216
-0.0178	-0.0456	0.0126	0.138
0.0093	-0.0139	0.0344	0.272
-0.0051	-0.031	0.0234	0.445
-0.0194	-0.0542	0.0173	0.749
0.0122	-0.0161	0.0416	0.812
0.0075	-0.0253	0.0427	0.614
-0.0026	-0.0238	0.0198	0.543
-0.0071	-0.0301	0.0178	0.467
0.0033	-0.0173	0.0246	0.575
-0.0111	-0.0335	0.0135	0.149
-0.0148	-0.0399	0.0114	0.968
-0.018	-0.0421	0.0069	0.893
-0.0194	-0.0439	0.0072	0.181
-0.0103	-0.0316	0.0116	0.053
-0.0272	-0.0502	-0.0014	0.561
0.0041	-0.0151	0.0242	0.404
-0.0028	-0.0299	0.027	0.263
-0.003	-0.0252	0.0207	0.024
0.0036	-0.0191	0.0266	0.451
-0.0106	-0.0341	0.014	0.516
-0.0198	-0.041	0.0027	0.023
-0.0199	-0.0457	0.0074	0.929
-0.0143	-0.0306	0.002	0.755
0.0037	-0.0243	0.0334	0.577
-0.0068	-0.0334	0.0209	0.828
-0.0305	-0.0534	-0.0065	0.549
0.0099	-0.0291	0.0515	0.973

0.0061	-0.0226	0.0358	0.93
-0.0021	-0.028	0.0252	0.5
0.0012	-0.0241	0.0274	0.952
-0.0041	-0.0273	0.0203	0.592
0.0186	-0.0108	0.0491	0.524
-0.001	-0.0249	0.0255	0.005
-0.0131	-0.0265	0.0012	0.716
0.0093	-0.0239	0.0439	0.177
-0.0042	-0.0233	0.0153	0.946
0.0101	-0.0183	0.041	0.866
-0.0114	-0.0329	0.0128	0.017
-0.0165	-0.0425	0.0122	0.113
-0.0127	-0.0327	0.0087	0.156
-0.0111	-0.0328	0.0125	0.173
0.0166	-0.0058	0.0397	0.325
-0.0085	-0.0279	0.0116	0.118
-0.0256	-0.0523	0.0026	0.713
0.0061	-0.0178	0.0312	0.255
0.0228	-0.0017	0.049	0.533
0.0056	-0.0175	0.031	0.196
-0.0029	-0.0273	0.0234	0.178
0.0074	-0.0138	0.0297	0.573
0.0066	-0.011	0.0249	0.557
0.0048	-0.0229	0.0388	0.44
-0.0151	-0.0371	0.0082	0.624
-0.0007	-0.0235	0.023	0.242
-0.0123	-0.0365	0.0124	0.301
0.0114	-0.0175	0.0418	0.575
-0.0057	-0.0284	0.0183	0.541
0.0117	-0.0092	0.0338	0.792
0.0235	-0.0068	0.0554	0.747
-0.0248	-0.044	-0.0044	0.907
-0.0137	-0.0432	0.0182	0.816
-0.0206	-0.0454	0.0054	0.054
-0.0072	-0.0333	0.0192	0.761
-0.0107	-0.0431	0.0229	0.526
0.0112	-0.014	0.0367	0.642
-0.0091	-0.0317	0.0145	0.926
0.009	-0.0211	0.0422	0.702
-0.0028	-0.0249	0.0196	0.696
0.0107	-0.0085	0.0312	0.34
-0.0066	-0.027	0.0146	0.446
0.0135	-0.0047	0.0324	0.398
0.0036	-0.0125	0.0202	0.821
-0.0097	-0.0341	0.0155	0.444

0.0072	-0.0136	0.0293	0.742
0.0156	-0.0113	0.0436	0.586
0.0211	-0.0127	0.0559	0.296
0.0066	-0.0148	0.0297	0.976
0.0033	-0.031	0.0406	0.953
-0.004	-0.0292	0.0233	0.548
-0.0016	-0.0294	0.0273	0.973
-0.0079	-0.0319	0.0168	0.63
-0.0015	-0.0221	0.0208	0.526
0.003	-0.0233	0.0306	0.57
-0.0061	-0.0294	0.0182	0.155
0.0055	-0.0226	0.0375	0.534
-0.0318	-0.0548	-0.005	0.003
-0.0049	-0.0266	0.0177	0.74
-0.018	-0.0388	0.0051	0.341
0.0141	-0.0275	0.0578	0.572
0.0225	-0.0084	0.0553	0.783
0.0089	-0.019	0.038	0.454
0.0084	-0.0217	0.0397	0.167
0.0132	-0.0142	0.0422	0.296
-0.0106	-0.0318	0.0116	0.274
-0.0105	-0.0329	0.0133	0.197
0.0117	-0.014	0.0383	0.644
0.0214	-0.0086	0.053	0.592
0.0011	-0.0253	0.0298	0.458
0.0017	-0.0315	0.0382	0.848
0.0212	-0.0018	0.0468	0.033
0.0009	-0.0332	0.0383	0.821
0.0156	-0.0126	0.0455	0.951
0.0232	-0.0094	0.0575	0.287
-0.0023	-0.0244	0.0207	0.03
-0.0042	-0.0296	0.023	0.92
0.0001	-0.0277	0.0293	0.407
0.0095	-0.0167	0.037	0.283
0.0094	-0.0171	0.0395	0.121
0.0155	-0.0146	0.0478	0.917
-0.0005	-0.0217	0.0223	0.617
0.0077	-0.0173	0.0337	0.079
-0.0095	-0.033	0.0149	0.613
-0.0015	-0.0268	0.0247	0.663
0.0127	-0.0202	0.0472	0.613
0.0069	-0.0198	0.0353	0.533
0.0242	-0.0069	0.0557	0.02
-0.0149	-0.0365	0.0089	0.349
-0.0173	-0.0408	0.0081	0.739

-0.0159	-0.0379	0.0074	0.007
0.0007	-0.0274	0.0323	0.472
-0.0096	-0.0312	0.0135	0.688
-0.0004	-0.0321	0.0349	0.656
0.0102	-0.0088	0.0302	0.609
-0.0131	-0.0351	0.0099	0.415
0.003	-0.0275	0.0364	0.599
0.0189	-0.0089	0.0494	0.102
0.0082	-0.0133	0.0306	0.428
-0.0058	-0.0254	0.0141	0.835
-0.0196	-0.0381	-0.0002	0.681
-0.0236	-0.0469	0.0001	0.009
0.03	0.0054	0.0565	0.036
0.0068	-0.0157	0.0304	0.256
-0.0097	-0.0336	0.0171	0.893
-0.0308	-0.0601	0.0009	0.039
0.0042	-0.0203	0.0307	0.768
-0.0052	-0.0266	0.0166	0.94
0.0132	-0.0064	0.0334	0.665
-0.0203	-0.0446	0.0037	0.16
0.0065	-0.0233	0.0371	0.682
-0.0115	-0.027	0.0053	0.161
-0.0085	-0.0315	0.0153	0.146
-0.0209	-0.0462	0.0056	0.058
-0.019	-0.0426	0.0056	0.897
0.0001	-0.0221	0.0236	0.992
0.0074	-0.022	0.0377	0.473
0.0182	-0.0086	0.0487	0.889
-0.0049	-0.0288	0.0217	0.879
0.0204	-0.0064	0.0505	0.056
0	-0.0231	0.0243	0.8
0.0485	0.0169	0.0831	0.297
0.0089	-0.0145	0.0336	0.318
-0.0112	-0.0371	0.0176	0.646
0.0028	-0.019	0.026	0.312
-0.009	-0.0315	0.014	0.348
-0.0194	-0.0376	0.0003	0.619
-0.0041	-0.0326	0.0263	0.548
-0.011	-0.0297	0.0072	0.448
-0.002	-0.0213	0.0201	0.533
-0.0068	-0.0267	0.0146	0.645
0.0077	-0.0165	0.0331	0.396
0.01	-0.0143	0.0346	0.502
-0.0278	-0.0564	0.0024	0.551
0.0164	-0.0023	0.0354	0.893

-0.0071	-0.0236	0.01	0.832
0.0073	-0.0176	0.0326	0.088
-0.0008	-0.0212	0.02	0.808
0.0251	-0.0135	0.0666	0.035
0.0045	-0.0171	0.0259	0.603
-0.0019	-0.0183	0.0155	0.219
-0.0113	-0.029	0.0079	0.063
0.014	-0.0084	0.038	0.76
0.0022	-0.0184	0.0238	0.987
0.0115	-0.0125	0.0367	0.942
0.0295	0.0004	0.061	0.682
-0.0034	-0.0322	0.0262	0.563
0.0132	-0.0081	0.0355	0.554
-0.0063	-0.0291	0.0183	0.41
-0.0003	-0.0311	0.0329	0.701
-0.0088	-0.0285	0.0121	0.926
-0.0218	-0.0453	0.0031	0.336
-0.0034	-0.021	0.0151	0.027
-0.0111	-0.0342	0.0132	0.789
-0.0155	-0.0341	0.0044	0.011
-0.0215	-0.0465	0.0061	0.311
-0.0271	-0.0514	-0.0019	0.714
0.0086	-0.0299	0.0499	0.614
0.0052	-0.0181	0.0287	0.191
-0.0128	-0.0375	0.0129	0.134
0.0282	-0.013	0.0739	0.771
-0.0392	-0.0616	-0.0167	0.05
-0.0037	-0.0279	0.0217	0.302
0.0021	-0.027	0.0314	0.594
-0.0162	-0.0416	0.0096	0.894
0.0134	-0.0096	0.0364	0.166
-0.0022	-0.0209	0.0179	0.346
-0.0002	-0.0231	0.024	0.877
0.016	-0.0081	0.0415	0.832
-0.004	-0.0281	0.0218	0.434
-0.0274	-0.0484	-0.0054	0.077
-0.0061	-0.0304	0.0195	0.494
-0.0297	-0.0594	0.0022	0.022
-0.02	-0.0397	0.0014	0.876
0.0026	-0.0279	0.0336	0.759
0.0178	-0.0144	0.054	0.425
0.0116	-0.0185	0.0456	0.115
-0.0023	-0.0267	0.0235	0.435
0.0059	-0.0221	0.0354	0.397
-0.0221	-0.0411	-0.0022	0.567

-0.0019	-0.023	0.0212	0.966
-0.0227	-0.044	-0.0012	0.074
-0.0001	-0.0298	0.0305	0.579
-0.0607	-0.0868	-0.0331	0.112
-0.0005	-0.0208	0.0208	0.723
-0.0075	-0.0238	0.0095	0.074
0.0074	-0.0163	0.0325	0.242
0.0011	-0.0101	0.0123	0.131
-0.0038	-0.0196	0.0131	0.293
-0.0166	-0.0379	0.0052	0.465
-0.0071	-0.0242	0.0104	0.588
-0.0101	-0.0356	0.0173	0.621
0.0069	-0.016	0.0307	0.743
0.0061	-0.0178	0.0312	0.255
-0.0072	-0.0247	0.0103	0.669
0.0048	-0.0234	0.0355	0.662
0.0099	-0.0293	0.0518	0.479
0.009	-0.0225	0.0422	0.712
-0.0016	-0.021	0.0199	0.757
0.0089	-0.019	0.038	0.454
0.0129	-0.012	0.0388	0.226
0.0004	-0.0248	0.0269	0.625
-0.0025	-0.0193	0.0156	0.538
0.0089	-0.0092	0.028	0.025
0.01	-0.0084	0.0296	0.978
-0.0142	-0.0393	0.0134	0.531
0.0196	-0.0151	0.0576	0.216
0.0085	-0.0156	0.0334	0.72
-0.03	-0.0595	0.0018	0.101
0.004	-0.0215	0.0304	0.712
-0.0278	-0.0498	-0.0043	0.109
-0.0067	-0.0307	0.0187	0.724
0.0309	0.0028	0.0599	0.654
0.0025	-0.026	0.0326	0.91
-0.0224	-0.0454	0.0017	0.227
-0.0216	-0.0429	0.0013	0.561
-0.0208	-0.044	0.0032	0.319
0.0153	-0.014	0.0466	0.646
-0.0102	-0.0363	0.0182	0.174
0.0189	-0.0064	0.045	0.339
0.006	-0.0249	0.0386	0.13
0.0272	-0.0086	0.0664	0.086
-0.0258	-0.0541	0.006	0.566
-0.0103	-0.0272	0.0071	0.458
0.006	-0.017	0.0314	0.785

0.013	-0.0125	0.04	0.251
0.0023	-0.0252	0.0325	0.744
0.0088	-0.0196	0.0381	0.912
-0.0121	-0.0393	0.0196	0.289
-0.0152	-0.0343	0.0046	0.579
-0.0067	-0.0314	0.0204	0.291
-0.0134	-0.0409	0.0154	0.705
-0.0048	-0.0323	0.025	0.3
0.0133	-0.0221	0.0545	0.354
-0.0182	-0.0461	0.0097	0.443
0.0062	-0.0259	0.0407	0.503
0.0227	-0.0076	0.055	0.196
-0.0005	-0.0182	0.0179	0.024
0.0161	-0.0127	0.0465	0.417
-0.0166	-0.0464	0.0167	0.225
0.0104	-0.0174	0.0407	0.087
-0.0052	-0.0394	0.0336	0.714
-0.0386	-0.0705	-0.0045	0.155
-0.0331	-0.0527	-0.0119	0.164
0.0034	-0.0216	0.029	0.604
-0.0202	-0.0442	0.0069	0.809
-0.0293	-0.0544	-0.0011	0.388
-0.0165	-0.0383	0.0065	0.088
-0.0129	-0.0351	0.0112	0.397
-0.0113	-0.0375	0.0161	0.053
-0.0193	-0.0421	0.005	0.617
0.0198	-0.009	0.0501	0.311
-0.0045	-0.0337	0.0293	0.311
-0.0155	-0.0507	0.0263	0.482
0.0243	-0.0082	0.0576	0.297
-0.0173	-0.0519	0.0161	0.779
-0.0153	-0.0419	0.0126	0.847
-0.0168	-0.0463	0.0145	0.538
0.0069	-0.0222	0.0371	0.37
-0.0109	-0.04	0.0203	0.473
-0.0025	-0.0337	0.0306	0.461
0.0229	-0.0109	0.058	0.417
-0.0037	-0.0273	0.0204	0.535
-0.0139	-0.0442	0.0184	0.568
0.0098	-0.0229	0.0454	0.151
-0.0343	-0.0582	-0.0097	0.055
0.0206	-0.0164	0.0605	0.896
-0.0026	-0.0338	0.0341	0.791
-0.0064	-0.0366	0.0266	0.423
0.0189	-0.01	0.0503	0.508

-0.0217	-0.0449	0.0035	0.159
-0.0002	-0.0226	0.0236	0.316
-0.0097	-0.04	0.0232	0.767
-0.0145	-0.0439	0.0168	0.512
0.0265	0.0021	0.0519	0.378
0.027	-0.0076	0.0631	0.993
-0.0146	-0.0375	0.009	0.182
0.007	-0.0211	0.0363	0.442
-0.0042	-0.0219	0.0144	0.5
0.0216	-0.0106	0.0559	0.813
-0.011	-0.0332	0.0115	0.808
-0.0075	-0.0321	0.0186	0.786
0.0048	-0.0229	0.0388	0.44
-0.0045	-0.0407	0.0369	0.537
0.0336	0.0057	0.0624	0.072
-0.0057	-0.0356	0.0267	0.812
0.0013	-0.0192	0.0236	0.758
0.0333	-0.0001	0.0718	0.119
-0.0193	-0.044	0.0067	0.917
-0.0231	-0.0438	-0.0003	0.206
-0.0088	-0.0388	0.0235	0.064
0.0054	-0.0208	0.0342	0.187
-0.0067	-0.0339	0.0217	0.481
0.0102	-0.0161	0.0405	0.252
-0.0025	-0.0225	0.0186	0.257
-0.0085	-0.0391	0.0238	0.484
0.0019	-0.0319	0.0402	0.521
0.0359	0.0033	0.0675	0.938
0.0116	-0.0196	0.0461	0.721
-0.008	-0.0333	0.0189	0.948
-0.005	-0.027	0.0192	0.433
0.0134	-0.0167	0.0448	0.281
-0.0071	-0.0369	0.0238	0.401
-0.0007	-0.0155	0.0148	0.967
-0.0127	-0.0386	0.018	0.543
0.0181	-0.0073	0.0446	0.18
0.0118	-0.0135	0.038	0.5
-0.0005	-0.0182	0.0179	0.024
0.0076	-0.0163	0.0323	0.194
0.0031	-0.0354	0.0444	0.95
-0.0082	-0.0496	0.0375	0.745
0.0015	-0.017	0.0209	0.877
-0.0102	-0.0477	0.033	0.171
0.0153	-0.0146	0.0467	0.901
-0.0026	-0.0253	0.0211	0.576

0.0025	-0.023	0.0291	0.308
0.0157	-0.0082	0.0401	0.668
0.0005	-0.0295	0.0322	0.338
-0.0044	-0.031	0.0243	0.64
-0.0063	-0.0281	0.0169	0.301
-0.018	-0.0379	0.0023	0.087
-0.0034	-0.0387	0.0335	0.477
0.0047	-0.021	0.0326	0.744
-0.0255	-0.053	0.0064	0.508
-0.0291	-0.054	-0.0035	0.196
-0.0149	-0.0395	0.0104	0.979
-0.0096	-0.0359	0.0188	0.579
0.0174	-0.0094	0.045	0.204
0.0047	-0.0276	0.0408	0.951
-0.0339	-0.0615	-0.0041	0.344
0.0092	-0.0138	0.0328	0.352
-0.0109	-0.0309	0.0107	0.456
-0.025	-0.0494	0.0021	0.496
-0.0185	-0.043	0.0081	0.03
-0.0098	-0.0386	0.0238	0.731
-0.0154	-0.0416	0.0125	0.996
0.0019	-0.0268	0.0324	0.813
-0.0046	-0.032	0.0251	0.363
-0.0122	-0.0334	0.0107	0.63
0.0111	-0.0163	0.0399	0.265
0.0074	-0.025	0.0404	0.231
-0.0115	-0.0332	0.0117	0.188
0.0086	-0.017	0.0352	0.343
0.0049	-0.0211	0.0339	0.967
-0.0178	-0.0486	0.0149	0.293
0.0361	0.0037	0.069	0.249
0.0024	-0.0221	0.0273	0.986
-0.0166	-0.0434	0.0108	0.616
0.0065	-0.0231	0.0406	0.621
0.0017	-0.0394	0.05	0.708
-0.0198	-0.0376	-0.0001	0.291
0.0188	-0.0109	0.0498	0.194
-0.0293	-0.0562	0.0039	0.144
0.0048	-0.0157	0.0271	0.744
0.0075	-0.0221	0.0409	0.998
0.007	-0.0281	0.0443	0.439
-0.0005	-0.0182	0.0179	0.024
0.0011	-0.017	0.0204	0.617
0.0051	-0.0136	0.0246	0.324
0.0423	0.0102	0.0754	0.018

-0.0046	-0.029	0.0199	0.428
0.0106	-0.0084	0.0309	0.387
0.0041	-0.0153	0.0243	0.658
-0.0023	-0.0277	0.0262	0.686
0.0246	0.0014	0.0481	0.122
0.0079	-0.0182	0.0368	0.927
-0.0141	-0.0422	0.0159	0.628
0.0104	-0.0137	0.0358	0.297
0.0073	-0.024	0.0404	0.502
-0.0168	-0.0464	0.015	0.817
-0.0003	-0.0249	0.0263	0.019
0.0077	-0.0168	0.033	0.42
0.0012	-0.0204	0.0233	0.962
0.0103	-0.018	0.0407	0.787
0.019	-0.0046	0.0437	0.187
0.0064	-0.0133	0.0272	0.512
0.0059	-0.0219	0.0344	0.325
-0.0138	-0.0365	0.0114	0.394
-0.0115	-0.0332	0.0117	0.188
0.0026	-0.0248	0.032	0.582
-0.0192	-0.0445	0.0075	0.142
0.019	-0.0068	0.0464	0.203
0.0177	-0.0195	0.0587	0.348
-0.0084	-0.0275	0.0114	0.031
-0.0009	-0.0225	0.0221	0.485
-0.0293	-0.0562	0.0039	0.144
-0.0324	-0.05	-0.0131	0.005
0.0078	-0.028	0.047	0.975
-0.0149	-0.0382	0.0096	0.164
0.002	-0.0215	0.0277	0.155
-0.0284	-0.0542	0.0007	0.267
-0.0107	-0.0273	0.0063	0.433
-0.011	-0.029	0.0081	0.797
-0.0023	-0.0237	0.0211	0.328
-0.0037	-0.0241	0.0181	0.904
-0.0153	-0.04	0.0109	0.82
0.008	-0.0121	0.0294	0.59
-0.0215	-0.0418	0.0003	0.618
-0.0156	-0.0451	0.0167	0.068
0.0083	-0.0253	0.0452	0.336
-0.0213	-0.0454	0.0038	0.303
-0.0155	-0.0489	0.0217	0.534
-0.0229	-0.0473	0.0017	0.152
-0.0044	-0.0285	0.022	0.556
-0.0123	-0.0376	0.0152	0.254

-0.0051	-0.035	0.0275	0.741
0.0084	-0.0189	0.0385	0.139
0.0029	-0.0231	0.0304	0.525
-0.0174	-0.044	0.0121	0.262
-0.0066	-0.0252	0.014	0.962
0.0057	-0.0162	0.0289	0.931
0.0088	-0.0245	0.045	0.781
-0.0279	-0.0557	0.0051	0.159
0.007	-0.0156	0.03	0.467
-0.0008	-0.0275	0.0278	0.989
-0.0345	-0.0572	-0.0103	0.297
0.0348	0.0045	0.0653	0.11
0.021	-0.0069	0.0514	0.668
0.0182	-0.009	0.0483	0.154
-0.0115	-0.0341	0.0112	0.926
0.0138	-0.0103	0.0397	0.932
-0.0016	-0.0358	0.0354	0.673
-0.0022	-0.028	0.0284	0.451
-0.0084	-0.0321	0.0178	0.964
-0.0053	-0.042	0.0312	0.703
-0.0189	-0.0497	0.015	0.672
-0.002	-0.0218	0.0188	0.542
0.0046	-0.0261	0.0387	0.229
-0.0036	-0.025	0.0187	0.302
-0.002	-0.0258	0.024	0.994
0.041	0.0099	0.073	0.111
-0.023	-0.0502	0.0072	0.677
0.0107	-0.0159	0.0388	0.023
-0.0028	-0.0312	0.0281	0.908
0.0126	-0.0096	0.0372	0.981
-0.0092	-0.0327	0.0148	0.067
-0.0195	-0.0385	0.0015	0.086
-0.0132	-0.0299	0.0048	0.696
-0.0059	-0.0283	0.0186	0.163
-0.0103	-0.0332	0.0141	0.867
-0.0158	-0.0364	0.0058	0.928
-0.0137	-0.0372	0.0109	0.121
0.0065	-0.0197	0.0341	0.11
0.0028	-0.0207	0.027	0.895
-0.0057	-0.0285	0.018	0.722
-0.0348	-0.0613	-0.0028	0.29
0.0007	-0.0224	0.025	0.698
-0.0065	-0.0287	0.0171	0.146
-0.016	-0.035	0.0039	0.979
0.0032	-0.019	0.0268	0.582

0.011	-0.0156	0.039	0.915
0.0019	-0.0204	0.0268	0.079
-0.0005	-0.0211	0.0215	0.446
-0.0035	-0.0294	0.0242	0.677
0.0082	-0.0155	0.0352	0.204
-0.0054	-0.0414	0.037	0.008
0.0217	-0.0072	0.0537	0.822
0.0228	-0.0136	0.0615	0.398
-0.0049	-0.0378	0.0297	0.789
-0.0147	-0.0411	0.013	0.932
-0.0051	-0.0319	0.0247	0.085
0.0258	-0.0082	0.0612	0.433
0.0204	-0.0051	0.0472	0.493
-0.0124	-0.0292	0.0052	0.919
-0.0083	-0.0348	0.018	0.304
0.0306	0.0008	0.0621	0.685
0.0014	-0.0182	0.0226	0.81
-0.0042	-0.0292	0.0214	0.371
-0.0102	-0.0293	0.0105	0.022
0.0092	-0.0175	0.0367	0.729
0.0269	-0.012	0.0687	0.952
-0.0023	-0.0206	0.017	0.759
0.0372	0.0087	0.0674	0.101
-0.0037	-0.0212	0.0139	0.937
0.0277	-0.0004	0.058	0.638
-0.0317	-0.0552	-0.0061	0.318
-0.0113	-0.0279	0.0058	0.357
-0.0054	-0.0235	0.0137	0.834
-0.0019	-0.0188	0.0161	0.413
-0.0087	-0.0249	0.0079	0.482
-0.0044	-0.0297	0.0215	0.654
-0.0008	-0.023	0.0231	0.887
-0.0128	-0.0403	0.0167	0.461
-0.0111	-0.0364	0.0175	0.646
0.0048	-0.0131	0.0238	0.055
-0.0174	-0.0375	0.0036	0.735
0.0206	-0.0149	0.0587	0.441
0.0072	-0.0297	0.0455	0.723
0.0104	-0.01	0.0317	0.262
0.01	-0.0087	0.0295	0.217
-0.0307	-0.0529	-0.0064	0.604
-0.0142	-0.0381	0.0116	0.758
-0.0099	-0.031	0.0121	0.644
0.0181	-0.006	0.0444	0.002
-0.0118	-0.033	0.0103	0.148

-0.0014	-0.0328	0.0353	0.7
-0.0023	-0.0189	0.0157	0.735
0.0103	-0.0085	0.0304	0.914
-0.0054	-0.0322	0.0237	0.989
0.002	-0.0242	0.0302	0.931
0.0021	-0.0195	0.0246	0.289
0.0103	-0.0069	0.028	0.412
-0.0126	-0.0273	0.0031	0.382
-0.0008	-0.0249	0.0258	0.954
-0.0036	-0.0296	0.0251	0.835
0.0095	-0.0135	0.0332	0.268
-0.0057	-0.0199	0.0097	0.25
0.0117	-0.013	0.0378	0.553
0.0009	-0.019	0.0221	0.031
-0.0115	-0.0355	0.0145	0.072
-0.0016	-0.0274	0.0246	0.986
-0.0031	-0.0298	0.0243	0.219
-0.0007	-0.0204	0.0195	0.801
-0.002	-0.0282	0.0251	0.33
0.0128	-0.0085	0.0341	0.147
-0.0068	-0.0305	0.0176	0.278
0.0073	-0.0136	0.03	0.578
-0.0143	-0.0298	0.0021	0.828
-0.0082	-0.03	0.0161	0.754
-0.0213	-0.0492	0.0099	0.198
-0.0032	-0.0323	0.0285	0.111
0.0036	-0.0081	0.0158	0.875
0.0025	-0.0287	0.0348	0.79
-0.0023	-0.0206	0.017	0.759
0.0019	-0.0209	0.0257	0.603
-0.0248	-0.0459	-0.0017	0.169
-0.0015	-0.0225	0.0195	0.903
-0.0029	-0.0334	0.0299	0.232
-0.0161	-0.0411	0.0096	0.438
0.0179	-0.0108	0.0487	0.105
-0.0147	-0.0379	0.0097	0.661
0.0004	-0.0256	0.0284	0.351
0.0074	-0.0238	0.0398	0.272
0.0104	-0.0203	0.0428	0.824
-0.001	-0.0208	0.02	0.275
-0.0059	-0.0261	0.0147	0.532
0.0075	-0.0144	0.0301	0.32
-0.019	-0.0513	0.0148	0.591
0.0085	-0.018	0.0347	0.444
-0.0039	-0.0264	0.0193	0.797

-0.0212	-0.0395	-0.0022	0.639
0.0061	-0.0224	0.0388	0.994
-0.0054	-0.0252	0.0156	0.929
-0.0037	-0.0297	0.0241	0.089
0.0018	-0.0247	0.0301	0.476
-0.0142	-0.0401	0.0123	0.738
-0.0127	-0.0356	0.012	0.697
-0.0036	-0.0253	0.0185	0.413
-0.0227	-0.044	-0.0012	0.074
-0.0001	-0.0298	0.0305	0.579
-0.0022	-0.0274	0.0235	0.868
0.0018	-0.0236	0.028	0.346
0.0178	-0.0067	0.0433	0.254
0.014	-0.017	0.0482	0.336
-0.0249	-0.0523	0.0041	0.001
-0.0079	-0.0303	0.0154	0.534
0.0202	-0.0063	0.0475	0.319
-0.0058	-0.0317	0.0224	0.069
-0.0112	-0.0369	0.0163	0.372
-0.013	-0.0436	0.0206	0.493
0.0013	-0.0147	0.0179	0.942
-0.0019	-0.0243	0.0218	0.19
-0.0058	-0.02	0.0095	0.949
-0.0052	-0.0329	0.0242	0.621
-0.0048	-0.0289	0.0196	0.887
-0.0089	-0.0441	0.0309	0.864
0.0032	-0.0263	0.0339	0.592
-0.0126	-0.0311	0.0064	0.708
-0.0002	-0.0313	0.0324	0.69
-0.0037	-0.0301	0.0247	0.971
-0.0161	-0.0452	0.0144	0.585
-0.0142	-0.0411	0.014	0.483
-0.0215	-0.0444	0.0024	0.06
-0.0114	-0.0361	0.0152	0.874
0.0015	-0.0271	0.0328	0.531
0.0087	-0.0104	0.029	0.279
-0.0121	-0.0363	0.0137	0.103
-0.0023	-0.0228	0.019	0.641
-0.0126	-0.0318	0.0077	0.682
-0.0037	-0.0273	0.0204	0.535
0.0116	-0.0163	0.0408	0.24
-0.0128	-0.0468	0.0241	0.697
-0.002	-0.0323	0.0308	0.952
-0.004	-0.0253	0.0176	0.886
-0.0055	-0.0327	0.0244	0.335

0.01	-0.0136	0.0354	0.177
-0.0007	-0.0155	0.0148	0.967
0.0029	-0.0191	0.0266	0.373
-0.021	-0.0462	0.0077	0.229
0.0217	-0.0115	0.0583	0.969
-0.0182	-0.0433	0.01	0.318
0.0118	-0.0245	0.0497	0.14
0.005	-0.0213	0.0332	0.157
-0.0037	-0.0306	0.0274	0.991
0.3396	0.3054	0.3734	0
-0.0127	-0.0384	0.0151	0.054

A.2 Parkfield - Cut off magnitude 2

Correlation	Confidence Interval	Confidence interval2	p value
0.0244	-0.0389	0.0868	0.981
-0.0740	-0.1545	0.0138	0.119
0.0085	-0.0334	0.0519	0.611
0.0523	-0.0463	0.1580	0.119
-0.0435	-0.0974	0.0127	0.663
-0.0473	-0.0986	0.0041	0.253
-0.0062	-0.0335	0.0222	0.770
-0.0353	-0.0919	0.0234	0.148
0.0017	-0.0760	0.0820	0.756
-0.0039	-0.0877	0.0793	0.241
0.0330	-0.0188	0.0873	0.117
-0.0100	-0.0466	0.0285	0.951
0.0274	-0.0297	0.0917	0.249
0.0719	-0.0489	0.2180	0.327
-0.0052	-0.0936	0.0860	0.839
0.0268	-0.1105	0.1842	0.474
-0.0216	-0.0763	0.0361	0.327
-0.0197	-0.0446	0.0059	0.664
0.0045	-0.0705	0.0834	0.305
-0.0138	-0.0597	0.0332	0.965
-0.0107	-0.0429	0.0211	0.943
-0.0020	-0.0458	0.0425	0.992
0.0178	-0.0642	0.1123	0.650
-0.0263	-0.0638	0.0129	0.150
-0.0115	-0.0704	0.0466	0.423
0.0092	-0.0749	0.0971	0.852
0.0245	-0.0428	0.1033	0.329
-0.0484	-0.0992	0.0042	0.251
-0.0015	-0.0456	0.0446	0.542
-0.0121	-0.0481	0.0251	0.571
-0.0219	-0.0927	0.0632	0.569
0.0166	-0.0195	0.0543	0.843
-0.0285	-0.1041	0.0521	0.337
-0.0201	-0.0486	0.0116	0.243
0.0020	-0.0882	0.0995	0.368
-0.0479	-0.1015	0.0087	0.080
-0.0057	-0.0434	0.0335	0.819
-0.0688	-0.1257	-0.0058	0.008
-0.0327	-0.1088	0.0509	0.741
0.0392	-0.0197	0.1021	0.434
0.1022	-0.0292	0.2345	0.108
-0.0519	-0.1226	0.0235	0.583
0.0861	-0.0786	0.2567	0.564
-0.0925	-0.1713	0.0124	0.137

0.0051	-0.0229	0.0333	0.782
-0.0302	-0.0716	0.0147	0.329
-0.0526	-0.1236	0.0262	0.716
0.0587	-0.0968	0.2248	0.543
-0.0271	-0.0941	0.0449	0.787
0.0397	-0.0227	0.1018	0.138
-0.0020	-0.0720	0.0683	0.689
-0.0298	-0.0679	0.0114	0.873
-0.0078	-0.0448	0.0289	0.576
-0.0099	-0.1181	0.1089	0.377
-0.0178	-0.0621	0.0311	0.981
-0.0290	-0.0797	0.0276	0.051
-0.0130	-0.0682	0.0500	0.750
0.0142	-0.0570	0.0870	0.921
0.0642	-0.0527	0.2177	0.486
-0.0221	-0.0651	0.0235	0.301
-0.0152	-0.0499	0.0208	0.197
-0.0311	-0.1170	0.0672	0.735
-0.0453	-0.0861	-0.0007	0.558
0.0977	0.0002	0.2006	0.014
-0.0789	-0.1748	0.0202	0.238
-0.0053	-0.0352	0.0276	0.669
0.0253	-0.0377	0.0934	0.938
-0.0014	-0.0283	0.0254	0.495
-0.0738	-0.1824	0.0501	0.821
0.0323	-0.1193	0.2222	0.860
0.0124	-0.0781	0.1159	0.541
-0.0279	-0.1044	0.0547	0.482
-0.0214	-0.0478	0.0056	0.739
-0.0236	-0.0855	0.0386	0.099
-0.0534	-0.0908	-0.0129	0.126
0.0106	-0.0614	0.0835	0.917
0.0083	-0.0538	0.0748	0.096
-0.0843	-0.1305	-0.0315	0.452
-0.0359	-0.0814	0.0118	0.047
-0.0233	-0.0636	0.0203	0.111
0.0342	-0.0611	0.1395	0.312
-0.0722	-0.1621	0.0325	0.484
-0.0390	-0.0866	0.0109	0.566
0.0068	-0.0351	0.0496	0.613
-0.0162	-0.0812	0.0483	0.734
-0.0113	-0.0446	0.0233	0.571
0.0738	-0.1145	0.2794	0.864
0.0257	-0.0526	0.1111	0.457
0.0649	-0.0122	0.1443	0.336

-0.0035	-0.0936	0.0910	0.958
0.0196	-0.0322	0.0693	0.533
0.0136	-0.0341	0.0675	0.899
-0.0319	-0.0673	0.0056	0.462
-0.0474	-0.1605	0.0727	0.948
0.0035	-0.0478	0.0564	0.208
-0.0092	-0.0442	0.0279	0.274
-0.0104	-0.0453	0.0251	0.967
0.0828	-0.0994	0.3217	0.626
-0.0302	-0.0783	0.0197	0.489
-0.0459	-0.0793	-0.0113	0.004
-0.0388	-0.0707	-0.0023	0.946
0.0196	-0.0770	0.1152	0.602
0.0014	-0.0350	0.0383	0.900
0.0476	-0.0673	0.1659	0.648
-0.0363	-0.1280	0.0634	0.301
0.0132	-0.1204	0.1685	0.505
-0.0511	-0.1034	0.0026	0.019
-0.0271	-0.0734	0.0205	0.576
0.0062	-0.0769	0.0977	0.918
-0.0117	-0.0551	0.0330	0.646
-0.0032	-0.0505	0.0455	0.936
0.0259	-0.0466	0.1065	0.220
-0.0527	-0.0443	0.0049	0.264
0.0662	-0.0970	-0.0077	0.130
0.0573	-0.0264	0.1600	0.093
0.0183	-0.0247	0.1417	0.114
0.0039	-0.0303	0.0661	0.236
-0.0474	-0.0254	0.0365	0.015
0.0058	-0.1107	0.0205	0.631
-0.0460	-0.0705	0.0845	0.966
-0.0226	-0.1193	0.0343	0.995
0.0801	-0.0590	0.0181	0.563
-0.0345	-0.0039	0.1713	0.981
-0.0327	-0.0864	0.0206	0.477
-0.0501	-0.1098	0.0563	0.526
-0.0463	-0.1146	0.0177	0.931
-0.0325	-0.0847	-0.0077	0.214
-0.1211	-0.0635	-0.0006	0.096
0.0245	-0.1964	-0.0116	0.311
-0.0166	-0.0295	0.0820	0.712
-0.0434	-0.0415	0.0088	0.337
-0.0459	-0.1115	0.0284	0.045
-0.0122	-0.1442	0.0638	0.585
-0.0230	-0.0565	0.0331	0.417

0.0003	-0.1025	0.0720	0.767
0.0357	-0.0488	0.0501	0.695
-0.0027	-0.1934	0.2444	0.706
-0.0468	-0.0455	0.0409	0.690
0.0023	-0.0735	-0.0189	0.265
0.2004	-0.0838	0.0901	0.484
0.0105	0.0086	0.3794	0.404
-0.1100	-0.0104	0.0326	0.427
0.0453	-0.1958	-0.0147	0.018
-0.0436	-0.0020	0.0927	0.789
-0.0308	-0.1005	0.0165	0.674
0.0271	-0.0986	0.0392	0.948
-0.0103	-0.1067	0.2180	0.829
0.0804	-0.0596	0.0406	0.258
-0.0079	-0.0341	0.2064	0.027
0.0631	-0.0526	0.0378	0.883
-0.0077	-0.0476	0.2031	0.165
-0.0046	-0.0477	0.0369	0.226
-0.0328	-0.0314	0.0226	0.712
-0.0016	-0.0871	0.0232	0.840
-0.0210	-0.0981	0.1031	0.576
0.0223	-0.0666	0.0274	0.458
0.0013	-0.0245	0.0684	0.921
-0.0247	-0.0479	0.0549	0.838
0.0121	-0.1218	0.0915	0.870
0.0344	-0.0745	0.1074	0.306
0.0321	-0.0042	0.0749	0.058
0.0019	-0.0262	0.1031	0.160
-0.0742	-0.1555	0.1830	0.172
-0.0848	-0.1781	0.0432	0.204
0.1027	-0.1620	0.0008	0.306
0.0042	0.0260	0.1812	0.005
-0.0012	-0.1224	0.1524	0.525
-0.0730	-0.0714	0.0762	0.342
0.0889	-0.1061	-0.0355	0.423
0.0055	-0.0169	0.2042	0.064
-0.0148	-0.0408	0.0533	0.345
0.0180	-0.0549	0.0264	0.915
0.0148	-0.0564	0.1051	0.884
-0.0192	-0.0880	0.1218	0.871
-0.0161	-0.0977	0.0567	0.660
-0.0036	-0.0625	0.0332	0.183
0.0165	-0.0546	0.0526	0.116
0.0046	-0.0732	0.1188	0.891
-0.0026	-0.0460	0.0603	0.840

-0.0210	-0.0728	0.0749	0.919
-0.0295	-0.0776	0.0362	0.085
0.0127	-0.1272	0.1433	0.706
0.0393	-0.0638	0.0935	0.829
0.0107	-0.0326	0.1117	0.485
-0.0104	-0.0471	0.0685	0.799
-0.0125	-0.0919	0.0744	0.544
0.0097	-0.0595	0.0371	0.183
-0.0314	-0.0184	0.0385	0.515
-0.0092	-0.0831	0.0206	0.548
0.0015	-0.0651	0.0499	0.966
-0.0073	-0.0457	0.0517	0.770
-0.0110	-0.0711	0.0673	0.238
-0.0250	-0.0768	0.0565	0.251
-0.0266	-0.0656	0.0166	0.672
0.1306	-0.0597	0.0107	0.114
-0.0204	0.0179	0.2572	0.810
-0.0371	-0.0705	0.0354	0.356
-0.0235	-0.0847	0.0134	0.059
-0.0160	-0.0475	0.0009	0.719
-0.0041	-0.0348	0.0025	0.193
-0.0569	-0.0434	0.0356	0.614
-0.0086	-0.1428	0.0344	0.339
0.1522	-0.0276	0.0111	0.372
-0.0089	0.0293	0.2738	0.008
-0.0022	-0.0742	0.0623	0.881
-0.0303	-0.0305	0.0265	0.820
0.0900	-0.0939	0.0405	0.483
-0.0056	0.0140	0.1694	0.069
-0.0194	-0.1118	0.1072	0.594
0.0037	-0.0795	0.0436	0.201
-0.0245	-0.0469	0.0578	0.396
-0.0441	-0.0622	0.0139	0.415
-0.0736	-0.1103	0.0218	0.122
-0.0239	-0.1682	0.0345	0.908
0.0135	-0.0665	0.0221	0.598
-0.0194	-0.0490	0.0800	0.309
-0.0224	-0.0549	0.0171	0.241
0.0036	-0.0886	0.0491	0.647
0.0177	-0.0473	0.0550	0.838
-0.0288	-0.0298	0.0662	0.372
0.0006	-0.0770	0.0214	0.058
0.0221	-0.1356	0.1658	0.213
-0.0562	-0.0506	0.1029	0.092
-0.1011	-0.0981	-0.0137	0.001

0.0233	-0.1509	-0.0466	0.043
-0.0337	-0.0220	0.0694	0.491
-0.0340	-0.0793	0.0158	0.894
-0.0530	-0.2088	0.1712	0.997
0.0088	-0.2476	0.1778	0.489
0.0058	-0.0455	0.0638	0.893
0.0337	-0.0262	0.0384	0.627
-0.0350	-0.0425	0.1000	0.996
-0.0109	-0.1081	0.0447	0.262
-0.0542	-0.0529	0.0368	0.196
-0.0125	-0.1195	0.0149	0.571
-0.0160	-0.0685	0.0463	0.167
-0.0425	-0.1222	0.1148	0.200
0.0051	-0.0899	0.0094	0.116
-0.0322	-0.0319	0.0447	0.073
0.0296	-0.0658	0.0025	0.222
-0.0154	-0.0237	0.0823	0.468
-0.0418	-0.0808	0.0505	0.993
0.0102	-0.0746	-0.0063	0.681
-0.0317	-0.0205	0.0413	0.253
0.0478	-0.0773	0.0158	0.158
0.0939	-0.0279	0.1282	0.934
-0.0882	-0.0324	0.2246	0.257
-0.0172	-0.1611	-0.0095	0.001
-0.0350	-0.0444	0.0111	0.937
-0.0662	-0.0827	0.0146	0.298
-0.0202	-0.1468	0.0244	0.277
-0.0466	-0.0806	0.0432	0.160
0.0095	-0.1485	0.0678	0.343
-0.0187	-0.0500	0.0749	0.631
-0.0075	-0.0787	0.0418	0.411
-0.0085	-0.0695	0.0580	0.484
-0.0323	-0.0601	0.0453	0.854
-0.0396	-0.1019	0.0356	0.258
-0.0118	-0.1024	0.0344	0.883
0.0185	-0.0860	0.0661	0.415
0.0090	-0.0265	0.0644	0.328
0.0628	-0.0174	0.0349	0.475
-0.0388	-0.0250	0.1513	0.382
-0.0251	-0.1078	0.0354	0.767
0.0140	-0.0753	0.0267	0.371
-0.0541	-0.0403	0.0696	0.545
0.0092	-0.1068	0.0005	0.198
-0.0560	-0.0522	0.0749	0.910
0.0040	-0.1128	0.0009	0.073

0.0041	-0.0297	0.0393	0.421
-0.0233	-0.0806	0.0960	0.531
-0.0739	-0.1194	0.0798	0.961
-0.0256	-0.1183	-0.0279	0.001
-0.0632	-0.0560	0.0059	0.437
-0.0232	-0.1157	-0.0088	0.053
-0.0629	-0.1097	0.0584	0.445
-0.0295	-0.1567	0.0313	0.499
0.0476	-0.0718	0.0137	0.483
-0.0038	-0.0245	0.1218	0.730
-0.0347	-0.0858	0.0884	0.445
-0.0506	-0.0824	0.0152	0.595
0.0011	-0.0917	-0.0087	0.043
-0.0070	-0.0402	0.0464	0.567
-0.0529	-0.0566	0.0437	0.722
-0.0100	-0.0938	-0.0117	0.033
0.0334	-0.0449	0.0261	0.742
-0.0108	-0.0642	0.1328	0.588
-0.0483	-0.0699	0.0487	0.695
-0.0264	-0.1260	0.0386	0.751
-0.0051	-0.0874	0.0493	0.584
0.0635	-0.0546	0.0456	0.722
-0.0496	-0.0362	0.1701	0.737
-0.0245	-0.0952	-0.0023	0.185
0.0227	-0.0575	0.0089	0.184
-0.0083	-0.0636	0.1118	0.027
-0.0113	-0.0432	0.0278	0.683
-0.0091	-0.0733	0.0555	0.910
0.0674	-0.0336	0.0159	0.958
-0.0178	-0.0054	0.1502	0.278
-0.0006	-0.0606	0.0281	0.386
0.0032	-0.0337	0.0329	0.361
0.0576	-0.0383	0.0463	0.618
0.0496	-0.0170	0.1288	0.172
0.0023	-0.0308	0.1276	0.526
0.0189	-0.0848	0.0987	0.456
0.0090	-0.0257	0.0650	0.489
-0.0121	-0.0279	0.0485	0.153
-0.0650	-0.0475	0.0260	0.311
-0.0040	-0.1266	0.0028	0.009
-0.0051	-0.0417	0.0347	0.414
0.0226	-0.0658	0.0561	0.853
-0.0186	-0.0760	0.1338	0.948
0.0241	-0.0801	0.0463	0.669
-0.0090	-0.1191	0.1818	0.740

0.0640	-0.0603	0.0415	0.970
0.0226	-0.0298	0.1661	0.663
0.0212	-0.0549	0.1006	0.664
-0.0263	-0.0063	0.0487	0.382
0.0025	-0.0908	0.0461	0.423
-0.0370	-0.0365	0.0448	0.266
-0.0092	-0.0620	-0.0108	0.652
-0.0260	-0.0607	0.0447	0.552
0.0000	-0.0712	0.0235	0.344
-0.0409	-0.1481	0.1445	0.617
0.0009	-0.1048	0.0244	0.051
-0.0174	-0.0637	0.0746	0.485
0.0243	-0.0801	0.0517	0.938
0.0030	-0.0218	0.0726	0.784
0.0230	-0.0219	0.0292	0.520
-0.0312	-0.0869	0.1502	0.253
-0.0331	-0.0829	0.0396	0.143
-0.0533	-0.0883	0.0246	0.747
0.0031	-0.1139	0.0088	0.013
-0.0252	-0.0465	0.0538	0.464
-0.0262	-0.0649	0.0176	0.290
0.0088	-0.0524	-0.0003	0.110
0.0207	-0.0461	0.0647	0.118
0.0218	-0.0209	0.0634	0.084
-0.0096	-0.0114	0.0559	0.039
-0.0085	-0.0679	0.0535	0.310
0.0259	-0.0465	0.0298	0.776
-0.0050	-0.0521	0.1050	0.247
0.0892	-0.0323	0.0229	0.724
-0.0113	-0.0560	0.2441	0.355
-0.0067	-0.0682	0.0459	0.686
0.0062	-0.0951	0.0891	0.695
-0.0430	-0.0488	0.0652	0.447
0.0875	-0.0794	-0.0064	0.216
-0.0666	-0.0548	0.2571	0.683
0.0499	-0.1762	0.0495	0.383
-0.0113	0.0006	0.0999	0.055
0.0038	-0.0895	0.0743	0.448
0.0189	-0.0676	0.0808	0.997
0.0306	-0.0402	0.0805	0.849
-0.0240	-0.0580	0.1128	0.990
-0.0441	-0.0672	0.0319	0.408
0.0176	-0.0949	0.0171	0.919
0.0014	-0.0409	0.0770	0.113
0.0165	-0.0566	0.0601	0.160

-0.0382	-0.0392	0.0757	0.664
-0.0138	-0.1260	0.0530	0.307
-0.0149	-0.0764	0.0504	0.679
-0.0399	-0.0577	0.0299	0.041
0.0187	-0.1041	0.0305	0.709
0.0074	-0.0481	0.0862	0.680
-0.0132	-0.0292	0.0443	0.428
0.0278	-0.0426	0.0164	0.743
-0.0054	-0.0231	0.0829	0.603
-0.0440	-0.1036	0.1066	0.474
-0.1256	-0.1156	0.0330	0.499
0.0362	-0.2556	0.0172	0.184
-0.0082	-0.0587	0.1263	0.571
-0.0132	-0.0977	0.0840	0.629
-0.0610	-0.0485	0.0221	0.422
-0.0273	-0.1357	0.0195	0.058
0.0692	-0.0905	0.0412	0.803
0.0043	-0.0497	0.2139	0.980
-0.0565	-0.0495	0.0599	0.851
-0.0091	-0.1059	-0.0040	0.019
-0.0670	-0.1387	0.1175	0.396
0.0316	-0.1897	0.0662	0.651
0.0001	-0.0869	0.1706	0.895
0.0083	-0.0319	0.0325	0.339
0.0342	-0.0387	0.0589	0.678
-0.0269	-0.0844	0.1853	0.788
-0.0094	-0.0848	0.0340	0.843
0.0297	-0.0643	0.0495	0.980
0.0021	-0.0157	0.0772	0.019
-0.1085	-0.0447	0.0532	0.412
-0.0182	-0.1760	-0.0338	0.023
0.0168	-0.1345	0.1101	0.278
-0.0020	-0.0911	0.1454	0.822
-0.0578	-0.0627	0.0616	0.787
0.0404	-0.1433	0.0361	0.985
0.0119	-0.0793	0.1622	0.239
0.0083	-0.0281	0.0585	0.534
0.0035	-0.0420	0.0603	0.072
-0.0497	-0.0729	0.0819	0.790
0.0271	-0.1046	0.0071	0.114
0.0596	-0.0344	0.0932	0.106
0.1360	-0.0311	0.1564	0.243
-0.0051	-0.0605	0.3220	0.226
0.0282	-0.0924	0.0806	0.677
-0.0307	-0.0369	0.1028	0.741

-0.0173	-0.0631	0.0033	0.838
-0.0400	-0.0637	0.0333	0.729
0.0149	-0.0919	0.0143	0.034
-0.0581	-0.0269	0.0583	0.596
0.0504	-0.1571	0.0488	0.189
-0.0171	-0.0127	0.1152	0.071
-0.0599	-0.1225	0.1003	0.910
-0.0098	-0.1047	-0.0097	0.020
0.0019	-0.0902	0.0789	0.230
-0.1319	-0.0406	0.0460	0.308
-0.0280	-0.2340	-0.0129	0.051
0.0099	-0.0740	0.0200	0.266
0.0143	-0.0749	0.1053	0.006
0.0039	-0.0342	0.0618	0.886
-0.0478	-0.0219	0.0302	0.546
-0.0246	-0.1030	0.0122	0.407
-0.0273	-0.1196	0.0862	0.406
0.0514	-0.0938	0.0445	0.995
-0.0061	-0.0585	0.1775	0.309
-0.0042	-0.0809	0.0698	0.275
0.0009	-0.0769	0.0776	0.330
0.0685	-0.0935	0.1097	0.516
0.0218	0.0022	0.1406	0.194
-0.0072	-0.0774	0.1139	0.368
-0.0320	-0.0298	0.0152	0.390
-0.0195	-0.1519	0.0969	0.327
0.0205	-0.0741	0.0370	0.429
-0.0057	-0.0469	0.0945	0.434
0.0185	-0.0600	0.0523	0.990
0.0005	-0.0302	0.0711	0.501
-0.0021	-0.0332	0.0363	0.469
-0.0157	-0.0894	0.0937	0.548
-0.0584	-0.0585	0.0286	0.717
0.0074	-0.1113	-0.0025	0.712
-0.0034	-0.0262	0.0432	0.513
-0.0867	-0.0487	0.0445	0.856
-0.0206	-0.1601	0.0021	0.551
0.0131	-0.0607	0.0202	0.640
0.0425	-0.1011	0.1420	0.626
0.0135	-0.0202	0.1088	0.250
0.0504	-0.0297	0.0595	0.896
0.0149	-0.0576	0.1656	0.279
0.0125	-0.0729	0.1032	0.591
-0.0237	-0.0203	0.0459	0.161
-0.0346	-0.0585	0.0150	0.490

0.0041	-0.1063	0.0401	0.669
0.0255	-0.0142	0.0227	0.774
-0.0830	-0.0598	0.1236	0.952
0.0101	-0.1595	0.0072	0.187
0.0299	-0.0279	0.0497	0.091
-0.0054	-0.0309	0.0940	0.992
-0.0011	-0.0687	0.0572	0.521
0.0119	-0.0453	0.0429	0.847
0.0084	-0.0433	0.0719	0.422
-0.0070	-0.1290	0.1736	0.581
-0.0242	-0.0750	0.0761	0.655
0.0206	-0.0944	0.0635	0.396
-0.0135	-0.0329	0.0750	0.991
0.0466	-0.1232	0.0981	0.987
-0.0065	-0.0961	0.2198	0.261
-0.0246	-0.0675	0.0596	0.708
-0.0272	-0.0688	0.0213	0.371
-0.0219	-0.0732	0.0210	0.958
0.0174	-0.0727	0.0330	0.441
0.0415	-0.0583	0.1092	0.522
-0.0461	-0.0418	0.1299	0.887
-0.0266	-0.1378	0.0541	0.456
-0.0441	-0.0755	0.0222	0.006
-0.0193	-0.0803	-0.0064	0.380
-0.0218	-0.0477	0.0099	0.261
-0.0058	-0.0667	0.0237	0.051
-0.0262	-0.0819	0.0747	0.459
-0.1010	-0.0953	0.0509	0.907
-0.0477	-0.1619	-0.0323	0.101
-0.0095	-0.1112	0.0360	0.557
-0.0109	-0.0687	0.0505	0.705
0.0487	-0.0605	0.0580	0.720
-0.0033	-0.0158	0.1173	0.471
0.0266	-0.0646	0.0560	0.204
-0.0020	-0.0382	0.0966	0.108
-0.0166	-0.0406	0.0372	0.780
0.0101	-0.1012	0.0783	0.730
-0.0145	-0.0593	0.0897	0.624
-0.0579	-0.0914	0.0650	0.513
0.0540	-0.1011	-0.0034	0.306
-0.0183	-0.0356	0.1431	0.790
-0.0171	-0.0675	0.0319	0.961
0.0188	-0.0615	0.0286	0.473
-0.1416	-0.0996	0.1440	0.090
-0.0088	-0.2598	0.0107	0.845

0.0337	-0.0708	0.0500	0.495
-0.0153	-0.0096	0.0827	0.094
-0.0087	-0.0541	0.0237	0.582
0.0098	-0.0442	0.0295	0.572
-0.0025	-0.0485	0.0727	0.553
0.0134	-0.0525	0.0555	0.420
-0.0014	-0.1022	0.1402	0.929
-0.0409	-0.0592	0.0575	0.802
0.0104	-0.1045	0.0275	0.301
0.0162	-0.0630	0.0844	0.536
-0.0106	-0.0335	0.0669	0.445
0.0457	-0.0644	0.0446	0.489
0.0043	-0.0301	0.1292	0.007
0.0694	-0.0602	0.0714	0.503
-0.0977	-0.0374	0.1764	0.717
0.0318	-0.1797	-0.0110	0.062
-0.0312	-0.0553	0.1242	0.486
0.0387	-0.0880	0.0276	0.202
0.0044	-0.0089	0.0896	0.679
0.0082	-0.0441	0.0504	0.361
-0.0459	-0.0723	0.0964	0.625
0.0346	-0.1073	0.0182	0.367
-0.0963	-0.0598	0.1495	0.283
0.0219	-0.1561	-0.0335	0.105
0.0275	-0.0156	0.0606	0.470
0.0085	-0.0290	0.0876	0.553
-0.0555	-0.1012	0.1438	0.639
0.0141	-0.0976	-0.0092	0.220
-0.0313	-0.0337	0.0662	0.720
-0.0735	-0.0711	0.0111	0.688
-0.0296	-0.1244	-0.0206	0.002
0.0106	-0.0836	0.0296	0.797
0.0037	-0.0424	0.0672	0.308
-0.0488	-0.0466	0.0553	0.385
-0.0258	-0.1381	0.0443	0.609
0.0015	-0.0846	0.0356	0.972
-0.0297	-0.0607	0.0682	0.566
0.0189	-0.0689	0.0085	0.253
0.0299	-0.0597	0.0947	0.264
0.0014	-0.0336	0.1007	0.683
-0.0085	-0.0340	0.0364	0.426
0.0058	-0.0994	0.0982	0.395
-0.0400	-0.0526	0.0684	0.763
-0.0169	-0.0943	0.0095	0.313
0.0075	-0.0718	0.0396	0.664

-0.0201	-0.0267	0.0428	0.479
0.0125	-0.1067	0.0732	0.113
-0.0157	-0.0814	0.1146	0.608
-0.0105	-0.0575	0.0279	0.647
-0.0162	-0.0547	0.0346	0.197
-0.0030	-0.0360	0.0045	0.352
-0.0067	-0.0317	0.0276	0.778
-0.0036	-0.0560	0.0445	0.924
-0.0042	-0.0630	0.0576	0.325
-0.0124	-0.0800	0.0636	0.501
-0.0241	-0.0475	0.0251	0.227
-0.0166	-0.0803	0.0380	0.896
-0.0434	-0.0731	0.0470	0.609
-0.1134	-0.1153	0.0417	0.496
-0.0338	-0.2085	0.0096	0.500
0.0105	-0.1006	0.0379	0.953
-0.0273	-0.0216	0.0444	0.780
-0.0346	-0.0960	0.0480	0.842
-0.0530	-0.0979	0.0336	0.244
0.0612	-0.0779	-0.0272	0.030
-0.0601	-0.1357	0.3209	0.931
0.0014	-0.1182	-0.0007	0.121
-0.0785	-0.0457	0.0522	0.783
-0.0828	-0.1701	0.0254	0.097
-0.0742	-0.1747	0.0257	0.360
-0.0151	-0.1361	-0.0084	0.495
0.0052	-0.0679	0.0429	0.527
-0.0051	-0.0820	0.1023	0.380
0.0154	-0.0997	0.1029	0.576
0.0014	-0.0202	0.0532	0.926
-0.0179	-0.0690	0.0811	0.908
-0.0230	-0.0710	0.0395	0.891
-0.0482	-0.0819	0.0381	0.046
0.0262	-0.1225	0.0383	0.329
0.0300	-0.0864	0.1440	0.316
0.0424	-0.1034	0.1709	0.802
0.0405	-0.0324	0.1231	0.633
-0.0244	-0.1227	0.2225	0.952
0.0255	-0.0920	0.0478	0.945
0.0737	-0.0082	0.0596	0.563
-0.0081	-0.0221	0.1764	0.306
-0.0047	-0.0672	0.0544	0.529
-0.0514	-0.0674	0.0584	0.895
0.0097	-0.0942	-0.0087	0.906
0.0982	-0.0482	0.0728	0.889

-0.0248	0.0294	0.1665	0.013
-0.0294	-0.0476	-0.0024	0.117
-0.0248	-0.0648	0.0091	0.150
0.0970	-0.1529	0.1131	0.746
-0.0081	0.0065	0.1922	0.437
-0.0206	-0.0884	0.0873	0.599
-0.0056	-0.0870	0.0561	0.348
0.1446	-0.0556	0.0471	0.641
-0.0378	0.0090	0.2949	0.003
0.0185	-0.0812	0.0093	0.593
-0.0387	-0.0984	0.1566	0.975
-0.0443	-0.0774	0.0026	0.068
-0.0564	-0.1224	0.0425	0.650
-0.0042	-0.1083	-0.0023	0.043
0.0147	-0.0449	0.0410	0.463
0.0086	-0.0983	0.1365	0.287
0.0053	-0.0378	0.0568	0.923
-0.0275	-0.0551	0.0689	0.848
0.1497	-0.0587	0.0058	0.726
-0.0350	-0.0602	0.3873	0.054
0.0186	-0.1175	0.0546	0.846
-0.0543	-0.0768	0.1207	0.997
-0.0005	-0.1124	0.0100	0.129
-0.0078	-0.0638	0.0639	0.753
0.0112	-0.0308	0.0160	0.506
0.0219	-0.0614	0.0869	0.506
0.0259	-0.0122	0.0584	0.115
-0.0123	-0.0346	0.0908	0.565
-0.0423	-0.0494	0.0255	0.943
0.0084	-0.1015	0.0207	0.637
-0.0403	-0.0313	0.0499	0.760
0.0080	-0.0640	-0.0159	0.396
-0.0283	-0.0576	0.0811	0.821
-0.0672	-0.0841	0.0304	0.882
0.0234	-0.1387	0.0176	0.261
-0.0029	-0.1324	0.1815	0.717
-0.0311	-0.0574	0.0558	0.629
-0.0091	-0.1006	0.0704	0.996
-0.0615	-0.0438	0.0275	0.302
0.0239	-0.1177	-0.0017	0.003
-0.0272	-0.0360	0.0870	0.607
-0.0585	-0.1330	0.1001	0.275
0.0148	-0.1047	-0.0052	0.031
0.0095	-0.0176	0.0496	0.896
0.0266	-0.0495	0.0733	0.510

0.0332	-0.0197	0.0765	0.421
-0.0047	-0.0420	0.1140	0.785
-0.0277	-0.0897	0.0857	0.825
-0.0115	-0.0672	0.0121	0.030
0.0163	-0.0914	0.0731	0.940
0.0071	-0.0559	0.0960	0.284
-0.0280	-0.0803	0.0986	0.872
0.0189	-0.1006	0.0518	0.522
-0.0523	-0.0545	0.0963	0.363
-0.0681	-0.0971	0.0025	0.540
-0.0054	-0.1776	0.0663	0.678
0.0080	-0.0649	0.0577	0.833
-0.0096	-0.0380	0.0568	0.417
-0.0203	-0.0352	0.0155	0.819
0.2267	-0.0543	0.0142	0.492
-0.0755	-0.1069	0.5272	0.224
-0.0149	-0.1480	0.0004	0.028
-0.0061	-0.0953	0.0654	0.718
0.0343	-0.0550	0.0440	0.486
-0.0144	-0.0310	0.1090	0.557
-0.0062	-0.0856	0.0548	0.830
-0.0434	-0.1029	0.0893	0.587
0.0197	-0.1153	0.0336	0.096
-0.0703	-0.0672	0.1144	0.852
-0.0341	-0.1795	0.0560	0.158
0.1087	-0.0864	0.0170	0.453
0.0152	-0.0287	0.2440	0.561
-0.0182	-0.0283	0.0595	0.405
0.0313	-0.0613	0.0282	0.220
-0.0212	-0.0096	0.0746	0.054
0.0143	-0.0548	0.0128	0.268
-0.0017	-0.0485	0.0803	0.849
0.0052	-0.0420	0.0391	0.461
-0.0219	-0.0741	0.0871	0.780
-0.0685	-0.0843	0.0437	0.352
-0.0061	-0.1519	0.0208	0.270
-0.0457	-0.1059	0.1022	0.642
0.0387	-0.1090	0.0210	0.320
0.0205	-0.0502	0.1274	0.312
0.0002	-0.0564	0.1076	0.959
-0.0443	-0.0865	0.0866	0.672
-0.0283	-0.0820	-0.0072	0.066
0.0385	-0.0792	0.0263	0.811
-0.0432	-0.0119	0.0917	0.248
-0.0408	-0.0956	0.0156	0.651

-0.0298	-0.1484	0.0770	0.734
-0.0212	-0.0908	0.0379	0.708
-0.0217	-0.0740	0.0317	0.962
-0.0238	-0.1786	0.1552	0.792
-0.0332	-0.1596	0.1220	0.930
0.0249	-0.0771	0.0107	0.271
0.0080	-0.0390	0.0950	0.521
-0.0419	-0.1109	0.1404	0.987
-0.1895	-0.1726	0.0798	0.530
-0.0056	-0.3231	-0.0220	0.111
-0.0334	-0.0544	0.0445	0.896
-0.0167	-0.1270	0.0975	0.456
-0.0054	-0.0421	0.0099	0.830
-0.0072	-0.0552	0.0461	0.339
0.0260	-0.0491	0.0367	0.543
0.0056	-0.0234	0.0785	0.059
0.0081	-0.0543	0.0692	0.655
-0.0616	-0.0390	0.0562	0.488
-0.0269	-0.1302	0.0393	0.224
-0.0137	-0.0532	-0.0003	0.418
0.0081	-0.0699	0.0463	0.490
-0.0166	-0.0638	0.0915	0.563
-0.0111	-0.0656	0.0337	0.864
0.0051	-0.0778	0.0604	0.581
-0.0200	-0.0315	0.0420	0.915
-0.1181	-0.0450	0.0076	0.752
-0.0184	-0.1893	-0.0359	0.060
0.0508	-0.1399	0.1335	0.255
-0.0051	-0.0244	0.1364	0.859
-0.0280	-0.0856	0.0848	0.650
-0.0044	-0.0640	0.0082	0.493
0.0103	-0.0450	0.0389	0.755
0.0024	-0.0359	0.0598	0.104
0.0300	-0.0377	0.0440	0.572
-0.0300	-0.0173	0.0815	0.915
0.0553	-0.1396	0.1052	0.048
-0.0325	-0.0482	0.1789	0.952
-0.0975	-0.0794	0.0189	0.188
0.0485	-0.1621	-0.0299	0.013
0.0315	-0.0661	0.1765	0.355
-0.0368	-0.0462	0.1124	0.025
-0.0139	-0.1338	0.0712	0.988
0.0472	-0.0598	0.0343	0.972
0.0135	-0.0126	0.1131	0.381
0.0013	-0.0761	0.1135	0.847

-0.0712	-0.0622	0.0818	0.070
0.0001	-0.1741	0.0421	0.391
0.0011	-0.0319	0.0334	0.737
-0.0024	-0.0543	0.0592	0.170
0.0063	-0.0419	0.0393	0.499
0.0027	-0.0735	0.0904	0.786
0.0079	-0.0753	0.0851	0.976
-0.0141	-0.0149	0.0313	0.760
0.1728	-0.0574	0.0315	0.626
-0.0248	0.0463	0.3011	0.023
-0.0348	-0.1037	0.0671	0.273
0.0005	-0.1635	0.1335	0.959
-0.0335	-0.0457	0.0469	0.713
-0.0177	-0.1018	0.0380	0.528
-0.0248	-0.1037	0.0820	0.904
-0.0239	-0.1085	0.0713	0.985
0.0484	-0.0750	0.0341	0.619
-0.0259	-0.0311	0.1345	0.219
-0.0512	-0.0922	0.0430	0.850
-0.0230	-0.1194	0.0271	0.715
0.0079	-0.0665	0.0200	0.092
0.0127	-0.0271	0.0445	0.687
0.0302	-0.0396	0.0691	0.913
0.0235	-0.0232	0.0844	0.290
0.0149	-0.0403	0.0940	0.770
-0.0757	-0.0798	0.1185	0.944
0.0727	-0.1534	0.0023	0.032
0.0458	-0.1084	0.2889	0.564
0.0172	-0.0012	0.0976	0.031
-0.0147	-0.0160	0.0517	0.686
-0.0507	-0.0577	0.0303	0.332
-0.0247	-0.1035	0.0043	0.513
-0.0289	-0.0543	0.0063	0.526
-0.0347	-0.0719	0.0152	0.741
-0.0021	-0.0685	0.0005	0.131
-0.0248	-0.1275	0.1681	0.666
-0.0407	-0.1096	0.0615	0.218
-0.0297	-0.0832	0.0033	0.222
-0.0163	-0.0699	0.0153	0.186
-0.0594	-0.0563	0.0250	0.998
-0.0041	-0.0929	-0.0232	0.241
0.0326	-0.0515	0.0438	0.864
0.0216	-0.0489	0.1215	0.744
0.0712	-0.0708	0.1306	0.974
-0.0039	-0.0516	0.2036	0.172

-0.0048	-0.0489	0.0430	0.737
-0.0320	-0.0686	0.0661	0.299
0.0875	-0.0695	0.0121	0.988
-0.0177	-0.0194	0.2048	0.071
0.0121	-0.0690	0.0380	0.123
-0.0518	-0.0168	0.0412	0.297
-0.0608	-0.1056	0.0019	0.006
-0.0517	-0.1510	0.0409	0.389
0.0071	-0.1240	0.0297	0.191
-0.0049	-0.0535	0.0736	0.745
-0.0136	-0.1205	0.1124	0.167
-0.0082	-0.0863	0.0676	0.754
-0.0661	-0.0555	0.0420	0.467
0.0199	-0.1212	-0.0068	0.176
-0.0053	-0.0465	0.0892	0.725
-0.0527	-0.0467	0.0368	0.470
0.0761	-0.0926	-0.0097	0.059
0.0132	-0.0501	0.2017	0.233
-0.0190	-0.0614	0.0939	0.868
-0.1173	-0.0699	0.0384	0.640
0.0064	-0.2251	0.0230	0.306
-0.0378	-0.0906	0.1185	0.377
0.0553	-0.1019	0.0385	0.749
0.0252	-0.0095	0.1207	0.088
0.0118	-0.0257	0.0796	0.793
0.0055	-0.0411	0.0649	0.602
0.0123	-0.0704	0.0801	0.753
0.0285	-0.0688	0.0958	0.685
0.0542	-0.0427	0.1056	0.421
-0.0091	-0.0540	0.1688	0.372
0.0211	-0.0941	0.0869	0.584
0.0467	-0.0324	0.0765	0.503
-0.0143	-0.0209	0.1168	0.255
-0.1014	-0.1164	0.0966	0.790
-0.0277	-0.1610	-0.0372	0.214
0.0089	-0.1122	0.0597	0.297
-0.0561	-0.0468	0.0604	0.704
-0.0153	-0.1090	-0.0015	0.333
-0.0192	-0.0735	0.0442	0.075
-0.0044	-0.1320	0.1040	0.258
0.0429	-0.0918	0.0930	0.703
-0.0414	-0.0577	0.1448	0.920
0.0304	-0.1074	0.0287	0.163
-0.0487	-0.0660	0.1313	0.592
-0.0548	-0.1173	0.0198	0.828

-0.0047	-0.1287	0.0354	0.040
0.0049	-0.0517	0.0463	0.709
-0.0446	-0.0899	0.0985	0.494
-0.0122	-0.0935	0.0080	0.044
-0.2169	-0.0989	0.0832	0.136
-0.0170	-0.3246	-0.0718	0.055
0.0884	-0.0530	0.0204	0.168
0.0158	-0.0388	0.2390	0.244
-0.0253	-0.0485	0.0807	0.440
-0.0457	-0.1299	0.0894	0.973
-0.0931	-0.1044	0.0217	0.757
-0.0994	-0.1537	-0.0278	0.214
-0.0367	-0.2018	0.0192	0.021
-0.0036	-0.1528	0.0958	0.480
-0.0281	-0.0744	0.0742	0.598
0.0525	-0.0758	0.0192	0.205
0.0435	-0.0454	0.1616	0.419
-0.0069	-0.0388	0.1281	0.519
-0.0158	-0.0860	0.0819	0.948
-0.0076	-0.0551	0.0313	0.154
0.0120	-0.0940	0.0870	0.824
-0.0002	-0.0628	0.0955	0.961
-0.0208	-0.0726	0.0785	0.397
0.0009	-0.0595	0.0171	0.882
-0.0064	-0.0559	0.0618	0.311
0.0145	-0.0928	0.0880	0.551
0.0550	-0.0531	0.0894	0.696
-0.0782	-0.0546	0.1714	0.438
-0.0071	-0.1446	-0.0066	0.071
0.0681	-0.0760	0.0703	0.579
-0.0103	-0.0819	0.2412	0.405
-0.0435	-0.0589	0.0408	0.480
-0.0766	-0.2551	0.3102	0.425
0.0269	-0.1868	0.0413	0.412
-0.0539	-0.0250	0.0808	0.228
-0.0210	-0.1269	0.0266	0.357
-0.0331	-0.0547	0.0140	0.519
-0.0241	-0.1050	0.0450	0.506
-0.0163	-0.1188	0.0803	0.839
-0.0557	-0.0504	0.0174	0.050
0.0153	-0.1316	0.0259	0.738
-0.0299	-0.0258	0.0604	0.085
-0.1000	-0.0612	0.0026	0.322
-0.0727	-0.1647	-0.0258	0.171
-0.0555	-0.1211	-0.0135	0.325

0.0036	-0.1368	0.0310	0.023
-0.0388	-0.0326	0.0402	0.672
-0.0513	-0.1171	0.0454	0.807
-0.0212	-0.1146	0.0147	0.318
-0.0217	-0.0540	0.0133	0.335
0.0141	-0.0514	0.0080	0.422
0.0161	-0.0372	0.0681	0.963
-0.0449	-0.0417	0.0752	0.604
-0.0327	-0.0722	-0.0170	0.028
-0.0051	-0.0667	0.0024	0.519
-0.0058	-0.0476	0.0380	0.987
0.0153	-0.0353	0.0233	0.783
0.0532	-0.0259	0.0581	0.111
0.0349	-0.0242	0.1402	0.578
0.0043	-0.0476	0.1305	0.529
-0.0346	-0.0331	0.0422	0.122
0.0179	-0.0946	0.0391	0.635
-0.0277	-0.0582	0.0932	0.151
0.0381	-0.0819	0.0311	0.074
0.0498	-0.0201	0.1011	0.201
0.0017	-0.0571	0.1731	0.981
-0.0437	-0.0428	0.0460	0.769
-0.0084	-0.1114	0.0303	0.293
-0.0173	-0.2361	0.2283	0.879
-0.0618	-0.0972	0.0704	0.726
0.0032	-0.2037	0.0686	0.134
0.0063	-0.0490	0.0568	0.645
-0.0280	-0.0514	0.0698	0.037
-0.0236	-0.0776	0.0242	0.421
-0.0380	-0.0741	0.0296	0.980
-0.0626	-0.0658	-0.0101	0.576
-0.0394	-0.1740	0.0623	0.418
-0.0490	-0.0731	-0.0056	0.288
-0.0134	-0.1576	0.0827	0.962
-0.0254	-0.0506	0.0250	0.834
-0.0430	-0.0941	0.0494	0.498
0.0082	-0.0887	0.0099	0.038
-0.0218	-0.0542	0.0735	0.586
-0.0047	-0.0940	0.0534	0.500
0.0273	-0.1115	0.1195	0.681
0.0204	-0.0768	0.1437	0.963
0.0034	-0.0320	0.0753	0.510
0.0144	-0.0644	0.0773	0.733
0.1014	-0.0478	0.0788	0.138
0.0099	-0.0405	0.2738	0.021

-0.0077	-0.0201	0.0398	0.166
0.0326	-0.0847	0.0753	0.429
-0.0382	-0.1041	0.1869	0.537
-0.0098	-0.1162	0.0471	0.297
0.0001	-0.1115	0.1079	0.257
-0.0093	-0.1353	0.1434	0.521
-0.0686	-0.0427	0.0257	0.779
0.0364	-0.1724	0.0502	0.502
-0.0762	-0.0216	0.0990	0.072
0.0322	-0.1816	0.0364	0.595
-0.0782	-0.0217	0.0903	0.297
-0.0385	-0.1565	0.0108	0.071
-0.0145	-0.0801	0.0052	0.093
-0.0371	-0.0345	0.0058	0.557
0.1033	-0.0610	-0.0123	0.369
-0.0211	-0.0522	0.2550	0.871
-0.0638	-0.1123	0.0766	0.932
0.1613	-0.1215	0.0018	0.085
-0.0106	0.0055	0.3199	0.533
0.0071	-0.0602	0.0388	0.237
0.0049	-0.0278	0.0418	0.484
0.0259	-0.0801	0.0974	0.345
0.0531	-0.0979	0.1736	0.482
0.0098	-0.0855	0.1908	0.987
0.0017	-0.0449	0.0636	0.814
-0.0157	-0.0538	0.0595	0.564
-0.0191	-0.0600	0.0292	0.812
0.0158	-0.0460	0.0082	0.053
-0.0214	-0.0326	0.0720	0.077
-0.0159	-0.0820	0.0443	0.792
-0.0367	-0.0843	0.0605	0.402
0.0276	-0.1251	0.0599	0.524
0.0321	-0.0554	0.1155	0.589
0.0211	-0.0382	0.1037	0.622
0.0475	-0.0536	0.0962	0.262
-0.0107	-0.0152	0.1162	0.779
0.0020	-0.0429	0.0211	0.926
-0.0415	-0.0314	0.0358	0.790
-0.0023	-0.1110	0.0377	0.324
-0.0714	-0.1069	0.1075	0.602
-0.0001	-0.1482	0.0069	0.015
0.0426	-0.0983	0.1008	0.721
-0.0825	-0.0437	0.1402	0.339
0.0321	-0.1880	0.0333	0.946
-0.0109	-0.0320	0.0986	0.463

-0.0218	-0.0630	0.0459	0.557
-0.0306	-0.0575	0.0165	0.906
-0.0061	-0.0865	0.0287	0.381
0.0956	-0.0423	0.0306	0.623
-0.0146	-0.0239	0.2216	0.095
0.0434	-0.0683	0.0429	0.042
0.0171	-0.0608	0.1541	0.747
0.0097	-0.0461	0.0876	0.705
-0.0049	-0.0326	0.0521	0.955
-0.0215	-0.0502	0.0423	0.602
-0.0093	-0.0501	0.0092	0.799
-0.0755	-0.0839	0.0674	0.872
-0.0548	-0.1640	0.0212	0.133
-0.0218	-0.1038	0.0013	0.548
-0.0338	-0.0748	0.0333	0.405
-0.0112	-0.0816	0.0187	0.660
0.0025	-0.0563	0.0341	0.588
-0.0072	-0.0372	0.0442	0.793
-0.0055	-0.0609	0.0514	0.432
-0.0355	-0.0258	0.0149	0.733
-0.0433	-0.0978	0.0286	0.056
-0.0219	-0.1563	0.0776	0.300
0.0282	-0.0891	0.0639	0.410
-0.0207	-0.0878	0.1508	0.740
0.0235	-0.1525	0.1282	0.439
-0.0118	-0.0418	0.0947	0.964
-0.0207	-0.0887	0.0765	0.301
0.0120	-0.0414	0.0005	0.698
-0.0352	-0.0327	0.0597	0.098
0.0249	-0.0791	0.0126	0.495
-0.0166	-0.0619	0.1161	0.922
0.0889	-0.0687	0.0381	0.522
0.0298	-0.0011	0.1817	0.147
-0.0111	-0.0244	0.0874	0.416
-0.0053	-0.1279	0.1111	0.406
-0.0015	-0.1002	0.0964	0.859
-0.0648	-0.0730	0.0790	0.685
0.1141	-0.1390	0.0200	0.676
0.0304	-0.0068	0.2371	0.463
-0.0058	-0.0809	0.1491	0.921
-0.0422	-0.0339	0.0238	0.939
0.0191	-0.1060	0.0296	0.831
0.0310	-0.0203	0.0624	0.210
0.0165	-0.0150	0.0809	0.024
0.0143	-0.0174	0.0518	0.508

-0.0370	-0.0275	0.0551	0.269
-0.0117	-0.0769	0.0101	0.563
-0.1173	-0.0505	0.0277	0.862
-0.0162	-0.2673	0.0747	0.549
-0.0306	-0.0576	0.0278	0.514
-0.0040	-0.0740	0.0182	0.215
-0.0608	-0.0180	0.0105	0.483
-0.0051	-0.1420	0.0341	0.242
-0.0495	-0.0465	0.0406	0.902
-0.0272	-0.1114	0.0178	0.375
-0.0062	-0.1093	0.0602	0.371

A.3 Southern California - Cut off magnitude 3.5

Correlation	Confidence Interval	Confidence interval2	p value
-0.015	-0.034	0.006	0.659
0.017	-0.077	0.1256	0.83

Appendix B

Constant strain rate experiments

B.1 Stress-Time plots

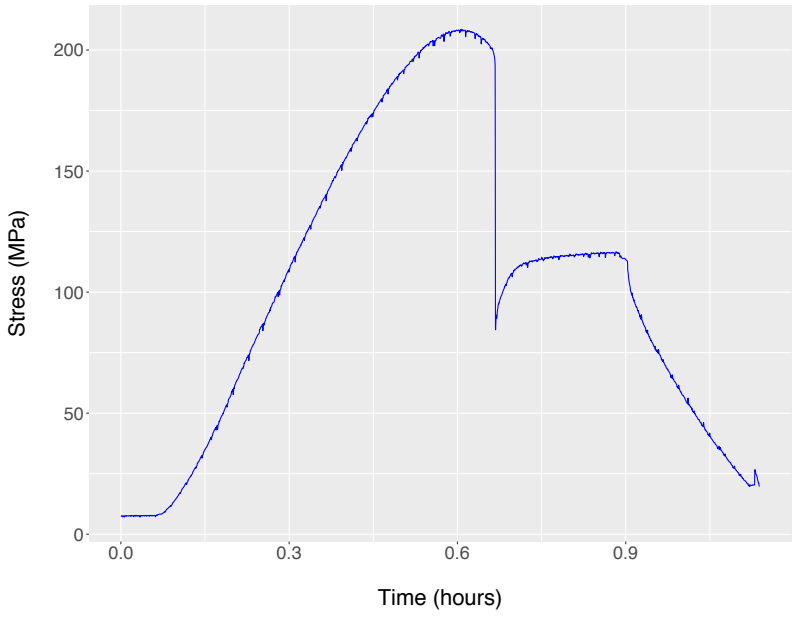

Figure B.1: Stress-Time plot. Dry experiment at 30 MPa confining pressure

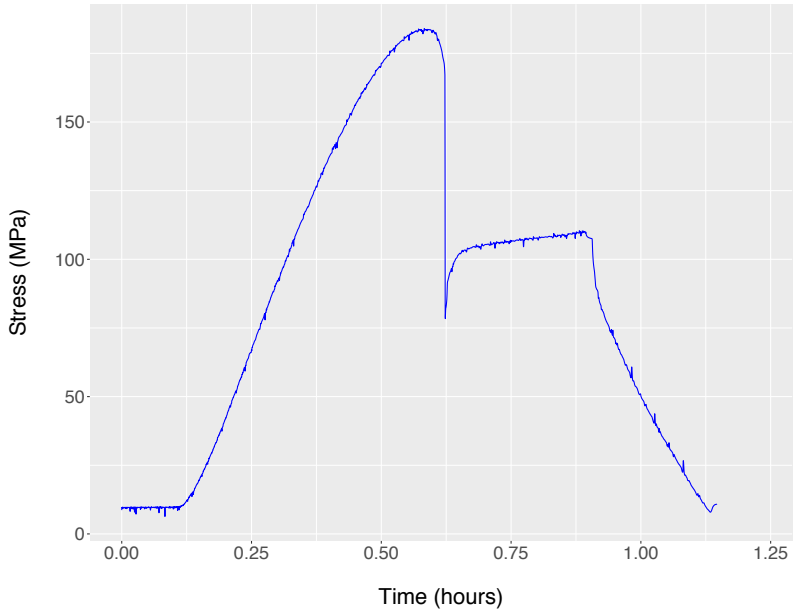

Figure B.2: Stress-Time plot. 50 MPa confining pressure and 20 MPa pore pressure, constant pressure experiment

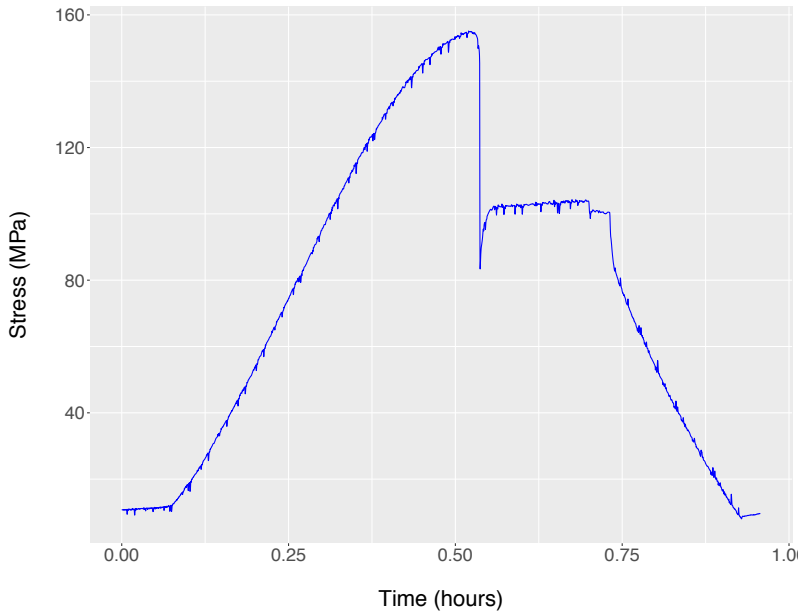

Figure B.3: Stress-Time plot. 50 MPa confining pressure and 20 MPa pore pressure, constant volume experiment

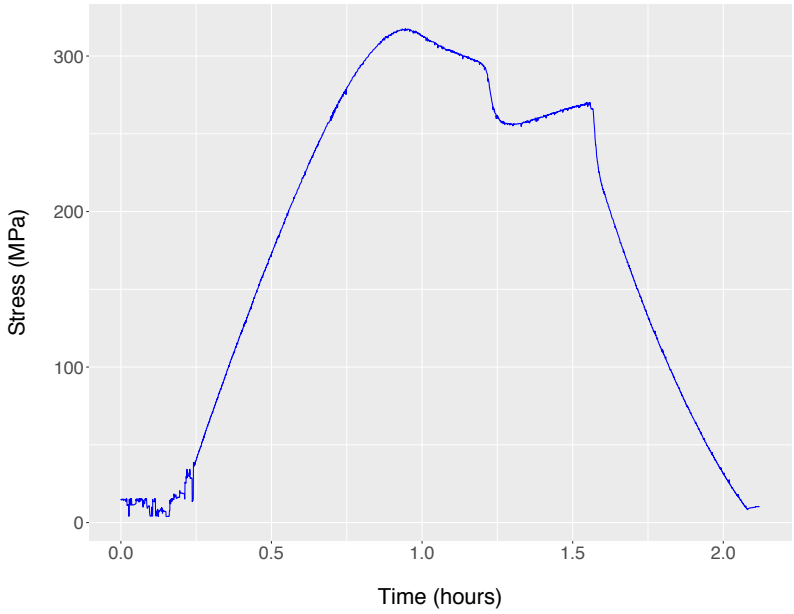

Figure B.4: Stress-Time plot. Dry experiment at 80 MPa confining pressure

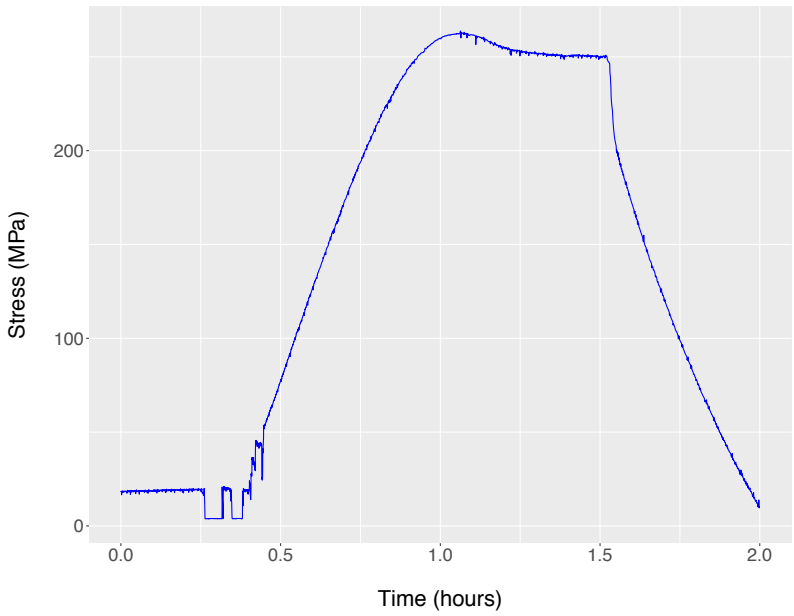

Figure B.5: Stress-Time plot. 100 MPa confining pressure and 20 MPa pore pressure, constant pressure experiment

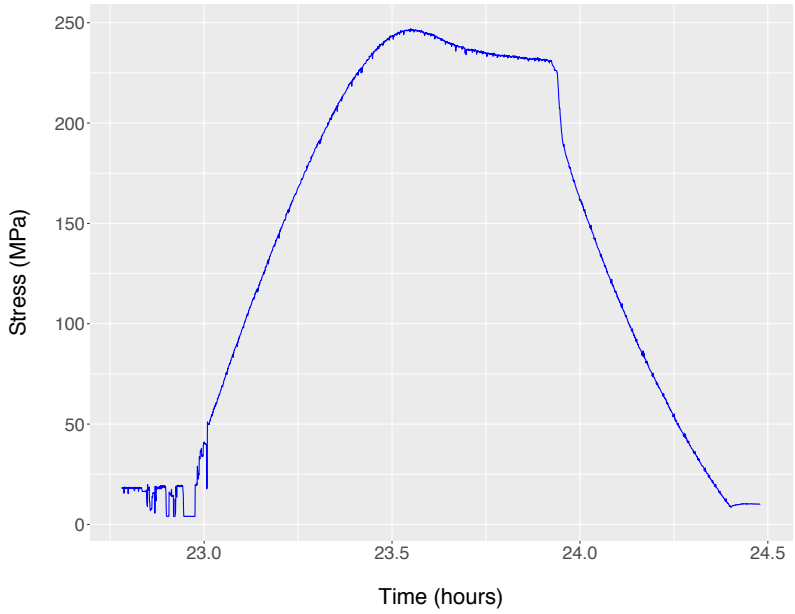

Figure B.6: Stress-Time plot. 100 MPa confining pressure and 20 MPa pore pressure, constant volume experiment

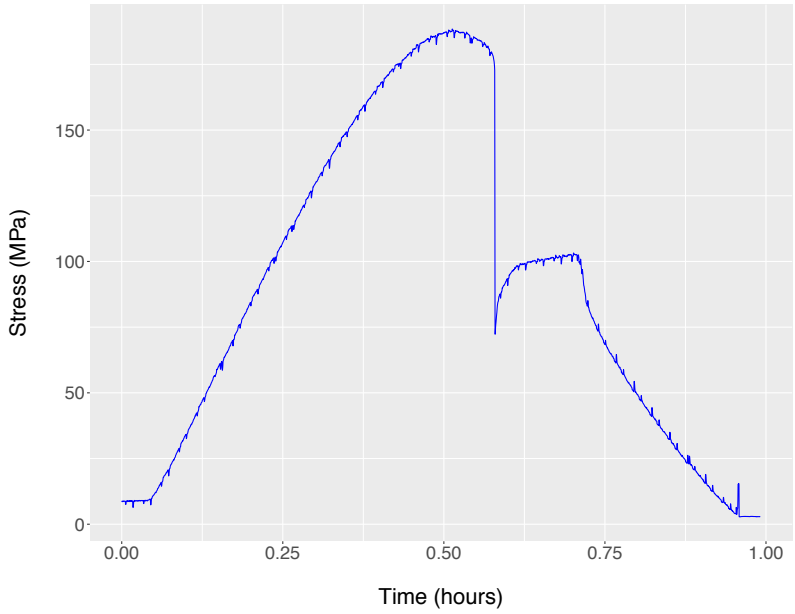

Figure B.7: Stress-Time plot. 40 MPa confining pressure and 10 MPa pore pressure, constant pressure experiment

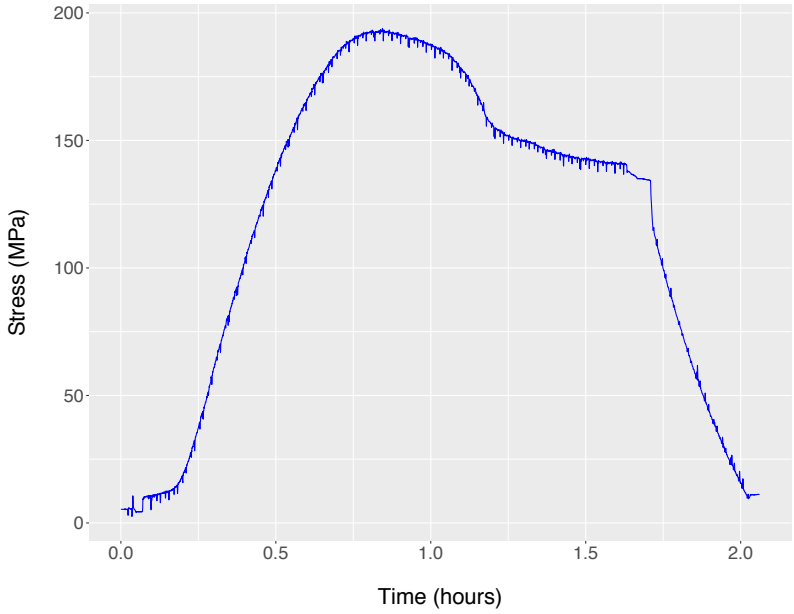

Figure B.8: Stress-Time plot. 50 MPa confining pressure and 20 MPa pore pressure, constant volume experiment

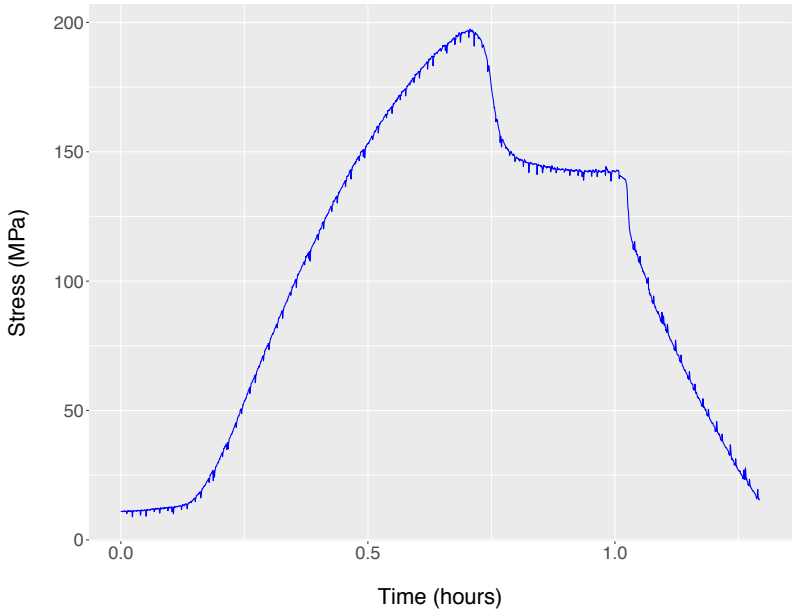

Figure B.9: Stress-Time plot. 50 MPa confining pressure and 20 MPa pore pressure, constant volume experiment

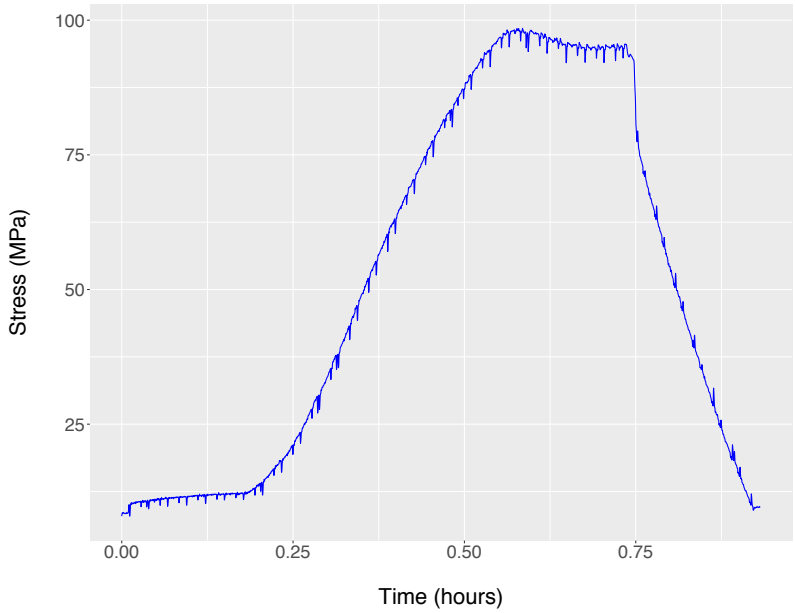

Figure B.10: Stress-Time plot. 50 MPa confining pressure and 20 MPa pore pressure, constant volume experiment. Saw cut sample.

Appendix C

Constant load experiments

C.1 Axial strain (%)-Time plots

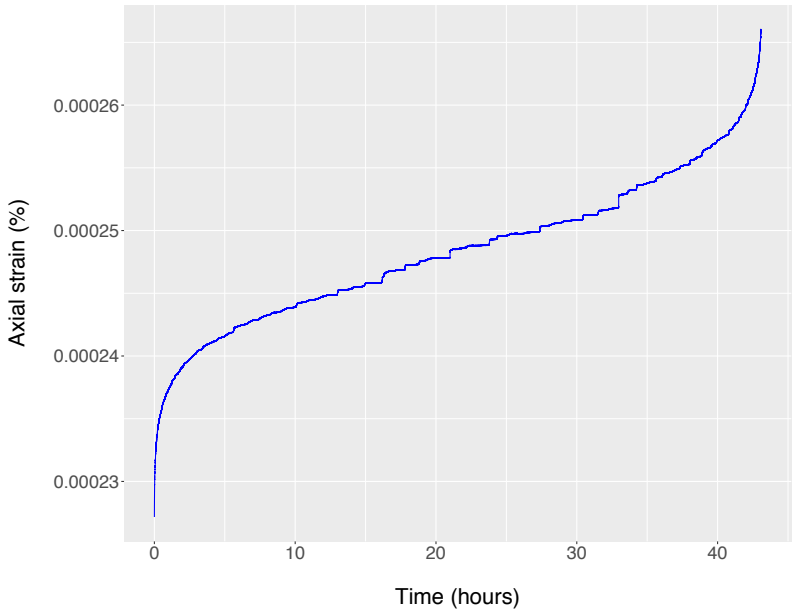

Figure C.1: Axial strain (%)-Time plot. 50 MPa confining pressure and 20 MPa pore pressure.

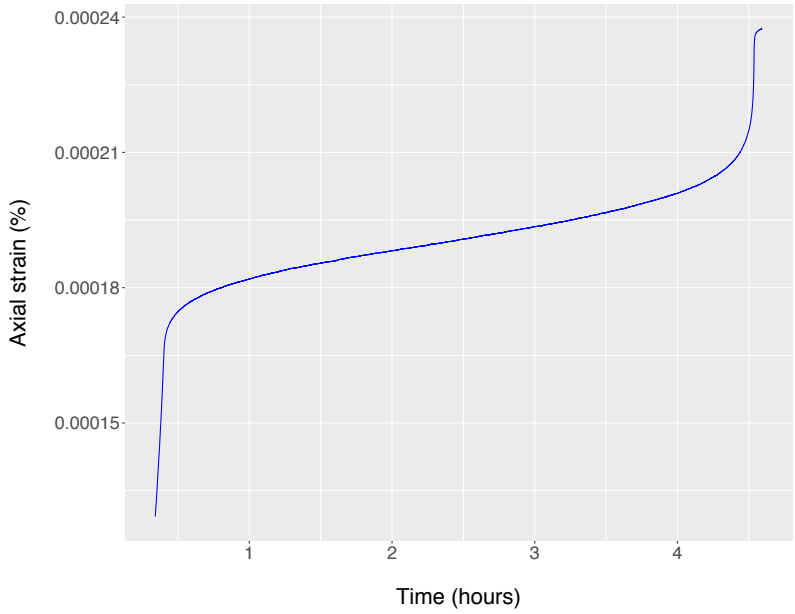

Figure C.2: Axial strain (%)-Time plot. 40 MPa confining pressure and 10 MPa pore pressure.

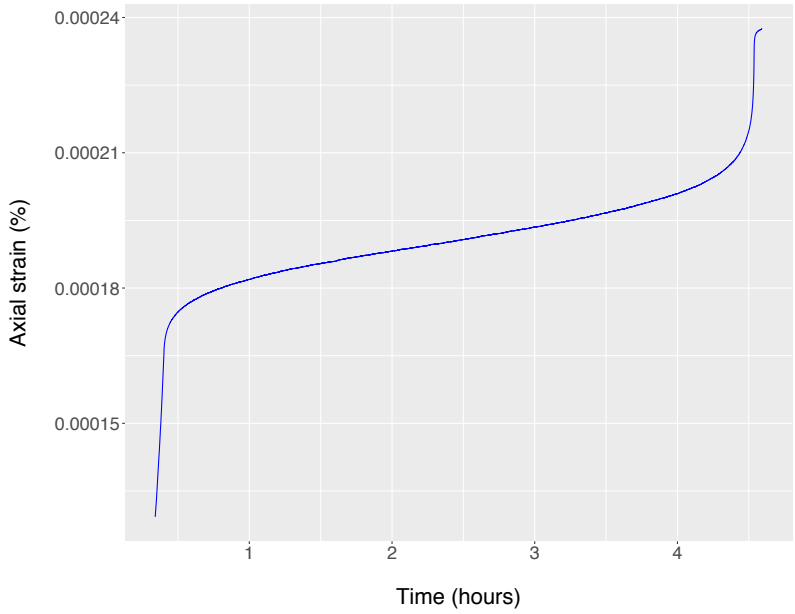

Figure C.3: Axial strain (%)-Time plot. 40 MPa confining pressure and 10 MPa pore pressure.

Appendix D

RMS Amplitude Method

The following description for the Geiger algorithm is from the user manual of the InSite software.

The RMS auto-picking algorithms operate by first calculating an auto-picking function using a moving window approach. At each waveform data point, i, two windows are generated: a front window and a back window. The value of the auto-picking function, F_i, is calculated by equation D.0.0.1 where A_j is the amplitude, NF is the length of the Front-window in data points, NB is the length of the Back-window in data points and n=2.

$$F_i = \frac{\sum_{j=i-1}^{i-NB} A_j^n}{\sum_{j=i+1}^{i+NF} A_j^n} \tag{D.0.0.1}$$

The auto-picking function represents a difference in energy contained in the front window compared to the back window. It can be viewed for a particular channel in the Waveform Visualiser. Peaks occur in the function where waveform signals suddenly increase in amplitude relative to data behind it. These peaks can then be used to estimate the arrival time of the different phases. The P-wave arrival can often be picked with high certainty as it emerges from just a background noise level. S-wave arrivals often emerge out of the P-wave coda (higher amplitude than the background noise) and so tend to have more uncertainty in their picking.

The following options are also available on the Auto-picking Property Sheet in order to tune the algorithm to the data.

- Use Analytic Envelope in RMS runs the auto-picking function on the analytic envelope of the data rather than the raw waveform amplitudes.
- Use Optimised Picking can be checked if the user wishes to use optimised picking algorithms. The user can carry out auto-picking by either of the following methods:

  - RMS Amplitude-picking function using the RMS.
  - Envelope Method-similar method used as for the RMS but the Envelope function is used.
  - AIC Method-Autoregressive (AR) modelling to provide improved estimates of the pick position.

- The user can choose how the maximum peak in the auto-picking function is obtained. The options include the following:
  - Use first peak in the auto-pick function-the algorithm looks for the first peak in the auto- picking function that is greater than the given threshold level.
  - Use max. peak in the auto-pick function-he algorithm searches the entire auto-picking function and finds the maximum peak above the given threshold level.
- When a Min. Peak to Peak Amplitude is set then the algorithm checks that the signal has sufficient amplitude to warrant a pick. This allows the user to discard picks automatically from waveforms when signals are below a desired level.
- Allow Automatic Amplitude Picking performs an automatic pick of the arrival's peak amplitude. This operation scans forward through NF data points (the length of the auto-picking front window) looking for a peak in the waveform. If there is more than one peak then the maximum is picked. A signal:noise ratio for this amplitude is also generated by dividing the amplitude by an RMS noise value calculated from in a pre-signal window before the arrival.
- Use Velocity Window Picking is a useful option for picking Active Events. The algorithm only generates an auto-picking function for a section of the waveform. The start and end points of this section are calculated knowing the signal T0 on the waveform and signal minimum and maximum velocities through the medium ? a homogeneous-isotropic medium is assumed between the shot/transmitter location and the receiver location for the channel being processed. This option is particularly useful in scenarios where noise appears on the waveforms before the signals of interest.
- Use Waveform Visualiser Window allows the user to define a window within an event waveform to be used for phase auto-picking.
- Autoprocess Source Vectors allows source vectors to be automatically calculated during the autopicking where applicable. Additional settings, for S-wave source vectors, are available through the Dialogue launched using the Further Source Vector Settings button (section 4.9.2.5).
- Linearity Threshold is the minimum linearity (in percent) that will be accepted when rotating the P- wave arrivals into the source vector orientation. The linearity represents the effectiveness of the P- wave rotation, thus source vectors with lower linearity can be regarded as having higher uncertainty.

- Rotation Back Window and Rotation Front Window set the window, in sample points, around the P pick that is used to calculate the P-wave rotation.
- Normalise Picking Functions finds the maximum peak in the auto-picking function and then normalizes all values to this maximum ? thus producing a function that has a maximum of 1.0. It should be noted that if the user defines an auto-picking threshold in the range 0.0 to 1.0, then using this operation will mean that a pick on the waveform is always produced; as there will always be a maximum in the auto-picking function above the threshold.
- Fix Rotation Window to Pick forces the source vector window to sit around the phase pick when calculating source vectors automatically. The default behaviour is for the window to be moved within the limits of the FFT window (Channel Processing tab) until a maximum linearity is achieved.

  The autopicking function behaves differently depending on whether the user is processing the event by Channel or by Instrument.

- In Channel mode the algorithm processes each channel individually using the amplitude from the waveform samples, A_j=W_j in equation D.0.0.1.
- In Instrument mode the algorithm uses the RMS waveform generated from the M channels (where

  $$1 \leq M \leq 4$$

). The RMS waveform is calculated using equation D.0.0.2 where W_{im} is the waveform amplitude on channel m at point i.

$$W_i = \sqrt{\frac{\sum_{m=1}^{m=M} W_{im}^2}{M}} \tag{D.0.0.2}$$

Appendix E

The Geiger algorithm

The following description for the Geiger algorithm is from the technical Appendix user manual of the InSite software.

The Geiger algorithm solves for the origin time t_0, and source location (x_0, y_0, z_0), such that the sum of the square of the residuals is a minimum, where the residual r is equal to the observed time minus t_0 minus the calculated time at (x_0, y_0, z_0). The algorithm iterates towards the correct location using the magnitudes of the time derivatives (the change in time for small changes in x, y, or z). The routine uses SVD (Singular Value Decomposition) inversion from P- and/or S-wave arrival times. Advantages of the Geiger method are:

1. The robustness of the inversion is estimated by the condition number.
2. Advanced analysis of the covariance matrix can be made to give error ellipsoids (X, Y, Z error estimates).

The Geiger method is an inverse least squares (L2 norm) problem. The source location is defined by four parameters, the coordinates (h) and the time:

$$\theta = (x_0, y_0, z_0, t_0) \tag{E.0.0.1}$$

The time residual, r_i (where i equals 1 to the number of stations n) is the difference between the calculated arrival times, T_i, and the observed arrival times, t_i, corrected to the time zero of the event, t_0:

$$r_i = t_i - t_0 - T_i \tag{E.0.0.2}$$

The function relating the arrival times and the location is nonlinear since there is no single step approach to find the best event location. The standard technique is to linearise the problem:

$$\theta = \theta^* + \Delta\theta \tag{E.0.0.3}$$

Where θ^* is a source location estimate near the true location, and $\Delta\theta$ is a small perturbation.

Using the first term in the Taylor series expansion, the observed times may be approximated by:

$$t_i = t_0^* + \Delta t_0 + t_i\left(h^*\right) + \frac{\delta T_i}{\delta h}\Delta h \tag{E.0.0.4}$$

The time residuals at the location h^* are given by:

$$r_i\left(h^*\right) = t_i - t_0^* - T_i\left(h^*\right) \tag{E.0.0.5}$$

Combining equation E.0.0.4 and equation E.0.0.5 gives:

$$r_i\left(h^*\right) = \Delta t_0 + \frac{\delta T_i}{\delta h}\Delta h \tag{E.0.0.6}$$

$$r_i\left(h^*\right) = \frac{\delta T_i}{\delta \theta}\Delta\theta \tag{E.0.0.7}$$

In matrix notation, equation E.0.0.7 can be expressed as:

$$r = A \cdot \Delta\theta \tag{E.0.0.8}$$

Where A is a $n \times 4$ matrix of partial derivatives.

The minimization of the sum of the squared time residuals can be given by:

$$b = B \cdot \Delta\theta \tag{E.0.0.9}$$

Where

$$b = A^\tau r \tag{E.0.0.10}$$

and

$$AB = A^\tau A \tag{E.0.0.11}$$

Is termed the covariance matrix. The Geiger location is found by choosing a starting location, solving the matrix problem (e.g. by Singular Value Decomposition) for $\Delta\theta$, and then iterating until this adjustment parameter reaches a user set minimum.